UNIVERSITY OF LONDON THESIS

Degree PhD Year 2007 Name of Author FABES Jeremy St John

Investigating the Role of Ephrin Signalling in Spinal Cord Injury

Jeremy Fabes

A Thesis Submitted for the Degree of Doctor of Philosophy to the University of London

Department of Physiology
University College London
September 2006

ProQuest LLC
789 East Eisenhower Parkway
P.O. Box 1346
Ann Arbor, MI 48106-1346

Abstract

Spinal cord injury in adult mammals commonly leads to the permanent loss of motor and sensory function in regions of the body below the level of injury. The inability of the central nervous system to regenerate is, in part, due to the presence of growth-inhibitory agents surrounding the lesion site. This thesis presents a previously unreported, inhibitory interaction between ephrinB2 expressed on reactive astrocytes and the EphA4 receptor present on lesioned corticospinal tract axons. This interaction appears to mediate the unusually large retraction of the corticospinal tract away from spinal cord injury sites. An attempt to interfere with this interaction by implanting a cell line secreting the ephrinA5 receptor binding domain is reported. While this approach induced improvements in regenerative sprouting from the corticospinal tract, complications with immune rejection and cell proliferation stopped further investigation. A second intervention using a small peptide with high affinity and specificity for the EphA4 receptor is also reported. Intrathecal infusion of this peptide for 14 or 28 days after injury reversed the retraction of the corticospinal tract and induced improvements in regenerative sprouting from corticospinal and rubrospinal tracts following dorsal or lateral white matter transection injuries. Sprouts were seen to migrate long distances, often to the astrocyte margin of the lesion cavity. Astrocyte behaviour following injury was also altered with the formation of astrocytic 'bridges' into the lesion cavity along which regenerating axons grew. Functional recovery was also enhanced with improvements in the paw reaching assay within 10 days of a unilateral dorsal column lesion with a 30% recovery of function at 28 days post-operation. The simplicity of this intervention and direct translation to human application make it a promising candidate for use in combinatorial approaches to human spinal cord injury treatment.

Acknowledgements
A lot of people have helped me keep sane through the ups and downs of this PhD so they deserve a lot of thanks.

Firstly I would like to thank my supervisors Steve Bolsover and Caroline Brennan for putting up with my total lack of organisation and having the foresight to anticipate the growing field of ephrins in CNS injury. Also Pat Anderson who, despite not officially supervising me, helped me with untold hours of surgery and provided enthusiastic and expert knowledge. I doubt this PhD would exist as it does without his help.

If for no other reason than putting up with the microwave curries on Thursday mornings the members of the Squash Court labs, past and present, should also be thanked. Steve, Sam, Sandip, Will, Rachel, Vinita and Dev were all great and fun people to work with and, more importantly, to chat to about totally unscientific things. The Anderson lab were very generous in letting me use their lab space and make a mess everywhere for over two years. They also taught me the secrets of immunohistochemistry without which there would be very few pretty pictures in this thesis. The kindness, expertise and friendliness of Pat, Greg, Bob, Kismet, Julia and Gemma was invaluable.

Last but not least I would like to thank my family who have always encouraged and supported me, despite often seeming somewhat rudderless in my approach to getting a career. Without their help and faith in me I doubt I would have finished this PhD and certainly would not have applied for medicine. My girlfriend Franci has always been lovely and stuck with me despite invariably being late, useless, distracted, asleep, working, ruining Sunday mornings and failing to take a Summer holiday. I should also mention my puppy Bailey who helped me keep everything in perspective and whose ability to climb stairs to tell me it was his lunch time also reminded me I had to eat too. I think I should thank the pet mice too who stoically ate too much food and got overweight.

There are many more people I should thank but I already sound like Gwyneth Paltrow at the Oscars so I'll leave it there.

P.S. I promised to mention the alien cells and neurons (happy Grace?).

Note to the reader
This complete thesis is presented in an abnormal format to simplify correlation of legend text with appropriate images. Legends are arranged such that they face towards their corresponding image panels to minimise page-leafing. Please note this may, of occasion, give the impression of 'missing' pages in the thesis.

Abbreviations used in the Thesis

ACSF	Artificial Cerebrospinal Fluid
AMPA	α-amino-3-hydroxy-5-methylisoxazole-4-propionate-kainate
AMV	Avian Myeloblastosis Virus
AP	Alkaline Phosphatase
BBB	Blood Brain Barrier
BDA	Biotinylated Dextran Amine
BDNF	Brain-Derived Neurotrophic Factor
cDNA	Complementary Deoxyribonucleic Acid
CHO	Chinese Hamster Ovary
CMV	Cytomegalovirus
CNF	Ciliary Neurotrophic Factor
CNS	Central Nervous System
cRNA	Complementary Ribonucleic Acid
CSF	Cerebrospinal Fluid
CSPG	Chondroitin Sulphate Proteoglycan
CST	Corticospinal Tract
C_t	Threshold PCR Cycle Number
DABCO	1,4- diazabicyclo[2.2.2]octane
DIG	Digoxigenin
DMEM	Dulbecco's Modified Eagle's Medium
DNA	Deoxyribonucleic Acid
DNase	Deoxyribonuclease
DREZ	Dorsal Root Entry Zone
DRG	Dorsal Root Ganglion
ECM	Extracellular Matrix
EDTA	Ethylenediaminetetraacetic Acid
EF	Elongation Factor
EGFP	Enhanced Green Fluorescent Protein
FBS	Foetal Bovine Serum
FCS	Foetal Calf Serum
FFA	Free Fatty Acid
FGF	Fibroblast Growth Factor
FGFR	Fibroblast Growth Factor Receptor
FITC	Fluorescein
GABA	Gamma-Aminobutyric Acid
GDNF	Glial Cell-Derived Neurotrophic Factor
GEF	Guanine Nucleotide Exchange Factor
GFAP	Glial Fibrillary Acidic Protein
GPI	Glycosylphosphatidylinositol
GTPase	Guanosine trisphosphatase
HBS	HEPES buffered saline
HBSS	Hank's Buffered Saline Solution
HEK	Human Embryonic Kidney
HIV	Human Immunodeficiency Virus
HRP	Horse Radish Peroxidase
IL	Interleukin
IP	Immunoprecipitation
Jak	Janus Kinase
JM	Juxtamembrane
LCST	Lateral Corticospinal Tract
LIF	Leukemia Inhibitory Factor
MAG	Myelin-Associated Glycoprotein
MAP	Mitogen-Activated Protein
MHC	Major Histocompatibility Complex
MMP	Matrix Metalloproteinase
MOI	Multiplicity of Infection
mRNA	Messenger Ribonucleic Acid
MS	Multiple Sclerosis

NGF	Nerve Growth Factor
NMDA	N-Methyl-D-Aspartate
NO	Nitric Oxide
NT	Neurotrophin
NYU	New York University
OEG	Olfactory Ensheathing Glia
OMgp	Oligodendrocyte Myelin Glycoprotein
PAF	Platelet Activating Factor
PSA-NCAM	Polysialic Acid-Neural Cell Adhesion Molecule
PBS	Phosphate Buffered Saline
PDGF	Platelet-Derived Growth Factor
PDZ	Postsynaptic Density-95/Discs Large/Zona Occludens-1
PFA	Paraformaldehyde
PLA_2	Phospholipase A_2
PNS	Peripheral Nervous System
qRT-PCR	Quantitative Reverse Transcriptase Polymerase Chain Reaction
RAG	Regeneration-Associated Gene
RAP	Receptor Affinity Probe
RGC	Retinal Ganglion Cell
RNA	Ribonucleic Acid
RNase	Ribonuclease
ROS	Reactive Oxygen Species
RST	Rubrospinal Tract
RT	Room Temperature
RTK	Receptor Tyrosine Kinase
SCI	Spinal Cord Injury
SDS-PAGE	Sodium Dodecyl Sulphate-Polyacrylamide Gel Electrophoresis
SEAP	Secreted Placental Alkaline Phosphatase
SEM	Standard Error in the Mean
SFK	Srk Family Kinase
SH2	Src Homology-2
SSC	Standard Saline Citrate
TBS	Tris Buffered Saline
TGF	Transforming Growth Factor
Tm	Annealing Temperature
TNF	Tumour Necrosis Factor
TU	Transforming Units
UTP	Uracil Trisphosphate

Contents

Chapter I

Introduction

Time Line of Spinal Cord Injury Development

Acute Phase

The initial mechanical insult of a spinal cord injury (SCI) commonly spares the peripheral white matter with a propensity for damage to the grey matter. The most likely explanation for this phenomenon is the greater vascularisation of the grey matter as well as its inherently softer consistency[1]. Within minutes of injury, the central grey matter microvasculature begins to develop scattered punctuate haemorrhages with localised oedema and serum and erythrocyte extravasation. This develops rostrally and caudally over the following eight hours through much of the grey matter and to a limited extent into the white matter[2] with anterior structures presenting changes first. With time this induces haemorrhagic necrosis in these areas that affects both neurons and glial cells to a similar extent and with a similar time scale[2]. The extent of haemorrhagic necrosis that develops appears to correlate closely with the severity of the injury[3] and anterior spinal artery damage is common at later time points. Typical observations of necrotic tissue include cellular atrophy, nuclear disorganisation, granulation of chromatin and disorganisation of the endoplasmic reticulae. Under these conditions, estimates of the timescale of irreversible damage to neural tissue following injury suggest that white matter may survive up to 72 hours following injury whereas the more susceptible grey matter is likely to be unrecoverable within an hour.

Sub-Acute Phase

This phase, also referred to as secondary injury, is typified by recruitment and invasion of cells into the lesion vicinity as well as reactive responses to injury by surviving cells. The main phenotypic change common to most CNS (central nervous system) injuries is reactive gliosis, comprising microglia and astroglia. However, while the pathophysiology of spinal cord injury develops relatively predictably over a period of weeks to months, different injury types do evolve distinctly and involve a wide range of cell types and signalling mechanisms.

The progression of secondary injury leads to expansion of the initial damage and hence incomplete lesions may often develop such that they are functionally equivalent to a transection[4].

Blood Flow Changes, Ischaemia

Injury to vasomotor output pathways commonly induces neurogenic shock through the loss of vasoregulation. Clinically this is observed in the form of bradycardia and hypotension. This vasospasm, combined with the primary insult damage to the microcirculation and other complications such as intravascular thrombosis, leads to the formation of hypoxic and ischaemic conditions in the injured cord. Furthermore, release of cytokines, serotonin, endogenous opioids and platelet-activating factor (PAF) in the secondary phase of injury may also induce vasoconstriction and hence limit perfusion. This hypoperfusion of the grey matter subsequent to injury is a common occurrence and probably expands to the white matter also, although some studies suggest that white matter may be more tolerant of the hypoxic and ischaemic consequences[5]. Ischaemic conditions develop rapidly and contribute to the formation of a depressed metabolic state relying mostly on anaerobic respiration for the first few hours post-injury. The uncoupling of cellular metabolism through free radical damage and sodium/calcium overload that occurs after injury (discussed below) is likely to combine with the ischaemic state of the tissue to induce this metabolic depression. Mitochondrial function, already diminished through secondary hypoxic and ischaemic damage, is further impaired by this build-up of intracellular calcium. However, a semblance of metabolic recovery occurs within 24 hours in surviving tissue[6].

The accumulation of lactate and other acidic metabolites during the ischaemic period has been proposed to reduce perivascular pH and hence induce hyperaemia[7]. As is typical for any ischaemia-reperfusion injury, oxygen-derived free radical generation in excess of the cellular antioxidant capacity occurs in the form of superoxide, nitric oxide, etc. These high-energy oxidants place oxidative stress on the injured nervous tissue and induce the oxidation of cellular components such as proteins and lipids. Action on mitochondrial

and metabolic enzymes, as well as ion channels and lipid peroxidation all contribute to secondary damage and other forms of secondary injury such as apoptosis and excitotoxicity.

Excitotoxicity

Accumulation of excitatory neurotransmitters induces damage to the injured cord[8] and the release of glutamate and aspartate occurs within minutes of injury[9, 10]. Much research has focussed on the role of glutamate in this context and glutamate-induced excitotoxicity appears to play a central role in the secondary ischaemic phase of CNS injury[11]. Activation of NMDA (N-methyl-D-aspartate) and AMPA (α-amino-3-hydroxy-5-methylisoxazole-4-propionate-kainate) receptors leads to the accumulation of sodium within neural cells with subsequent development into calcium overload through the Na^+-Ca^{2+} exchanger. Sodium overload within the cell induces cytotoxic oedema and acidosis which is exacerbated by inactivation of the Na^+-K^+ ATPase by reactive oxygen species. Calcium-dependent enzymes such as calpains, cyclooxygenase and phospholipase A_2 (PLA_2) degrade structural components of the cell such as neurofilaments and also axon-myelin proteins. Calcium-dependent lipoxygenase, cyclooxygenase and lipase also induce the production of cytokines such as prostaglandins, leukotrienes and thromboxanes. As well as their role in disruption of blood flow secondary to injury and formation of reactive lipid species, these cytokines are known to mediate astrocyte reactivity and the formation of the glial scar[12].

Free Fatty Acid Release and Free Radical Formation

Excessive activation of calcium-dependent phospholipases leads to hydrolysis of phospholipids and free fatty acid (FFA) release. FFA accumulation occurs rapidly after injury and also in a later phase between four and 24 hours that mirrors metabolic depression[13]. The severity of tissue damage apparent in the stable long-term injury correlates well with the extent of FFA build-up that occurs during secondary injury, highlighting the importance of these mediators of secondary damage. FFA metabolism leads to the formation of thromboxanes and other cytokines released from arachindonic acid, as well

as PAF derived from activated PLA_2, that will contribute to diminished local blood flow and inflammation.

Numerous components of the secondary phase of injury contribute to the formation of free radicals. Metabolism of arachindonic acid by cyclooxygenase can lead to free radical release. Invading cytotoxic neutrophils release oxygen free radicals to kill target cells and the excessive release of ROS (reactive oxygen species) and the high numbers of neutrophils within the lesion area leads to free radical levels beyond the ability of surviving tissue to cope. Furthermore, calcium overload induces the formation of free radical species as do glutamate excitotoxicity, inflammation and ischemia, and catecholamine autoxidation. Under less pathological conditions endogenous defence mechanisms such as anti-oxidants, superoxide dismutase and peroxidases sequester and inactivate ROS. However, the diminished viability of large quantities of spared tissue in the secondary phase of injury, combined with the high levels of free radicals means that free radical-mediated cell death is common. Furthermore, sequestration of iron to prevent the propagation of oxygen and lipid free radical formation is impaired as the ready availability of haemoglobin following haemorrhage provides a source of iron to overcome cellular defences.

Electrolyte Balance

As discussed, the initial primary insult results in local rupture of the vasculature and blood-brain barrier that induces radially spreading vasogenic oedema that is likely to imbalance the precise electrolytic homeostasis of the CNS tissue for at least the first week after injury. Disruption to the electrolyte balance is one leading candidate for the development of spinal shock following injury. Spinal shock occurs transiently following damage to the spinal cord with flaccid paralysis below the level of the damage and a loss of stretch and flexor reflexes. Loss of impulse conduction in intact fibres in spinal shock is common and rapid accumulation of intra-axonal calcium[14] and extra-cellular potassium[15] would be expected to interfere with normal conduction. Intracellular calcium accumulation might deregulate sodium and potassium electrochemical gradients. Extracellular potassium would be expected to

induce excessive depolarisation of surviving fibres and neurons hence diminishing their function[15].

Inflammation

The inflammatory response to SCI occurs rapidly (within hours) and develops over days[2]. Inflammatory cell invasion commences with polymorphonuclear granulocytes and this is followed by infiltration of monocytes and macrophages with a phagocytic role. At later time points, a minor influx of lymphocytes has also been observed.

The leukocyte response following injury initially involves the invasion of neutrophils that release lytic enzymes, potentially inducing secondary damage to surviving neuronal and circulatory tissue[16]. These neutrophils, whose primary role is anti-bacterial, still invade lesions (experimental or clinical) that are closed, sterile wounds. Subsequent recruitment of macrophages leads to large-scale phagocytosis of damaged tissue. The microglial response is graded in a well-controlled manner to the extent of injury and cellular regulation appears to be relatively precise as only moderate invasion of healthy, non-degenerative tissue is apparent[2]. Microglial activation involves upregulation of major histocompatibility complex class I and II antigens (MHCI and II) and the activated macrophage marker ED1 as well as an increase in the number of processes. Full transformation into phagocytic brain macrophages can occur with associated cytotoxic activity, however it appears that these cells attack healthy as well as necrotic tissue and contribute to inflammatory damage. Macrophage and neutrophil overreaction to injury results in destruction of spared tissue through release of granule components and formation of oxygen free radicals. These two immune system agents are proposed to induce the rapid demyelination of spared axons seen ~24hrs after injury[16]. Oligodendrocyte lysis through secretion of tumour necrosis factor-α (TNFα) and nitric oxide (NO) production is a likely mediator of this.

The role of the immune system in the secondary phase of spinal cord injury is controversial with components proposed to be both beneficial and detrimental to recovery[17]. Macrophages and microglia highlight the duality of the role the

immune system can play following injury to neural tissue. Further to their negative influence on the recovery process, macrophages have been shown to secrete a wide range of pro-recovery molecules that contribute to the destruction of myelin, aid tissue repair, stimulate Schwann cell proliferation and promote tissue homeostasis. The massive influx of macrophages to the distal stump of severed PNS (peripheral nervous system) axons is credited with the rapid clearance of myelin debris within days and subsequent regeneration. Poor macrophage recruitment in the CNS is likely to blame for persistence of myelin debris for months after injury. It should be noted however that other work suggests that the Schwann cell-derived myelin sheaths of the PNS are more amenable to macrophage degradation than oligodendrocyte myelin in the CNS[18].

Glial Cells

Following CNS injury glial cells play a variety of roles, positive and negative. Some secrete neurotrophic factors that can modulate regenerative sprouting either positively or negatively[19]. Others that have a phagocytic role play a detrimental role as either oxidative or enzymatic functions overreact to the injury, as discussed above. In many cases the homeostatic role of glial cells often becomes uncoupled following injury facilitating the excitotoxic and acidosis processes.

Following injury astrocytes typically become hypertrophic and upregulate the expression of intermediate filament proteins such as GFAP (glial fibrillary acidic protein), nestin and vimentin within hours. The extent of astrocyte reactivity is remarkable with a gradient of GFAP expression visible rostral and caudal to the injury over millimetres in the adult rat, while nestin and vimentin appear localised to the lesion margin. In addition to the hypertrophic response, glial cell oxidative and lysosomal activity is increased as well as the production of inhibitory extracellular matrix[20] (ECM). Limited division of astrocytes occurs within the first few days after injury often restricted to the margin of the lesion site. However, ablating these mitotic astrocytes[21] has been shown to diminish repair of the blood brain barrier (BBB) leaving the spinal cord without effective homeostasis or protection leading to extensive

inflammation and degeneration[21]. The BBB is permeable for as long as two weeks following spinal cord injury and extensive scarring is observed in those areas where the BBB is most heavily damaged as reactive astrocytes work to restore it.

Roughly a week following injury a flexible intermixed aggregation of cells develops at the lesion margin, comprising reactive astrocytes, meningeal cells and endoneural tissue. Interactions between meningeal cells and astrocytes appear to regulate the formation of the glial scar and the new glial limitans and this interaction appears to be ephrin mediated, as discussed below. Injuries that do not damage the dural layers significantly, and hence do not have a meningeal cell component, develop a scar without these interactions. Reactive astrocytes around the lesion penumbra form the bulk of the glial scar[22] and begin to develop connexin-43-based junctional complexes similar to those found in the tightly-knit BBB. The development of the glial scar begins around one week after injury, similar in time-scale to the reformation of the BBB, and this astrocyte response continues for weeks after injury. As discussed later, cytokine signalling through transactivation of the EphA4 receptor appears to mediate this astroglial response to injury[12]. The close association between scar astrocytes develops into a mechanically strong lining, probably developed to permit the reformation of the glial limitans and to exclude invading meningeal cells such as fibroblasts. Invading meningeal fibroblasts in both brain and spinal cord injuries[23, 24] proliferate rapidly in the basic fibroblast growth factor (bFGF)-rich spinal cord environment[25]. These invading cells often divide extensively hence a mechanically strong barrier is required to maintain the integrity of surviving neural tissue. However, the tight interaction between reactive astrocytes at the lesion penumbra and their expression of anti-regenerative agents presents a formidable barrier to regeneration. The astrocyte response to CNS injury is well conserved throughout evolution and hence must provide some benefit to the animal. However, the procreative capacity of any animal following severe spinal cord injury is likely to be minimal; hence the astrocyte response has evolved to ensure survival of an animal following a minor CNS injury where such a response can be inherited. Preventing massive secondary inflammation and

damage following minor injury is evolutionarily preferable to permitting regeneration of lesioned axons through more extensive areas of damage.

With time the glial scar stabilises and segregation of astrocytes and fibroblasts occurs with deposition of a new basal lamina that develops into the reformed glial limitans[26]. Deposition of new ECM by invading cells such as Schwann cells, macrophages and fibroblasts will also contribute to the development of the cavity and scar. Laminin, collagen and fibronectin are all produced and may contribute to wound closing, reformation of the basal lamina or providing a permissive environment for regeneration.

Apoptosis and Axons

Apoptosis in the secondary phase of injury results from free radical damage, excitotoxicity, cytokine exposure and inflammation; all extensive following spinal cord damage. Neuronal apoptosis leads to a significant reduction in functional outcome[27], while microglial apoptosis has been suggested to contribute to the inflammatory component of secondary injury[28]. Demyelination, already in progress through immune cell activity, is increased by apoptosis within the oligodendrocyte population[29].

A rim of spared peripheral white matter is common in many patients once the lesion site has stabilised, however these patients often score as suffering a complete spinal cord transection injury in functional and sensory tests. In some cases the tracts that are spared do not mediate motor or sensory function, but in many others demyelination or necrosis of spared fibres and supporting cells appears to be responsible. Demyelination begins within 24 hours of injury and continues throughout the injury process, completely baring some axons within a week. Demyelination exacerbates the post-injury loss of function significantly as spared axons with little or no myelin are typically unable to conduct or at best will be unstable in their conduction properties. Haemorrhagic necrosis induces separation of the axon from its myelin sheath with axonal swelling[30] that will further disrupt function.

Late Phase

Despite differing subacute and late stages of development, most spinal cord injuries develop into similar stable lesions with cavitation walled off by a scar and the Wallerian degeneration of white matter distal to the lesion. Following the immediate inflammatory phase, macrophages migrate away from the centre of the lesion to leave a cerebrospinal fluid (CSF)-filled cavity that is surrounded by scar tissue. In some cases slow development of syringomyelia in the months following injury can lead to the formation of an extensive cavity that induces further functional loss.

The Neuronal Response to CNS Injury

Unlike the perinatal response to injury, where many injured neurons die, adult spinal and supraspinal neurons survive axotomy as long as the injury is not too proximal. In some cases an axotomised neuron will die through lack of target-derived neurotrophic factors[31], but this is often dependent on the neuronal population in question. Similarly the intrinsic ability of neurons to regenerate varies significantly between tracts[32]. The neurons of the corticospinal and rubrospinal tracts, often studied for their obvious functional role, ease of access, established anatomy and simple labelling, have both been shown to survive for significant periods after injury, despite neuronal atrophy[33].

The initial intrinsic response to CNS injury is encouraging with upregulation of regeneration-associated genes and moderate sprouting of lesioned processes. Sprouts from lesioned axons have been seen in many animal models of CNS injury and generally follow a similar morphology and time frame of behaviour. Thin, unmyelinated sprouts are put out from lesioned axon stumps for short distances (often less than 1mm[34]) and persist for a few weeks[35]. However, these sprouts do not elongate and within a week regeneration-associated genes have been downregulated and axotomised neurons become atrophied[31]. Subsequent to this period of sprouting, sprout regression occurs (termed die-back) in nearly all cases such that only minimal functional recovery typically occurs[36, 37]. The extent of this retraction has not been conclusively defined[34, 38] but retraction from the initial mechanical

disruption of over 2mm is standard for the corticospinal tract (CST). During and subsequent to retraction, sprouts and axonal stumps develop retraction bulbs (also termed termination bulbs or end bulbs) with a highly characteristic swollen morphology[37] – large swellings similar to growth cones filled with mitochondria, neurofilaments and other organelles[39]. While these structures have traditionally been viewed as stagnant attempts at sprouting that hold little regenerative potential, recent evidence suggests that they are remarkably flexible and have been shown to respond to favourable changes in their environment with impressive regeneration despite long periods of stability[40]. Furthermore, damage to spinal roots permits the slow invasion of the lesion site by Schwann cells and these have been found to secrete neurotrophic factors and permit the formation of myelinated sprouts from endbulbs in chronic injuries over a period of years[36, 41].

After PNS lesion, rapid degeneration of the distal stump occurs with myelin breakdown. Local proliferation of Schwann cells occurs concomitantly with synthesis of growth-promoting substrates and neurotrophic factors. Subsequently sensory and motor fibres regenerate through the cleared lesion site, often close to their previous paths, and grow for long distances, usually resulting in target reinnervation with good specificity. Over a longer period Schwann cells remyelinate the newly grown axons to restore near-normal conduction. While extrinsic factors such as neurotrophic support and the presence of scar-associated growth-inhibitors in the CNS are likely to be important differentiating factors (discussed below), intrinsic differences should not be ignored. It is important to consider that the mechanism of CNS regeneration, whether endogenous or treated, is likely to be different to that seen in the PNS as the usual substrates for PNS regeneration and development, such as laminin, fibronectin and collagen, are not present in great quantities in CNS injury. PNS regeneration is characterised by upregulation in tubulin and actin mRNAs (messenger ribonucleic acid) with downregulation in neurofilament mRNAs[42, 43]. In contrast, the growth rate for CNS neurites is around ten percent of their peripheral counterparts[44] and they appear to be neurofilament-dense, with little of the F-actin seen in other growth cones[45]. It is likely therefore that the CNS does not use the standard

actin-filopodial approach to regeneration but may be driven by neurofilament polymerisation inside the growth cone. Furthermore, microtubule-associated proteins, required for stable axon growth, may also contribute to the differences in regeneration rate and capacity: isoforms expressed in the adult are different to those in development and expression does not revert following injury[46].

It is a well-accepted phenomenon that embryonic and newborn CNS tissue regenerates significantly better than the equivalent adult tissue. Analysis of CST regeneration in the newborn hamster following pyramidotomy showed extensive plastic growth into spared tissue with subsequent growth down distal spinal cord[47]. While targetting of regenerating axons was imperfect, functional improvements were readily apparent[47]. Subsequent work identified late developing axons to be a major constituent of this recovery process, but the presence of regenerating axons was also confirmed[48]. While embryonic neurons implanted into adult CNS tissues can put forward processes that can successfully navigate the inhibitory glial environment, adult processes are unable to do so[49]. The ability of embryonic neurons to modify their expression of integrins such that they can navigate the adult spinal cord ECM appears to be the differentiating factor. Adult neurons have lost this capacity[50] and hence the mature CNS appears to be more sensitive to growth-inhibitory mediators[51]. Occasional reports have identified some moderately successful regenerative sprouting in the untreated CST[34] but no progress into the lesion site has ever been reported in the untreated adult animal.

Regeneration of long myelinated tracts in the adult mammal is limited to only a few specific tracts[52, 53]. However, significant functional recovery can be made following stroke, partial SCI and other CNS injuries. Plasticity of the remaining nervous structure is probably responsible for this long-term functional improvement and extensive reorganisation has been observed in all CNS regions associated with spinal cord injuries[54]. This plasticity usually takes the form of activation of 'silent' pathways, collateral sprouting from injured or uninjured pathways and reorganisation of neural networks and pattern generators. Silent synapses, often inhibited by GABAergic (gamma-

aminobutyric acid) interneurons, become active shortly after injury and the presence of numerous vacated post-synaptic densities stimulates sprouting of local spared fibres to fill these sites. However, in a similar manner to the ability of tracts to regenerate, the plasticity response diminishes with age but even in humans over eighty years of age recovery from stroke is still readily apparent.

Gene Expression

Some studies comparing recovery from injury in the PNS and CNS indicate that the main differentiating factor is the presence of the inhibitory glial environment within the CNS[55]. This was initially highlighted by the pioneer peripheral nerve transplant experiments where brainstem axons were seen to regenerate into a peripheral nerve implant in the spinal cord but not beyond it[56, 57]. However, subsequent experiments by Richardson[58] demonstrated that the cell body response was also critical. DRG (dorsal root ganglion) neuron central processes were only able to regenerate into peripheral nerve grafts in the dorsal columns of the spinal cord if a pre-conditioning lesion of their peripheral processes had been performed. The cell body response elicited by this pre-conditioning lesion involves expression of a range of regeneration-associated genes[59] (RAGs). These studies have been extended and more recently central DRG processes have been observed to regenerate strongly following dorsal column injury subsequent to a preconditioning lesion[60]. This result, combined with similar studies in the rat optic nerve[61], have shown that the intrinsic growth state of the neuron is as important as the extrinsic microenvironment to the extent that strong neurotrophic support may facilitate regeneration through growth-inhibitory sites.

The genetic cell body response to injury of PNS neurons with central processes comprises upregulation of a range of RAGs encompassing ion channels, trophic factors and their receptors, neuropeptides, cytoskeletal and cytoskeletal regulatory proteins, axon guidance and cell adhesion mediators, cytokines and their receptors and transcription factors. Transgenic approaches to determine the role of these RAGs individually have shed some light on the topic suggesting that proteins such as integrin α-7 receptors[62] and galanin[63] are important in regeneration. However, as these studies are not in

conditional or targetted transgenic animals, it is hard to determine whether changes in extrinsic (i.e. non-neuronal cell) expression may also be influencing the regeneration phenotype. For example, knocking out a cytoskeletal regulating protein could readily alter microglial or astroglial behaviour and hence give the impression of diminished regeneration attributed to the absence of a neuronal RAG.

Re-expression of developmental proteins is a common response to CNS injury with numerous immediate-early genes expressed[64]. Different neurons show different transcriptional responses to injury and different primary and secondary injury pathologies induce varying expression patterns as well. However, a number of genes are commonly upregulated in the immediate-early response. A comparison between gene expression changes following spinal cord injury and sciatic nerve injury in mice[65] identified a range of interesting genes that may be responsible for the remarkable difference in regenerative capacity of these two tissues. Immediate-early and heat shock proteins (HSPs) are well represented in this population and probably act to stabilise surviving neural tissue. Growth-associated protein of 43kDa (GAP-43[66]) and CAP-23[67] show dramatic upregulation following PNS injury and have received much attention[68, 69]. GAP-43 is expressed in developing neuronal growth cones and regenerating axons[70, 71] and has been correlated with the rapid growth cone progress that initiates regeneration[72]. GAP-43 mediates the interaction between membrane rafts and actin[73] and appears to promote sprouting of the axon terminal through directed mobilisation of actin, a mechanism that appears to be shared by CAP-23[73]. The gene expression pattern of CNS neurons following injury differs significantly from their PNS counterparts, not just in the individual proteins expressed but, as mentioned previously, in the duration and degree of expression. For instance, while CNS neuron expression of GAP-43 correlates with the ability of transected fibres to successfully sprout into peripheral nerve grafts, this expression is typically transient and only occurs in descending tracts when the injury is sufficiently proximal[74, 75]. Proximal injuries also induce the expression of a wider range of RAGs in CNS neurons; in addition to GAP-43, L1 and c-jun are also

upregulated under these conditions[76] and are likely to be at least partially responsible for the regenerative response seen after proximal injury.

Targetted overexpression of RAGs has revealed an interesting requirement for synergy between these proteins for successful regeneration. Attempts to promote regeneration into peripheral nerve grafts in the thalamic[77] and Purkinje cell[78] systems by overexpression of GAP-43 resulted in no improvement. However, co-overexpression of CAP-23 and GAP-43 increased sprouting of dorsal column axons into peripheral nerve grafts[79] but still significantly less than that seen with preconditioning lesions suggesting that a more suitable target for manipulation may be an upstream expression regulator capable of turning on the whole battery of RAGs seen following preconditioning PNS lesions. This conclusion fits well with analysis of the intrinsic regenerative capacity of CNS neurons when compared to their RAG expression[80]: neurons expressing more than one RAG following injury demonstrate better regeneration. Hence, synergy between the RAGs appears to be necessary for effective regeneration and this requirement for more than one growth-associated gene for successful regeneration is common.

Neurotrophic Deficiency

Changes in the expression of neurotrophins and their receptors, as well as atypical secretion of neurotrophins from endogenous and invading/recruited cells, play a significant role in the post-injury survival and response of most cells affected by injury. Considering the differences in intrinsic CNS and PNS regeneration it is unsurprising that neurotrophic factors and their receptors are also differentially regulated and expressed in these tissues following injury. Target- or glial cell-derived neurotrophic support following PNS injury is required for maintenance of the neuron – administering anti-NGF (nerve growth factor) antibodies leads to PNS neuron atrophy where usually none occurs[81]. A similar phenomenon appears to occur in the CNS as the initial rapid cell death of retinal ganglion cells following injury can be reversed by the application of neurotrophic factors[82]. Hence the observed atrophy and cell death of CNS neurons following axotomy is likely to be due to insufficient autocrine or paracrine neurotrophic support. The downregulation in

expression of neurotrophin and growth factor receptors in adult neurons, and the lack of re-expression following injury is also likely to exacerbate the loss of regenerative capacity. However, upregulation in the Trk family of neurotrophin receptors does occur. Penetrating lesions to adult rat spinal cord induce upregulation in the glial expression of TrkB receptor mRNA and that is localised to the glial scar[83]. Lateral column injuries have shown TrkC upregulation in transected fibres[84] while contusion injuries in the rat induce TrkA upregulation and the expression of bFGF[25, 85, 86]. Expression of bFGF appears to be localised to motor and grey matter neurons as well as peri-lesion astrocytes. However, a lack of expression of appropriate receptors for available neurotrophins may be the critical factor – rubrospinal axons show a downregulation in the FGF receptor FGFR-1 after axotomy and signalling through this receptor may be required for regenerative growth[87].

The corticospinal tract illustrates this neurotrophic dependency well: lesion of the CST at the level of the internal capsule leads to death of over half of the corticospinal neurons[88]. However, this response can be rescued by exogenous BDNF (brain-derived neurotrophic factor) in sufficient quantities[89], while application of anti-BDNF antibodies exacerbates the cell death. Hence, the endogenous supply of BDNF following injury is sufficient to maintain the survival of a proportion of the BDNF-sensitive CST neuron population but not all of it. The complex neurotrophic requirements of CNS neurons is also likely to require considerable work to unravel. In the adult rat CST, quantification of sprouting following lesion showed a significant response to injury that was enhanced by NT3 (neurotrophin), unaffected by BDNF and impaired by NGF[90]. Hence, broad-range application of neurotrophic factors to encourage neuronal survival and regenerative outgrowth is unlikely to resolve the impaired CNS recovery. Implantation of embryonic rat spinal cord tissue into adult animal spinal cord permits good regeneration and recovery[91] suggesting that an approach based on developmental expression of neurotrophins may have some merit.

Myelin-based Inhibitors of Regeneration

In vitro neurite outgrowth is inhibited by CNS myelin and this activity appears to be mediated by a range of myelin-associated inhibitors[92, 93]. Nogo, OMgp (Oligodendrocyte myelin glycoprotein) and MAG (Myelin Associated Glycoprotein) will be discussed here although other molecules are known and others are likely to be discovered. These proteins are expressed in the intact CNS[94, 95], where they are likely to play a role in preventing aberrant plasticity and sprouting, and at the site of CNS injury[22, 96] where they present a strong growth-inhibitory obstacle.

The Nogo proteins comprise three members: Nogo-A (the largest), Nogo-B and Nogo-C (the smallest). The common inhibitory domain, Nogo-66, induces growth cone collapse and neurite retraction[97]. Nogo-A contains a further N-terminal inhibitory domain that enhances its potency[98] and is found in CNS myelin oligodendrocytes. OMgp, also known as arretin[99], is a GPI-linked (glycosylphosphatidylinositol) inhibitory extract from CNS myelin capable of causing growth cone collapse and inhibiting axonal regeneration[100, 101]. Recent evidence suggests an expression of OMgp by glial cells that contribute to nodes of Ranvier[102]; whether this protein is found on reactive astrocytes at the lesion margin is unknown. MAG is a sialic acid–binding Ig-family lectin that binds glycoconjugates, predominately two major axonal gangliosides, GD1a and GT1b[103]. MAG has a wide growth-inhibitory spectrum that includes action on adult DRG cells, cerebellar granule cells and many other neurons[99, 104]. However, despite compelling *in vitro* data, regeneration studies using both MAG[105] and OMgp[102] knock-out mice show no improvement in regeneration.

NgR1 mediates signalling for all three of these molecules and acts as a co-receptor with LINGO-1 and either p75 or TROY[106]. The Nogo receptor homologues NgR2 and NgR3 may also play a role in inhibitory signalling - NgR2 binds MAG in a sialic acid-dependent manner and acts as a functional receptor for that protein[107].

Knock-out of Nogo isoforms in mice have resulted in mixed regenerative responses following injury[108]. Nogo-$A^{-/-}$ mice show a slight improvement in CST sprouting after injury[109] while Nogo-$A^{-/-}B^{-/-}$ mice demonstrated no regeneration of the hemisected CST[110] nor impressive anatomical and functional recovery[111]. Genetic background or compensatory expression could account for these differences, although further investigation is required to resolve the disparity. One safe conclusion is that Nogo-A cannot be the only mediator of growth inhibition in CNS injury. The best evidence to date for the role of Nogo as a key growth-inhibitory mediator is derived from experiments using antibodies that neutralise Nogo signalling[112, 113], notably IN-1. Expression of NgR1 and Nogo-A on corticospinal neurons and axons make the CST an obvious target for regenerative studies. IN-1 administration to midthoracic dorsal column injuries in young rats[114] led to remarkable CST regeneration beyond the lesion site. However, the presence of the regenerating axons in the normal anatomical location for the CST and the impressive regeneration seen in control animals (2.5mm beyond the lesion site) suggests that some fibres recorded as regenerating may have been spared. A separate study on IN-1 treatment of adult rat pyramidotomies demonstrated increased regeneration (2mm) and in this study regenerated axons were found everywhere but the degenerating CST[115]. Other approaches using anti-Nogo antibodies have found similar results[116]. Functional recovery has also been demonstrated following partial lesions of the cord[117, 118] but acute administration is required for full anatomical and functional benefits – an eight week delay in treatment significantly diminishes the regenerative response[119].

As discussed previously, combinatorial approaches combining IN-1 antibodies with neurotrophic support[90] or embryonic spinal cord implants[34] led to enhancement of the regenerative response above that observed for IN-1 alone. Further evidence that neutralisation of Nogo alone does not lead to successful regeneration comes from studies of more severe injuries involving extensive scarring or cyst formation[116, 118]. The presence of numerous other inhibitors of regeneration at these lesions is the likely explanation[96, 120, 121].

The sum of current literature on Nogo neutralisation suggests that the functional improvements seen following injury stem predominately from sprouting and plasticity of injured[122, 123] and spared[122] fibres, although some regeneration of CST fibres into spared tissue may also contribute to motor functions. The most telling experiment to highlight this demonstrated that rostral relesioning of the corticospinal tract after functional recovery was induced by IN-1 administration had no significant effect on the recovered function[124]. Hence, sprouting from fibres very rostral to the primary injury into spinal cord tissue untouched by the secondary injury, must have mediated the functional recovery. The expression of Nogo-A on regenerating CST and other cell bodies and access to the cell body by neutralising antibodies suggests that plasticity may be induced by an antibody-mediated cell body response. However, regardless of the source of regeneration, neutralisation of Nogo appears to be strongly pro-regenerative. Primate experiments[125] have found similar functional recovery to that seen in rodent studies which is very encouraging for clinical initiatives.

Endogenous antibodies to myelin can be generated by immunisation with CNS myelin preparations. Pre-immunised animals show improved CST regeneration following injury[126] and the presence of regenerating axons in the dorsal white matter suggests that myelin breakdown following injury may be more rapid, similar to PNS regeneration. Similar techniques involving immunisation against MAG and Nogo-66[127] or AminoNogo, Nogo-66, MAG and tenascin-R[128] have reported improved regeneration but not to the extent seen with whole-myelin immunisation. Knock-out experiments aimed at the NgR1 receptor have produced ambiguous results, suggesting either slightly enhanced[129] or unimproved[130] regeneration; neither study demonstrated CST regeneration however. Pharmacological approaches using the Nogo-66 blocking peptide NEP1-40 have shown regeneration and sprouting of descending spinal tracts following injury after either immediate[97] or seven day delayed[131] administration. NgRecto, the NgR1 ectodomain, also encourages CST regeneration and functional recovery[132] but significantly more than that seen with NEP1-40 despite it's wider range of pharmacological action (blockade of Nogo-66, MAG and OMgp activity). Interestingly these

pharmacological studies report CST regeneration unlike the genetic approaches to NgR1 inactivation discussed above; compensatory changes in gene expression may account for this discrepancy however.

As already discussed, DRG neurons microtransplanted into the spinal cord white matter[133] or the corpus callosum[134] successfully put out growing processes. This occurred whether in undamaged spinal cord or white matter undergoing Wallerian degeneration subsequent to dorsal column injury. The rate of regeneration was similar to that found in peripheral nerve regeneration (approximately 2mm per day) despite the presence of numerous myelin-associated growth-inhibitory molecules. Growth stopped upon arrival at the chondroitin sulphate proteoglycan (CSPG)-rich lesion scar suggesting that scar- rather than myelin-associated inhibitory molecules may prove to be more potent. The lack of expression of NgR1[135, 136] and p75[137] in many DRG neurons may account for part of this behaviour, however.

Other Inhibitors at the Lesion Site

Semaphorins

The semaphorin family of proteins share a conserved 500 amino acid motif termed the sema domain. Semaphorins are classified based on membrane topology (transmembrane, secreted or GPI-linked) and primary sequence. The vertebrate semaphorins include secreted (class 3) and membrane-anchored (classes 4 to 7) family members, however Sema 3A has received most attention in spinal cord injury to date. Recent research into other family members has identified strong Sema4D expression in myelin and upregulation by oligodendrocytes around an injury[138]. Sema4D is a potent inhibitor of DRG and cerebellar granule cell neurite outgrowth and hence is likely to contribute to myelin-associated inhibition. Plexins and neuropilins act as co-receptors for Sema3A as well as further accessory proteins such as the L1 adhesion molecule. Complex intracellular signalling mechanisms develop from many of the developmental guidance proteins and semaphorin signalling is no different. Currently recognised mediators of growth cone guidance include cyclic nucleotides, redox signalling[139], kinases, Rho family guanosine trisphosphatases[140] (GTPases) and eicosanoids[141].

Expression of Sema3A depends on the type of damage sustained by the spinal cord (or any other CNS tissue). Meningeal fibroblasts express Sema3A and hence transection and stab wound injuries are Sema3A-positive[96]. Contusion injuries where meningeal cell invasion does not occur do not contain Sema3A[96, 142]. These injuries are still highly inhibitory however, suggesting that Sema3A may not be a significant growth-inhibitory mediator. However, regenerating ascending dorsal column axons avoid areas of Sema3A expression [96], suggesting further work on semaphorins in spinal cord injury is warranted.

Slits and Netrins

Slit and Netrin family members are pathfinding proteins that play critical roles in CNS development. Depending on cyclic nucleotide levels and neuron type either repulsion or attraction can result from Netrin signalling and midline expression of Netrin in mammals preserves left-right integrity of various nervous tracts. Adult rat and mouse Netrin-1 expression is localised to neurons and oligodendrocytes as well as ECM surrounding these cells[143]. Recent research indicates that Netrin-1 is strongly expressed in mouse spinal cord lesions[144] but no regenerative studies have yet been reported. Vertebrate Slit proteins play a role as repulsive guidance markers for developing spinal cord axons[145] and the retina[146] through the Robo family of receptors. Slit-1 and -3 are expressed in mouse spinal cord lesions by macrophages and/or meningeal fibroblasts[144] and would be expected to repel regenerating axons from Robo-positive tracts such as the CST[147]. While no studies have yet to confirm the role of slits and Netrins in spinal cord injury, they clearly require further study in this context as potential mediators of growth-inhibitory signalling.

Scar Formation and Approaches to Overcome Scar-Associated Inhibition

As discussed, the glial scar begins to develop at the physical margin of the lesion site around a week following injury. The main components are reactive astrocytes as well as invading meningeal fibroblasts and endoneural tissue

(when dural or spinal root damage has occurred, respectively). These astrocytes are predominately derived by migration from surviving tissue although limited division of astrocytes occurs within the first few days after injury. Meningeal fibroblasts rapidly invade both brain and spinal cord injuries[23, 24] and proliferate in the bFGF-rich spinal cord environment[25]. At early time points oligodendrocyte precursors are also major constituents of the scar; the limited migration of these cells during injury suggests that the majority of the precursors present in the scar must be derived from proliferation, probably driven by the presence of FGF and PDGF (platelet-derived growth factor) in the lesion vicinity.

Depending on the cellular composition of the lesion margin, the interactions that mediate the development of the scar vary. In the case of the most common human injuries where dural and spinal root tissues are disrupted, ephrin-mediated interactions appear to contribute to cell sorting and the deposition of a new basal lamina that develops into the reformed glial limitans[148]. In all cases however, reactive astrocytes develop connexin-43-based junctional complexes and form a tightly-knit physical barrier. Not only does this barrier prevent any further invasion of surviving spinal cord tissue by fibroblasts, it restricts the migration of parencyhmal astrocytes such that the scar rapidly evolves into an astrocyte-free zone[149]. Further to the deposition of ECM molecules that contribute to the reformation of the blood-brain barrier, growth-inhibitory substrates are expressed throughout the scar – both on cells and deposited in the ECM.

Hence, the lesion scar appears to prevent regeneration in three main ways:

- A physical barrier to regeneration of axons into the lesion cavity
- Preventing migration of astrocytes into the cavity
- Expression of growth-inhibitory agents

While the strength of the tight junctions between scar astrocytes is beneficial to repel the pressure of proliferating meningeal fibroblasts, axons are unable to penetrate this physical blockade. Hence, even those axons with sufficient regenerative capacity to overcome the numerous growth-inhibitory molecules

surrounding the scar are unable to regenerate through it. Sprouting into spared white and grey matter presents navigation difficulties and successful growth around lesion scars is unlikely without strong neurotrophic support. However, the scar developed following injury to the mediobasal hypothalamus is permissive for growth and has few gap junctions and expresses some PSA-NCAM (Polysialic Acid-Neural Cell Adhesion Molecule) and laminin[150]. Hence in some cases the glial scar can be permeable to axons and permit regeneration. Furthermore, NGF-responsive neurons may be able to put forward processes onto reactive astrocytes[151, 152] and neurotrophic factors such as NGF, bFGF and TGF-β (transforming growth factor) may, under the right circumstances, be able to modulate the expression of some astroglial growth-inhibitory proteins such as L1 and tenascin[153]. Hence, modification of the glial scar such that it becomes permissive for growth is likely to be a component of any successful approach to inducing regeneration.

The role of astrocytes in CNS injury is unresolved with robust evidence for both growth-promoting and -inhibitory roles. Approaches to diminish the formation of the glial scar by ablating mitotic astrocytes[21] have shown diminished repair of the blood brain barrier leaving the spinal cord without effective homeostasis or protection leading to extensive inflammation and degeneration. Furthermore, migrating astrocytes aid wound closure and provide a substrate upon which other cells and axons may repopulate disrupted tissue and provide reinnervation[133, 134]. However, generic approaches aimed at minimising the formation of the scar and astrocyte gliosis have reported some improvements in regeneration. Administration of 7β-hydroxy-cholesterol-oleate appears to improve serotonergic axon sprouting[154] while transgenic animals without GFAP and vimentin demonstrate improved regeneration following injury[155]. Other experiments have shown that removing hyperplasic astrocytes with low-dose X-irradiation or ethidium bromide injection reduces secondary injury[156] and improves functional recovery[157, 158]. Targetting the cytokines that mediate gliosis, i.e. with anti-TGF-β antibodies or IL-10 (interleukin) application to prevent cytokine synthesis, also appears to minimise the overall CNS damage[159]. Elegant implant studies by the Silver laboratory highlight the dual role played by

astrocytes. Microtransplantation of adult DRG neurons into the spinal cord white matter such that no local reaction occurs permit sensory processes to regenerate long distances at rates of 1mm per day or more, implying that quiescent astrocytes are growth-supportive. Implantation into white matter of a spinal cord that had received a distal (caudal) lesion also results in good regeneration of DRG processes through oligodendrocytes, damaged myelin and reactive astrocytes. Hence, reactive astrocytes also appear to be growth-permissive. However, upon reaching the growth inhibitor-dense scar the processes rapidly terminated to produce typical dystrophic endbulbs[133, 134]. Hence, reactive astrocytes expressing moderate levels of growth-inhibitors are permissive for regeneration but, when a critical expression level is reached, are highly effective inhibitors of growth.

While astrocytes do express growth-promoting molecules, numerous experiments have highlighted the inhibitory nature of the ECM developed by reactive astrocytes[160, 161], despite the fact that it contains laminin. Expression of ECM proteoglycans by astrocytes in the glial scar is upregulated following CNS injury in adult animals[120, 161, 162]. Proteoglycans consist of a protein cord linked to a sulphated glycosaminoglycan (GAG) chain. Four classes of proteoglycan are expressed by astrocytes; heparin, dermatan, karatan and chondroitin sulphate proteoglycans. The CSPG family includes brevican, aggrecan and NG2 and these differ in their protein core as well as their side chain composition (reviewed by Carulli et al., 2005, Hartmann and Maurer, 2001). Some CSPGs are neurotrophic[163] while others appear to minimise astrogliosis and scarring[164, 165], although the majority are thought to be growth-inhibitory and induce retraction[166, 167]. Both the protein core[168] and the GAG side chains are thought to be inhibitory[169]. CSPG expression and secretion appears to be a common mechanism within CNS injuries[170, 171] with CSPGs secretion by astrocytes within 24hrs and a maintained presence in the lesion vicinity for months[120, 161, 162]. The distribution and time-course of CSPG expression varies with the subtype in question[120] and different cells express different CSPGs. Reactive astrocytes predominately express neurocan while NG2 and phosphacan are present on meningeal fibroblasts. Significantly, early mammalian embryos and cold-blooded species where effective

regeneration occurs following central injury do not express CSPGs[172, 173]. Furthermore, *in vitro* hippocampal neuron cultures regenerate better on 'scar-in-a-dish' cultures from neonatal animals than on those derived from adult animals, with evidence that neonatal cultures are in fact supportive and promote growth[174]. Similarly, astrocyte cultures derived from adult lesioned optic nerve are strongly growth-inhibitory towards adult DRG regeneration *in vitro* whereas those from neonatal injuries promote outgrowth[175]. Adult CNS and PNS responses to CSPG exposure *in vivo* appear to be varied with sensory neurons capable of growing further into a proteoglycan-positive lesion site than motor processes[176]. In a similar manner to the repulsion of DRG processes by a CSPG-positive spinal cord scar[133], central DRG processes are repelled from the CSPG-dense DREZ (dorsal root entry zone) following spinal nerve transection, even when the DREZ is free from injury[177].To date, there are no published reports suggesting significant regeneration into a proteoglycan-positive spinal cord lesion site without intervention.

Application of the *Proteus vulgaris* enzyme chondroitinase selectively cleaves GAG side chains from CSPGs and hence diminishes the glycoprotein inhibitory activity. Regeneration of retinal ganglion cells in 'scar-in-a-dish' experiments is substantially improved by the application of chondroitinase[167] and chondroitinase has been applied to contusion injuries with significant reductions in CSPG immunoreactivity[178] that persist for weeks[179]. The precise mechanism of chondroitinase action – i.e. improvements in plasticity or regeneration – has not been fully elucidated[180]. Regardless, chondroitinase has been found to encourage the regeneration of various ascending and descending spinal tracts following lesion[181, 182] including spinocerebellar[183] and rubrospinal[184] tract axons. Growth into peripheral nerve grafts following injury[185] is also enhanced as well as regeneration in a range of other CNS injuries[181]. Improvements in functional recovery have also been demonstrated – intrathecal chondroitinase ABC injections induced moderate functional recovery following dorsal column injury[181] or forcep compression of the cord[186]. However, the remaining protein core and digested GAG stubs from chondroitinase digestion retain inhibitory activity[187] and approaches to minimise this further show improved regeneration[188].

Approaches to Improve CNS Regeneration

Neurotrophic Support

Most experiments aimed at neurotrophic supplementation have used the neurotrophin family members NGF, BDNF and NT3 as well as GDNF (glial cell-derived neurotrophic factor). Signalling for the neurotrophins is through the TrkA, B and C receptors and in some cases the p75 receptor. GDNF acts through the RET tyrosine kinase and an accessory subunit. Most spinal pathways appear to express TrkB and TrkC, motoneurons have been found to express RET and different subpopulations of DRG neurons express varying Trk receptors. In culture neurotrophins and GDNF have been shown to promote neurite outgrowth[189, 190] and to facilitate growth on inhibitory myelin substrates[191]. Convergence of signalling on RhoA is a likely mechanism of action for the neurotrophic ability to facilitate growth over inhibitory substrates. The p75 receptor is involved in transmitting both neurotrophin and myelin-based inhibitor signalling to induce either growth or retraction of growth cones. Inactivation of RhoA by neurotrophin-mediated p75 signalling prevents growth cone collapse and retraction mediated by myelin-induced activation of RhoA by p75[192, 193].

NGF, GDNF and various cytokines are upregulated in the PNS following injury[194, 195]. These growth-promoting factors undoubtedly contribute to PNS recovery. Furthermore, inhibition of Jak2 (Janus kinase 2, a cytokine signalling mediator) prevents axon growth following preconditioning lesion[196] and leukaemia inhibitory factor (LIF) or IL-6 knock-out mice show reduced regeneration[197, 198]. Sensory axons have been found to regenerate into the spinal cord and provide functional improvements following NGF or FGF2 delivery via an adenoviral vector[199] or intrathecal neurotrophin delivery[200]. Similarly, long regenerative sprouts from the central processes of DRG neurons similar to those found following a preconditioning lesion occur following application of NT3, NGF and GDNF[200-203].

Neurotrophic support does not just promote regeneration from severed axons but also appears to play a neuroprotective and cell-survival role following injury such that neuronal apoptosis can be counteracted by neurotrophic factors. Lesion of adult rat or mouse facial or sciatic nerves leads to motoneuron atrophy and death and this effect is counteracted by NT3, CNF (ciliary neurotrophic factor) and GDNF[204]. Various neurotrophins have been found to enhance motor neuron regeneration[205, 206] and an alternative method of neurotrophic delivery through genetically modified fibroblasts has also yielded encouraging results. Lesioned RST (rubrospinal tract) axons were seen to regenerate towards an implant of BDNF-secreting cells with subsequent navigation through the implant or into spared tissue[207]. Axons able to grow into cord distal to the injury site were seen to regenerate for remarkable distances and behavioural testing suggested the formation of useful nervous connections. Similarly, NGF-secreting fibroblasts induced some regeneration[208] following injury, although motor axon recovery was not seen to improve. However, most reports of neurotrophic intervention alone have documented only moderate regeneration. Combinatorial therapy however, whether with embryonic spinal cord implants or anti-Nogo antibodies, induces good growth. Regeneration of descending fibres have also been found to improve following embryonic spinal cord implants combined with intrathecal BDNF[209, 210] and the combination of NT3 and neutralisation of myelin-associated growth-inhibitors also results in improved spinal cord regeneration[90].

The diverse roles of neurotrophins during development include cell survival, axon guidance, plasticity, neurotransmitter release and synapse/dendritic arbour formation[211]; hence it should be expected that neuronal sensitivity and response will vary. BDNF appears to encourage chronically injured spinal cord axons to grow into a peripheral nerve graft[212] but in the acute injury plays a neuroprotective role for CST axons while not inducing regeneration[213]. This change in activity as the lesion develops is not uncommon – BDNF and NT3 induce greater RST neuron survival and regeneration when administered non-acutely[209, 214].

Filling the Lesion Site

Numerous approaches to fill the lesion site with synthetic materials have been used (for reviews see references 215 and 216). These materials are usually seeded with growth-promoting neurotrophic factors or cells such as Schwann cells. In some cases astrocytic rejection of the implant as a 'foreign body' results in rapid exclusion of the implant from the spinal cord similar to that seen with normal scarring. However fibronectin-based conduits appear to offer a good balance of properties[215] including effective resorption, no immune rejection and orientation for regenerating axons. Fibrin gels present another synthetic material with similar properties[216] and also appears to prevent excessive scar and cavity formation.

Schwann cells have been found to promote the regeneration of the CST when injected into spinal cord[217] and their incorporation into implanted materials enhances regeneration of a range of CNS tracts[218]. Implantation of exogenous or endogenous neural stem cells or neuron and oligodendrocyte precursors has been investigated[213, 219, 220]. Ventral horn motoneurons produced by expansion and targetted differentiation in culture of rodent embryonic stem cells successfully integrated with endogenous ventral horn tissue and extended axons that successfully synapsed on muscle[221]. Other studies have found successful myelination and neuronal repopulation by embryonic stem cells when implanted into a contusion injury[219, 222]. However, the neurotrophic environment of the spinal cord following injury appears to promote differentiation into glial lineages, rather than neuronal[223].

Olfactory ensheathing glia (OEGs) present one of the best current implant treatments for a range of CNS injuries. OEGs have been found to migrate into spared neural tissue rostral and caudal to a spinal cord injury and, following alignment of their processes to provide regenerative channels, facilitate the growth of CNS tracts through the lesion site, shielded from potential growth-inhibitory factors[224, 225]. The regenerative drive induced by these cells stems from their expression and deposition of growth-permissive substrates and secretion of numerous neurotrophic factors. Following CST injury OEGs have been found to promote long distance regeneration with limited plastic

sprouting that led to moderate recovery of locomotor function. The ability of OEGs to elicit a regenerative response when implanted into chronic injuries highlights the promise of this developing field.

Ephrins in Spinal Cord Injury

Introduction

The Eph family of receptor tyrosine kinases[226] and their membrane-bound ligands, the ephrins, are critical regulators of development, particularly neuronal pathfinding[227-229]. The ligands are grouped into two sub-families[226] – the A-subclass (ephrinA1-A6) that are glycosylphosphatidylinositol coupled and the B-subclass (ephrinB1-B3) that are integral membrane proteins with one transmembrane domain and a short cytoplasmic region. To date, 16 Ephs have been found in vertebrates and are divided into A- and B-subclasses on the basis of ligand affinity and sequence similarity. Ephs and ephrins bind promiscuously with most members of the corresponding subclass interacting in the nM affinity range[229]. Some promiscuity exists between subclasses[230-232], in particular EphA4 binds ephrinB ligands with high affinity[233-236]. The Eph extracellular domain is composed of the ligand-binding globular domain, a cysteine rich region and two fibronectin type III repeats – a 90 amino acid long stretch repeated 15-17 times in the fibronectin molecule, commonly found in many cell-surface proteins. The cytoplasmic domain of the Eph receptor family is divided into 4 parts – a juxta-membrane (JM) domain containing two conserved tyrosines, a classical protein tyrosine kinase domain, a sterile α-motif thought to participate in protein-protein interactions and a PDZ-domain (postsynaptic density-95/Discs large/zona occludens-1) binding motif in the last 4-5 residues important in protein scaffolding[237]. As is the case with classical RTKs[238] (receptor tyrosine kinases), Eph receptor kinase activity is autoinhibited by the JM domain[239, 240]. Ligand-induced autophosphorylation relieves this conformational inhibition, permitting kinase activity and adaptor protein recruitment, required for most signalling[241].

Ephrin Signalling with relation to Spinal Cord Injury

Soluble monomeric ephrin ligands do not induce functional signalling, instead artificial preclustering or membrane attachment is required[242-245], indicating a

requirement for cell-cell contact *in vivo*. The single transmembrane nature of the Eph family necessitates receptor dimerisation for activation through clustering of ephrins and leads to phosphorylation of 10 or more specific Eph tyrosine residues, several of which are involved in upregulation of the tyrosine kinase activity[246]. Phosphorylation also permits phosphotyrosine-binding proteins to bind to the 4 or more phosphotyrosines that are docking sites for SH2 (Src homology-2)-domain containing proteins. This regulatory mechanism is highly reminiscent of that proposed for the platelet-derived growth factor receptor β and the TrkB receptor. X-Ray crystallographs show that Ephs and ephrins form a cyclic heterotetramer with a 2:2 stoichiometry[247], this planar arrangement is necessary for binding to occur between two cell surfaces. The complexity of Eph signalling means that the receptor modulates many pathways and cell responses, many of which affect growth cone guidance or cell migration[248]. The principal mediators of ephrin-induced repulsion and morphogenesis are the Rho family of small GTPases, RhoA, Rac1, and Cdc42, through modulation of actin cytoskeleton dynamics[249-252]. These signalling mediators permit repulsive or adhesive interactions between cells[230, 253-258], partially mediated by differential activation of the Rho, Rac1 and Cdc42 GTPase pathways, which regulate actin depolymerisation (repulsion) and polymerization (adhesion), respectively[248, 259]. Further signalling diversity comes from PDZ-binding domains in ephrin and Eph family members that can induce protein clustering[260-263] and hence specify regulation.

Recruitment of Src family kinases (SFKs) is a common Eph receptor theme[264, 265] and recent work suggests that EphA4-mediated growth cone collapse requires the phosphorylation of ephexin1 by SFKs[266, 267]. Ephrin signalling through ephexin1 (Eph-interacting exchange protein, a Rho GTPase guanine nucleotide exchange factor, GEF), a member of the Dbl family of exchange factors has been shown to activate RhoA to induce growth cone collapse and inhibit cdc42 and Rac1 to inhibit filopodial and lamellipodial outgrowth, respectively[259, 268]. This interaction appears to be required for EphA-receptor-mediated repulsive guidance. Similarly, EphB receptors interact with other GEF proteins, e.g. kalirin[269] and intersectin[270], that exhibit exchange activity

towards Rac1 and Cdc42. The ability of the ephrin system to signal in either direction is now a common theme with reverse, ephrin-based, signals acting through PDZ domains to activate SFKs[230, 243, 244, 255, 260, 271-273]. For example, A-class ephrin signalling[274] has been implicated in vomeronasal axon mapping to the accessory olfactory bulb[275] and B-class signalling mediates commissural axon repulsion[276] and attraction[241]. Ephrin signalling is complicated by emerging data that ligand co-expression can modulate receptor sensitivity[277, 278]; increasing evidence for co-expression of ligands and receptors on neurons[279, 280] suggests this may play a significant developmental role. As well as their well-defined role in the regulation of cytoskeletal dynamics, there is also evidence for transcriptional modulation by ephrin signalling. Examples include the NMDA receptor[264, 281] and, interestingly, ephrinA2 itself[282]. Furthermore, Eph-mediated activation of the MAP (mitogen-activated protein) kinase pathway[283, 284] and the Rho GTPases[285, 286] would be expected to have further transcriptional roles.

Many of the Eph receptor signalling roles require differential responses to gradients of ligand expression. A number of studies suggest that, unlike classical RTKs, activation of Eph receptor kinase activity is not sufficient for signalling[287] but clustering is also required. Furthermore, increasing densities of ephrin ligand lead to further oligomerisation of receptors and hence recruitment of different cytoplasmic effectors[288].

Developmental Functions and Expression of Ephrins relevant to Spinal Cord Injury

Ephrins represent major contact-dependent guidance molecules in development of the nervous system. A selective list of their roles would encompass the guidance of corticospinal tract fibres down the spinal cord to their terminal field[235, 236, 289, 290], thalmocortical[291-293] and hippocamposeptal[294, 295] fibres, spinal motoneuron outgrowth[296, 297], target selection[279, 296-301] and neuromuscular junction formation and maintenance[302]. Other critical roles involve the visual system[303-307], the segmental organization of spinal nerves[308, 309], selective bundling (fasciculation) and dispersal (defasciculation) of axons[310], the formation of the anterior commissure[241, 311] and spinal central

pattern generators[290, 300, 312, 313], local neuronal networks within the spinal cord that mediate locomotion[314].

Ephrin Expression in the Adult CNS

Ephrin family member expression is most prominent during development; following birth most tissues downregulate ephrin expression and it is only preserved in selected areas where it performs maintenance and regulatory roles in the adult. Adult human[315, 316] and non-human primate[317] studies indicate substantial Eph and ephrin expression in adult brain and spinal cord, with particularly strong expression in cortical and hippocampal neurons. This staining pattern appears to be similar or identical to that highlighted in mouse and rat[318-325] suggesting that data from rodents is relevant to human studies. Of particular interest is the evolutionarily conserved expression of EphA4 in cortical neurons[315] suggesting a conserved guidance mechanism for the CST[235, 236, 289]. In the rodent, extensive neuronal expression in adult brain has been found, in particular in the hippocampus, cortex, striatum, thalamus, and cerebellum[321, 326-329] and studies have highlighted expression of ephrins in both motor[330] and sensory[26, 281] systems. Furthermore, supporting cell types such as astrocytes[26, 321] and oligodendrocyte[331] in both brain and spinal cord and the surrounding meningeal fibroblasts[26] have been shown to express ephrin family members. Expression of Eph receptors and ligands in complementary systems such as axons[321] and myelin[331] or hippocampal dendrites and supporting astrocytes[332-335] suggest in the adult system ephrins may act to constrain and modulate plasticity. This role has been highlighted in both learning[265] and sensory[281] scenarios.

Ephrin Functions in the Adult CNS

Accumulating evidence suggests that the ephrin family plays a significant role in the adult animal, discarding the conventional view of these proteins as solely developmental. Recent evidence has revealed a complex ephrin-mediated regulation of hippocampal plasticity with multiple EphB receptors acting via Rho to regulate the actin-based cytoskeleton[249, 269, 270, 336] required for dendritic spine morphogenesis[337], development and maturation[338]. B-class ephrin signalling is essential for dendritic spine morphogenesis, neuronal–glial

communication[335] and plasticity in synaptic signalling[264, 334, 339, 340]. Furthermore, sensory plasticity in the spinal cord regulated by EphB–ephrinB interactions may contribute to sensory abnormalities in persistent pain states[281].

Complementary to this role in regulating plasticity, the more typical repulsive role of ephrin signalling[235, 341] is employed in constraining plasticity of 'fixed' neural connections where ectopic connections would be unwanted. Evidence suggests that continued expression of EphA4 in adult cortical neurons giving rise to the CST[315, 321] may be required to maintain specificity – localised expression of ephrinB3 in myelinating oligodendrocytes around the adult CST[331] would prevent aberrant sprouting. Similarly, EphA5 may constrain hippocamposeptal and olfactory system plasticity in the adult mouse[295]. This model is similar to that proposed for the non-pathological function of Nogo, MAG, and OMgp[342] and is supported by the observation that aberrant sprouting occurs when EphA receptors are not expressed[234-236, 343].

Other critical adult roles of ephrin signalling include neural stem cell migration, proliferation and function[290, 344-346], immune system functions such as T- and B-cell signalling, immunoregulation and costimulation[347-349], ECM attachment through integrin receptor signalling[350-352] and chemokine responses[263]. All of these may be important in the response of the CNS to injury, furthermore it is possible that Eph receptor activation may play a trophic role in cell survival[353], although solid evidence for this is lacking.

The Role of Ephrins in Spinal Cord Injury

The presence of ephrin family members in the uninjured animal, particularly within the spinal cord, means that following injury ephrin-mediated pathological interactions will occur that are likely to be detrimental to regeneration. These interactions are not restricted to typical growth cone repulsion but are fundamentally involved in the acute and long-term post-injury environment.

As discussed, astrocyte proliferation and gliosis following injury leads to the formation of glial scar[354] that protects surviving neural tissue from invasion by meningeal fibroblasts[148, 355, 356]. While this process is essential for restoring the blood-brain barrier[356], astrocytes in the scar not only present a mechanical barrier to regeneration but also induce the expression of numerous scar-associated neurite growth-inhibitory molecules in the basal lamina deposited during this astrocytic-fibroblast interaction. Bundesen *et al.* have shown that, in mouse SCI, upregulated expression of ephrinB2 in reactive astrocytes and EphB2 in fibroblasts following injury[26] mediates these astrocyte-meningeal fibroblast interactions. Their results suggest that bidirectional signalling prevents cell population intermingling in a manner similar to that found during ephrin-regulated rhombomere boundary formation[230, 271, 357]. The authors suggest that astrocytes and fibroblasts are initially repelled via cell contact-mediated ephrin signalling and subsequent segregation is maintained by the basal lamina. This interaction may also regulate cellular morphology to induce the well-documented parallel-lesion orientation of astrocytic processes. Activation of Rho in astrocytes, as well as in neurons and oligodendrocytes, has also recently been reported in spinal cord after injury[358]. Ephrin signalling is likely to regulate Rho activity and may be the mechanism behind the reactive astrocyte morphogenesis. The juxtaposition of ephrinB2-positive astrocytic end feet onto EphB2-positive fibroblasts at the newly formed glia limitans suggests these proteins may play a role in the deposition of this basal lamina or the cellular attachment to it through integrin signalling[350-352, 359]. The presence of ephrinB2 throughout the extent of the glial scar will present a further regenerative barrier to Eph-positive axonal tracts. As discussed, the disruption of this non-permissive glial environment[154, 156] is likely to contribute to CST regeneration and the recovery of motor function, as shown previously[157, 158].

Further work by Goldshmit *et al.*[12] has identified astrocytic EphA4 as a major constituent of the post-SCI signalling cascade. The authors report that EphA4 null mice regain significant functional capacity following a dorsal hemisection. Importantly, the hemisected spinal cord showed almost no astrocytic gliosis with minimal glial scarring and the authors demonstrate that astrocytic EphA4

may be required for gliosis following cytokine exposure[12]. The inhibition of this pathway may be the basis of the attenuated astroglial reaction[360] and improved SCI environment[159] following IL-10 administration (an inhibitor of microglial cytokine synthesis). The EphA4$^{-/-}$ mice also show decreased CSPG expression at the lesion site suggesting that EphA4-mediated reactivity may be a crucial component of the formation of the growth-inhibitory basal lamina. However, reactive astrocytes play numerous beneficial roles following SCI including phagocytosis[21, 361, 362] to remove degenerated material[114, 363], the production of growth-promoting molecules[364, 365] and other roles[21]. A transient increase in astrocytic ephrinB expression has been seen following hippocampal deafferentation[332, 366] and the temporal profile of the expression suggests a potential role in denervation-induced reorganization events and regulation of Rho-mediated astrocytic phagocytosis[367, 368]. In the EphA4$^{-/-}$ mouse, it appears that astrocytic gliosis is not entirely abrogated which may permit growth-enhancing properties of gliosis such as phagocytosis and growth factor secretion while limiting negative effects such as the formation of the glial scar. Similarly, GFAP and vimentin double null mice present a mild gliosis following entorhinal cortex lesion and these animals demonstrate improved regeneration[155].

EphrinB3, well established as the midline developmental guidance marker for EphA4-expressing CST axons[235, 289], is also expressed in adult myelin[331]. Adult cortical neurons continue to express EphA4[323] which is activated by ephrinB3[369] and induces growth cone collapse[370]. In culture the cortical neuron repulsion/retraction response was equivalent to that of all three of the p75-mediated inhibitors combined[331]. EphrinB3 was also shown to induce a repulsive reaction in cerebellar granule neurons through an EphB-mediated mechanism[331]. The CST, unlike other axonal tracts which may extend short sprouts into or around a lesion, undergoes a progressive retraction in the months following a lesion[38, 97, 176]. The continued expression of EphA4 in the adult CST and its interaction with astrocytic ephrinB2 and myelin-based ephrinB3 is a likely cause of this phenomenon. One emerging aspect of ephrin signalling following SCI is that, due to the huge range of expression profiles, different cellular and axonal populations respond in different manners

to unique combinations of inhibitory molecules. This may be the basis for differential regeneration of rubrospinal, raphespinal and corticospinal tracts in NgR1 knockout mice[111] where ephrinB2/3-responsive CST axons cannot take advantage of the improved SCI environment. Furthermore, regeneration approaches aimed at Rho signalling[371, 372] might benefit from the abrogation of ephrin signalling as well as that mediated by p75-mediated inhibitors.

Contrary to the larger body of work on the ephrin proteins, some interactions do favour axonal growth[373-378]. Wang *et al.*[332] propose that dendritic EphB-astrocytic ephrinB neuroglial crosstalk may mediate dendritic spine regrowth in the hippocampus after entorhinal deafferentation, perhaps though mechanisms seen in adult plasticity[334]. Furthermore, there is evidence that ephrins may be re-expressed to supply their developmental role as guidance molecules for appropriate reinnervation of targets. During optic nerve regeneration in goldfish, specific EphAs and ephrin-As are up-regulated coincident with restoration of retino-tectal topography[282, 379]. Ephrin family members also appear to be transcriptional regulators, and in the goldfish EphA/ephrin-A interactions appear to regulate ephrin-A2 expression in the tectum[282].

Other studies have implicated changes in ephrin expression in the post-injury CNS environment. Thoracic contusion models have shown an upregulation in A[318] and B[380] family Eph receptors and EphB3 upregulation in astrocytes has been implicated in the astrocytic gliosis that contributes to scar formation in adult rat SCI[12, 381]. Furthermore the expression of Eph family members is upregulated in adult animals following central neural damage[282, 382-385]. An as yet unresolved role for ephrin signalling post-SCI in inflammation is probable: perivascular mononuclear cells express numerous A-class ligands and receptors[315] where they may regulate migration[349], cytokine production[386] and T-cell adhesion[387]. In multiple sclerosis tissue, EphA3 staining indicated expression in microglia[315]. Considering the similarity[315, 318] in expression of ephrin family members in MS (multiple sclerosis) and SCI, this suggests a possible role for ephrin signalling in post-injury regulation of activated microglia. This correlation also suggests a common injury mechanism.

The concept of developmental proteins being re-employed following injury is not limited to ephrins[388]. Many regenerative processes parallel prior ontogenesis and frequently the molecular mechanisms involved seem to resemble development. The upregulation and re-expression of ephrins following CNS injury might be an attempt to re-implement developmental expression profiles that promote neuron survival, neurite outgrowth and reorganisation/guidance. Enhanced expression might supply some topographic guidance information for re-establishing organisation and connections, but these signals will invariably inhibit regrowth. Approaches to specifically target ephrin signalling *in vivo* with synthetic peptides and chimera proteins have been successful[344, 345, 389] suggesting the ephrin system is amenable to intervention to improve regeneration. Evidence to date suggests that a careful modulation of ephrin signalling could bring about significant improvements in glial scarring and astrocytic gliosis.

Chapter II

Expression of Ephrin Family Member Protein and mRNA following Spinal Cord Injury

ABSTRACT

It is likely that a number of factors combine to make the injured spinal cord a non-permissive environment for axonal growth. Most cut axons, including those of the corticospinal tract, generate sprouts in the days following lesions of the adult mammalian spinal cord[217]. However, in the absence of other manipulation, no sprouts successfully grow back to their synaptic targets. Indeed, axons within the corticospinal tract undergo an usually large degree of retraction or 'die-back' in the months following a lesion[38, 390]. The results presented in this chapter suggest that a significant, previously unreported, factor inhibiting the regeneration of corticospinal tract axons is ephrin:Eph receptor interaction. Two events combine to cause this inhibition. First, following a lesion, ephrinB2 is upregulated in white matter astrocytes, such that the distal stumps of the cut corticospinal tract, and any sprouts they generate, are invariably surrounded by high levels of ephrinB2 expression. Second, continued transport of the EphA4 receptor down corticospinal tract axons causes the accumulation of the receptor at the axonal termination bulbs where it interacts with ephrinB2 and generates an inhibitory, retraction-evoking response. In contrast neighbouring rubrospinal axons, which do not express EphA4, retract less following spinal cord injury and can advance some way towards the lesion before they are stopped by other inhibitory factors[391-393]. Regrowth of corticospinal tract axons through and across a lesion is markedly enhanced in mice lacking EphA4[12]. In normal mice EphA4 was present at only low levels in descending axons, and it was suggested that the major mechanism by which EphA4 inhibited growth after spinal cord lesions was by encouraging the formation of a glial scar. Further to this finding, our results indicate that in the rat transected CST axons express significant amounts of EphA4 and that this may allow a direct inhibitory action on the axons by ephrinB2-positive reactive astrocytes.

METHODS

Animal Housing and Surgery

Animals were housed at the UCL Biological Services Central Facility. Adult female 200-220g Sprague-Dawley rats were housed in groups of one to four animals with food and water available *ad libitum*. A 12/12h light/dark cycle was used with the lights on at 7.00am. Housing conditions were identical for all animals discussed in this thesis. Professor Anderson (Department of Anatomy, UCL) assisted in the majority of the surgical procedures discussed and helped develop the techniques used.

All surgical procedures were approved by the UCL ethical committee and licensed by the Home Office. Before surgery rats were anaesthetised with a mixture of halothane, nitrous oxide, and oxygen. Microsurgical scissors were used to transect part of the left dorsal column, the entire right dorsal column and part of the dorsal horn of grey matter at C6, or to transect the lateral column at C6. In other experiments the spinal cord was compressed with a 50 gram weight applied at C6 for 5 minutes using an apparatus derived from that used by Nystrom and Berglund[394]. In each case, animals were sacrificed seven or ten days after injury by overdose with halothane.

For qRT-PCR (quantitative reverse transcriptase polymerase chain reaction) experiments, up to 100µg tissue was taken from the region encompassed by, and including, the lesion site. For immunohistochemical procedures, the animal was either transcardially perfused with 4% paraformaldehyde before removal of the spinal cord or, following exsanguination, approximately 2cm of spinal cord tissue was removed and fresh-frozen in OCT Compound (Tissue-Tek), cooled by dry ice followed by storage at -20°C until use. Perfused tissue was stored at 4°C in 30% sucrose, 10% Thiermesol in phosphate buffer until use.

Anterograde Tracing of Nerve Tracts

Where anterograde labelling of the CST was required, 5µl of 10% biotinylated dextran amine (BDA, Molecular Probes, Oregon, USA) was injected into the motor cortex using standard coordinates[395]. Labelling of the rubrospinal tract

was carried out by stereotaxic injection into the red nucleus of 3µl of a replication-deficient human immunodeficiency virus (HIV) vector encoding enhanced green fluorescent protein (EGFP, 6.5×10^8 EGFP transfecting units/ml) 10 days before spinal cord injury. The HIV vector was produced using transfer plasmid pHR'SIN-cPPT-CE and following standard procedures. In this vector EGFP is driven by the CMV (cytomegalovirus) promotor[396]. The viral vector injected in this way only infected midbrain neurons, so that only rubrospinal axons were labelled with EGFP. This was done because BDA injection into the red nucleus has in some cases in the Anderson laboratory been found to produce some corticospinal labelling in addition to rubrospinal labelling.

Quantitative RT-PCR

Tissue dissection was performed using sterile instruments, the tissue was then cleaned in RNase-free PBS (ribonuclease, phosphate buffered saline) and homogenised in TRIzol (Invitrogen) or QIAzol (Qiagen), RNA (ribonucleic acid) stabilisation agents. When the tissue under study was of CNS or PNS origin the Qiagen RNeasy Lipid Tissue Extraction Kit was used. Otherwise, the material was then cleared of sediment and phase-separated using chloroform. An upper, aqueous, phase that contained the tissue RNA was precipitated at -80°C with isopropanol overnight, washed with ethanol and resuspended in RNase-free distilled water. RNA samples were treated with DNase I (deoxyribonuclease, Qiagen DNase Free kit) to remove any genomic contamination. 20µl of complete cDNA (complementary deoxyribonucleic acid) was prepared from 1µg of each RNA using random hexamers (500ng, Promega) and AMV reverse transcriptase (avian myeloblastosis virus, 20U, Promega) for 45min at 42°C. Primers for qRT-PCR were designed using the Applied Biosystems Primer Express software due to the stringency of the parameters required for effective PCR in the system. Primers were designed based on either the published rat sequence of each gene, where available, or the mouse sequence in all other cases. 96 parallel 25µL PCRs were set up, each containing 0.5µL (approx. 25ng) cDNA and 300nM of each primer. Forty cycle PCR was performed on the Applied Biosystems LightCycler™ with a 30 second denaturation step at 94°C followed by 30 seconds at 59°C for primer

annealing and 30 seconds at 72°C for polymerase extension. At the end of this amplification phase, a slow dissociation step was performed starting at 60°C and finishing at 85°C that permitted analysis of the DNA (deoxyribonucleic acid) product from the PCR for purity. As the temperature rose and double-stranded DNA species began to denature, the SYBR Green fluorescence reduced. As each species has a different denaturation temperature depending on length and GC base percentage, the fluorescence change peak corresponding to that species differed in temperature to other PCR products. Hence, a single DNA product in each PCR produced only one peak and indicated a highly specific PCR with minimal background signal. DNA synthesis was monitored using the fluorescent AmpliGOLD compound (Applied Biosystems). Following the selection of a suitable threshold DNA concentration, the PCR cycle (C_t) at which each PCR breached this threshold was used to determine the original cDNA concentration for each mRNA (See Figure 2.M1). Normalising each cDNA with β-actin expression permitted comparison between cDNAs (see Results), hence the C_t for β-actin expression was analysed for each cDNA as well. Each PCR was performed in triplicate with a parallel well containing a cDNA preparation that lacked reverse transcriptase. This eliminated the occasional spurious PCR result and allowed an analysis of genomic, or other, contamination in the assay.

The efficiency of each primer pair is a numerical representation of the efficacy of each pair to amplify specific DNA amplicons. Theoretically each cycle should generate one copy of each existing amplicon, giving an efficiency of 2. However, experimentally C_t values of correctly designed primer pairs range from 1.7 to 2.1. Primer efficiencies were calculated using a 20-fold dilution series (from 1 to 1:2000) of one cDNA that strongly expressed the amplicon of interest. The C_t value for each of these dilutions was then plotted against the log (base 10) of the relative cDNA concentration. As shown in Figure 2.1, this gives a linear plot, the gradient of which (termed *m*) can be used to derive the primer efficiency (*Eff*) using the equation:

$$Eff = 10^{\left(\frac{-1}{m}\right)}$$

Mathematical manipulation of the qRT-PCR data was performed to normalise expression of each gene in each cDNA sample to β-actin expression independently of all other samples. Direct comparison between genes and tissue treatments was then possible. The original cDNA concentration of an amplicon can then be derived by placing the primer efficiency for that amplicon to the power of the C_t for any cDNA (i.e. $Eff_{\beta actin}$ ^ $Ct_{\beta actin}$). Due to the inverse relationship between C_t values and the starting cDNA expression of the amplicon of interest, the normalised expression of any gene in a given cDNA preparation (*R*) is calculated inversely (i.e. β-actin expression / EphA4 expression). Hence the following equation[397] was used to calculate the final normalised mRNA expression values for each tissue of interest:

$$R = \frac{Eff_{\beta actin}^{Ct_{\beta actin}}}{Eff_{Eph}^{Ct_{Eph}}}$$

This gives a normalised value for gene expression based on β-actin expression in the cDNA analysed to account for variations in tissue collection and processing, cDNA production and PCR efficiency. Typically the values are less than one due to the high level of expression of β-actin in many tissues.

EphA, EphrinA and EphrinB expression following spinal cord injury

Two spinal injuries have been investigated. In the first, a dual dorsal hemisection was performed at C5 and tissue taken from the region encompassed by, and including, the lesion sites. In the second injury a 50gram weight application was performed at C5 and an equivalent volume of tissue removed from the injury site. Control animals underwent a laminectomy but no spinal cord injury and were treated identically to the injured animals. In all cases tissue was excised 7 days after injury and limited to 100μg.

Primers were designed to minimise the likelihood of cross-amplification due to the high sequence homology in the Eph and ephrin family (see Figures 2.M2-

4). Thermal dissociation analysis and agarose gel electrophoresis of qRT-PCR products revealed distinct DNA species without splice variants (Figure 2.3). BLAST searches of the rat genome also confirmed that each primer pair would only anneal to their intended targets and that there would be no cross-priming.

Immunocytochemistry

Fresh frozen samples of brain and spinal cord from operated and unoperated animals were sectioned in the horizontal or para-sagittal planes at 12µm thickness on a cryostat. Fixed tissue was cut at 40µm thickness on a freezing microtome. Samples were rinsed three times in TNT buffer (Tris Buffered Saline (TBS) with 0.05% Tween-20, Sigma) prior to incubation for one hour at room temperature in blocking solution (TBS, 1% BSA, 0.1% Triton X-100) supplemented with 10% normal serum as appropriate for the secondary antibody in use. Where biotinylated secondary antibodies were used, 2% normal horse serum was also included in the blocking solution. The samples were then incubated with primary antibodies, diluted appropriately in blocking solution, at 4°C. The samples were rinsed three times with TNT buffer and incubated with fluorophore- or biotin-conjugated secondary antibodies, diluted in blocking solution for two hours at room temperature. Again, the samples were rinsed several times in TNT solution before being stained with bisbenzamide (1µg/ml) for 5min. Primary antibodies used included rabbit anti-EphA4 antibody (1:5000, kindly provided by David Wilkinson, National Institute for Medical Research, UK), goat anti-ephrinB2 antibody (1:750, R & D Systems), goat anti-EphA4 antibody (1:750, R & D Systems) and mouse anti-GFAP (1:400, Sigma) in blocking medium overnight at 4°C. Secondary antibodies used were goat anti-rabbit-Alexa 488 (1:400, Molecular Probes), rabbit anti-goat-FITC (Fluorescein, 1:200, Sigma), chicken anti-mouse-Alexa 594 (1:400, Molecular Probes) and biotinylated horse anti-goat (1:200, Vector Labs.). Visualisation of either biotinylated secondary antibodies or anterogradely labelled corticospinal tract axons was performed using either streptavidin-Alexa 568 (1:200 in 0.1M TBS, Molecular Probes) or avidin-HRP reagent (horse radish peroxidase, Vectastain ABC kit, Vector Labs.) followed by exposure to tyramide-Cy3 (1:400 in 0.1M Tris Buffer, New England

Nuclear) for 30min at room temperature. Where tyramide-Cy3 enhancement was used sections were exposed to 0.3% H_2O_2 for 15min at room temperature followed by three washes in TNT buffer before application of blocking solution. The samples were rinsed three more times in TNT buffer before being coated with 1,4- diazabicyclo[2.2.2]octane (DABCO) and sealed under a coverslip with nail-varnish. Control sections, which were not incubated with primary antibodies but otherwise processed identically, were used to ensure signal specificity.

Generation of digoxigenin-labelled riboprobes

Primers were designed against the 364-1282bp region of the mouse EphA4 gene (GenBank Accession NM_007936) that encompassed the C-terminal end of the ligand binding domain and the N-terminal end of the fibronectin type-3 repeat region. The 5' primer was designed to contain a T7 RNA polymerase recognition sequence and similarly, the 3' primer was designed to contain a T3 RNA polymerase recognition sequence.

Primer sequences used were:

5'-EphA4 AATTAACCCTCACTAAAGGG**AGCGCTTCATCAGAGAGAGCC**

3'-EphA4 TAATACGACTCACTATAGGG**GGTCCGGGCTAGGGTTATACT**

with sequence-specific regions in bold font.

Antisense probes were generated by gel purification of the ~950bp PCR product and phenol:chloroform precipitation of the DNA fragment followed by *in vitro* transcription with T7 RNA polymerase (Roche Applied Science). Sense probes were produced from the same purified DNA fragment but *in vitro* transcription was performed with T3 RNA polymerase (Roche Applied Science). Antisense and sense cRNA (complementary ribonucleic acid) probes labelled with digoxigenin (DIG) were generated according to the manufacturer's recommendations using a DIG-UTP (uracil trisphosphate) RNA labelling kit (Roche Applied Science). Unincorporated digoxigenin was removed from the probe using a Sephadex column (Roche Quickspin).

In situ hybridisation

In situ hybridisation was carried out using published methods[398, 399]. In brief, cryostat sections of brain and spinal cord were cut at a nominal thickness of 12µm, thaw-mounted onto slides coated with 3-aminopropyltriethoxy silane, and fixed with RNase-free 4% paraformaldehyde in PBS overnight at 4°C. After being washed in PBS, sections were treated with 0.1M hydrochloric acid and washed in PBS, incubated in 0.1M triethanolamine containing 0.25% acetic anhydride, and then washed with PBS, dehydrated in an ascending ethanol series, and air dried. Prehybridisation was carried out at 37°C overnight with a mixture of prehybridisation buffer/deionised formamide 1:1 (containing 50% formamide, 25mM ethylenediaminetetraacetic acid (EDTA), 50mM, pH7.6, Tris–HCl, Denhardt's solution (Sigma), 0.25mg/ml tRNA (Boehringer Mannheim), and 20mM NaCl). The digoxigenin labelled sense and antisense probes were prepared at a concentration of approximately 1µg/ml with hybridisation buffer containing 50% formamide, 20mM Tris–HCl (pH7.5), 1mM EDTA, 1x Denhardt's solution, 0.5mg/ml tRNA, 0.1mg/ml polyA RNA (Sigma), 0.1 M dithiothreitol and 10% dextran sulphate. Hybridisation was performed overnight at 65°C. After hybridisation, sections were washed in 0.2x standard saline citrate (SSC, containing 30mM NaCl and 3mM Na–citrate, pH7.0) and then three times in 0.1x SSC/50% formamide at the hybridization temperature. Sections were equilibrated with buffer 1 (100mM Tris–HCl, 150mM NaCl, pH7.5) and then incubated in buffer 2 (1% Boehringer blocking reagent, 0.5% BSA fraction V (Sigma) in buffer 1) and incubated with alkaline phosphatase-coupled antibodies to digoxigenin (Roche Applied Science, UK) at a dilution of 1:1500 in buffer 2 overnight at 4°C. Sections were washed in buffer 1, equilibrated in buffer 3 (100mM Tris–base, 100mM NaCl, 50mM MgCl2, adjusted to pH9.5), and developed in the dark with buffer 3 containing 0.34 mg/ml 4-nitroblue tetrazolium chloride (Roche Applied Science, UK), 0.175 mg/ml 5-bromo-4-chloro-3-indolyl phosphate (Roche Applied Science, UK), and 0.25 mg/ml levamisol (Sigma). Development was stopped by washing with buffer 4 (10mM Tris–HCl, 1mM EDTA, pH 8.0), following which the sections were air dried and mounted in DPX beneath glass coverslips. The specificity of the hybridisation signal was verified by comparison with the sections processed with the sense probe under identical

conditions. Comparison between tissues pre- and post-injury was performed using sections developed on the same slide.

Digital image capture and analysis

Fluorescence images were acquired on a Zeiss 510 confocal microscope using conventional filter based fluorescence optics. Excitation and emission wavelengths were, respectively: Hoechst = 351nm, 385 - 490nm; FITC, Alexa 488 and EGFP = 488nm, 505 - 550nm; Cy 3, Alexa 568 and Alexa 594 = 543nm, >560nm. Imaging of slides labelled with multiple dyes was always sequential, that is, the preparation was only illuminated with light of one wavelength at any one time. Transmitted light images were acquired on the same microscope using bright field illumination.

RESULTS

Quantitative RT-PCR was used to initially pan a range of possible ephrins and Eph receptors to define which family members were mostly likely to be important in spinal cord injury and hence warranted further investigation. Following selection of interesting genes (specifically the ephrinB2 ligand and the EphA4 receptor), *in situ* hybridisation and immunohistochemistry were employed to localise the expression of the corresponding proteins.

qRT-PCR for EphrinA1-5, EphrinB2-3 and EphA3-4,6-7

Primer Efficiency Calculations

Primer pairs were accepted for use in the qRT-PCR study only if their efficiency resided within the range of 1.8-2.05 and the linear regression coefficient for the dilution graph was $R^2 > 0.99$. The efficiency assays for all primer pairs used showed that the qRT-PCR assay is responsive to a range of PCR cDNA concentrations with a good regression fit potentially as low as 0.1pg/µl (for examples see Figure 2.1). Negative control assays using preparations without reverse transcriptase revealed no genomic signal or other background expression suggesting that DNase treatment of RNA preparations was successful and background PCR signal was not significant. Details of primer pairs used in this investigation are included in Figure 2.2.

Thermal Dissociation of qRT-PCR Products

Subsequent to each complete qRT-PCR, a thermal dissociation step was performed to assess the quality of DNA product produced. As shown in Figure 2.3, nearly all dissociation profiles for the qRT-PCR products showed a single, well-defined fluorescence change peak indicating a single DNA product with little or no background. Hence the primers used in this study appear specific for the cDNA sequence to which they are designed, the use of low-homology regions permitting differentiation between family members. Furthermore the dissociation profiles suggest there are no splice variants produced within these amplicon regions in the tissues of interest.

N.B. The thermal dissociation profile for ephrinA2 produces a double peak. This matter was not pursued further as ephrinA2 expression was seen to be negligible in control or injured tissue.

Matrix Metalloprotease-2 mRNA expression as a reporter for experimental confidence

RNA extraction from nervous tissue is often complicated by the presence of high lipid content. A lipid-specific RNA extraction kit (Qiagen RNeasy Lipid Tissue Extraction Kit) was used for all extractions. However, to ensure that the qRT-PCR technique was accurately reporting changes in gene expression, matrix metalloproteinase-2 (MMP-2) expression, an inflammation-associated protein that is known to be upregulated following some spinal injuries[400, 401], was examined. As shown in Figure 2.4A, the quantitative RT-PCR technique reported that expression of MMP-2 mRNA was significantly upregulated after crush injury, indicating that the technique is giving valid results. Hence, the changes in Eph and ephrin family member expression can be confidently interpreted as real and not an artefact due to complications with post-injury tissue.

EphA Receptor mRNA expression following Spinal Cord Injury

EphA3 and EphA7 show limited expression in control cord and there is little change in expression following either injury type. However, EphA4 and EphA6 show significant expression in control spinal cord and this is downregulated significantly following both injury types performed, the dual dorsal column

transection and controlled weight compression (Figure 2.4A). The degree of mRNA downregulation also appears to correlate with the extent and severity of the injury. Crush injuries reduce levels of EphA4 by ~90% and nearly abolish expression of EphA6.

EphrinA1-5 mRNA expression following Spinal Cord Injury

EphrinA expression following spinal cord injury has not been investigated to date. EphrinA4 was the only significantly expressed ligand subtype in the spinal cord tissue, either before or after injury (Figure 2.4B). In a similar manner to that seen in the EphA receptor data, the expression trend was negative with ephrinA4 expression reduced by around 95% following controlled compression injury. Unfortunately, the expression of ephrinA protein in adult rat or mouse spinal cord tissue has not been investigated to date so no comparison with the current literature can be performed.

EphrinB2 and B3 mRNA expression following Spinal Cord Injury

Of B class ephrins, only B2 and B3 have been reported to be expressed at significant levels in spinal cord[26, 236]. Quantitative RT-PCR indicated that the levels of ephrinB2 mRNA increased after spinal cord injury, consistent with previous findings (Figure 2.5, Bundesen *et al.*, 2003[26]). Upregulation of ephrinB3 following dorsal transection injury was not statistically significant. However, downregulation of ephrinB2 expression following crush injury was significant.

Immunohistochemistry and *In Situ* Hybridisation to Detect the EphA4 Receptor in Normal and Injured Spinal Cord

Immunocytochemical investigation of EphA4 expression following spinal cord injury

Horizontal sections of spinal cord from uninjured Sprague-Dawley rats revealed low levels of EphA4 expression (when compared to secondary antibody-only controls) in grey matter at all spinal levels and throughout the dorsal and ventral extent of the cord. Immunoreactivity was undetectable in white matter in these control animals (Figure 2.6A and B), or in lesioned axons remote from the lesion site (Figure 2.6C). However, strong EphA4

immunoreactivity was observed in dorsal and lateral white matter tracts just proximal to a transection injury 3-14 days following injury (Figures 2.6C, 2.6D and 2.7A). The anatomical location of the immunostaining was suggestive of a corticospinal expression. To confirm the identity of the EphA4 positive axons, a subpopulation of corticospinal tract axons was labelled by injection of biotinylated dextran amine into the motor cortex at the time of spinal cord lesion. Ten days later anterogradely transported BDA was seen to colocalise with EphA4 immunoreactivity in axon stumps and immediate intact axonal material (Figure 2.7B-D).

In addition to its appearance in CST axon terminations, EphA4 expression was present in blood vessels associated with GFAP-positive astrocytes (Figure 2.7E) as well as in GFAP-positive astrocytes in white and grey matter (Figure 2.8). Interestingly, a time course of EphA4 expression at 28 and 42 days following injury did not reveal EphA4 expression at or near the lesion site, although grey matter astrocytic staining was preserved.

Caudal to a spinal cord transection injury, punctate EphA4 immunostaining was observed in the central white matter (Figure 2.9A). OX-42 staining for macrophages and microglia did not reveal any colocalisation with EphA4 suggesting these are not invading immune system cells (Figure 2.9B-D). Bisbenzamide staining indicated the absence of a nucleus in these puncta and they appeared to be closely associated with astrocytic processes (Figure 2.9E). These puncta are therefore likely to be the swollen EphA4-filled remains of damaged CST axons or perhaps the termination bulbs of ascending dorsal column axons. The absence of any axonal EphA4 caudal to the lesion site would argue against the presence of EphA4 in ascending tracts, however.

In Situ Hybridisation for EphA4 mRNA expression in control and post-injury tissue

Localisation of EphA4 receptor protein to the injured CST suggests that either the protein is accumulating passively in the termination bulbs through continuing anterograde transport following injury, or the cell bodies of the CST

axons are actively upregulating expression of EphA4. To examine whether EphA4 transcription is increased in cortical pyramidal neurones following CST lesion in rats, *in situ* hybridisation was performed using a probe for EphA4 mRNA. Consistent with previous reports from the mouse[323], brains from uninjured animals showed EphA4 expression in layers II-VI of the hindlimb cortical region together with a particularly strong expression in the hippocampus (Figure 2.10). Seven days after a CST lesion, EphA4 mRNA expression in these regions was comparable to control (Figure 2.10C), consistent with previous findings that these neurons show little cell body response in the first 2 weeks following a remote axotomy[74]. Local axotomy, however, has been shown to induce an upregulation in EphA receptor expression in the hippocampus[385]. To investigate the expression of EphA4 following local neural damage, a stab wound was performed in the motor cortex and coronal sections through the cortex processed for EphA4 mRNA expression. Very local to the insult, EphA4 mRNA was clearly upregulated (Figure 2.11A). EphA4 mRNA was also detected in the CA1 and CA3 regions of the hippocampus (Figure 2.10) and the lining of the lateral and fourth ventricles (Figure 2.11B).

EphA4 mRNA in control spinal cord showed the expected pattern of staining indicative of astrocytic localisation (Figure 2.11C). White matter staining was weaker and more striated with EphA4-positive puncta aligned in small discrete groups. Grey matter staining was more intense and uniformly distributed in agreement with immunohistochemical staining of astrocytic EphA4. Around the lesion site, EphA4 mRNA staining is clearly visible in the white matter suggesting either an upregulation of EphA4 mRNA in surviving white matter astrocytes or the invasion of reactive EphA4-positive astrocytes from the grey matter (Figure 2.11D). Also of interest is the highly centralised staining of each astrocyte with close association of mRNA with the nucleus in each cell and little staining of processes.

Immunohistochemistry to detect the ephrinB2 ligand in normal and injured spinal cord

The qRT-PCR data indicated an upregulation of ephrinB2 mRNA in the lesion site (Figure 2.5). Previous studies have also reported this ephrinB2 upregulation at spinal cord lesions, particularly in reactive astrocytes at the glial scar margin[26]. The presence of ephrinB2 in the lesion site may present a further barrier to the regeneration of EphA4-positive CST axons following injury hence the probability of this interaction occurring at the astrocyte-axon interface was investigated. Remote from the lesion site, ephrinB2 immunoreactivity was relatively weak and was predominately in GFAP-positive grey matter astrocytes, with low levels of staining in white matter astrocytes (Figure 2.12). Consistent with existing reports, strong ephrinB2 immunoreactivity was observed in astrocytes of both grey matter and white matter at the lesion site (Figure 2.13). These astrocytes were observed to orient their processes perpendicular to the lesion margin (Figure 2.14). The effect of the continued expression of ephrinB2 in grey matter together with its upregulation in astrocytes at the lesion site is that EphA4-positive CST termination bulbs are completely surrounded by tissue expressing this inhibitory ligand (Figure 2.15). EphrinB2 immunoreactivity was also seen in small and medium dorsal root ganglion neurones and their unmyelinated processes (Figure 2.16), as previously reported[281].

EphA4 expression correlates with retraction after lesion

In the lateral white matter, axons of the lateral CST run alongside axons of the rubrospinal tract. The red nucleus, where the cell bodies of the rubrospinal axons are located, has no detectable expression of EphA4 in adult rodents[321, 323]. In order to compare the responses of neighbouring EphA4-expressing corticospinal axons and non-expressing rubrospinal axons to a spinal injury, a lentiviral vector encoding EGFP was injected into the red nucleus. Ten days later BDA was injected into the motor cortex to label corticospinal axons and a lateral column injury was performed. When the animals were killed, ten days following the spinal injury, EGFP-expressing neuronal perikarya were found only in the midbrain, indicating that there was no retrograde transfection of neurons by the viral vector via axons of passage (Figure 2.17A). In the

cervical spinal cord bright EGFP labelling of the rubrospinal axons was observed, without any EGFP labelling of dorsal CST axons (Figure 2.17B). Lentiviral delivery of EGFP therefore allowed complete separation of rubrospinal and corticospinal axons, unlike most conventional tracing techniques. This is clearly seen in coronal brain sections with separate zones of tracer expression and no colocalisation (Figure 2.17A). In the lateral white matter, BDA positive CST axons terminated well proximal to the lesion site, indicating that, as in the dorsal CST, they had retracted following the injury. In contrast the terminations of EGFP-positive RST axons were located closer to the lesion (Figure 2.18A). 63 CST axons in three cords terminated an average of 307±19μm (± SEM, standard error in the mean) from the boundary of the lesion, while in the same cords 209 RST axons terminated 103±7μm from the boundary (Figure 2.18B, $p<0.0001$, t test).

DISCUSSION

EphA Receptor qRT-PCR

The data indicates that expression of both A-class Eph receptors and ephrins is reduced in the tissue around a lesion site. Most, if not all, axonal EphA receptor mRNA will be located in the cell body some distance from the lesion site. Hence, the reduction in EphA mRNA expression around a spinal cord injury seen in the qRT-PCR study does not detract from the hypothesis that neuronal EphA receptors may play an important role in preventing axonal regeneration. However, the downregulation observed does imply that EphA receptors are not significantly expressed in surviving or invading cells local to the lesion. In apparent disagreement with this finding, published data suggests that EphA4 upregulation in astrocytes may contribute to their reactive behaviour following injury and to the formation of the glial scar[12]. One means to resolve the data presented here with the existing literature would be to consider the extensive loss of astrocytes following spinal cord injury. Uninjured grey matter tissue appears to express moderate amounts of EphA4 (see Figure 2.6) and this may be localised to astrocytes (Figure 2.8 and Willson *et al.*[318]). In contrast EphA4 appears in white matter astrocytes in a highly localised region at the lesion site itself. Hence, following an injury, the overall level of EphA4 expression (as seen in the qRT-PCR data) may fall due

to astrocytic loss, but the remaining astrocytic upregulation of EphA4 results in a positive result in published immunohistochemistry and *in situ* hybridisation studies presented here. This hypothesis is supported by Bundensen *et al.*[26] who note a similar downregulation in expression of ephrinB2 and EphB2 in injured spinal cord following an injury, despite increases in expression at later time points.

Data from Willson *et al.* indicates a two-fold or greater upregulation in EphA3, 4 and 7 receptors seven days following spinal cord injury[318]. This is in disagreement with the qRT-PCR data presented here regarding EphA receptor expression. There are some differences in experimental technique regarding the comparable data sets – i.e. spinal cord crush injury. Willson *et al.* make use of the New York University (NYU) Impactor injury to perform a 12.5mm 10gram weight drop whereas we used a controlled (non-impact) 50gram weight application to perform our crush injuries. It is likely that the NYU Impactor injury will induce a different type and location of injury to our controlled crush approach – an impact would be expected to induce more cavitation and possibly an injury close to the central canal whereas a controlled crush might induce the injury epicentre closer to the site of weight contact and produce less cavitation. Another possible cause of differences stems from the quantification used in the two studies. Whereas Willson *et al.* have used a semi-quantified approach looking at the intensity of PCR bands, we have used β-actin expression-normalised RT-PCR quantification based on fluorescence of the DNA-reporter SYBR Green. Such a deleterious tissue treatment as spinal cord injury could easily cause complications in expression quantification without some form of normalisation, due to tissue death and other confounding factors. These complex pathological changes include the invasion of meningeal fibroblasts and immune system cells, hypertrophy and death of astrocytes and for formation of a new glial limitans. Importantly, our data regarding ephrinB2 and MMP-2 expression agrees with that expressed in the literature[26, 400]. Identical cDNA preparations and qRT-PCR techniques were used in all gene expression studies, hence the data presented here is well founded. Nevertheless, work from another laboratory to confirm these findings would provide good grounding for future expression studies.

EphrinA qRT-PCR

Published data suggests a developmental expression of ephrinA4 in the hippocampus and cortex[402] but this is thought to disappear in the adult. However, as Figure 2.4B shows, ephrinA4 expression appears to be retained in the adult rat spinal cord. The severe downregulation in mRNA expression seen in Figure 2.4B implies there is no active upregulation in expression in surviving neural tissue subsequent to injury suggesting that ephrinA4 is unlikely to be significant in the post-injury environment. Without further data on adult expression and ligand localisation it is hard to postulate a possible role for ephrinA4 in the adult, however the fact that expression diminishes following both injury types suggests it is not expressed on an invading cell line such as meningeal fibroblasts or immune cells. Most likely it is expressed on astrocytes (where co-expression with ephrinB2 and EphA4 would open up a whole range of regulatory *cis*-interactions), oligodendrocytes or dorsal horn neurones, all of which suffer extensive cell death following injury. Further investigation of this ligand is warranted as it may play a role in constraining plasticity in the normal spinal cord. Ephrin signalling has also been shown to be supportive or trophic in nature in some cases[353], hence downregulation in the expression of some ephrins and Eph receptors may diminish the trophic support available to surviving tissue following injury. Neurotrophic deficiency following injury is a major factor in the lack of regeneration and approaches to replenish this growth support should consider trophic factors such as ephrins that may not act through the standard p75 receptor mediated signalling pathway.

EphrinB qRT-PCR

Both ephrinB2 and ephrinB3 have been implicated as major contact-repellent agents in the injured spinal cord environment. Our qRT-PCR analysis of ephrinB ligand expression in rat spinal cord demonstrated significant expression of ephrinB2 and ephrinB3 in control tissue, in agreement with published work[26, 236]. Furthermore, the qRT-PCR data indicates that ephrinB2 is upregulated following injury in agreement with the Western blot experiments of Bundensen *et al.*[26]. As ephrinB2 expression appears to be upregulated in

reactive astrocytes, ephrinB2 mRNA expression would be expected to be highest in tissues undergoing a crush injury where the degree of inflammation and astrocytic gliosis was greatest. However, as outlined above and in agreement with the data of Bundensen *et al.*[26], cell death following the more deleterious crush injury will mask a large extent of the increase in ephrinB2 expression. This is the likely cause of the smaller ephrinB2 mRNA expression upregulation seen seven days following crush injuries compared to dual dorsal hemisection injuries.

Immunohistochemistry and *in situ* hybridisation for EphA4 expression following spinal cord injury

EphA4 protein is not detectable in uninjured corticospinal tract axons, even though EphA4 transcription is proceeding in the cell body (Figures 2.6A-B and 2.10A). In contrast, EphA4 protein accumulates at the cut ends of corticospinal tract axons after injury, with distinct axonal 'tails' tracking rostrally from termination bulbs. The most likely explanation for these data is that uninjured pyramidal neurones of the motor cortex synthesize EphA4 and transport it down the axon to their presynaptic terminals, where it may play a role in synaptic plasticity[345]. In this model, although EphA4 is present in uninjured axons, the concentration is too low for immunological detection. Axotomy does not increase the rate of EphA4 synthesis as no increase in *in situ* hybridisation signal is apparent after injury, but as transport out of the cell body and down the axon continues the protein accumulates at the severed axon stump. In the non-pathological situation, EphA4 may act at CST termini to prevent axonal sprouting in the developed animal. At the injury site, however, the presence of high levels of EphA4 at the sites of potential neurite regeneration in the spinal cord is likely to be strongly inhibitory to any regenerative activity.

Expression of EphA4 in, and proximal to, termination bulbs of the CST is strong three days following injury and does not appear to strengthen over the subsequent 11 days. This is not surprising, as previous studies[403, 404] using transfected cell lines *in vitro* have shown that rapid uptake of ligand-receptor complexes occurs into both ligand- and receptor-expressing cells. This

process not only attenuates signalling to downstream processes (although some is likely to persist inside the endocytotic cell) but will also lead to rapid protein turnover – hence preventing excessive build-up of EphA4 at CST termination bulbs. However, at 4 and 6 weeks following injury, EphA4 expression disappeared from the dorsal or lateral white matter but is retained in the grey matter. While proximal injuries appear to induce a robust change in EphA expression in the cortex[385] (also see Figure 2.11A), cortical neuron responses to distal injury are generally negligible[74]. Death of cortical neurons may explain this change in expression, or perhaps a long-term decline in overall transcription as the axotomised neurons atrophy.

The recent discovery of ephrinB3 in myelin and evidence for its strong growth-inhibitory properties *in vitro*[331] suggests that the interaction between myelin ephrinB3 and CST EphA4 may also prove significant in the post-injury response. While the interaction with astrocytic ephrinB2 may diminish as the lesion scar becomes more stable and the majority of the CST fibers die back from the lesion site, the interaction with ephrinB3 will be maintained as damaged myelin will be present throughout the vicinity of the injury. EphrinB3 may prove to be the ligand which prevents regenerative sprouting of the CST from its final, retracted, position.

In addition to the axonal and astrocytic EphA4 discussed above, punctate EphA4 immunostaining caudal to the lesion site in the central white matter was also noted (Figures 2.6C and 2.9A). This did not colocalise with OX-42 staining (Figure 2.9B-D) arguing against a role for EphA4 in activated macrophages and microglia invading the lesion site. This was confirmed by the apparent absence of genetic material within the puncta following bisbenzamide staining (Figure 2.9E). GFAP staining suggested a close association with reactive astrocytic processes suggesting these strongly EphA4-positive puncta are likely to be the swollen remains of damaged CST axons undergoing Wallerian degeneration. As noted previously, the absence of any axonal EphA4 caudal to the lesion site would argue against the presence of EphA4 in ascending tracts.

The *in situ* hybridisation staining for EphA4 revealed astrocytic staining in the spinal cord in agreement with the immunohistochemical data (Figures 2.11C and 2.8). EphA4 staining in the lesion site is significantly stronger than that found in control white matter and injured white matter some distance from the lesion. However, mRNA expression of EphA4 in cells in the lesion site was not visibly higher than control or injured grey matter expression suggesting that either:

- Reactive grey matter astrocytes invading the lesion site do not increase their expression of EphA4 significantly.
- Reactive surviving white matter astrocytes near the lesion site greatly upregulate their EphA4 expression.

Both of these phenomena may occur but differentiating between them – and hence elucidating the source of EphA4-positive astrocytes in the lesion site – is difficult. When one considers the loss of white matter astrocytes subsequent to a lesion centred on the white matter, the most likely source of invading astrocytes would be from the grey matter. Hence, local upregulation of EphA4 mRNA is unlikely to be extensive. This conclusion is in agreement with the qRT-PCR data that suggests that, overall, the expression of EphA4 mRNA decreases following injury.

Immunohistochemistry for EphrinB2 expression following Spinal Cord Injury

The upregulation of ephrinB2 in reactive astrocytes (Figures 2.5 and 2.13) is proposed to interact with EphB2 expressed on invading meningeal fibroblasts following spinal cord injury[26]. In this context it is likely to play a role in the formation of the new glial limitans, limiting the invasion of meningeal fibroblasts into surviving tissue, and permitting the reformation of a stable CNS environment. However, an unexpected side-effect of this physiological mechanism is the possible interaction between astrocytic ephrinB2 and CST-based EphA4. EphA4 binds with high affinity to ephrinB2 and transduces a repulsive signal to the growth cone of any developing CST axon[235, 236, 405]. Hence, a similar response is likely in the context of spinal cord injury. As shown in Figure 2.12B, ephrinB2 expression is strong in the uninjured grey

matter surrounding the lesion site, preventing any regenerative sprouting into spared grey matter. It is also strongly expressed in reactive astrocytes (either from surviving white matter or invading grey matter) around the lesion centre. In this location there is an unavoidable interaction between astrocytic ephrinB2 and EphA4 strongly expressed in CST termination bulbs (Figure 2.15). The time-course of ephrinB2 expression[26] and CST retraction[38] are also closely interlinked with the period of greatest CST retraction occurring between 5 and 14 days after injury and rapid upregulation of ephrinB2 expression between 3 and 10 days after injury. This interaction is therefore likely to be a major contributor to the increased retraction seen in the CST response to injury when compared to other axonal tracts.

One question raised by the presence of ephrinB2 and EphA4 on reactive astrocytes is whether any form of *cis*-interaction occurs. Binding of ephrin ligands and receptors in *cis* has been documented[278] and, while it appears to not mediate any intracellular signalling, does interfere with *trans*-activation of the receptor (and mostly likely the ligand also). However, while astrocytic EphA4 is most likely to be important in the one to three day period post-injury when cytokine release from invading immune cells appears to induce astrogliosis via a mechanism involving EphA4[12], ephrinB2 expression is upregulated between the three and seven day period when it interacts with fibroblastic EphB2. Hence these two proteins are unlikely to be strongly co-expressed during their period of critical signalling and hence *cis*-interactions are unlikely to prove significant.

Comparing Corticospinal and Rubrospinal Tract responses to Lateral Column Injury

Evaluating the role of any single protein in a process as complex as spinal cord injury is difficult. Fortunately, the rubrospinal tract does not express EphA4[321, 323] and, to date, has not been found to be developmentally regulated by ephrin signalling of any kind. In all other respects the two descending motor tracts should respond to lesion in an identical manner. The lateral CST (LCST) and the RST also run in close proximity within the lateral white matter, often with interspersed fibers (Figure 2.17B) hence they can be

transected by a single injury with confidence that they will experience very similar post-lesion conditions. Hence a direct comparison of the post-injury response of the LCST and the RST should identify the role of EphA4 expressed on LCST termination bulbs (Figure 2.7A). As shown in Figure 2.18, transected lateral CST axons terminated with intensely BDA-positive termination bulbs on average ~200μm more rostral than their EGFP-stained RST counterparts. No other differences in gene expression or post-injury response published to date explain this difference in behaviour following lateral white matter injury. Hence, the likely cause is the presence of growth-inhibitory EphA4 present on CST axons that interacts with astrocytic ephrinB2 and myelin-based ephrinB3

CONCLUSION

An increasingly common theme in spinal cord injury is the emergence of developmental guidance proteins as major regulators of the spinal cord response to injury. EphA4, the critical regulator of repulsive developmental guidance of the CST down the spinal cord around embryonic day 17[234-236, 319], appears to be yet another member of this growing group of proteins. Manipulation of the environment within the injured spinal cord to allow useful recovery in humans is likely to require a combinatorial approach to overcome a number of different inhibitory cues. Indeed, even within the field of operation of ephrins and Eph receptors at spinal cord lesions, more complex interactions, such as a backwards signalling in which Ephs evoke effects upon ephrin expressing cells, may play a role[12]. Nevertheless, our results suggest that blockade or modification of ephrin:Eph receptor interactions may be a useful component of a successful treatment strategy.

Figure 2.M1

Sample qRT-PCR readout showing C_t analysis

Fluorescence from each well is plotted against the PCR cycle number. A threshold is defined that intersects all fluorescence traces in the linear phase. The corresponding PCR cycle number (termed C_t) is taken as a quantitative representation of the cycles required for that PCR to reach the threshold. Therefore a high C_t value implies more cycles were required to reach the expression threshold and hence the initial cDNA (and therefore by implication the mRNA and tissue) contained low levels of the gene of interest.

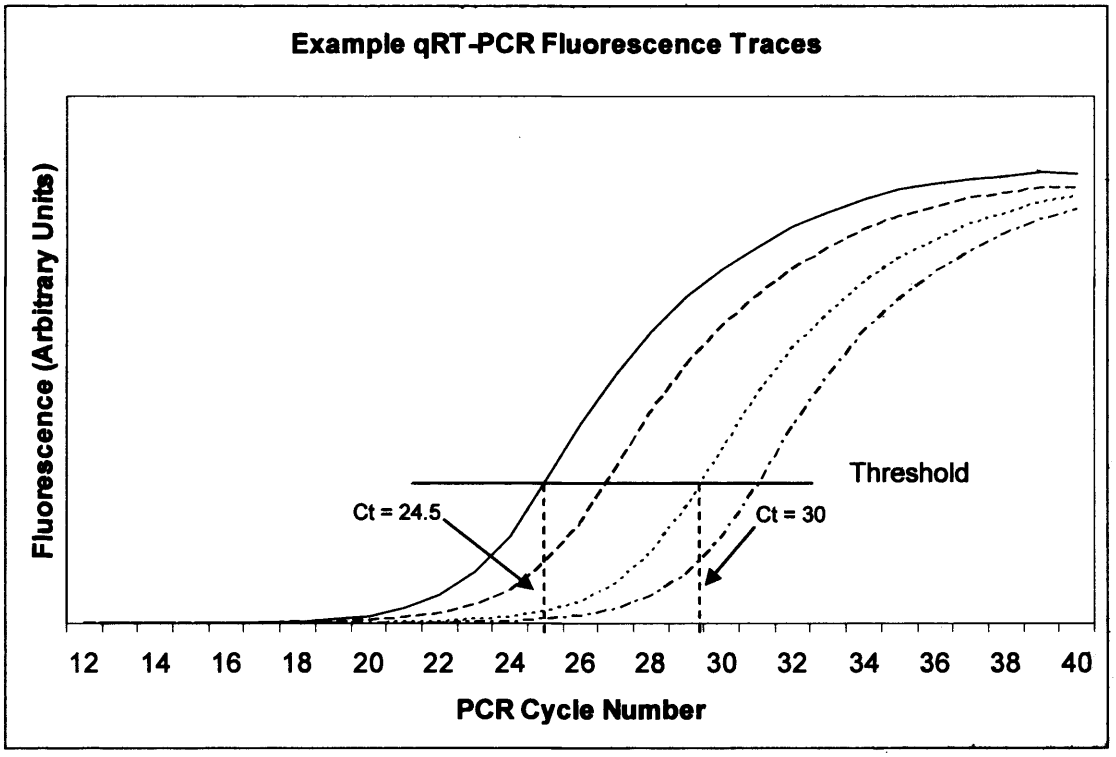
Example qRT-PCR Fluorescence Traces
Fluorescence (Arbitrary Units)
Threshold
Ct = 24.5
Ct = 30
12 14 16 18 20 22 24 26 28 30 32 34 36 38 40
PCR Cycle Number

Figure 2.M2

Multiple Sequence Alignment of investigated EphA receptors

Alignment of EphA receptor sequences used for qRT-PCR amplification demonstrating the use of primers in DNA regions that demonstrate less conservation. In this Multiple Sequence Alignment red characters indicate exact homology between all aligned sequences, blue show partially homologous areas and black characters represent those bases with no homology between aligned gene family members. Dashed regions show that insertions and deletions during evolution of the gene family have led to regions that do not correspond between family members.


EphA3 ATGGATTGTCA---------CCTCTCCATCCTCATCCTGTTCGGCTGCTGCGTCCTCAGCTGCTCCAGGGAACTGAGTCCACAGCCTTCCAACGAAG
EphA7 ATGGTTGTTCAAACTCGGTACCCTTCGTGGATTATTTTGTGTTACATCTGGCTGCTTGGCTTTGCACACACGGGGGAGGCGCAGGCTGCGAAGGAAG
EphA4 ATGGCTGGGATT------TTCTATTTCATCCTCTTTTCGTTTCTCTTTGGAATTTGCGACGCTGTCACCGGTTCTAGGGTATACCCGGCGAATGAAG
EphA6 ATGGGGGGCTGCGAAGTCCGGGAATTTCTTTTGCAATTTGGTTTCTTCTTGCCCCTGCTGACAGCTTGGACCGGCGACTGCAGTCACGTCTCCAACCAAG
TTAATCTACTAGATTCAAAAACGATTCAAGGAGAGCTGGGCTGGATCTCCTACCCATCCCACGG---GTGGGAAGAGATCAGTGGTGTTGATGAGCATTACACACCAATCAG
TACTGTTACTGGACTCGAAAGCACAACAAACAGAATTGGAATGGATTTCCTCTCCACCCAGTGG---GTGGGAAGAAATTAGTGGTTTGGATGAGAACTACACACCAATAAG
TTACTTTATTGGATTCCAGATCTGTTCAGGGAGAGCTTGGGTGGATAGCAAGCCCTCTGGAAGGAGGGTGGGAGGAAGTAAGCATTATGGATGAGAAAATACACCGATCCG
TTGTGTTGCTTGATACAACTACAGTGATGGGAGAACTAGGATGGAAAACATATCCACTGAATGG---GTGGGATGCCATTACTGAAATGGATGAACACAACAGGCCCATACA
GACTTACCAGGTATGCAATGTCATGGATCACAGCCAAAATAATTGGCTGAGGACAAACTGGGTGCCGAGAAACTCAGCTCAGAAGATC
AACATACCAGGTGTGCCAGGTCATGGAGCCCAACCAGAACAACTGGCTTCGGACTAACTGGATTTCTAAAGGCAACGCACAAGGATT
AGACTTACCAGGTATGCAATGTCATGGATCACAGCCAAAATAATTGGCTGAGGACAAACTGGGTGCCGAGAAACTCAGCTCAGAAGATC
TACATACCAGGTATGCAATGTCATGGAACCAAACCAGAACAACTGGCTTCGTACTAACTGGATCTCTCGTGATGCTGCTCAGAAAATC
5′ Primer
3′ Primer

Figure 2.M3

Multiple Sequence Alignment of investigated ephrinA proteins

Alignment of ephrinA sequences used for qRT-PCR demonstrating the use of primers in DNA regions that demonstrate less conservation. In this Multiple Sequence Alignment red characters indicate exact homology between all aligned sequences, blue show partially homologous areas and black characters represent those bases with no homology between aligned gene family members. Dashed regions show that insertions and deletions during evolution of the gene family have led to regions that do not correspond between family members.

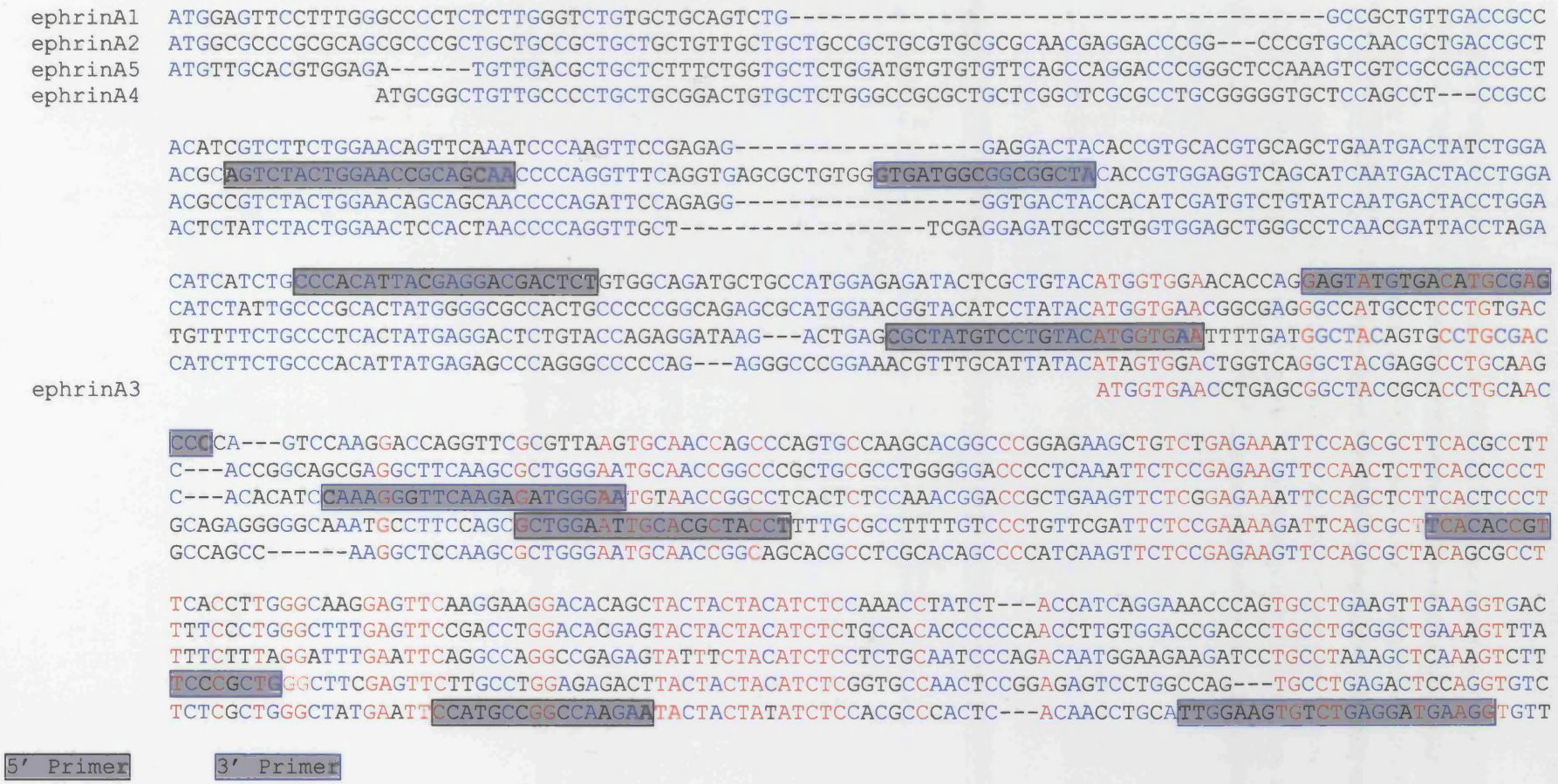
ephrinA1
ephrinA2
ephrinA5
ephrinA4
ephrinA3
5′ Primer
3′ Primer

Figure 2.M4

Multiple Sequence Alignment of investigated ephrinB proteins

Alignment of ephrinB sequences used for qRT-PCR demonstrating the use of primers in DNA regions that demonstrate less conservation. In this Multiple Sequence Alignment red characters indicate exact homology between all aligned sequences, blue show partially homologous areas and black characters represent those bases with no homology between aligned gene family members. Dashed regions show that insertions and deletions during evolution of the gene family have led to regions that do not correspond between family members.

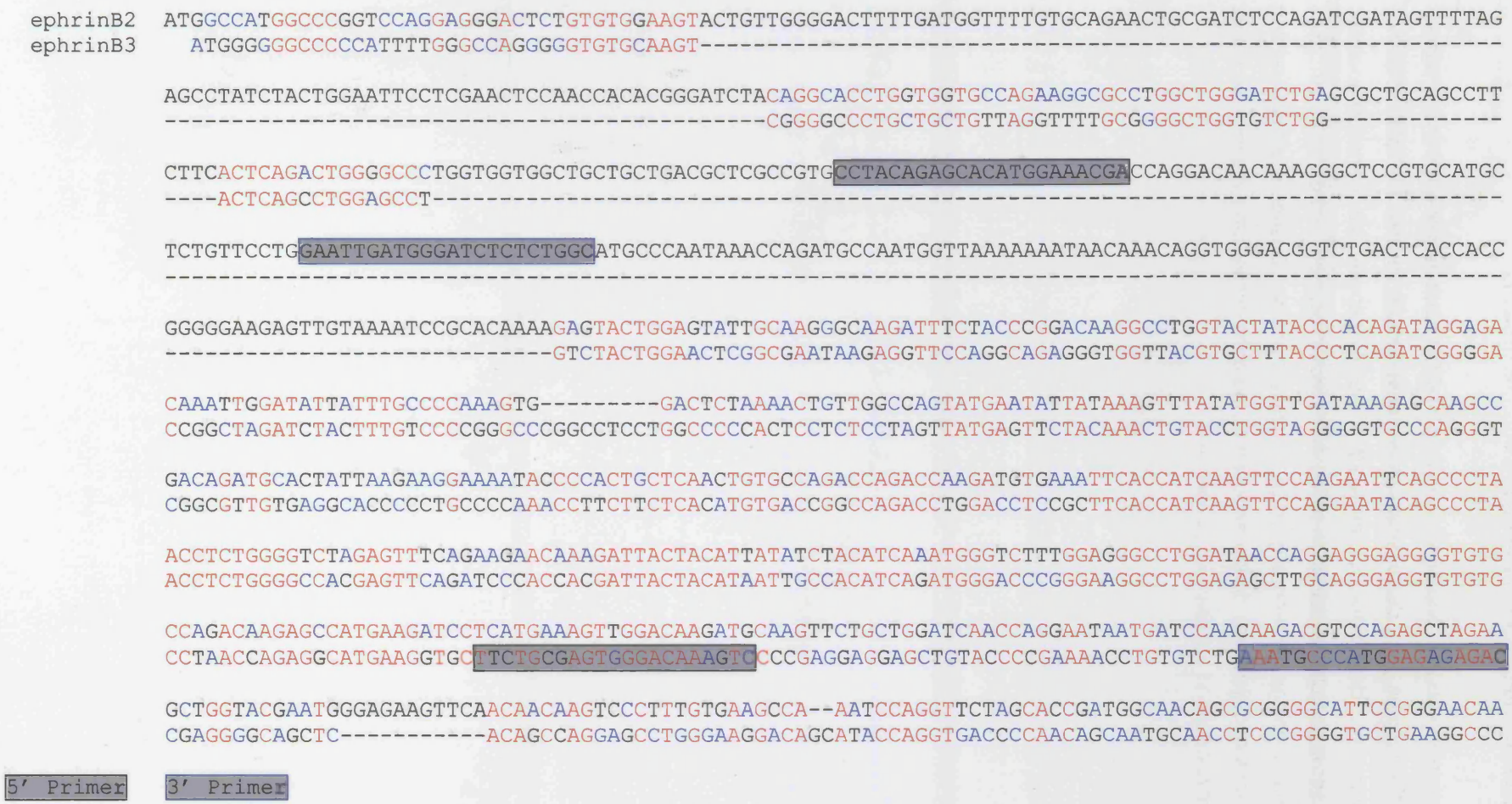
ephrinB2
ephrinB3
5′ Primer
3′ Primer

Figure 2.1

Example primer efficiency plots

Typical serial dilution graphs for primer efficiency calculations (EphA4 and EphA6 receptors shown). C_t values for the EphA4 and EphA6 receptors in serially diluted hippocampal cDNA plotted against the log (base 10) of the relative cDNA concentration. Starting cDNA concentrations were approximately 0.2ng/µl and good data was obtained from dilutions of 0.1pg/µl. As shown, regression analysis of the best-fit lines was good, indicating a good assay sensitivity for a range of cDNA concentrations.

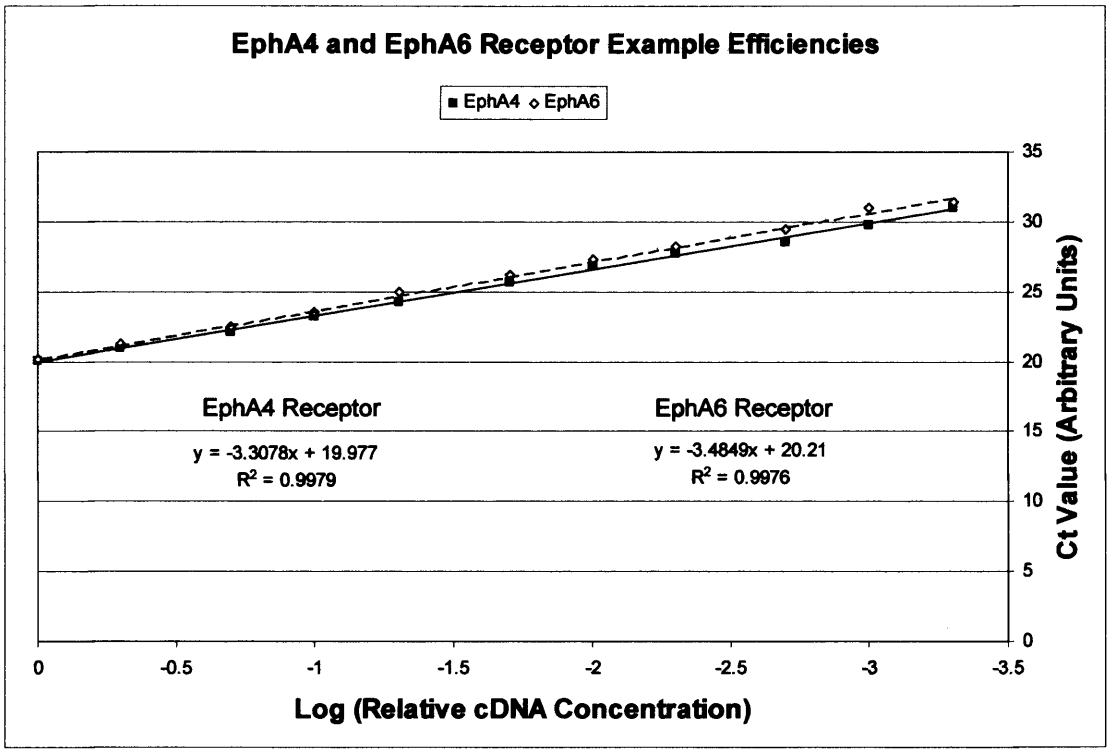
EphA4 and EphA6 Receptor Example Efficiencies
EphA4
EphA6
35
30
25
20
15
10
5
0
Ct Value (Arbitrary Units)
EphA4 Receptor
y = -3.3078x + 19.977
R2 = 0.9979
EphA6 Receptor
y = -3.4849x + 20.21
R2 = 0.9976
0
-0.5
-1
-1.5
-2
-2.5
-3
-3.5
Log (Relative cDNA Concentration)

Figure 2.2

Table of primers used in the qRT-PCR study

Primers were designed using the Primer Express Software (Ambion) due to the stringent conditions required for the LightCycler qRT-PCR machine. Primer annealing temperatures (T_m) were designed to be as close to the optimum of 59°C as possible and amplicons were maintained in the 60-120bp range to facilitate reliable and rapid replication.

Figure 2.3

Thermal dissociation graphs for qRT-PCR products

A-C. Plot of the thermal dissociation curve analysis for EphA (A), ephrinA (B) and ephrinB (C) qRT-PCR products. All but one RT-PCR product yielded a single fluorescence change peak indicating a highly specific PCR with minimal background signal. Control PCR dissociation profiles using control cDNA preparations where no reverse transcriptase was included yielded no DNA product, as shown, indicating the absence of genomic, or other, contamination.

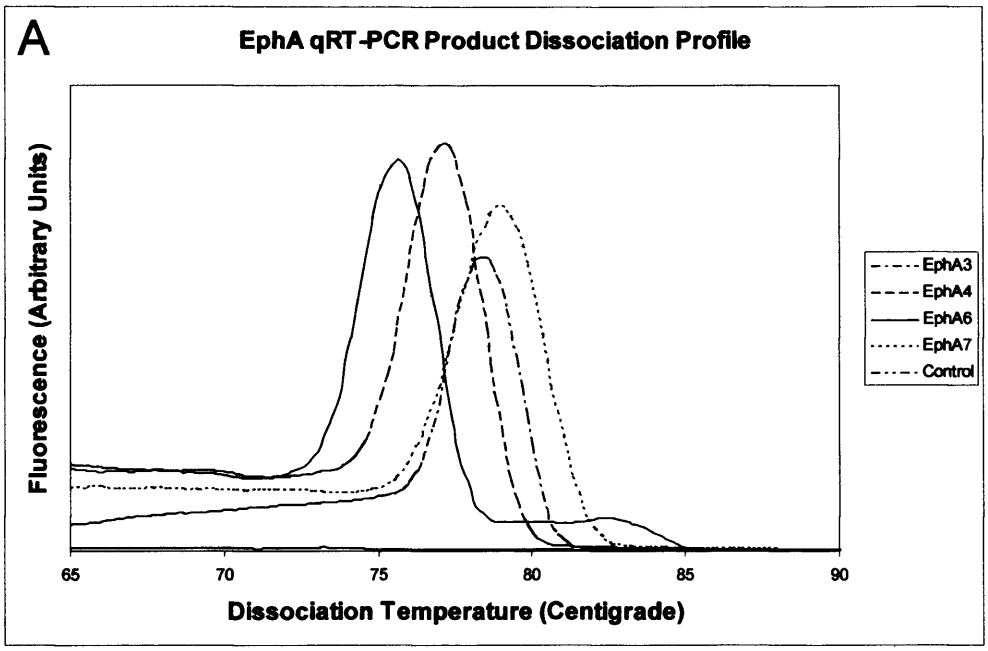
A
EphA qRT-PCR Product Dissociation Profile
Fluorescence (Arbitrary Units)
65
70
75
80
85
90
Dissociation Temperature (Centigrade)
EphA3
EphA4
EphA6
EphA7
Control

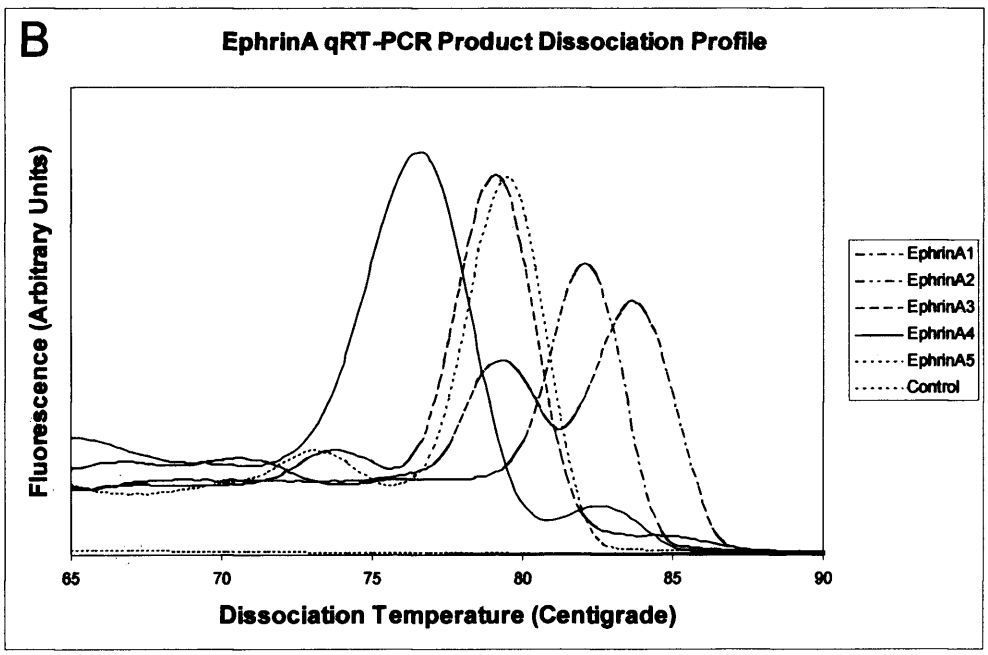
B
EphrinA qRT-PCR Product Dissociation Profile
Fluorescence (Arbitrary Units)
65
70
75
80
85
90
Dissociation Temperature (Centigrade)
EphrinA1
EphrinA2
EphrinA3
EphrinA4
EphrinA5
Control

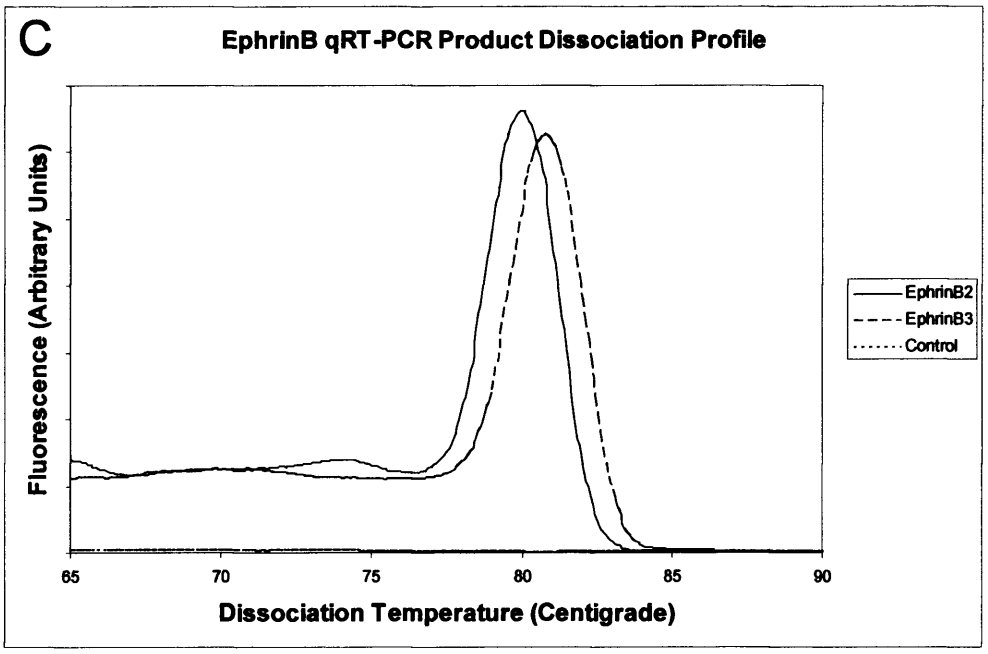
C
EphrinB qRT-PCR Product Dissociation Profile
Fluorescence (Arbitrary Units)
65
70
75
80
85
90
Dissociation Temperature (Centigrade)
EphrinB2
EphrinB3
Control

Figure 2.4

Relative EphA and ephrinA mRNA expression from qRT-PCR data

A-B. EphA receptor (A), ephrinA ligand (B) and Matrix Metalloprotease-2 (A) mRNA expression in spinal cord 7 days following control laminectomy, dual dorsal hemisection or controlled weight crush injuries. Mean ± SEM, n = 4 for each data set. * $p < 0.05$; unpaired *t*-test.

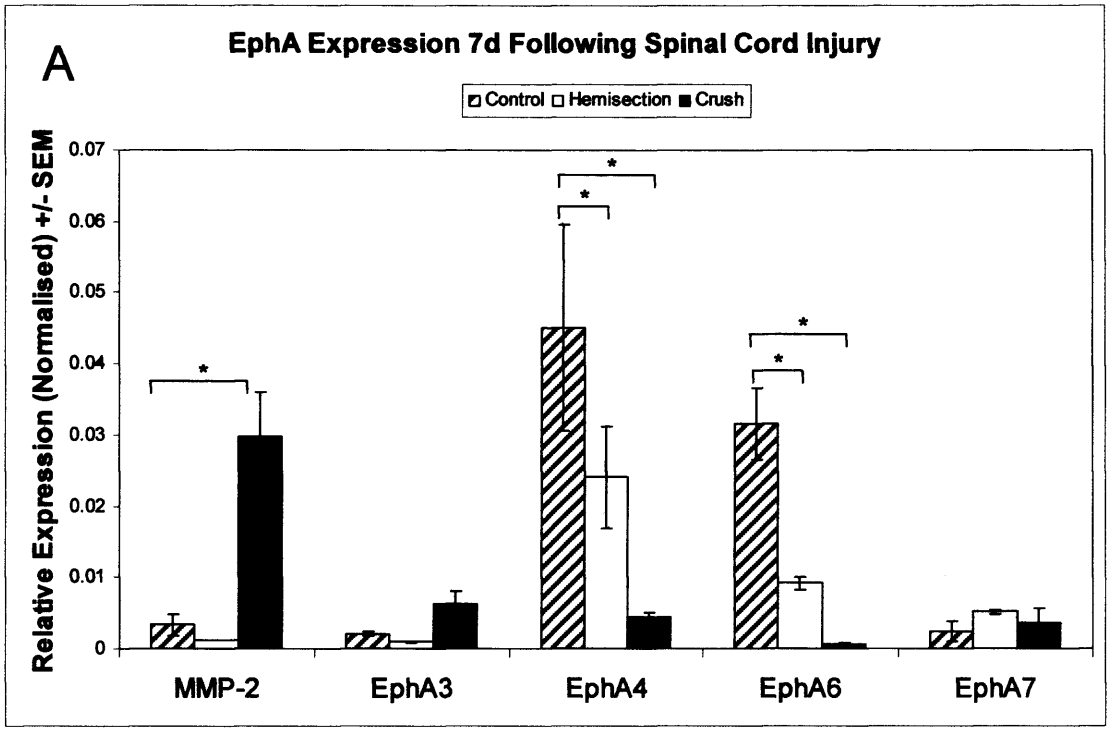
A
EphA Expression 7d Following Spinal Cord Injury
Control Hemisection Crush
Relative Expression (Normalised) +/- SEM
0.07
0.06
0.05
0.04
0.03
0.02
0.01
0
MMP-2
EphA3
EphA4
EphA6
EphA7

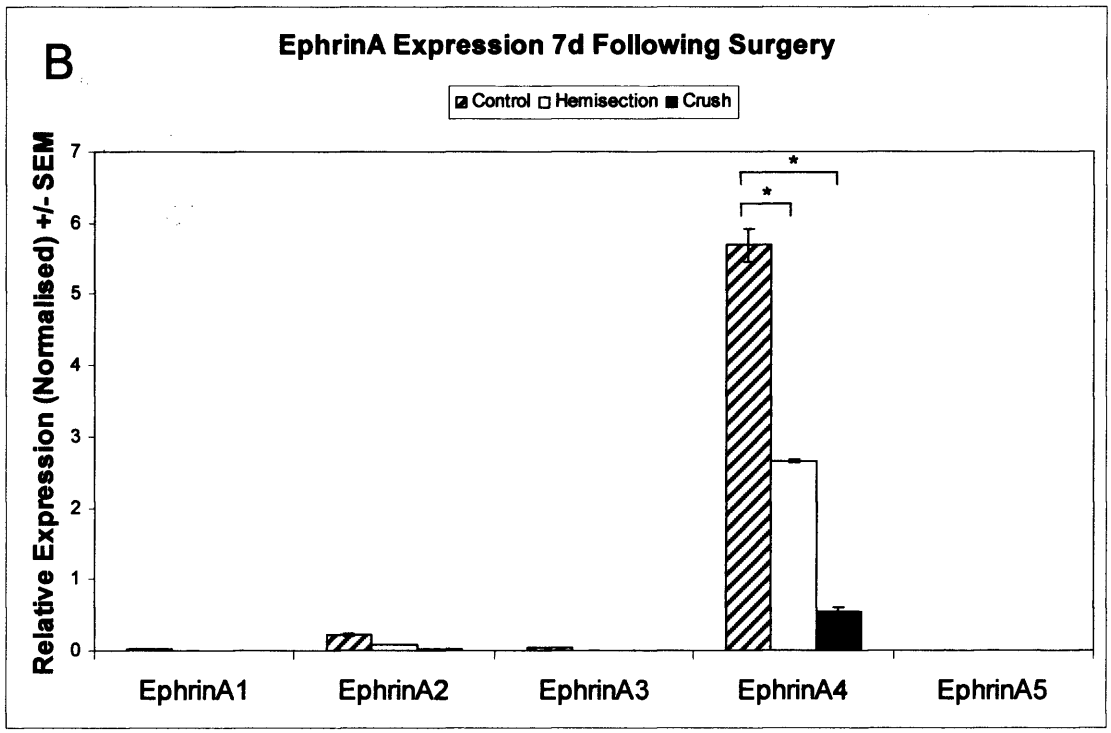
B
EphrinA Expression 7d Following Surgery
Control Hemisection Crush
Relative Expression (Normalised) +/- SEM
7
6
5
4
3
2
1
0
EphrinA1
EphrinA2
EphrinA3
EphrinA4
EphrinA5

Figure 2.5

Relative ephrinB mRNA expression from qRT-PCR data

EphrinB mRNA expression in adult rat spinal cord 7 days following control laminectomy, dual dorsal hemisection or controlled weight injuries. Mean ± SEM, n = 4 for each data set. * $p < 0.05$, ** $p < 0.001$; unpaired *t*-test.

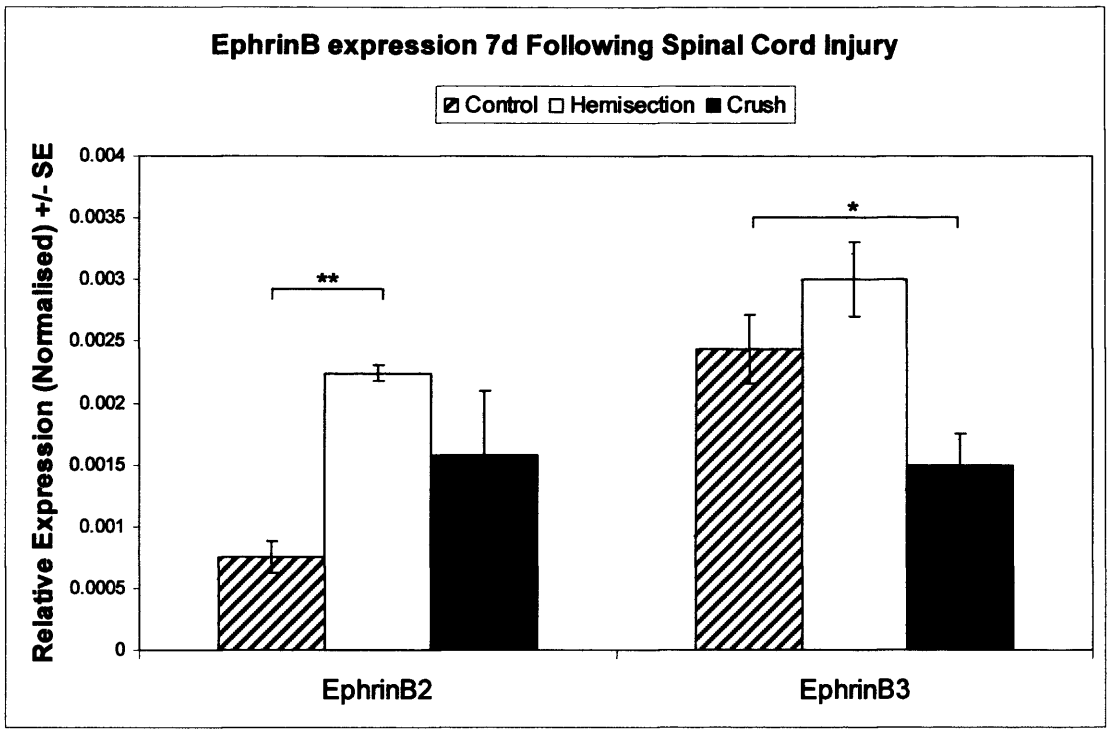
EphrinB expression 7d Following Spinal Cord Injury
Control
Hemisection
Crush
Relative Expression (Normalised) +/- SE
0.004
0.0035
0.003
0.0025
0.002
0.0015
0.001
0.0005
0
**
*
EphrinB2
EphrinB3

Figure 2.6

Immunohistochemical localisation of EphA4 receptor expression

A. EphA4 staining of control, uninjured adult Sprague-Dawley rat spinal cord tissue. Horizontal section taken through the dorsal corticospinal tract (*) showing no EphA4 expression with EphA4-positive dorsal horn grey matter (#) on either side. Scale bar 150μm.

B. EphA4 staining (green) of control, uninjured adult Sprague-Dawley rat spinal cord tissue. Horizontal section taken though the dorsal CST (*) with EphA4-positive dorsal horn grey matter visible (#). BDA labelling of the CST with streptavidin-Alexa^{568} processing (red) indicates that the CST in this region of cord is EphA4-negative. Scale bar 150μm.

C. Horizontal section through the dorsal corticospinal tract showing EphA4 staining. The lesion centre is highlighted by the dotted line and the retraction of the EphA4-positive CST (arrow) is clearly visible. White matter rostral and caudal to the lesion site is EphA4-negative (*) unlike the grey matter which shows minimal change in EphA4 expression proximal or distal to the injury (#). Punctate EphA4 expression is also visible caudal to the lesion site (triangle). Negative control immunohistochemistry using an identical protocol but excluding the primary antibody shows only normal tissue autofluorescence (square indentation). Scale bar 500μm.

D. Higher magnification image of Figure 2.8C highlighting the axonal appearance of the EphA4 staining (arrows) with the EphA4-dense termination bulbs closer to the lesion (triangles). Scale bar 150μm.

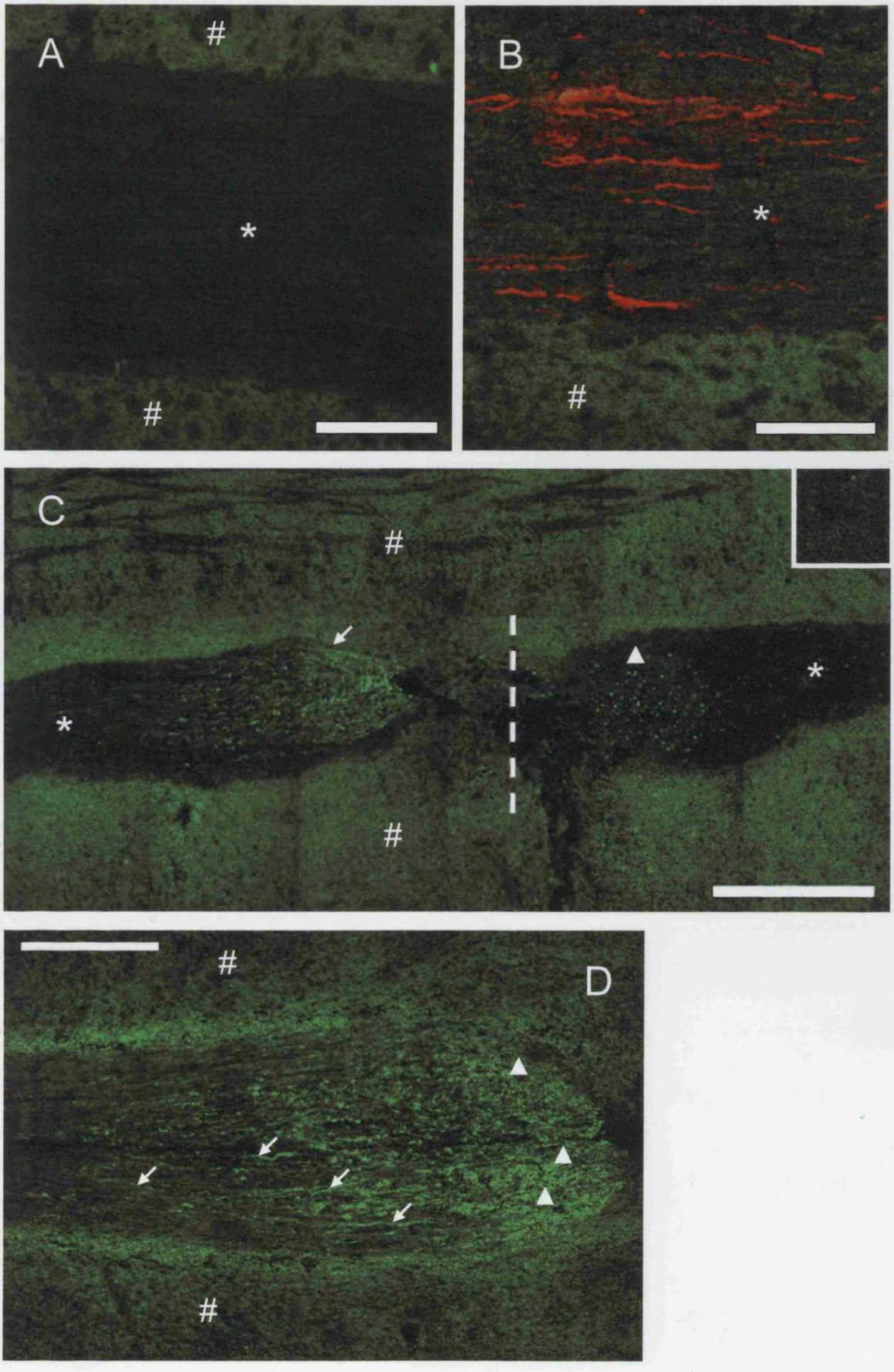
A
#
*
#
B
*
#
C
#
*
*
#
D
#
#

Figure 2.7

Immunohistochemical localisation of EphA4 receptor expression

A. Lesioned lateral white matter axons expressing EphA4. Horizontal 14µm fresh frozen section taken through the lateral corticospinal tract seven days following dorsal hemisection. Lateral corticospinal tract fibres with strong EphA4 expression are sparse but this axon demonstrates a clear EphA4-poisitive process with obvious termination bulbs at the end of abortive sprouts (arrows). Scale bar 50µm.

B-D. EphA4 receptor expression (A) colocalises with BDA labelling of the CST (C). Horizontal 14µm fresh frozen section taken through the dorsal corticospinal tract. To preserve the EphA4 antigen only a brief fixation was performed hence BDA labelling appears diffuse. Hence, some diffusion of BDA from the CST fibres occurs. However, it is apparent that EphA4 appears to be predominately located in the main part of the lesioned CST, rather than the smaller off-shoots and processes (arrows). Scale bars 50µm.

E. Fresh frozen 14µm section through the dorsal grey matter showing EphA4-positive blood vessels (green) associated with GFAP-positive astrocytes (red). Scale bar 50µm.

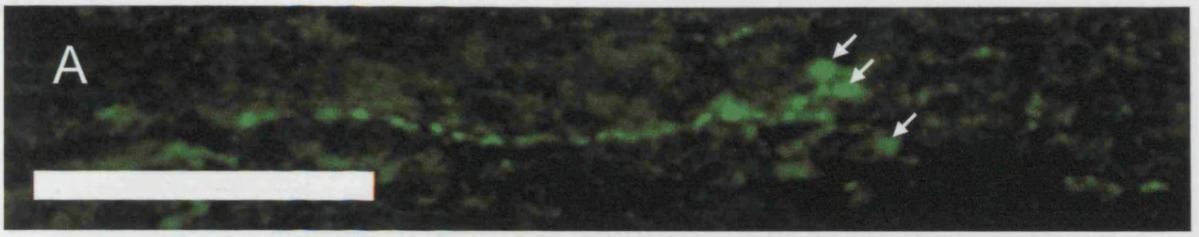
A

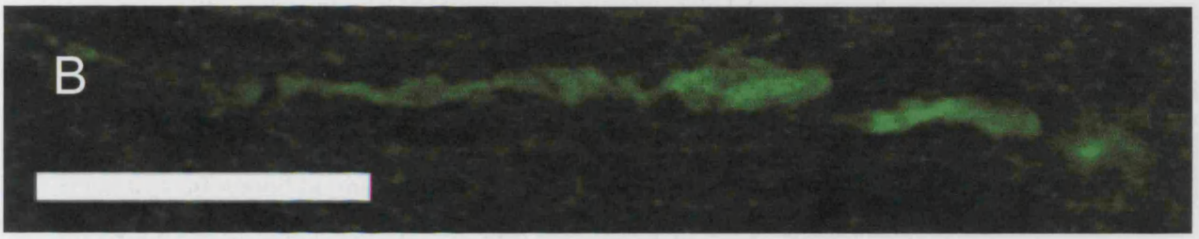
B

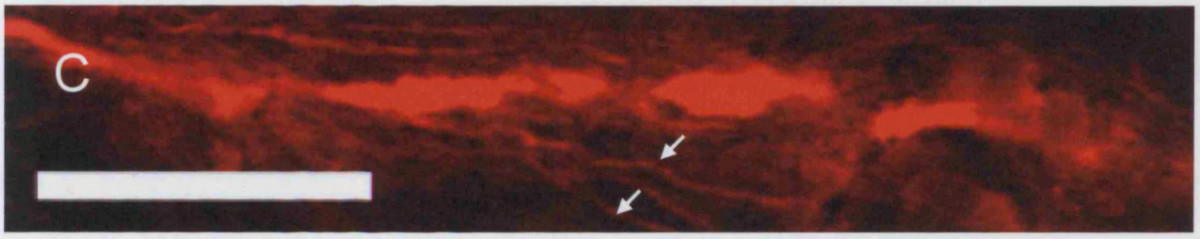
C


D

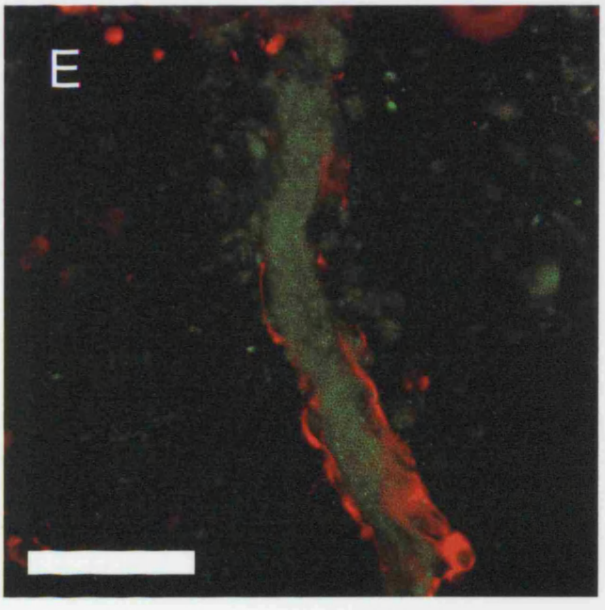
E

Figure 2.8

The EphA4 receptor is expressed in GFAP-positive astrocytes

A-C Fresh frozen 14μm section through the dorsal grey matter showing GFAP-positive grey matter astrocytes (red, A) expressing the EphA4 receptor (green, B). Merging these images with bisbenzamide staining for DNA (blue, C) demonstrates that EphA4 is present throughout most of the astrocytic processes (arrows) and the cell body (triangle). Scale bars 50μm.

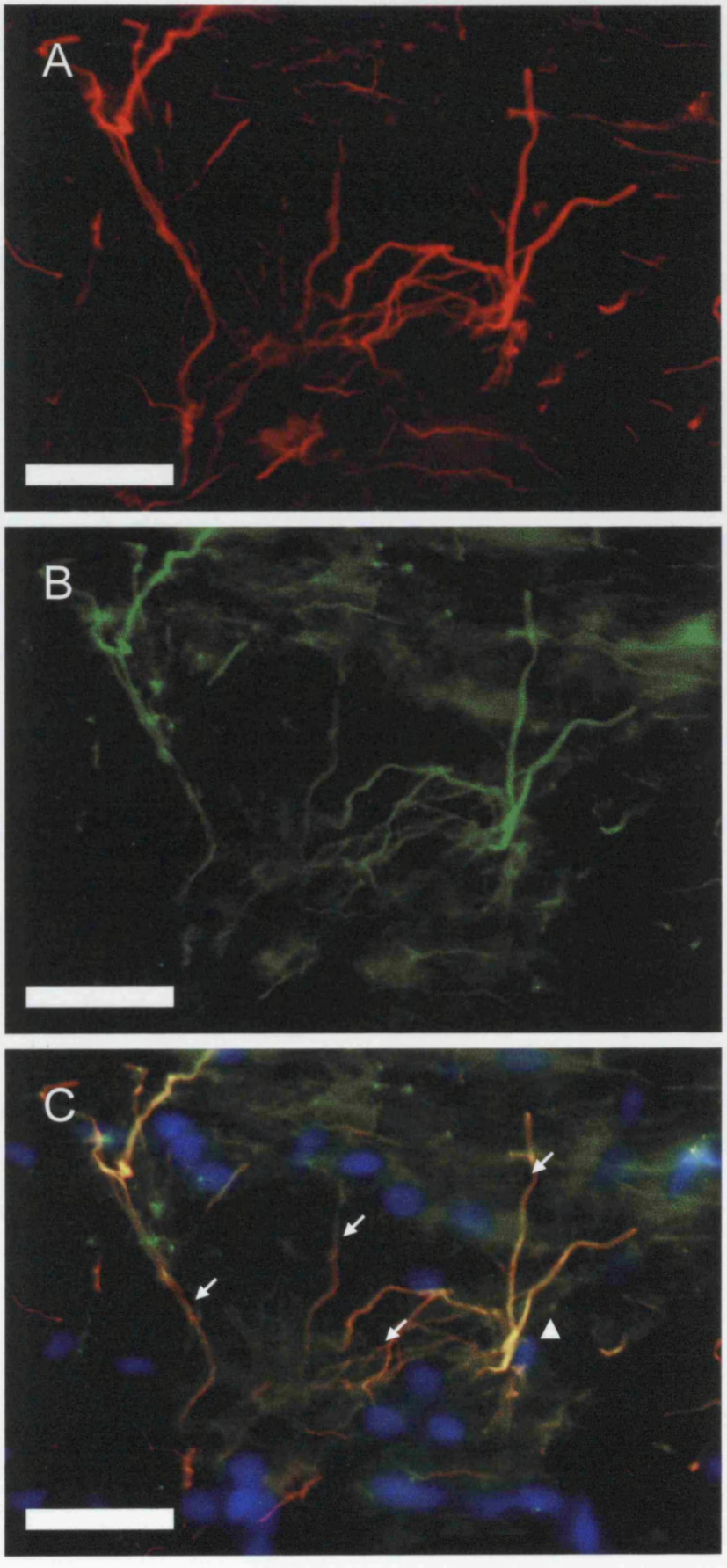
A
B
C

Figure 2.9

EphA4 positive puncta rostral to a spinal cord injury are not microglial but do associate strongly with astrocytes

A. EphA4-positive puncta present in the caudal region of the lesion site (arrows) do not have any distinct morphology by which they can be identified. Scale bar 100μm.

B-D. OX-42 staining for macrophages and microglia (red, B) shows no colocalisation with the EphA4-positive puncta (green, C and D). Scale bars 50μm.

E. GFAP staining (red) reveals reactive astrocytes closely associated with these EphA4 positive puncta (green). Bisbenzamide staining (blue) indicates the puncta contain no genetic material suggesting they are either termination bulbs from ascending tracts or degenerating EphA4-positive CST axon fragments. Scale bar 50μm.

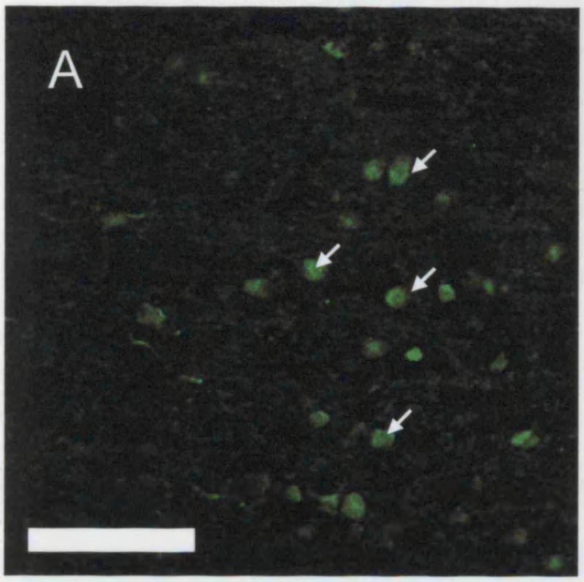
A

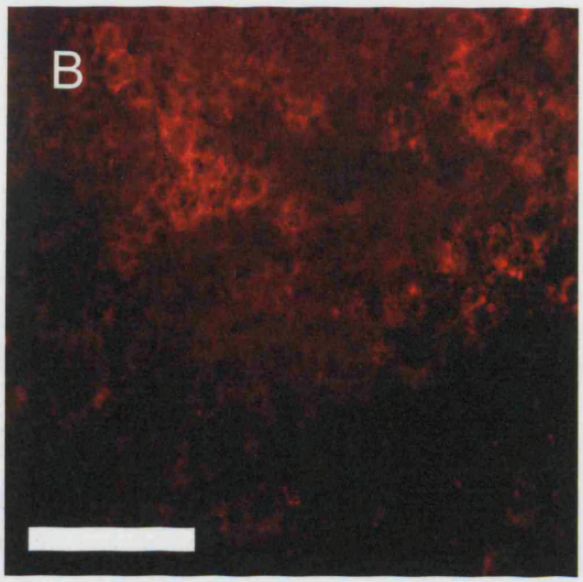
B

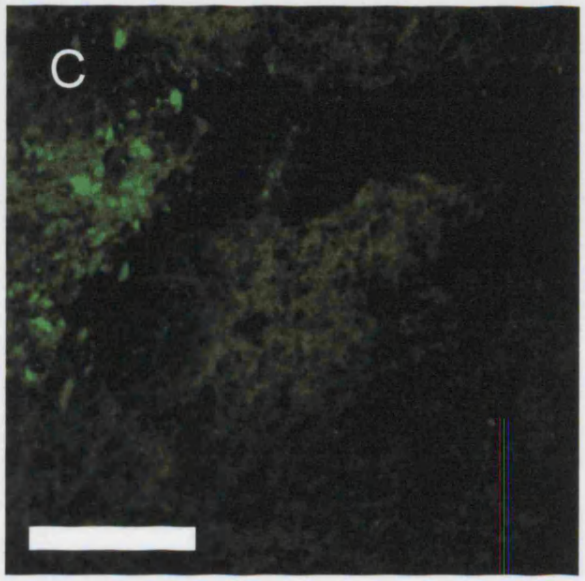
C

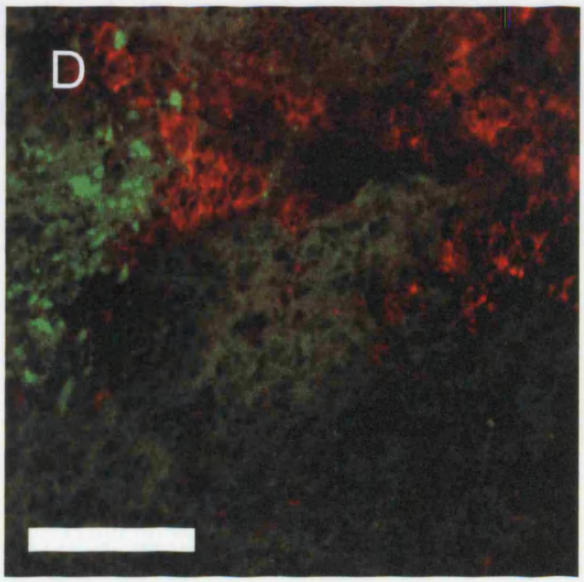
D

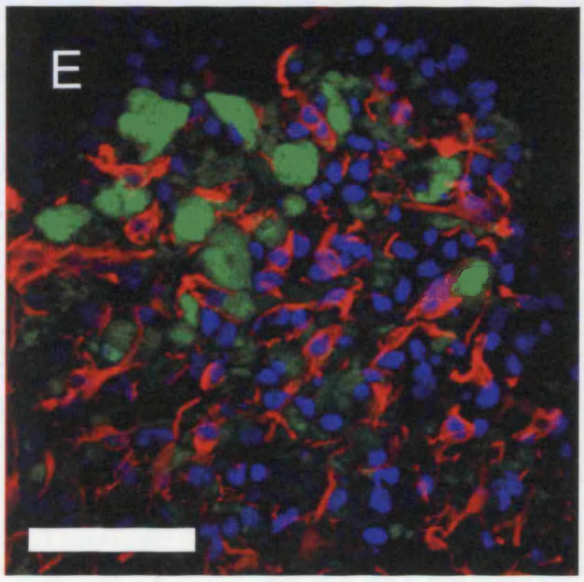
E

Figure 2.10

Pyramidal cells do not upregulate EphA4 expression following spinal cord injury

A-B. Coronal 14μm fresh frozen section from a control adult rat brain. *In situ* hybridisation for EphA4 mRNA expression using antisense (A) and control, sense (B) probes. EphA4 mRNA is localised to the hippocampus (h) and layers II-VI of the motor cortex (m). Non-specific probe binding is negligible (B). Scale bars 750μm.

C. Coronal 14μm fresh frozen section from an adult rat brain seven days following a dorsal hemisection that fully transected the dorsal and lateral corticospinal tract. *In situ* hybridisation for EphA4 mRNA expression reveals EphA4 mRNA localised to the hippocampus (h) and layers II-VI of the motor cortex (m). Scale bar 750μm.

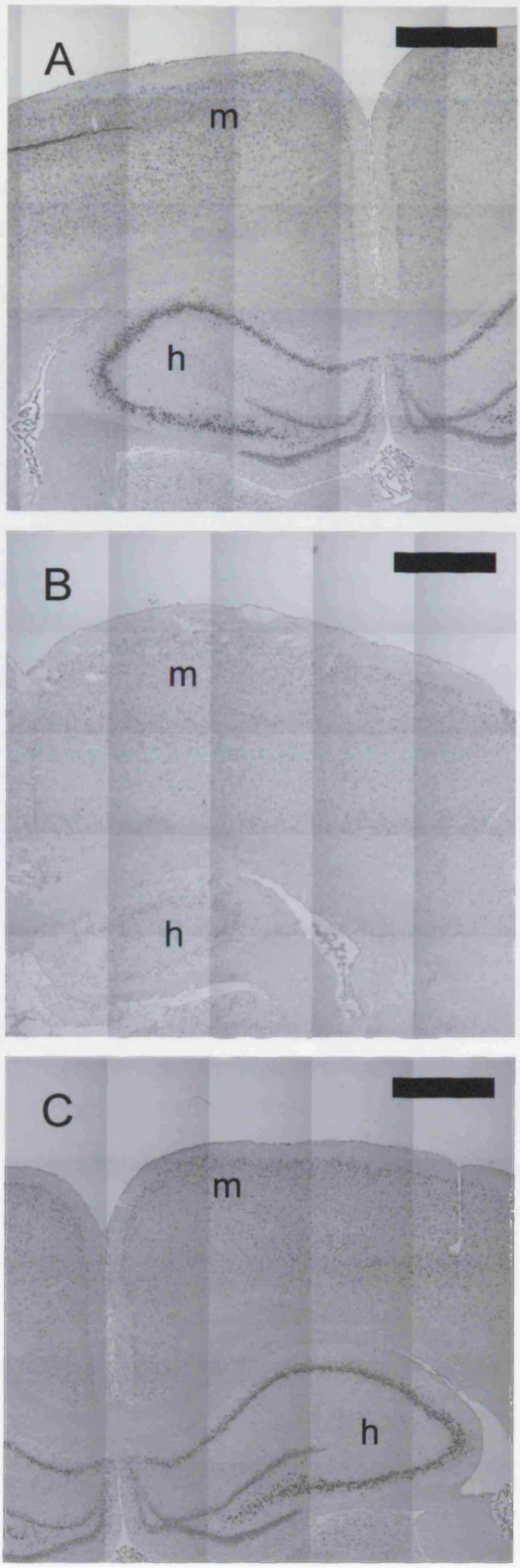
A
m
h
B
m
h
C
m
h

Figure 2.11

EphA4 receptor localisation by *in situ* hybridisation

A. Coronal 14μm fresh frozen section from an adult rat brain highlighting the site of a needle puncture. *In situ* hybridisation for EphA4 mRNA expression reveals an upregulation in the expression of EphA4 in motor cortex nuclei local to the injury. Scale bar 50μm.

B. Coronal 14μm fresh frozen section from an adult rat brain highlighting the lateral ventricle. EphA4 mRNA is strongly expressed in unidentified cells in the lining and plexus of the ventricle and a similar expression pattern is seen in other ventricles. Scale bar 150μm.

C. Horizontal fresh frozen 14μm section of the control adult rat spinal cord showing EphA4 mRNA localised to strongly expressing grey matter (#) cells and more weakly expressing white matter (*) cells. The *in situ* staining pattern and immunohistochemical data suggests these cells are likely to be astrocytes. Scale bar 200μm.

D. Horizontal fresh frozen 14μm section of the adult rat spinal cord seven days following injury demonstrating how the lesion epicentre becomes strongly EphA4 mRNA-positive with a likely combination of white matter astrocytes upregulating expression and reactive grey matter astrocytes invading the lesion site. Scale bar 200μm.

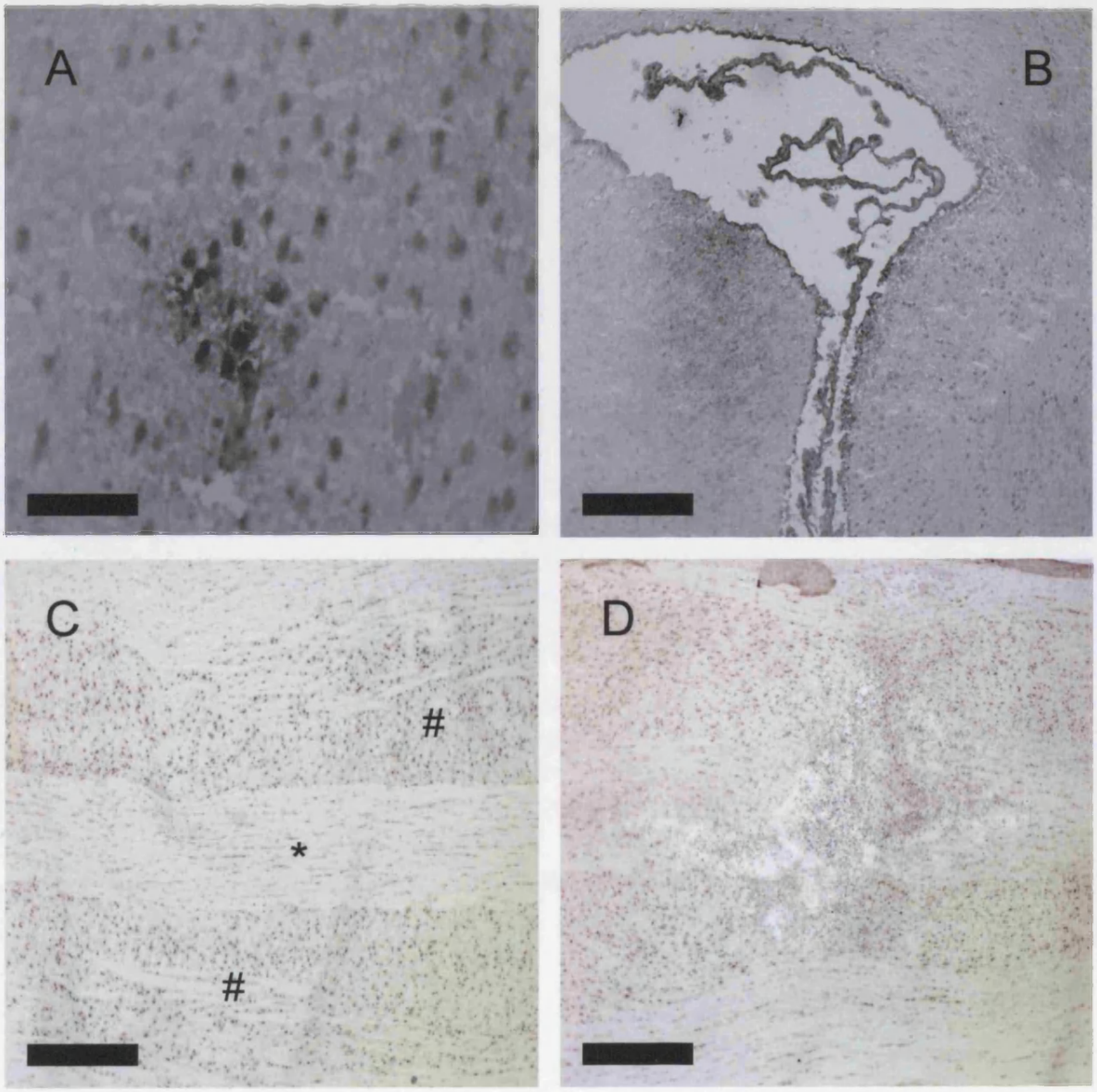
A
B
C
#
*
#
D

Figure 2.12

Grey matter astrocytes express ephrinB2

A-C. Horizontal 14μm fresh-frozen section through the uninjured dorsal corticospinal tract showing that GFAP-positive grey matter (#) astrocytes (red, A) strongly express ephrinB2 (green, B) while the less GFAP-positive white matter (*) astrocytes do not. Some weak staining of dorsal horn grey matter neurons was also apparent (arrows, C). Scale bars 200μm.

D-E. Higher magnification images of uninjured spinal cord confirm this colocalisation of GFAP (red, D) and EphA4 (green, E). Interestingly, merged images with bisbenzamide staining for DNA (blue, F) indicate that while GFAP expression is strongest close to the nucleus, EphA4 staining appears to extend throughout all the astrocyte processes with comparable intensity (arrows, E). Scale bars 50μm.

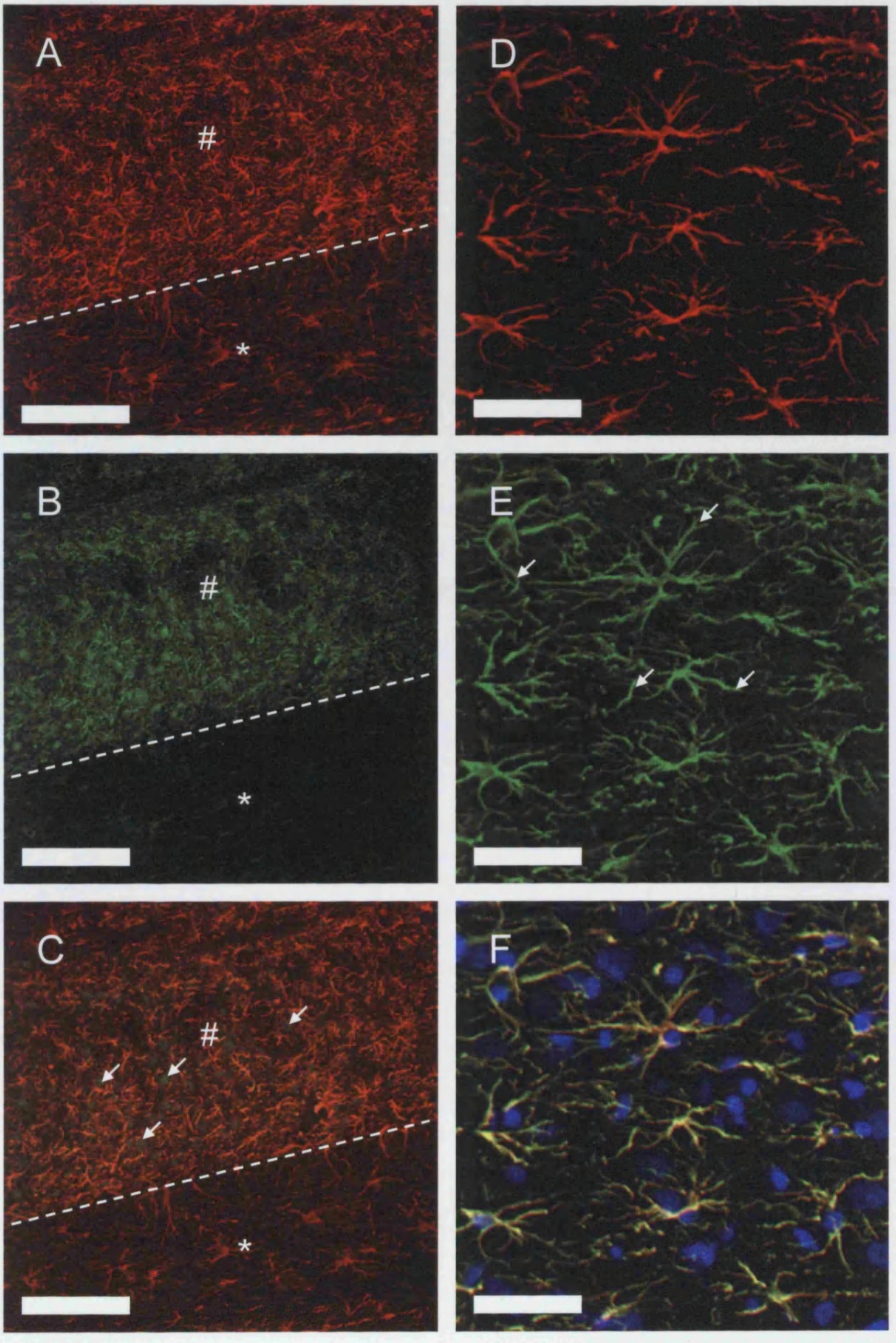
A
#
*
D
B
#
*
E
C
#
*
F

Figure 2.13

Astrocytes upregulate ephrinB2 expression following spinal cord injury

A-B. Low magnification image of a horizontal 14μm fresh frozen section through the dorsal corticospinal tract seven days following dorsal column transection. GFAP-positive astrocytes (green, A) strongly upregulate GFAP expression when undergoing gliosis in the vicinity of the lesion site. EphrinB2 in these astrocytes is similarly upregulated (red, B). Expression of both antigens is strong in the white (*) and grey (#) matter rostral and caudal to the injury although the spread of ephrinB2 expression does not appear as extensive. Scale bars 500μm

C-E. Higher magnification images of the grey/white matter margin near the lesion site. The expression margin of GFAP (red, C) and ephrinB2 (green, D) between the grey (#) and white (*) matter near the lesion site has become indistinct. The two proteins still strongly colocalise but expression in the white matter is now comparable to that seen in the grey matter. A combination of invading ephrin-B2 positive reactive grey matter astrocytes and upregulation of GFAP and ephrinB2 in surviving white matter astrocytes is likely to cause this expression change. Scale bars 200μm.

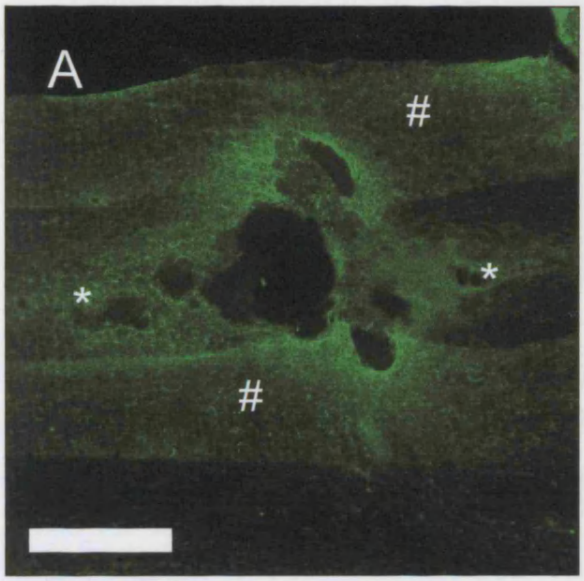
A
#
*
*
#

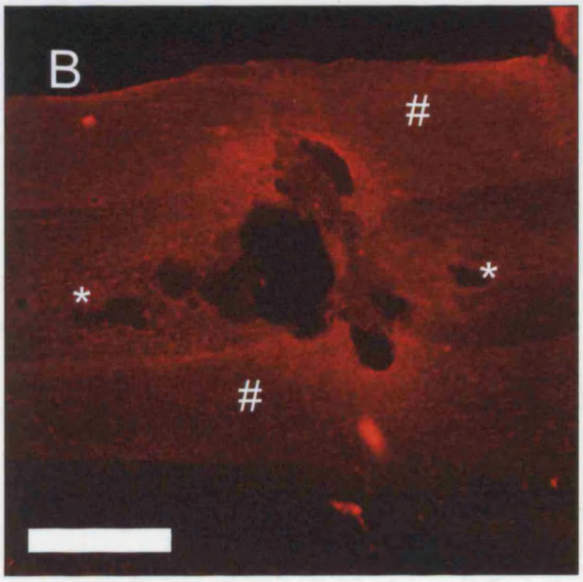
B
#
*
*
#

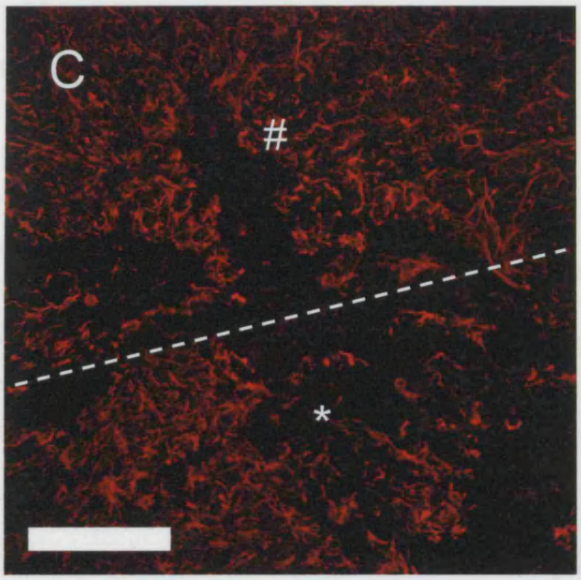
C
#
*

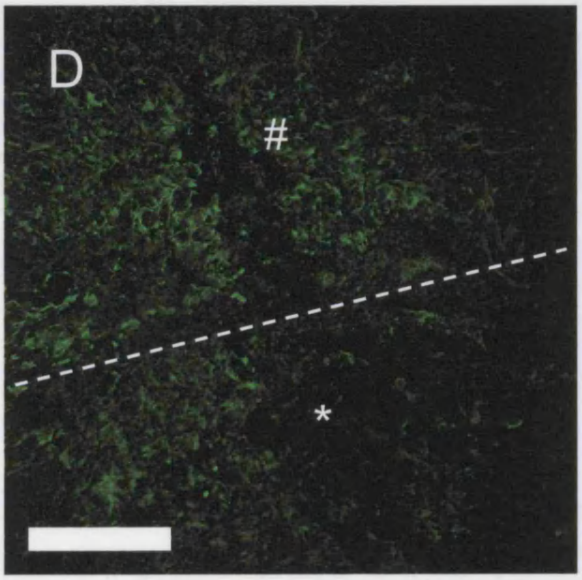
D
#
*

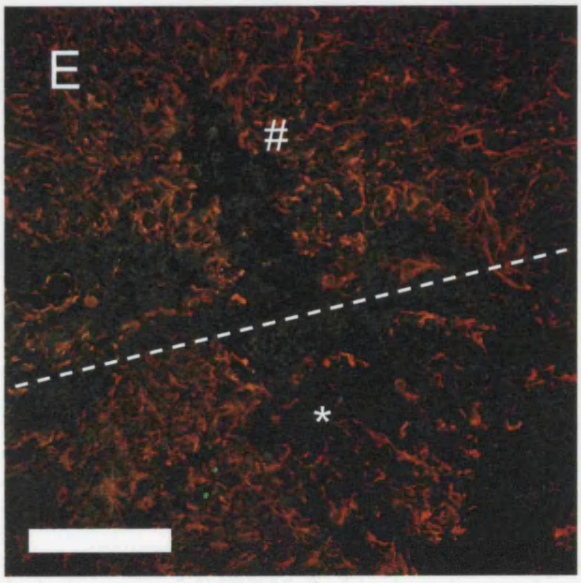
E
#
*

Figure 2.14

EphrinB2-positive astrocytes surround the lesion site

A-C. Horizontal 14μm fresh frozen section showing the margin of the grey matter astrocytes at the lesion cavity (*) seven days following dorsal column injury. GFAP-positive reactive astrocytes orient their processes towards the lesion epicentre (red, A and D) and ephrinB2 expression in these cells and their processes is clear (green; B and C, E and F). Scale bars 100μm.

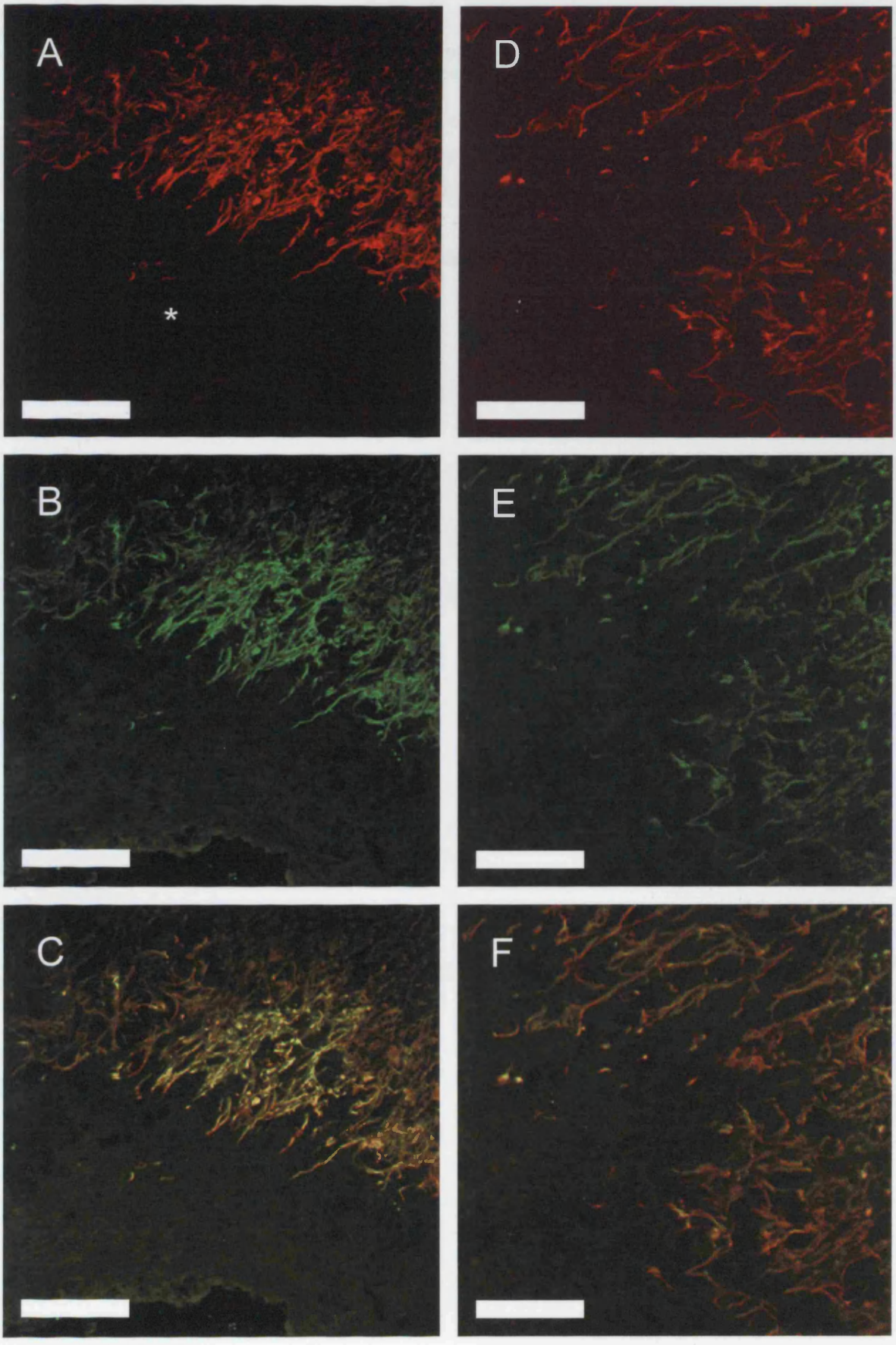
A
*
D
B
E
C
F

Figure 2.15

The EphA4-positive CST is surrounded by ephrinB2-positive astrocytes after injury

A-C. Horizontal 14μm fresh frozen section through the transected dorsal corticospinal tract seven days following injury. EphA4 in the corticospinal tract (green, A) is clearly in close proximity to ephrinB2-positive astrocytes (B) at the lesion margin (C). Scale bars 150μm.

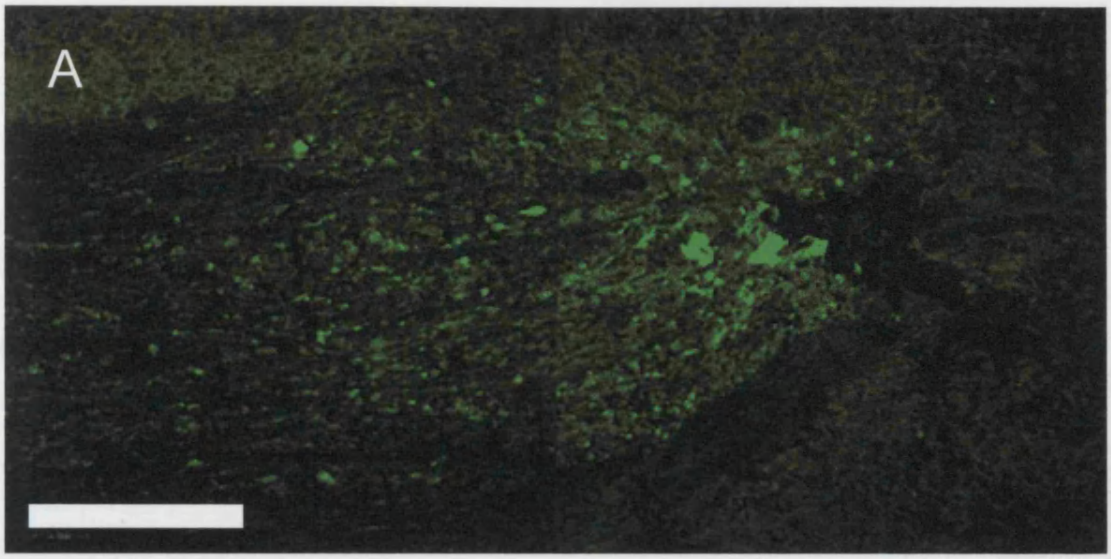
A

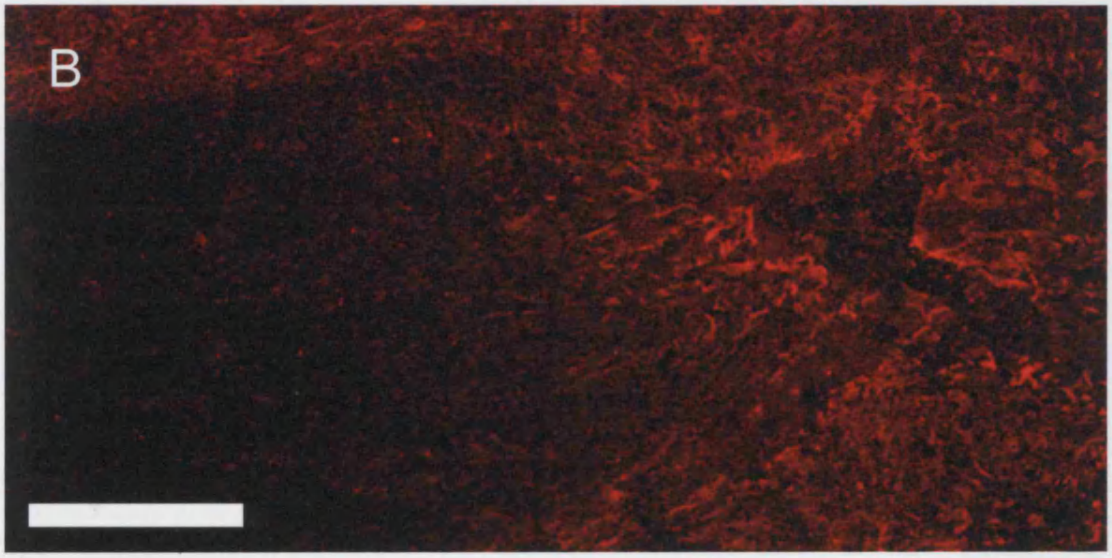
B

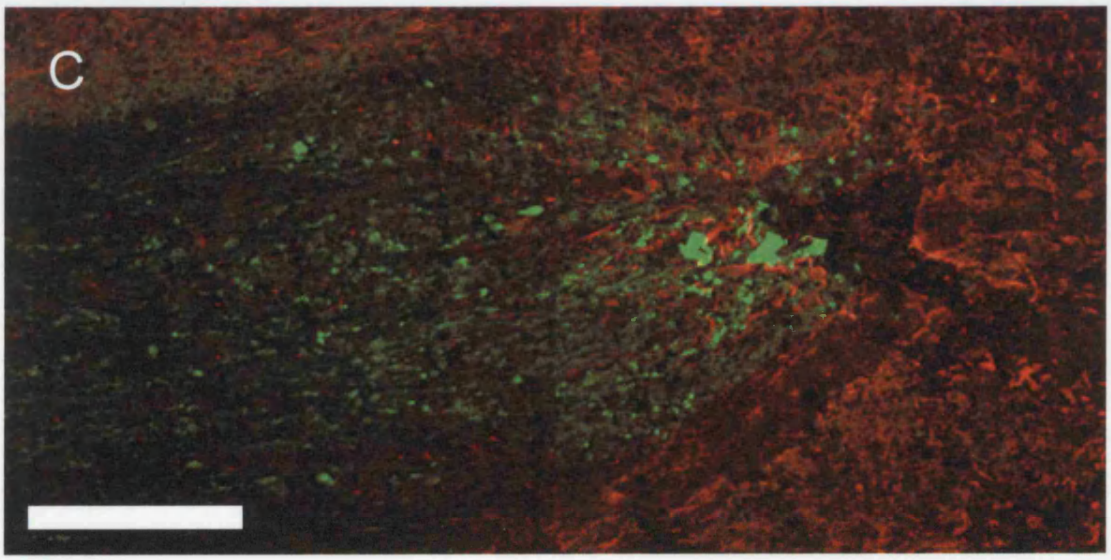
C

Figure 2.16

Immunohistochemical localisation of the ephrinB2 protein

A-C. Horizontal 14μm fresh frozen section though a dorsal root entry zone in the thoracic region. Sensory neuron axons originating in the dorsal root ganglion are ephrinB2-positive (green, A) although this expression diminishes as they approach the GFAP-positive DREZ (red, B and C). Scale bar 200μm.

D. Horizontal 14μm fresh frozen section though a dorsal root ganglion in the thoracic region. Small- and medium-sized DRG neurons are strongly ephrinB2-positive, as are their processes. Scale bar 200μm.

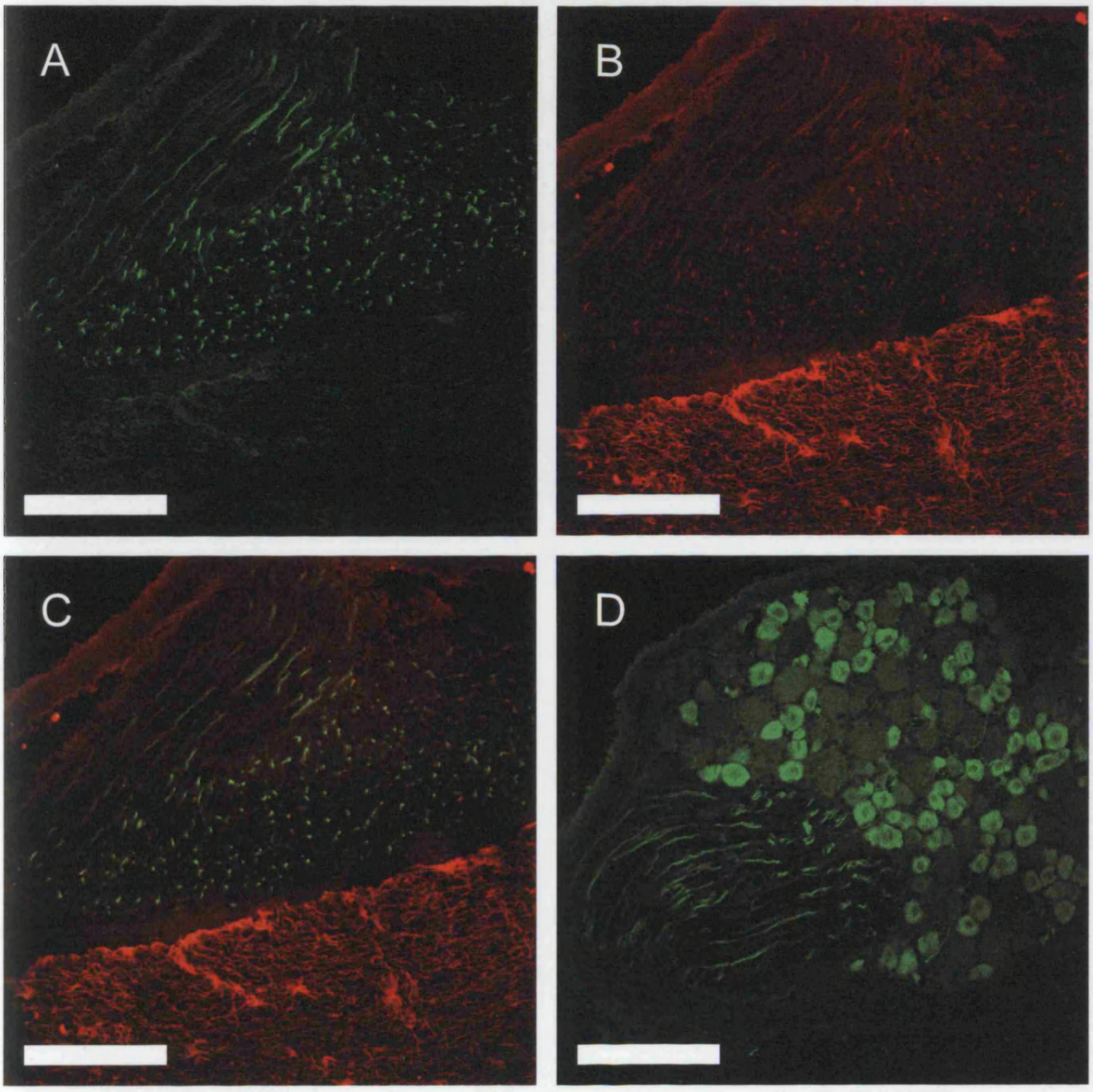
A
B
C
D

Figure 2.17

The CST and RST tracing methods do not co-label any axonal tracts

A. Coronal 40μm section through the perfused rat brain following corticospinal tract labelling by BDA injection to the motor cortex and rubrospinal tract labelling by EGFP-expressing lentivirus injection to the red nucleus. The section is taken just caudal to the level of red nucleus injection and the distinct expression domains of the BDA (red) and EGFP (green) are clear. Scale bar 500μm.

B. Transverse section of the lateral white matter from an animal receiving EGFP-expressing lentivirus to the red nucleus and BDA to the motor cortex. Lateral CST (red, arrows) and RST (green) fibres intermingle and occupy similar fields of the lateral white matter. Scale bar 100μm.

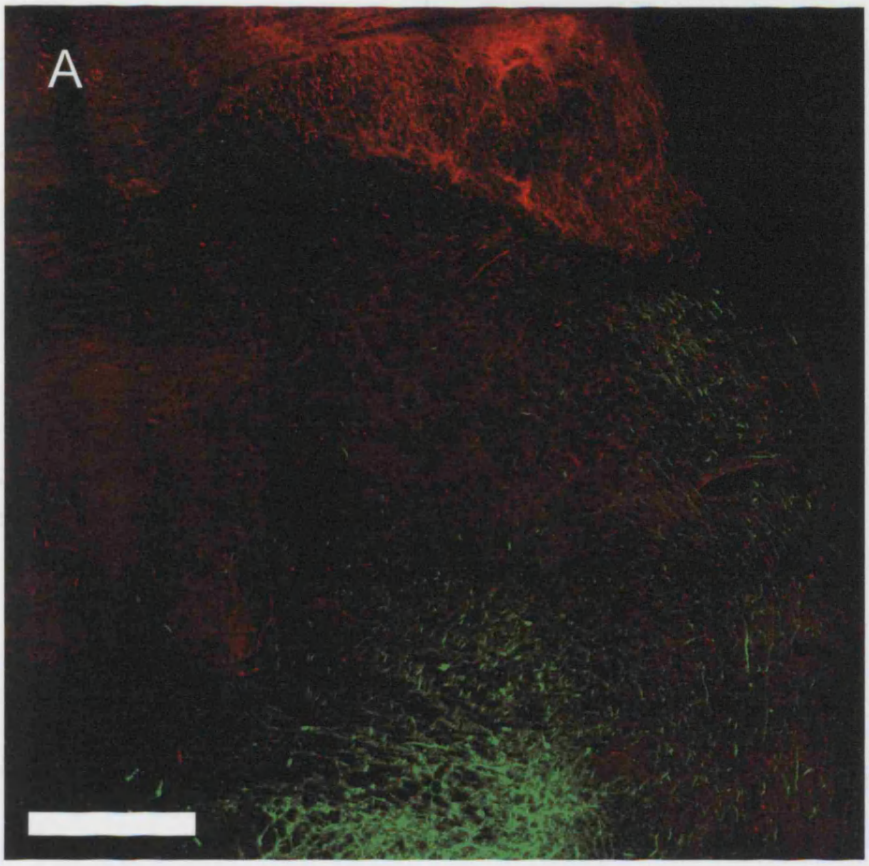
A

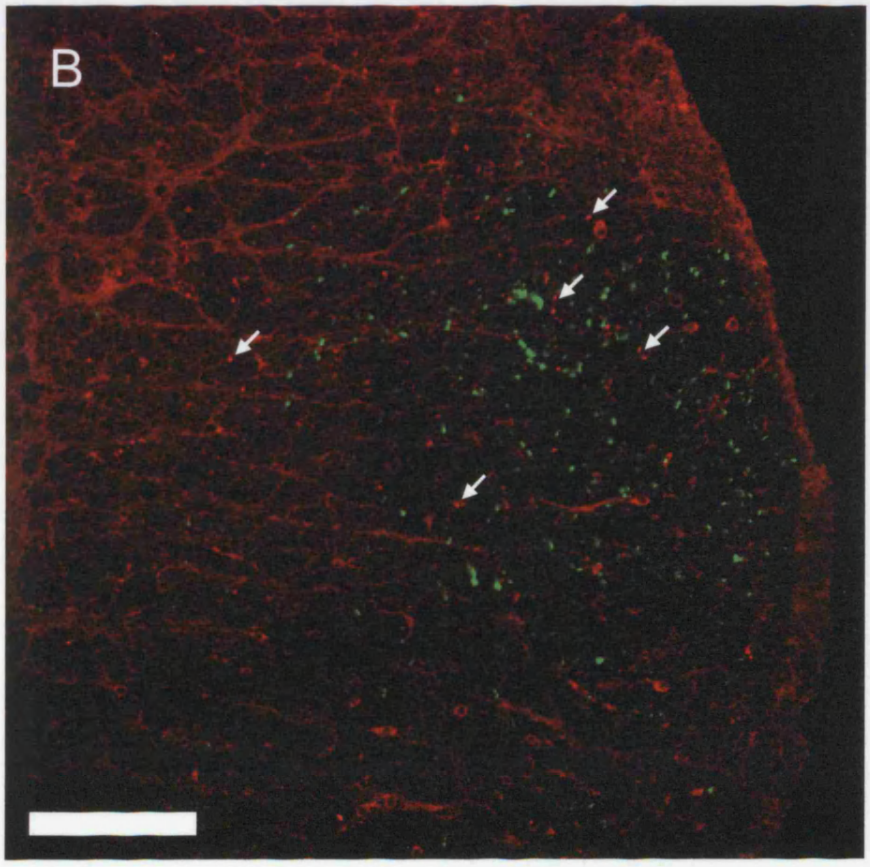
B

Figure 2.18

The EphA4-positive CST retracts further following injury than the EphA4-negative RST

A-B. EGFP-positive RST axons (green) are seen to retract to a smaller extent than BDA-positive CST axons (red). Hence the mean distance of RST termination bulbs from the lesion margin (delineated by the dotted line) is less than that for the lateral CST. Quantifying these regeneration distances for a series of animals (n = 3) highlights this difference in regenerative capacity (B, mean ± SEM). Scale bar 250μm.

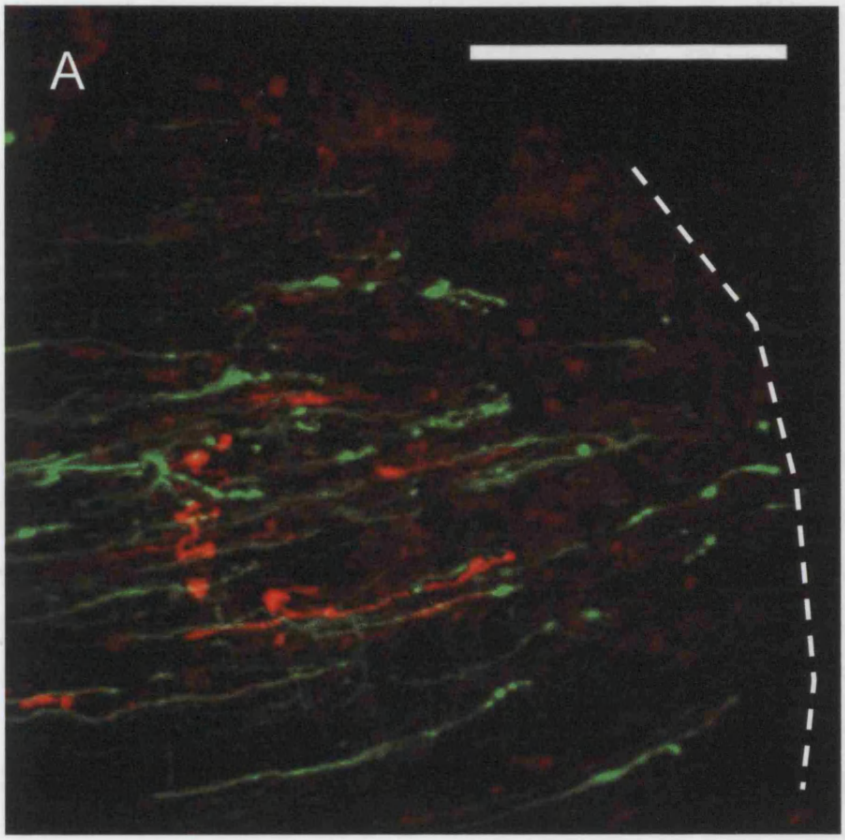
A

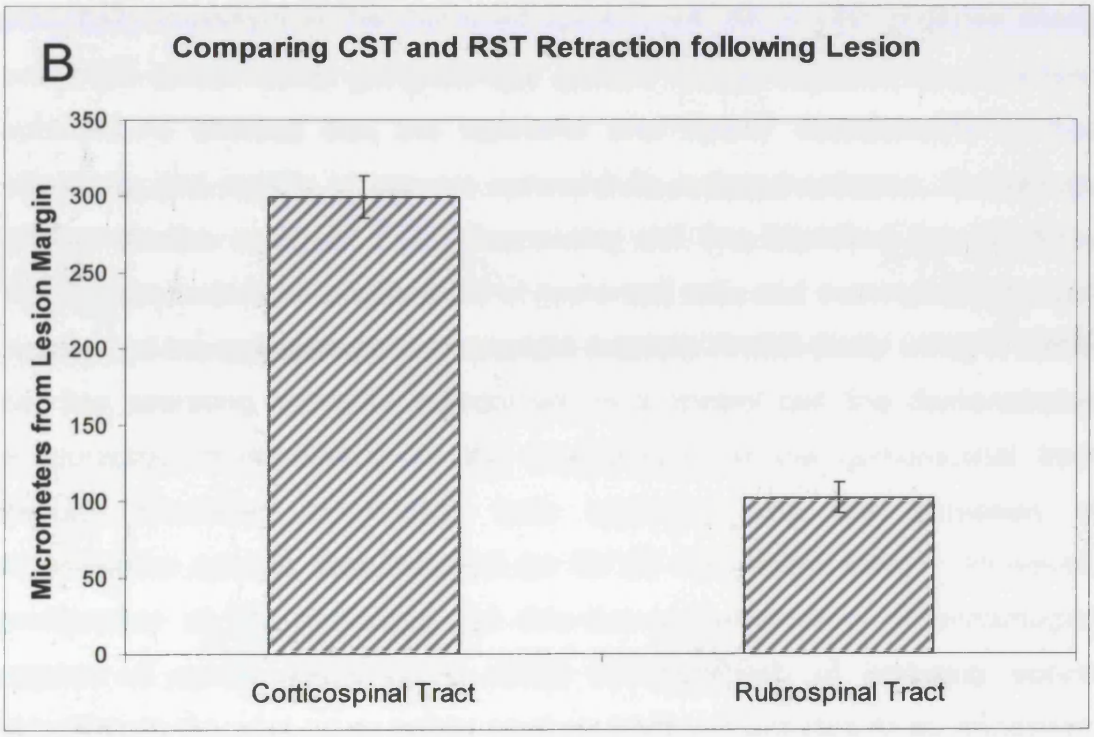
B
Comparing CST and RST Retraction following Lesion
Micrometers from Lesion Margin
350
300
250
200
150
100
50
0
Corticospinal Tract
Rubrospinal Tract

Chapter III

Production and Implantation of CHO Cell Lines Secreting Blockers of Ephrin Signalling

Abstract

Given the likely role of ephrin signalling in spinal cord injury as a negative regulator of regeneration and a possible mediator of the formation of the growth-inhibitory basal lamina, a method of neutralising ephrin signalling to encourage spinal cord regeneration was pursued. The aim of the project was to produce stably-transfected cell lines secreting monomeric ephrin/Eph ectodomains that would be capable of binding endogenous ligand and receptors. Implantation of these cell lines would permit a continuous supply of blocking protein to a lesion site and hence interrupt any ephrin signalling. EphrinB1, EphB3, EphA7 and ephrinA5 were selected for their ability to bind promiscuously and with high affinity to many Eph/ephrins identified as potentially important in the damaged spinal cord. An *in vitro* collapse assay using E6 chick retinal ganglion cell growth cones exposed to dimerised ephrinA5-Fc showed that the ephrinA5 and EphA7 ectodomains worked effectively and rapidly to prevent ephrinA5-Fc induced collapse. Preliminary implant studies using an EGFP-expressing cell line identified complications with immune rejection, proliferation of implanted cells and meningeal fibroblast invasion of the collagen gelfoam implant support. A pilot study using a stable cell line secreting ephrinA5 ectodomain or a control cell line demonstrated encouraging improvements in the regeneration of the corticospinal tract through increased termination bulb sprouting and the formation of regenerative sprouts that reached as far as the lesion margin. However, proliferation of the implanted cell line led to deformation of undamaged regions of spinal cord. Hence, while the approach of inhibiting ephrin signalling in the post-injury spinal cord environment appears to be beneficial, the use of implanted cell lines is not a viable long-term means of administration.

METHODS

Design of PCR Primers

To produce the desired protein ectodomains that would bind to endogenous ephrin ligands and Eph receptors, primers were designed to incorporate the entire ligand or receptor binding domain as appropriate. Each primer consisted of 6 bases of random sequence (ATGGAT) to permit binding of the Taq polymerase to the DNA followed by the desired digestion enzyme recognition sequences for subsequent ligation into pEF-BOS. In the 3' primers, a TTA STOP codon was introduced and in the case of the ephrinA ligand this was placed before the GPI attachment sequence[406] to ensure the translated product was not retained at the cell membrane. 16 to 19 bases of gene-specific sequence were then attached to the end of this non-specific sequence. In all cases, the locations of the digestion enzyme recognition sites were held in frame with the coding sequence to permit fusion protein production.

Primer sequences were based on published rat sequences or were derived from n-BLAST searches of rat genome using published mouse sequences.

EphrinB1 primers were designed based on the published mRNA sequence for Rattus norvegicus ephrinB1 [GenBank: gi 8393301; ref NM_017089.1].

Forward primer sequence

ATCGATTCTAGAACGCGTACGCCGTTGGCCAAGA

Reverse primer sequence

ATCGATACGCGTTTAGGAGTTAAAGAAGCTGTCG

EphB3 primers were designed using a BLAST search of the published NCBI rat genome using the published mRNA sequence for the Mus musculus EphB3 receptor [GenBank: gi 20892082; ref XM_148146.1].

Forward primer sequence

ATCGATGAATTCACGCGTTGCTGGGCGCTGGAAG

Reverse primer sequence

ATCGATACGCGTTTAAGTGGTGGATGCACACTTC

EphrinA5 primers were designed based on the published mRNA sequence for Rattus norvegicus ephrinA5 [GenBank: gi 16758777; ref NM_053903.1].

Forward primer sequence

ATCGATGGATCCACGCGTAAAGTCGTCGCCGACC

Reverse primer sequence

ATCGATACGCGTTTATGGCTCGGCTGACTCA

EphA7 primers were designed based on the published mRNA sequence for the Rattus norvegicus EphA7 receptor [GenBank: gi 19705436; ref NM_134331.1].

Forward primer sequence

ATCGATGGATCCACGCGTGAGGCGCAGGCTGCGA

Reverse primer sequence

ATCGATACGCGTTTAGGACCAGCACTTCTTGTAG

PCR and cloning

Rat whole brain RNA was made from the complete brain of an adult female 200g Sprague-Dawley rat dissected using sterile instruments. The tissue was cleaned in RNase-free PBS and homogenised in TRIzol (Invitrogen). The material was then centrifuged at 3500rpm for 10min to clear remaining sediment and phase-separated using 20% chloroform. An upper, aqueous, phase that contained the tissue RNA was precipitated at -80°C with isopropanol overnight, washed with ethanol and resuspended in RNase-free distilled water. Complete cDNA was prepared from 1µg of RNA using random hexamers (25mM, Promega), dNTPs (500µM, Promega), RNasin (2U, Promega) and AMV reverse transcriptase (20U, Promega) for 45min at 42°C. Initial cloning PCRs were performed using rat whole brain cDNA and subsequent PCR used the appropriate PCR product for second-round amplification. PCR products were analyzed on 1% agarose gels to ensure the presence of product. The product was gel purified and then digested with the appropriate digestion enzymes (all from Promega), as was purified vector DNA. Gel purification to select the appropriate digestion product was followed by ligation and transformation of ultracompetent E. coli (JM-109, Promega).

Colony selection and clone analysis through Mini-Prep (Qiagen Mini-Prep Kit) and restriction enzyme digestion permitted the production of large DNA quantities that were sent for sequencing analysis (DNA Sequencing Facility, Biochemistry Department, University of Cambridge) to confirm successful cloning (Figures 3.M1-3.M8).

Initially ectodomain inserts were cloned into pEF-BOS, a mammalian expression vector[407], to add immunorecognition and secretion signal tags to the eventual translation product. The enlarged insert was then cloned into pCS2+ to permit high level expression in transfected cells. Inserts were cloned into the MluI IL-3/c-myc cloning site of pEF-BOS (Figure 3.M9A). This provides an N-terminal domain secretion signal derived from the Interleukin-3 (IL-3) gene that induces strong mammalian expression[407] and is cleaved subsequent to secretion of the protein. The vector also encodes a *c-myc* C-terminal domain tag that permits tracing and purification through immunorecognition at this c-myc domain. Following successful insertion of correctly-oriented inserts into pEF-BOS, the ~750bp XbaI digestion fragment containing the DNA coding for the complete fusion protein was inserted into the XbaI cloning site of pCS2+, a high-level transient mammalian expression vector[408] (Figure 3.M9B). The calcium phosphate precipitation method (Calcium Phosphate Transfection Kit, Promega) was used to transiently transfect Human Embryonic Kidney (HEK) and Chinese Hamster Ovary (CHO) cells with the pEF-BOS and pCS2+ vectors at each cloning stage to check for successful expression. 96 hours post-transfection the medium was harvested, centrifuged for 1min at 2000g to pellet cell debris and then centrifuged for 15min at 2000g at room temperature through 10kDa NWM size-exclusion filters (Millipore). This yielded roughly 1ml supernatant per 10ml growth medium.

Cell Culture Media and Techniques

Standard aseptic cell culture techniques were used throughout. All work was performed in a class II laminar flow tissue culture hood. HEK and CHO cells were maintained at 37°C, 5% CO_2 in culture flasks containing supplemented DMEM medium (Dulbecco's Modified Eagle's Medium, High Glucose, with

FBS (foetal bovine serum), 10%; and occasionally also penicillin/streptomycin, 1%; final concentrations 5,000 units/ml and 5 mg/ml, respectively) or serum-free and protein-free medium for CHO cells transfected with ectodomains for use on SDS-PAGE (sodium dodecyl sulphate-polyacrylamide gel electrophoresis) gels.

Transfection of HEK and CHO cells

24hr before transfection HEK or CHO cells were split and plated (at 10^6 cells per dish) onto 10cm diameter cell culture dishes. Following 24hr incubation (37°C, 5% CO2), 20µg of DNA was used to transiently transfect the cells (using the calcium phosphate precipitation method). 24 hours post-transfection cells were washed twice in sterile PBS and returned to the incubator with fresh pre-warmed medium for a further 48 hours. Cytoplasmic β-galactosidase (in pCS2+) was used in a control transfection dish to assess the transfection ratio. The β-galactosidase plate was washed with PBS 24hrs post-transfection then fixed (2% w/v formaldehyde in PBS, 5min, 4°C), rinsed with PBS and stained (X-gal 1mg/ml, potassium ferricyanide 5mM, potassium ferrocyanide 5mM, magnesium chloride 2mM) for β-galactosidase expression for 30min at 37°C. Transfections producing a transfection ratio of less than 25% after 24hrs were discarded.

Alkaline Phosphatase-tagged Eph and Ephrin ectodomains

The RAP (Receptor Affinity Probe or Receptor Alkaline Phosphatase) staining method[304, 409, 410] uses soluble protein ectodomains fused to secreted placental alkaline phosphatase (SEAP[411]) to locate binding sites within cells or tissues. APtag-1 vector (alkaline phosphatase, Figure 3.M10A) containing EphA3 or ephrinA5a was used to transiently transfect HEK cells via the calcium phosphate precipitation method. The APtag-1 vector induces secretion of the EphA3 or ephrinA5a extracellular domain fused to SEAP, which can be visualised chromatogenically following binding and fixation[412].

To assay the level of ephrinA5 or EphA7 protein ectodomain expression EphA3-AP or ephrinA5a-AP fusion proteins were used as detection agents. The full method used is published on the Science STKE website[413]; briefly,

HEK293 cells are transfected with one AP-tag construct (or an empty construct for negative controls) using the calcium phosphate method. 96 hours post-transfection the medium is harvested, centrifuged for 1min at 2000g to pellet cell debris and then centrifuged for 15min at 2000g at room temperature through 10kDa NWM size-exclusion filters. The AP-tagged protein concentration in any sample was assayed using serial dilutions and addition of p-Nitro phenyl phosphate substrate (pNPP, Sigma) with detection at 405nm. The known rate constant of SEAP means that a change of 15 OD units over a 30 minute time period corresponds to 1pmol of AP-tagged protein.

Detection of Secreted Eph/Ephrin Ectodomains

Semi-purified supernatant derived from size-exclusion spin preparations was applied for 2hrs to 96-well plates coated in anti-*c-myc* antibody (Sigma), wells were then washed three times in PBS-0.1T PBS containing 0.1% Tween-20, Sigma). 2.5nM ephrinA2-AP fusion protein was then applied to each well for 2hrs, following three washes in PBS-0.1T, bound alkaline phosphatase was detected using the p-Nitro phenyl phosphate substrate system (pNPP) with detection at 405nm.

Immunoprecipitation and Coomassie Staining

Protein A (0.2g, Invitrogen) was resuspended in 40ml of distilled water and allowed to swell for 2 hours followed by two washes in distilled water. Beads were then spun at 1500rpm and resuspended in immunoprecipitation (IP) buffer (50mM Tris HCl, 150mM NaCl, pH 7.0). Ectodomain protein samples were adjusted to 0.5ml with IP Buffer and anti *c-myc* antibody added at 1:2000. Samples were rocked gently for one hour at 4°C when 50µl of Protein A slurry in prechilled IP Buffer was added. Samples were gently rocked for a further hour at 4°C and then spun at 10,000g for 30sec at 4°C. The supernatant was removed and the remaining protein A material was washed three times with IP Buffer at 4°C with gentle rocking. Following a further spin at 10,000g for 30sec, gel loading buffer was added and the sample was boiled for 10min. The supernatant from a final centrifugation at 10,000g was loaded onto a 10% Tris-HCl SDS-PAGE (Bio-Rad pre-cast gels) and electrophoresed

at 200V with constant current. Coomassie staining was performed with BioSafe Coomassie (Bio-Rad) for one hour with gentle rocking followed by extensive washing with distilled water.

Anti-c-myc Western Blotting

Samples were placed at 95°C in Laemmli Buffer for five minutes before being loaded onto 10% Tris-HCl SDS-PAGE pre-cast gels (Bio-Rad) and electrophoresed at 200V with constant current. Electrophoresed protein was then transferred onto nitrocellulose (Amersham) by semi-dry transfer blotting. Polyacrylamide gels were equilibrated in semi-dry transfer buffer for 20 minutes before being transferred for one hour at 15V. Nitrocellulose membranes were washed three times for five minutes in PBS-0.05T (PBS containing 0.05% Tween-20) before being blocked for one hour at room temperature in PBST containing 5% non-fat dried milk powder (Sainsbury's, UK). Membranes were then incubated overnight at 4°C in PBS-0.05T containing 1% milk supplemented with rabbit anti-*c-myc* antibody (1:5000, Covance). Three washes in PBS-0.05T were performed followed by two hour incubation in goat anti-rabbit-HRP secondary antibody (1:25,000, Autogen Bioclear) at room temperature. Following three washes in PBS-0.05T, membranes were developed in ECL Plus Western Detection reagent (Amersham Biosciences) and visualised using photosensitive film (Kodac).

Stripe Assays

The stripe assay, an axon pathfinding assay based on the chick retinotectal mapping system where EphA3-expressing retinal ganglion cells (RGCs) are guided by repulsive gradients of ephrinA5[414], was investigated as a possible assay of the efficacy of the secreted ectodomains in blocking ephrin signalling. The assay involves the production of alternating 90μm width stripes of substrate with/without ephrinA5 such that axons growing out from RGCs are faced with a choice of substrate[301, 305, 363, 415, 416]. Previous work has indicated that RGCs avoid the ephrin-containing lanes, growing solely on the lanes of control substrate. Addition of soluble ephrinA5 or EphA7 ectodomains would be expected to block ephrin signalling and permit growth on either lane[417-419].

Two different types of stripe substrate were used. When soluble proteins were used as the test substrate, stripes were deposited on a glass substrate. When cell membranes were used as the source of the test agent, the stripes were created on 0.1µm pore size filters.

Glass coverslips were treated with 1% acid alcohol for 2hrs, rinsed twice in sterile water and maintained in 70% ethanol at 4°C until used. Before use, coverslips were placed on 3MM filter paper (Whatman) and autoclaved, cooled and coated with poly L-lysine. Following aspiration and two rinses in sterile water, coverslips were dried and pressed onto silicone matrices (Figure 3.M10B; Bonhoeffer laboratory, Max-Planck Institute, Tubingen, Germany).

The primary stripe agent, 10µg/ml anti-human Fc antibody (~10µl, Sigma) was injected into the matrices and incubated at 37°C for 1hr. Sterile PBS was then injected through the matrices to wash the stripes. Coverslips were removed from the matrices and natural mouse laminin (5µg/ml, Invitrogen) was applied to the whole coverslip to provide a general growth-supporting layer against which any repulsion or avoidance behaviour could be observed. Each coverslip was then incubated with growth medium containing 10% foetal calf serum (FCS, Sigma) to block any non-specific binding. The coverslips were then washed in PBS and incubated with either homodimeric human Fc-tagged ephrinA5 or human IgG (both 20µg/ml, Sigma) at 37°C for one hour. Coverslips were placed in growth medium consisting of F12, 86%; FCS, 10%; chicken serum, 2%; 200mM L-Glutamine, 1%; and penicillin/streptomycin, 1% (final concentrations 5000 units/ml and 5 mg/ml, respectively) supplemented with 0.4% methylcellulose (all from Sigma)

Filter-based stripes were made in a two-step process[420]; a 0.1µm Whatman polycarbonate filter was placed onto a polymerised silicone rubber 'grill' consisting of horizontal channels 90µm in diameter and 9mm in length. This grill was then placed on a porous glass frit support through which a vacuum was applied to the microchannels (Figure 3.M11A). 150µL of the primary stripe agent was applied to the surface of the filter. The concentration of

primary stripe agent was calibrated to fully block the filter after 100µL of the suspension had been sucked through. 0.03bar suction was applied until the filter was blocked and then surplus liquid was removed and the filter placed on a nylon grid supported on another porous glass frit (Figure 3.M11B). 150µL of the secondary stripe agent was applied and 0.03bar suction applied to fill the alternating stripes. The filter was rinsed in PBS solution and then placed in culture medium (without methylcellulose) until use.

Resolution between the two stripes was good with both methods (See Figure 3.M11C) and this was preserved regardless of the substrate type and period of incubation.

Retinal Ganglion Cell Culture and Visualisation of Axons on Stripe Substrates
Retinas were dissected from 6-day-old chick embryos in Hank's Buffered Saline Solution (HBSS, Sigma). After removal of the pigment epithelium and vitreous body, the retina was spread on a 0.4µm Whatman nucleopore filter. Retina and filter were chopped together in a McIlwain tissue chopper into 250µm width strips and placed inverted on either glass coverslip or filter stripes. RGC/filter strips were held in place with platinum weights and incubated at 37°C and 5% CO_2 in the minimum volume of medium required to cover the explant in order to enhance adhesion of the explant to the stripes. After 1hr, 250µL of pre-warmed medium (containing methylcellulose) was added and explants were incubated at 37°C and 5% CO_2 for 40-48hrs.

Cultures were then fixed (2% w/v formaldehyde, 0.33M sucrose in PBS) for 4hrs at 4°C, washed twice in PBS, permeabilised with Triton X-100 (0.1% w/v in PBS, Sigma), washed twice in PBS and stained with phalloidin-Alexa 488 (1:40, Molecular Probes) for 20min at room temperature. After being washed twice in PBS, stripes were visualised using a goat anti-human Fc primary antibody (1:1000, Sigma) and a rabbit anti-goat secondary antibody coupled to Alexa-594 (1:400, Molecular Probes). Coverslips could be viewed directly under a fluorescence microscope. Filter-based cultures were inverted onto Petri-perm dishes and then analysed.

Neurite Outgrowth Assay

The neurite outgrowth assay[421] is based on *in vitro* assays used to assess the effects of astrocytes on dendrite or axon outgrowth from neuronal explants[422]. HEK cells or HEK cells transiently transfected with full-length ephrinA5a were grown to near-confluency (~85%, to permit further growth of cells during the experiment without reaching over-confluency). Culture medium was then replaced with RGC culture medium (this change induced no obvious phenotypic change in the HEK cells). An E6 chick retina was then dissected as normal and then dispersed with collagenase and repeated pipetting. RGCs were seeded onto the HEK cell monolayer, maintained in position by surface tension, and allowed to adhere. 48hrs later plates were fixed and immunocytochemically stained with a mouse anti-neurofilament antibody (1:500, Sigma) and Alexa 594 coupled goat anti-mouse secondary (1:400, Molecular Probes). Ectodomains were added in the co-culture stage where necessary and the average axonal lengths for neurons were assessed under a fluorescence microscope.

Collapse Assay

10mm diameter glass coverslips were treated with 20µg/ml poly-L-lysine for 30min at room temperature, washed in sterile PBS and then incubated with 25µg/ml mouse laminin for 1hr at 37°C. Following two washes in PBS 1ml of RGC medium was added to each well and placed at 37°C in 5% CO_2 until addition of primary retinal cultures. Temporal E6 chick retinas were chopped into ~1mm^2 squares and then triturated manually in Ca^{2+}/Mg^{2+}-free HBSS (Sigma) approximately 10 times to produce clumps of 10-20 cells that were still viable and extended axons in culture. Roughly 4 squares of tissue were added per coverslip and cultures were left for 24hrs at 37°C, 5% CO_2.

Once robust axon outgrowth was underway and axons of roughly 100-200µm length were visible, cultures were exposed to either ephrinA5-Fc (20nM, R & D Systems), NOC-7 (500µM, positive control, Sigma) or PBS (control) for 30mins at 37°C, 5% CO_2. In those cases where an ectodomain was co-added to the culture, a 4:1 molar ratio of blocker to collapsing agent was applied. Cultures were then fixed with warm 4% w/v paraformaldehyde at 37°C, 5%

CO_2, permeabilised with 0.1% Triton-X100 (5min) and stained with phalloidin-Alexa 488 (1:40, Molecular Probes) to identify F-actin. NOC-7, a nitric oxide donor, is known to induce strong growth cone collapse and hence acts as a positive control in this context[423]. Fluorescence images were acquired on a Zeiss 510 confocal microscope with both the experimental procedure and the analysis being performed blind. Analysis of randomised fluorescence images permitted a quantification of the percentage of growth cone collapse.

Stable Cell Line Production for EphrinA5-*cmyc* and EphA7-*cmyc*

For initial investigation the EphA7-*cmyc* and EphrinA5-*cmyc* ectodomains were selected. pC1-neo and pCS2+EphrinA5-*cmyc* or pCS2+EphA7-*cmyc* vectors were used to co-transfect CHO cells for subsequent clonal selection for neomycin resistance and ectodomain expression. Clonal selection in 600µg/ml neomycin for one week resulted in well-defined and isolated clones of neomycin resistant CHO cells. 384 clones were selected per ectodomain and grown in 600µg/ml neomycin for ~two weeks until nearly confluent. Colonies were assayed for ectodomain expression for each cell line using the *c-myc* capture assay; this identified numerous expressing clones of each line. Those colonies that were secreting at the highest levels and showed a normal cell morphology under a light microscope were selected for further large-scale growth and assessment. Following further selection in 600µg/ml neomycin for 2-3 weeks, the colony with the best combination of good secretion of ectodomain, normal cell morphology and standard growth rate in culture was selected to be used in the *in vivo* experiments.

Production of the EGFP-expressing Cell Line

CHO cells were grown to 50% confluency in CHO growth medium in a 6-well plate. On the day of transduction, one well was trypsinised and the cell number counted. Typically $2x10^5$ cells were present in this well. A non-replicative integrating HIV virus was used that contained EGFP driven by a CMV promoter[396]. The HIV vector was produced using transfer plasmid pHR'SIN-cPPT-CE and following standard procedures. This virus was diluted in CHO growth medium supplemented with polybrene (hexadimethrine bromide, 8µg/ml, Sigma) at $1x10^6$ Transforming Units (TU) to produce a

multiplicity of infection (MOI) of 5. Typically with this virus an MOI of one would suffice for >95% transduction but to ensure >99% of cells were EGFP-positive, an MOI of 5 was used. CHO culture medium was replaced with virus-containing medium overnight at 37°C, cells were then washed twice in sterile 37°C PBS before being returned to normal CHO culture medium. Some variability was apparent in EGFP expression but few cells developed aggregated protein clusters. Furthermore, growth rate and morphology appeared unaffected by EGFP transduction. Cells were observed for one month in standard culture conditions to ensure no loss of EGFP expression occurred.

Surgical Procedures and CST Labelling

All surgical procedures were approved by the UCL ethical committee and licensed by the Home Office. Adult female 200-220g Sprague-Dawley rats were anaesthetised with a halothane, nitrous oxide, and oxygen mixture. A number of surgical approaches were pursued to obtain the optimal cell implantation procedure but the spinal cord injury and CST labelling techniques remained the same. Microsurgical scissors were used to transect part of the left dorsal column, the entire right dorsal column and part of the dorsal horn of grey matter at C6. In each case, animals were sacrificed two weeks after surgery by overdose with halothane. Where anterograde labelling of the CST was required, 5µl of 10% biotinylated dextran amine (Molecular Probes, Oregon, USA) was injected into the left motor cortex using standard coordinates (Paxinos and Watson, 1986). Animals were injected subcutaneously with FK-506 (1mg/kg body weight) every day for three days prior to surgery to provide sufficient immunosuppression. Animals received further FK-506 injections daily for a further three days after surgery and then injections every other day until the end of the experiment. For immunohistochemical procedures, animals were transcardially perfused with 4% w/v paraformaldehyde before removal of the spinal cord. Perfused tissue was stored at 4°C in 30% sucrose, 10% Thiermesol in phosphate buffer until use.

Implantation Method I: Intraventricular

$2x10^5$ CHO-EGFP cells were trypsinised, pelleted and washed in sterile 37°C PBS before being resuspended in 5µl sterile PBS. Cells were injected into the right lateral ventricle using standard coordinates (Paxinos and Watson, 1986) by stereotaxic injection. Animals were transcardially perfused with 4% w/v paraformaldehyde after three days.

Implantation Method II: Lesion Site

Sterile collagen gelfoam was soaked overnight in CHO growth medium at 37°C. $2x10^5$ trypsinised, washed and dispersed CHO-EGFP cells were then seeded onto the gelfoam and left to settle for 24hrs. Animals underwent a normal spinal cord injury at C6 with the exception that the dura was not sutured back together. A small (2mm x 3mm) segment of collagen gelfoam was then inverted onto the injury and sutured into place, such that the cells were as close as possible to the spinal cord (Figure 3.M12A). Overlying muscle was then sutured over the gelfoam. Animals were transcardially perfused with 4% w/v paraformaldehyde after ten days.

Implantation Method III: Para-Lesion Site

Collagen gelfoams were prepared and spinal cord injury performed as directed above. The dura was once again left unclosed to permit good access of the ectodomains to the spinal cord injury, especially at early time points following injury. Gelfoam was then sutured inverted roughly 1mm rostral to the lesion site (Figure 3.M12B). Animals were transcardially perfused with 4% w/v paraformaldehyde after ten days.

Immunohistochemistry

Fixed tissue was cut at 40µm thickness on a freezing microtome. Samples were permeabilised in TBST buffer (0.1M Tris Buffered Saline with 0.5% Triton-X100, Sigma) for one hour prior to incubation for one hour at room temperature in goat blocking solution (0.1 M TBS, 1% BSA, 0.1% Triton X-100, 10% normal goat serum). Sections were incubated in monoclonal mouse anti-GFAP (1:1000 in goat blocking solution) overnight at 4°C and washed three times in TBST before a two hour incubation in goat blocking medium

containing steptavidin-Alexa 568 (1:1000) and goat anti-mouse FITC (1:400, Sigma) at room temperature. Sections were then washed three times in TBST before being mounted on gelatinised slides, coverslipped in DABCO and sealed with nail varnish.

Digital image capture and analysis

Fluorescence images were acquired on a Zeiss 510 confocal microscope using conventional filter based fluorescence optics. Excitation and emission wavelengths were, respectively: FITC, Alexa 488 and EGFP = 488nm, 505 - 550nm; Alexa 568 and Alexa 594 = 543nm, >560nm. Imaging of slides labelled with multiple dyes was always sequential such that the preparation was only illuminated with light of one wavelength at any one time. Transmitted light images were acquired on the same microscope using bright field illumination.

RESULTS

Selection of ephrin family members

To inhibit ephrin signalling in the injured spinal cord using monomeric ephrin/Eph ectodomains that would be capable of binding endogenous ligand and receptors, the choice of sub-family members was critical. A literature search was performed to identify those members of the Eph/ephrin family thought to play a role in axon guidance, neurite outgrowth or spinal cord injury, or those shown to be expressed in the adult or developing spinal cord[229, 323] One member of each family of ligand and receptor were then selected for their ability to bind with high affinity to all of the corresponding Eph/ephrins identified. The promiscuity of ligand-receptor binding in the ephrin family facilitates this approach[424] (Figure 3.1A). EphrinB1, EphB3, EphA7 and ephrinA5 were selected and show high affinity binding to many Eph/ephrins identified as potentially important in the damaged spinal cord (Figure 3.1B).

Cloning

The receptor/ligand binding domains of ephrinB1, EphB3, ephrinA5 and EphA7 were successfully cloned from rat brain cDNA and inserted into the MluI restriction site of pEF-BOS as determined by DNA sequencing (Figures

3.M1-4). These IL-6 secretion signal- and *c-myc*-tagged fusion protein coding regions were subcloned into the *Xba*I restriction site of pCS2+ in the correct orientation, also shown by sequencing (Figures 3.M5-8).

Predicted Ectodomain Structures

Based on the crystal structure of the EphB2 receptor extracellular domain[425] and the ephrinB2-EphB2 tetramer crystal structure[247], it is possible to produce a predicted protein structure for each of the ectodomains using the SWISS-PROT program. Due to the primary sequence and structural homology between the subfamily ligands and receptors, sequence-based structure matching should be sufficiently accurate to assess the location of critical binding domains.

For effective signalling blockade, the structure of the secreted globular domains must be effectively identical to the structure that exists in the native protein. Accurate folding of the second order structures is essential in the ectodomains to ensure correct internal packing of each domain, and hence its overall structure. Rasmol rendering of the SWISS-PROT data indicated that the α-helical and β-sheet structures within each globular domain would be preserved as would the overall domain structure of each ectodomain. Domains required for both the primary and secondary ephrin-Eph interactions are built from flexible loops and α-helices from various non-sequential regions of the primary structure[247, 425-427]. Based on the tertiary structure at the interface of ligand and receptor and the sequence conservation between family members, it is possible to predict those sequences required for the formation of ephrin-Eph dimers and ephrin-Eph-ephrin-Eph stereotetramers[247]. As shown in Figure 3.2, the residues that play essential roles in Eph-ephrin interactions are clearly positionally conserved in the predicted structure of the secreted ectodomains. The structural preservation of these binding interface components implies that specificity (or promiscuity in this case) of binding will be preserved. Obviously SWISS-PROT modelling is only an approximation of the real protein folding, but the general preservation of structure and the formation of the correct amino acid conformation at the binding sites suggests that cognate ligand/receptor

interactions with soluble ectodomains will be of high (nanomolar) affinity and hence be able to block signalling effectively.

Immunoprecipitation and SDS-PAGE of Secreted Ectodomains

The ephrinA5 and EphA7 ectodomain pCS2+ vectors were used to transiently transfect HEK and CHO cells via the calcium phosphate precipitation method. 10-20μg of DNA in an 80% confluent 10cm diameter culture dish (approx. $3x10^6$ cells) produced sufficient ectodomain to produce a 5nM solution. Spin filtration through a 10kDa size-exclusion filter therefore typically resulted in 1ml of 50nM ectodomain product. Detection was performed using the *c-myc* tag capture assay followed by exposure to ephrinA2-AP or EphA2-AP, alkaline phosphatase fusion proteins permitting chromogenic quantification of expression levels. This method indicated that binding was successful at both the immunorecognition tag and also the globular domain. The ability of the ectodomain to bind with high affinity to another soluble receptor/ligand globular domain *in vitro* was especially encouraging as the binding conditions in this scenario are much more stringent than those that will be encountered by the ectodomains *in vivo*.

Coomassie staining of SDS-PAGE gels of ephrinA5 and EphA7 ectodomains immunoprecipitated with anti-*c-myc* antibodies revealed strong, clear expression bands (Figure 3.3A). Immunoprecipitated ectodomains were also detected with anti-*c-myc* antibodies in a Western blot (Figure 3.3B). In all cases, ectodomains ran at the expected molecular weights, approximately 30kDa. Successful immunoprecipitation to pull down the ectodomains prior to electrophoresis and the Western blotting procedure also indicate good binding to the *c-myc* tag. Furthermore, the bands seen in the blots are sharp and distinct with no significant secondary bands nearby. This indicates reliable translation and glycosylation of the complete ectodomain product with minimal degradation.

Stable Cell Line Production for EphrinA5-*cmyc* and EphA7-*cmyc*

Stable cell lines selected for use in the implantation studies demonstrated normal growth rates and morphology. Secretion rates were estimated at

100pmol protein secretion per $3x10^6$ cells over a 24hr period. Immunoprecipitation and SDS-PAGE of the growth medium revealed bands of the appropriate size following Coomassie staining (as per Figure 3.3A). Combined with the successful *c-myc* capture assay with ephrin/Eph-AP detection this confirms that the cell lines are secreting the required ectodomain at good levels.

As well as the ectodomain-secreting lines developed, a number of cell lines were obtained from other researchers. CHO cell lines stably secreting ephrinA5-Fc, ephrinA2-Fc and ephrinA5-AP were a generous gift from Caroline Brennan (Queen Mary, University of London) and ephrinA5-FLAG from was a generous gift from Andrew Boyd (Queensland Institute of Medical Research, Canada).

Assaying Blocking Ectodomains *in vitro*

Before *in vivo* experiments commenced, an assessment of the capacity of each ectodomain to block ephrin signalling *in vitro* was performed.

Coverslip-based Stripe Assays

Stripe assay studies using glass coverslips coated in laminin and stripes of Fc-tagged ephrinA5 produced good outgrowth and lane selectivity. Staining of cultures with phalloidin-Alexa 488 revealed long straight axons (often fasciculated) growing up to 1mm in 48hrs (Figure 3.4A). However, co-staining of cultures with an anti-Fc primary antibody and detection with an Alexa 594-coupled secondary antibody (Figures 3.4B and 3.4C) revealed that, instead of avoiding the ephrinA5, axons were preferentially growing on stripes containing ephrinA5-Fc. Control assays using human IgG Fc on stripes produced an identical selection phenotype (Figure 3.5A). Subsequent experiments with stripes produced following injections of sterile PBS only also produced this outgrowth phenotype. A final round of experiments were performed to identify the cause of the complications. It appears that, on removing the matrix from the coverslip, the poly-L-lysine remains attached to the matrix rather than to the coverslip. This results in pronounced lanes of poly-L-lysine separated by glass. This is readily visible by washing the coverslips and then incubating

them with Albumin-Alexa 594 (see Figure 5.5B). Subsequent incubations therefore only deposit material on the 'channel' stripes hence, despite these stripes containing ephrinA5-Fc, they are the only substrate that will support growth as axons are unable to grow on glass. As the chemorepulsive action of ephrinA5 is only effective over long time periods when there are alternative growth substrates, the neurites eventually grow on the ephrinA5 lanes. Conversations with a number of groups who have worked with this form of stripe assay indicated that this is a commonly found, but little reported, problem with this assay. Hence, alternative assays were pursued to investigate the efficacy of ectodomain signalling block.

Filter-based Stripe Assays

CHO cell membrane fragments or ~300kDa Poly-D-Lysine appeared to successfully bind to the filter surface and remain in place for the period of incubation, as indicated by the preservation of Alexa^{594}-BSA staining (see Figure 3.M11B). Axons were successfully visualised using a phalloidin-Alexa 488 conjugate but outgrowth was frequently poor, especially on HEK293 membranes (Figure 3.5C), and did not show any evidence of responding to the substrate stripes.

Neurite Outgrowth Assay

As the stripe assay did not provide a useful framework to draw convincing conclusions about ectodomain efficacy, the outgrowth assay was used[421]. This is based on *in vitro* assays used to assess the effects of astrocytes on dendrite or axon outgrowth from neuronal explants[422]. Temporal E6 chick retinal ganglion cells were dispersed on near-confluent layers of HEK293 cells or HEK cells transiently transfected with full-length ephrinA5a. Following fixation and staining with an anti-neurofilament antibody, the effect of including the EphA7 or ephrinA5 ectodomains in the co-culture stage could be assessed (Figure 3.6A). The average axonal lengths for neurons cultured in each condition were assessed under a fluorescence microscope under blinded conditions. However, as shown in Figure 3.6B, growth on the HEK-ephrinA5 cells appears to be more robust. The time course of the growth cone-collapsing response induced by ephrins is short, with axons generally

recovering after 30min[405]. This means that the axon avoidance response will only be functional when there are alternative substrates available. Hence, in this culture, once axons have adapted to growing on the ephrinA5, there is no impediment to growth. The increased outgrowth may, in fact, be attributable to the ephrinA5a itself as this could provide a further substrate for attachment.

Collapse Assays

Because of these complications, it became necessary to use another technique to assess the efficacy of my ectodomain blockers. The collapse assay is a simple technique utilizing retinal ganglion cell growth cone collapse. EphrinA5-Fc (when homodimerised) induces growth cone collapse of EphA3-positive E6 chick temporal RGC axons. Co-application of a blocking ectodomain together with the ephrinA5-Fc to cultures should protect growth cones from collapse, permitting assessment of ectodomain efficacy. Explants of ~1mm square RGC tissue put out long, occasionally fasciculated axons (up to 300μm) in 24hrs. Uncollapsed growth cones were obvious due to their spread out phenotype with multiple extended filopodia and lamellipodia (Figure 3.7A). Collapsed growth cones were also readily identified by their compressed and highly actin-dense heads which often retained a single characteristic filopodium (Figure 3.7B).

Baseline collapse present following addition of pre-warmed sterile PBS was 28% in agreement with published data[341]. The positive collapse control, NOC-7, induced a large-scale collapse (80 ±12%) also equivalent to that reported in the literature[423] suggesting the system is responsive to collapse and this change is accurately picked up by the staining, imaging and quantification. Two monomeric blockers were assayed in this culture; the EphA7-*c-myc* ectodomain and the ephrinA5-Fc monomer. Both showed robust and reliable abrogation of the collapse action and, on their own, demonstrated no collapsing ability (Figure 3.8). Growth cones treated with sterile PBS alone showed a 28 ± 9% (± 95% confidence interval) collapse rate, similar to the 31 ± 12% collapse rate of growth cones treated with the EphA7-*cymc* ectodomain and the 19 ± 10% collapse rate of growth cones treated with the ephrinA5 ectodomain. The 68 ±6% collapse rate of growth cones exposed to 20nM

dimeric ephrinA5 was significantly different to all three control assays ($p < 0.001$ Fisher's Exact Two-Tailed Test). Co-application of 80nM monomeric ephrinA5 ectodomain or pre-incubation of the dimeric ephrinA5 with 80nM monomeric EphA7 induced a collapse rate of 34 ±5% and 31 ±9%, respectively. These values are significantly different from the collapse rate seen for dimeric ephrinA5 alone ($p < 0.001$ Fisher's Exact Two-Tailed Test).

Control Cell Implantation Studies

Cell implantation studies are established for some cell lines[428-430], notably some of the original work by Martin Schwab and co-workers used IN-1 secreting hybridomas implanted into the ventricular system[114]. However, there are no reports in the literature that describe the implantation of non-rat mammalian cell lines into rat nervous system. Hence, preliminary work focussed on minimising side-effects due to implantation and stabilising the cell mass within the animal. To identify and locate implanted cells, a normal CHO cell line was transduced with a lentivirus encoding soluble EGFP. The expression ratio for this virus was remarkably high (~99%) at a MOI of approximately 5 permitting the localisation of nearly all cells implanted in the animals (Figure 3.9A). Later studies using clonal cell lines secreting ectodomains incorporated a 5% cell population from this EGFP-expressing line to permit visualisation of the cell mass *in vivo*.

Injection of EGFP-expressing CHO cells into rat lateral ventricles using stereotaxic coordinates was successful and cells appeared to have integrated into the ventricular walls within 3 days. 40µm coronal sections through the injection site revealed numerous EGFP-positive cells (Figure 3.9B) with a typical CHO cell morphology suggesting that at this time point no immune rejection had occurred. However, staining for OX-42 revealed a strong macrophage and microglia response (Figures 3.9B and 3.9C) around the lesion with activated immune cells closely associated with implanted CHO cells. Hence, despite prior immunosuppression of animals with FK506, immune rejection of the implant occurred and OX-42-positive macrophages and microglia would be expected to clear EGFP-CHO cells within the following days.

An alternative approach was then employed; to enhance access of the soluble blocking proteins to the lesion site and to improve the immunosuppressant exposure, cells were implanted near the lesion site (Figure 3.M12A). Collagen gelfoams were seeded with EGFP-CHO cells and this material was sutured onto the dura at the lesion site. Preliminary studies indicated that these cells became highly metastatic following exposure to the injured spinal cord environment and invaded the lesion site in a similar manner to endogenous meningeal fibroblasts. As can be seen in Figure 3.10A, EGFP-positive CHO cells can be seen penetrating the original margin of the spinal cord and invading the lesion cavity, past surviving GFAP-positive astrocytes. Endogenous meningeal fibroblasts in the lesion site are a source of growth inhibitors and interact with reactive astrocytes to induce the formation of the glial scar. Hence, the presence of exogenous fibroblasts in the lesion site is unlikely to be conducive to successful regeneration. However, minimal immune rejection had occurred suggesting that this method of blocker delivery warranted further investigation. To avoid this complication, seeded collagen gelfoams were then implanted 1-2mm rostral to a lesion site (Figure 3.M12B). Ten days following dorsal column lesion, minimal invasion by endogenous macrophages or microglia was seen and the implanted cells demonstrated their typical spread-out morphology. No obvious invasion of tissue was apparent suggesting this technique would provide a reliable platform for ectodomain delivery.

The data presented in Chapter II and in the published scientific literature suggests that ephrinB ligand interactions with EphA4 are likely to be a major determinant of functional recovery following spinal cord injury. The ephrinA5 ectodomain was therefore selected as the primary blocker for investigation. Control CHO cells or secreting cells (CHO-ephrinA5) were seeded onto collagen gelfoams and maintained in culture for two days before being sown onto the dura over a region of undamaged spinal cord. Animals were investigated over a two week period, receiving FK-506 injections prior to, and throughout, the investigation. Corticospinal tract regeneration following implantation of the cell lines was traced using BDA injection to the motor

cortex at the time of injury. Two weeks following injury the animals were perfused with 4% paraformaldehyde and their spinal cords removed.

Ectodomain Effects on Spinal Regeneration

The main gross anatomical observation of the excised tissue was the presence, in all animals, of a large tumourific cell mass centred on the collagen gelfoam. Horizontal freezing microtome sections of the spinal cords revealed that the invasion of the gelfoam by meningeal fibroblasts (and also probably the proliferation of implanted fibroblasts) had placed pressure on the uninjured cord within the constraints of the dura, causing some deformation (Figure 3.10B). While there was no obvious locomotor deficiency in the animals other than that expected in the 48-72hrs following surgery, some disruption of ascending and descending pathways must have occurred. The BDA-labelled CST was seen to have been displaced by the cell mass to a level more deep than usual although both rostral and caudal to the implant it appeared anatomically normal. At the lesion site, caudal to the implant, BDA-labelled CST axons were seen to extend to the lesion site with typical dorsal CST morphology in all animals (Figure 3.11).

As the sample number for this study was small (n = 2 for control and experimental) no statistical conclusions can be drawn. Furthermore, the extent of the 'tumour' produced by the implant was such that it would not be humane to perform further experiments of this nature to draw more firm conclusions. However, observations of the injury site do permit some useful information to be gained from the investigation. In animals receiving CHO-ephrinA5 implants, the degree of CST retraction was visibly smaller than that found in the CHO animals (Figure 3.11B compared to 3.11A). Individual termination bulbs in the ephrinA5-treated animals were seen to be putting out sprouts towards the lesion site (Figure 3.12A) many of which reached the lesion margin, as defined by GFAP staining (Figure 3.12B). However, the extent of glial scarring and cyst formation did not seem to be affected by the presence of the ephrinA5 ectodomain. Similarly there was no change in the upregulation of GFAP by reactive astrocytes (Figure 3.12C).

DISCUSSION

Ectodomain Expression

Predictive modelling of each ectodomain using SWISS-PROT based on existing X-ray crystal structures suggested that the extracellular regions selected will correctly fold and will bind with good affinity to endogenous full-length Ephs and ephrins. Regions of the proteins known to be important in the formation of receptor-ligand complexes are retained and predictive folding suggests they will be correctly positioned for high affinity binding. Furthermore, sufficient secondary and tertiary structure appears to be preserved within the globular domains to retain correct folding and stability in solution. This is supported by the data from the *c-myc* capture assay that indicates not only binding at the *c-myc* immunorecognition tag to capture the ectodomain, but also high affinity binding at the binding domains to permit effective chromogenic detection of the ectodomains using the AP-tagged constructs. The SDS-PAGE data also shows the ectodomains migrate at the expected molecular weight and are immunodetectable under Western blotting conditions.

The release rate of the ectodomains from the stable cell lines was also encouraging. Assuming a 40µL volume of CSF within the spinal cord (the likely volume of dilution for secreted ectodomain), Figure 3.13 shows the likely concentration profile following implantation. Assuming a 50nM concentration is required (based on the *in vitro* findings of Murai et al.[389] and a 4:1 molar ratio for effective blockade) 22hrs will be required before a 'therapeutic' concentration has been reached. This is a reasonable time window for beneficial function. The use of a cell line as the means of production of the ectodomains means that the products should always be properly glycosylated and folded, a requirement for effective binding and signalling blockade.

Collapse Assays

The collapse assay offers the benefits of being highly responsive and readily quantifiable. The monomeric blockers produced by the stable cell lines CHO-ephrinA5 and CHO-EphA7 were assayed in this culture; the EphA7-*cmyc* and ephrinA5-*cmyc* ectodomains. The 70% collapse of the growth cone population

induced by dimeric ephrinA5 was almost completely attenuated by monomeric ephrinA5 or EphA7 in a 4:1 molar ratio. Hence, in the context of EphA3-based collapse of E6 chick RGC growth cones, the EphA7 and ephrinA5 ectodomains are both capable of interrupting Eph-ephrin interactions *in vitro*. The lack of toxic or other side-effects and the high affinity and very efficacious blockade of A-class ephrin signalling suggests the blockers will work effectively in the injured spinal cord environment.

Imaging data suggested that both NOC-7 and ephrinA5 induce lamellipodial withdrawal and growth cone collapse, but filopodia appear to remain attached and extended. This is unsurprising as it is known that following the initial collapse response to ephrinA family proteins, axons recover and continue to grow as long as the ephrin concentration remains constant, suggesting that the collapse response is rapidly reversible and does not involve large-scale actin depolymerisation.

Cell Implantation Studies

Considering the work of Professor Schwab's laboratory[114] using IN-1 secreting hybridomas implanted in the ventricular system, it was surprising to find such rapid and efficacious immune rejection of the ventricularly implanted CHO-EGFP cells following three days of FK-506 administration. However, communication with authors from this publication suggested that during these studies the balance of immunosuppression and cell implantation was a very delicate one that required many repetitions. Too great a dose of immunosuppressant and the cell line became malignant and proliferative and form a tumour mass, too small a dose of immunosupression and the implant was rapidly removed by invading macrophages and microglia. Our dosing of the FK-506 was identical to that used throughout all the other implants and the drug is known to pass the blood-brain barrier. Furthermore the size of the implant was small. However, perhaps the formation of a hole into the brain by the stereotaxic injection might have permitted an influx of meningeal cells that may have enhanced the immune response.

The opposite reaction, i.e. an aggressive implanted cell response, was seen in the second implant study (Figure 3.M12A). The implanted cells were obviously not held in check by the usual anti-proliferative mechanisms and were able to aggressively invade the lesion cavity. The proliferation of the implanted cell line, and the likely invasion of the collagen gelfoam by endogenous meningeal fibroblasts, were unexpected and unfortunate as this 'on lesion' implant offers the best delivery of ectodomain.

The final implantation method used (Figure 3.M12B), highlighted the main complication of the procedure – the difficulty in balancing the immunosuppression with the implantation volume. In the initial CHO-EGFP pilot animal, the cell implant remained quiescent and showed no proliferation or invasive tendency. However, an identical FK-506 dosing regime and cell implantation number with the CHO or CHO-ephrinA5 implant, produced massive proliferation/invasion and the formation of a tumour mass. Slight differences in the proliferative capacity of the three cell lines could perhaps have tipped the proliferation/engulfment balance towards growth.

Perhaps a method of encapsulating the cell implant, as has been used previously with PC12 cells[431], would prevent these unwanted side effects but still permit effective ectodomain delivery. Such a development would be costly and time-consuming and the para-lesion implant offers almost as effective delivery. The collagen gelfoam, while an excellent substrate for the growth of the fibroblastic CHO cells used in the study, is obviously also likely to provide an attractive target for meningeal fibroblasts. Perhaps a substrate that can support cells under media-rich *in vitro* culture conditions but does not provide a favourable platform for proliferation would be a more suitable choice.

Despite the low replication numbers (n of 2 for control and experimental), a number of interesting observations can be made. CHO-ephrinA5 animals show a clear reduction in the retraction of the bulk of the termination bulbs from the lesion margin (as defined by GFAP staining) compared to control animals (Figure 3.12). This supports the concept outlined in Chapter II that EphA4 in the CST axons mediates this retraction from the lesion site in the

first few days following injury. Furthermore, CHO-ephrinA5 animals show improvements in regenerative sprouting of processes towards the lesion site with many of these growing as far as the astrocyte margin (Figures 3.13A-B).

In the work of Goldshmit *et al.*[12], knocking out the EphA4 gene is shown to reduce astrocytic gliosis and reactivity following spinal cord injury and to diminish the wound-healing response *in vitro*. Furthermore, the lesion site produced 6 weeks after a lateral white matter injury in EphA4 knock-out mice was described as minimal and often hard to distinguish, with numerous spouting/regenerating axons traversing its length. However, in the CHO-ephrinA5 animals, the extent of glial scarring and cavity formation following central white matter injury did not seem to be affected by the presence of the ephrinA5-*c-myc* ectodomain (Figure 3.12C). Similarly there was no apparent change in the upregulation of GFAP by reactive astrocytes, when compared to spinal cord injuries in the CHO animals. Assuming that effective blockade is occurring at the EphA4 receptor, which is certainly indicated by the observations of increased sprouting, this suggests that blocking the EphA4 receptor encourages CST regenerative sprouting but does not prevent astrocytic gliosis. Two possibilities would account for this:

- EphA4 in astrocytes is transactivated by cytokines released after injury and the ligand binding domain of the receptor is not required for the role of the receptor in astrocytic gliosis.
- EphA4 on the CST is a major mediator of the inability of injured CST axons to regenerate (as outlined in Chapter II).

The concept of EphA4 being transactivated during astrocytosis is proposed in the work by Goldshmit *et al.*[12]. In this model activation of EphA4-mediated signalling is required for the cytokine-mediated signals that induce astrocyte reactivity. Which component of EphA4 signalling (i.e. PDZ-, SH-2- or kinase-mediated) is not known, but it is likely to be independent of ligand binding to the receptor, unless *cis*-interactions with co-expressed ephrinB2 were sufficient. This hypothesis would agree well with the data presented here. Hence, while inhibitory post-injury responses due to EphA4 on the CST are minimised, those due to EphA4 on astrocytes are unaffected.

The second possibility would account for the improvements seen in regenerative sprouting despite the lack of effect on the lesion site and astrocytic gliosis. Inhibiting EphA4 will minimise the repulsive interactions induced by ephrinB2 in reactive astrocytes and ephrinB3 expressed in damaged myelin. The ability of the CST termination bulbs to sprout and put forward regenerative processes towards the lesion site in animals receiving the ectodomain implant suggests that EphA4 is a major, if not the only, negative mediator preventing the CST from undergoing a normal regenerative response to injury. Furthermore, by reducing the extent of the CST die back, the platform for regeneration is significantly improved and presents a scenario for regeneration that will likely synergise with other treatments.

One other possibility is that other EphA receptors may be expressed in the lesion site. Data presented here (Figure 3.6A) and in published form[318] suggest that this is the case but as yet no localisation of these receptors has been performed. While it is possible that another EphA receptor may be partially responsible for the improvements in CST regeneration seen, this is unlikely as no study to date has identified any such receptor in the cortex during adulthood. Furthermore EphA4 alone is responsible for CST targeting during development[234, 319]. Also, Chapter IV demonstrates that the increased regeneration seen here can be entirely attributed to blockade of EphA4 alone.

CONCLUSION

While the observations detailed suggest that further experimentation with this implantation technique could yield exciting and interesting data, the invasion of non-pathological tissue by the implants suggests that this method of blocker delivery may cause discomfort to the animals and is hence not suitable for longer term investigation. The data highlights inhibition of EphA4 as a promising candidate for improving spinal cord regeneration following injury and this has been pursued pharmacologically in Chapter IV.

Figure 3.M1

EphrinB1 Ectodomain cloned into pEF-BOS

B1-Forw: Sequence derived from 5' cloning primer.
B1-R/C: Reverse complement of sequence derived from 3' cloning primer.
Expected: Anticipated sequence of clone.

Red boxes highlight the ATG translation start site, the GAGCAGAAGCTTATCCTCGGAGGAGGACCTG sequence encoding the *c-myc* tag and the TAA translation stop site.

Images produced using multiple sequence alignment with hierarchical clustering[432] with red text indicating perfect agreement between both sequences and the expected sequence and blue text highlighting regions where only one sequence agrees with the expected result.

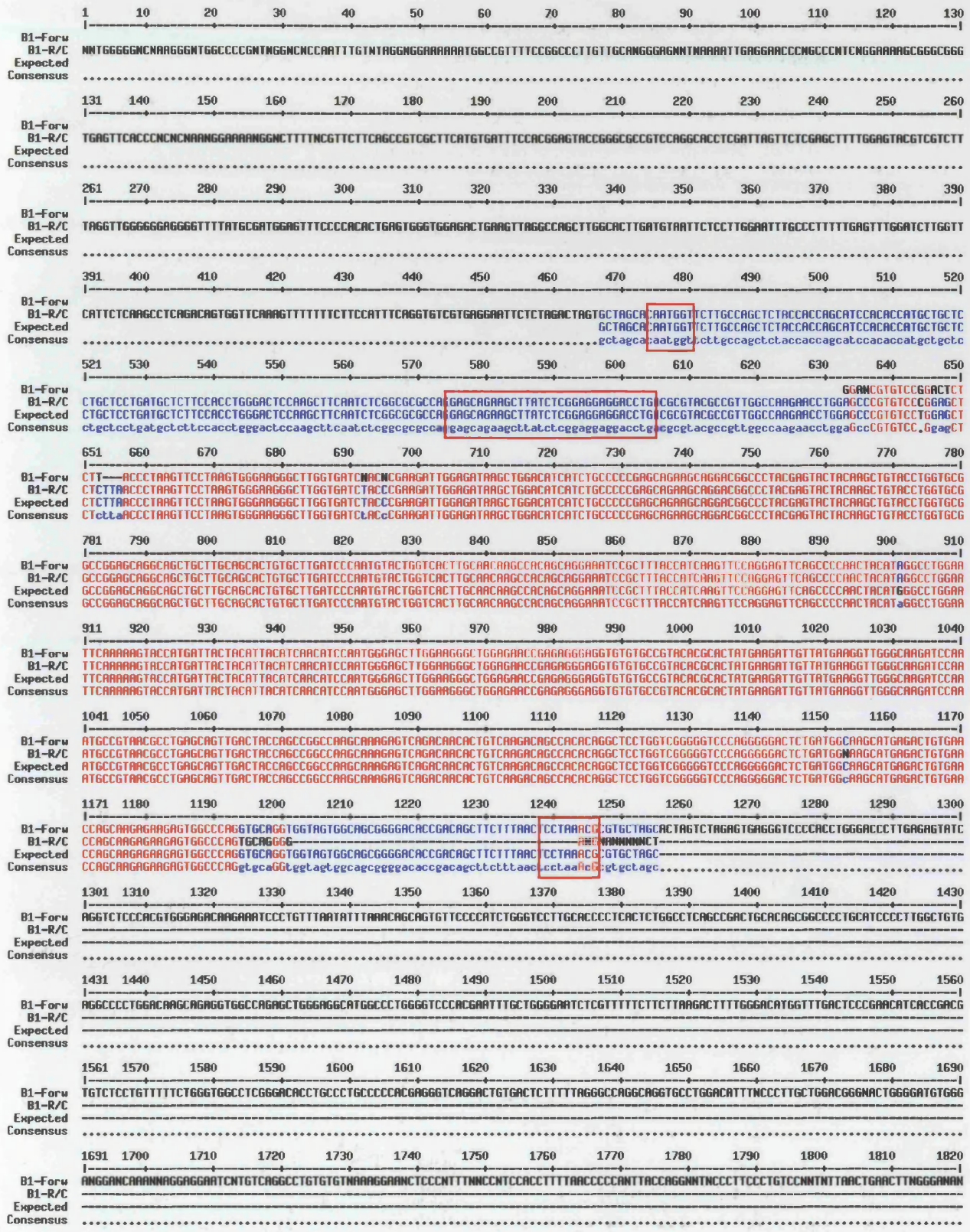
B1-Forw
B1-R/C
Expected
Consensus

Figure 3.M2

EphrinB1 Ectodomain cloned into pCS2+

B1-Forw: Sequence derived from 5' cloning primer.
B1-R/C: Reverse complement of sequence derived from 3' cloning primer.
Expected: Anticipated sequence of clone.

Red boxes highlight the ATG translation start site, the GAGCAGAAGCTTATCCTCGGAGGAGGACCTG sequence encoding the *c-myc* tag and the TAA translation stop site.

Images produced using multiple sequence alignment with hierarchical clustering[432] with red text indicating perfect agreement between both sequences and the expected sequence and blue text highlighting regions where only one sequence agrees with the expected result.

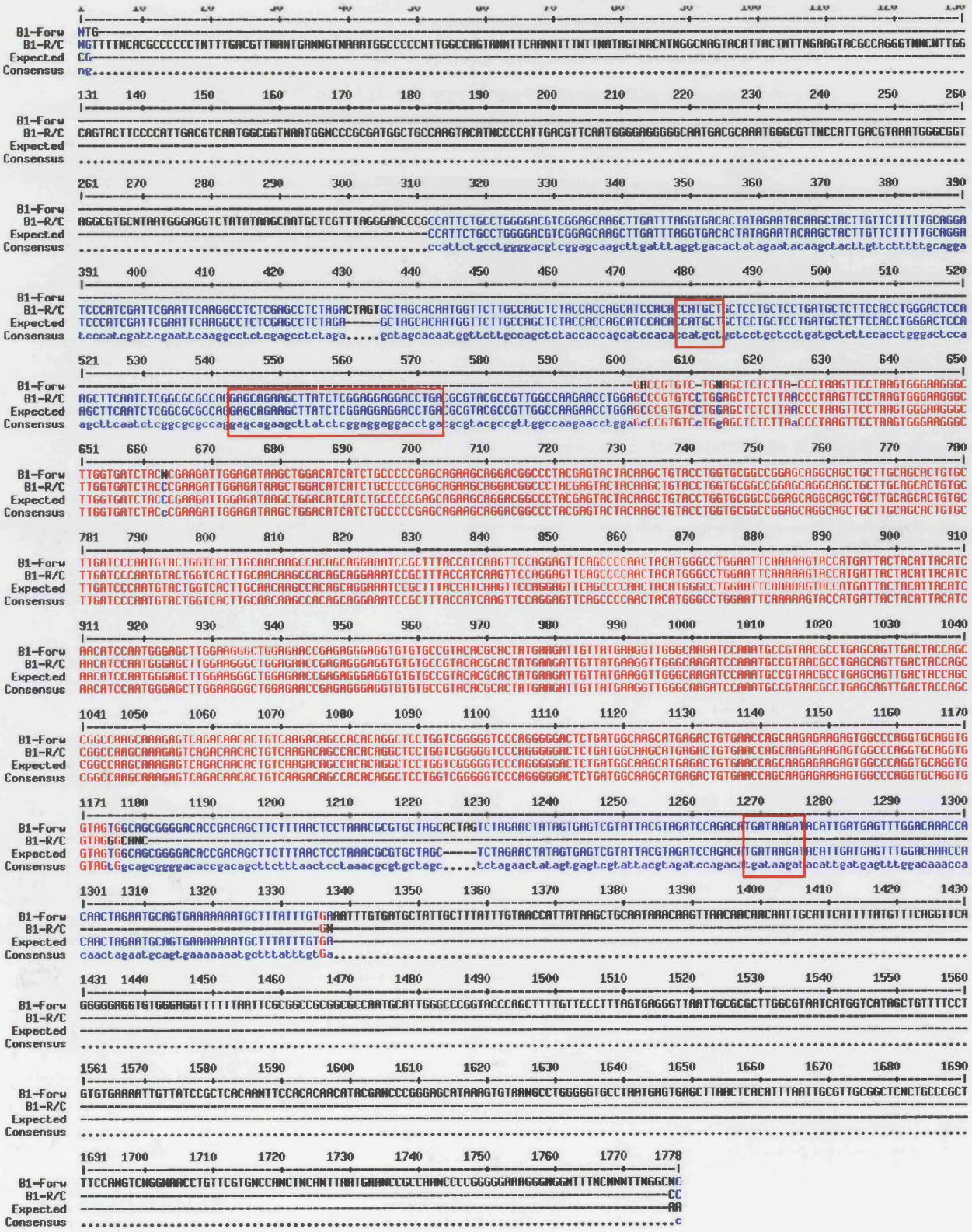

Figure 3.M3

EphB3 Ectodomain cloned into pEF-BOS

B3-Forw: Sequence derived from 5' cloning primer.
B3-R/C: Reverse complement of sequence derived from 3' cloning primer.
Expected: Anticipated sequence of clone.

Red boxes highlight the ATG translation start site, the GAGCAGAAGCTTATCCTCGGAGGAGGACCTG sequence encoding the *c-myc* tag and the TAA translation stop site.

Images produced using multiple sequence alignment with hierarchical clustering[432] with red text indicating perfect agreement between both sequences and the expected sequence and blue text highlighting regions where only one sequence agrees with the expected result.

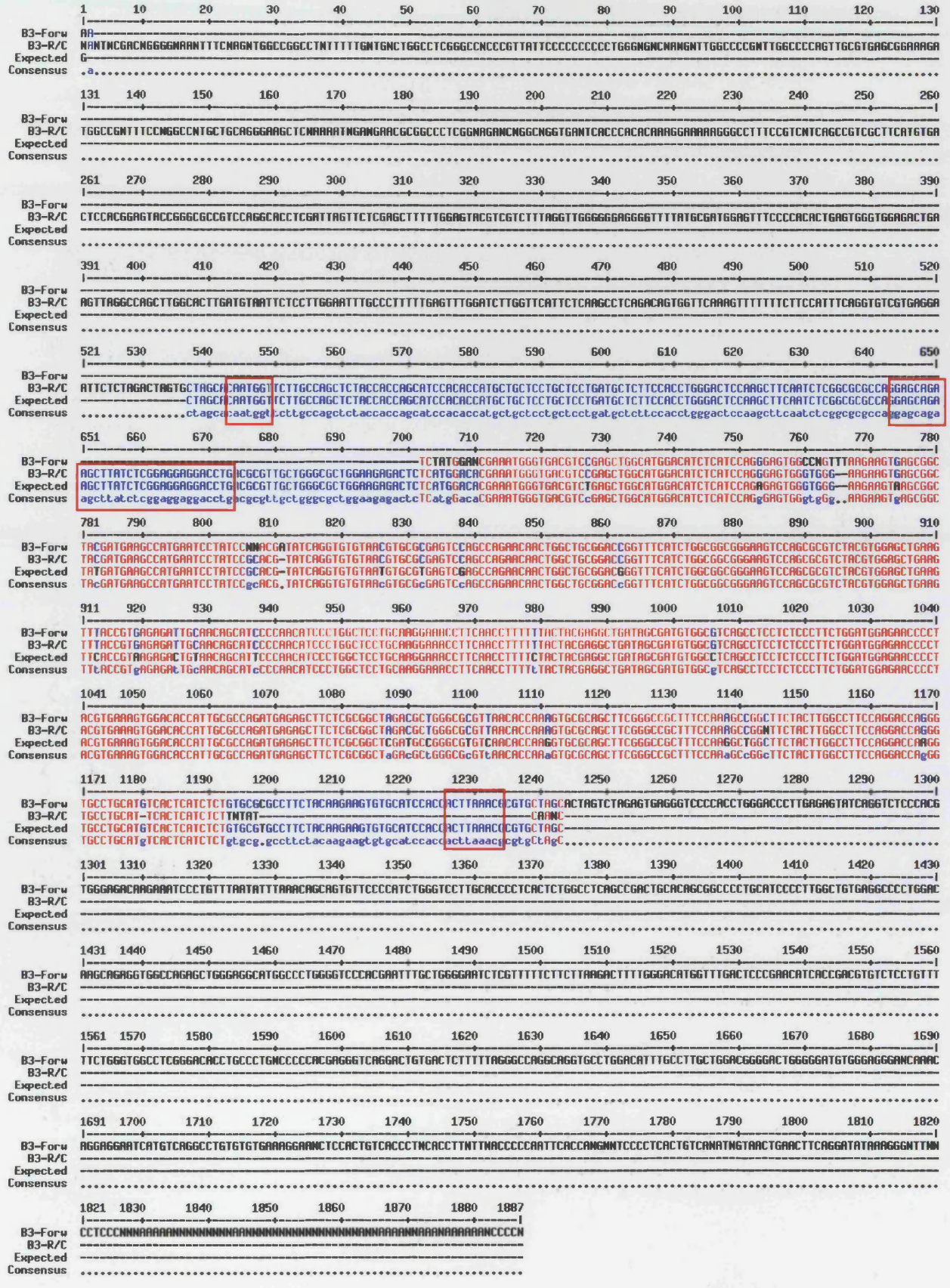
B3-Forw
B3-R/C
Expected
Consensus

Figure 3.M4

EphB3 Ectodomain cloned into pCS2+

B3-Forw: Sequence derived from 5' cloning primer.
B3-R/C: Reverse complement of sequence derived from 3' cloning primer.
Expected: Anticipated sequence of clone.

Red boxes highlight the ATG translation start site, the GAGCAGAAGCTTATCCTCGGAGGAGGACCTG sequence encoding the *c-myc* tag and the TAA translation stop site.

Images produced using multiple sequence alignment with hierarchical clustering[432] with red text indicating perfect agreement between both sequences and the expected sequence and blue text highlighting regions where only one sequence agrees with the expected result.

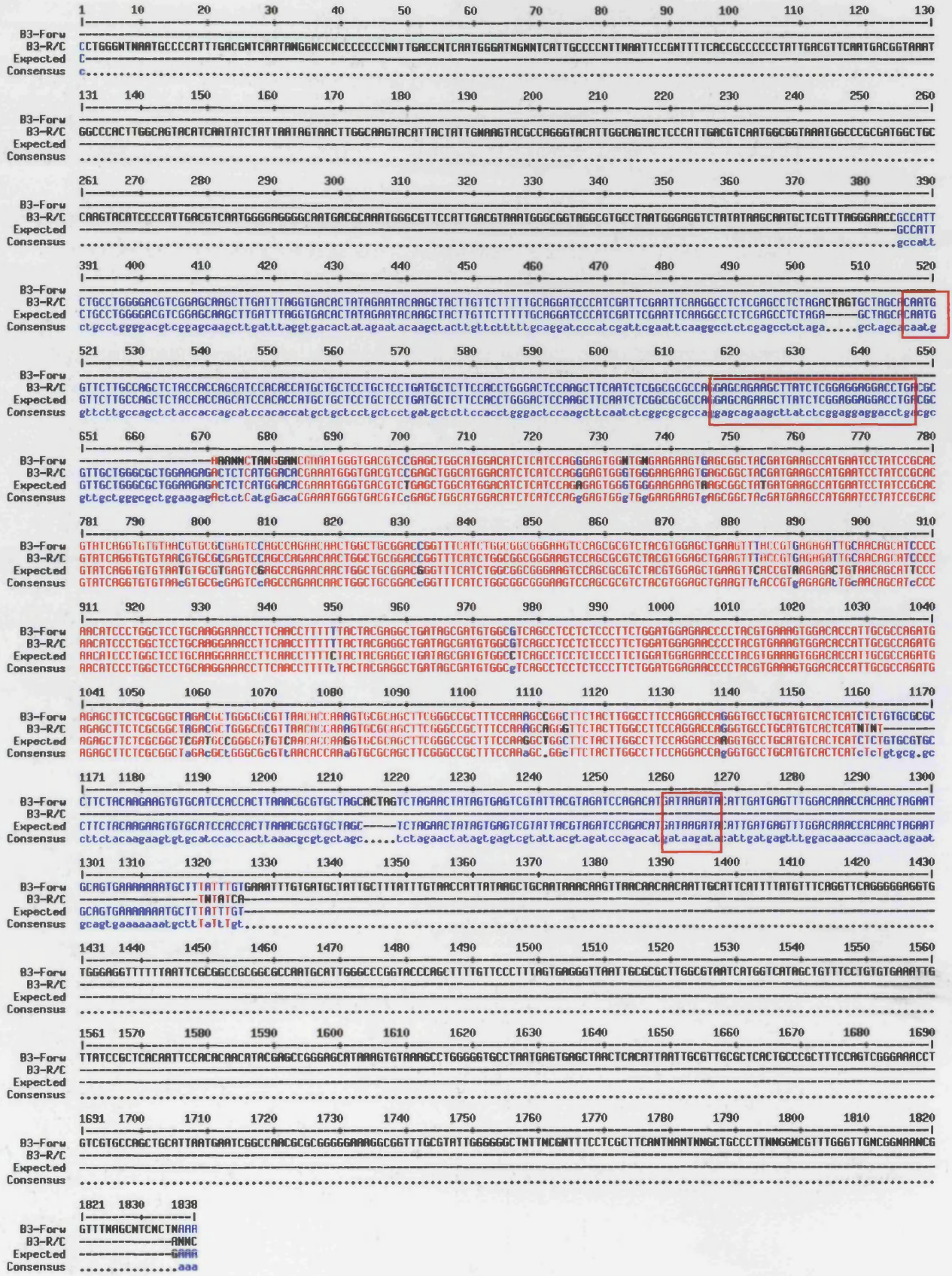

Figure 3.M5

EphrinA5 Ectodomain cloned into pEF-BOS

A5-Forw: Sequence derived from 5' cloning primer.
A5-R/C: Reverse complement of sequence derived from 3' cloning primer.
Expected: Anticipated sequence of clone.

Red boxes highlight the ATG translation start site, the GAGCAGAAGCTTATCCTCGGAGGAGGACCTG sequence encoding the *c-myc* tag and the TAA translation stop site.

Images produced using multiple sequence alignment with hierarchical clustering[432] with red text indicating perfect agreement between both sequences and the expected sequence and blue text highlighting regions where only one sequence agrees with the expected result.

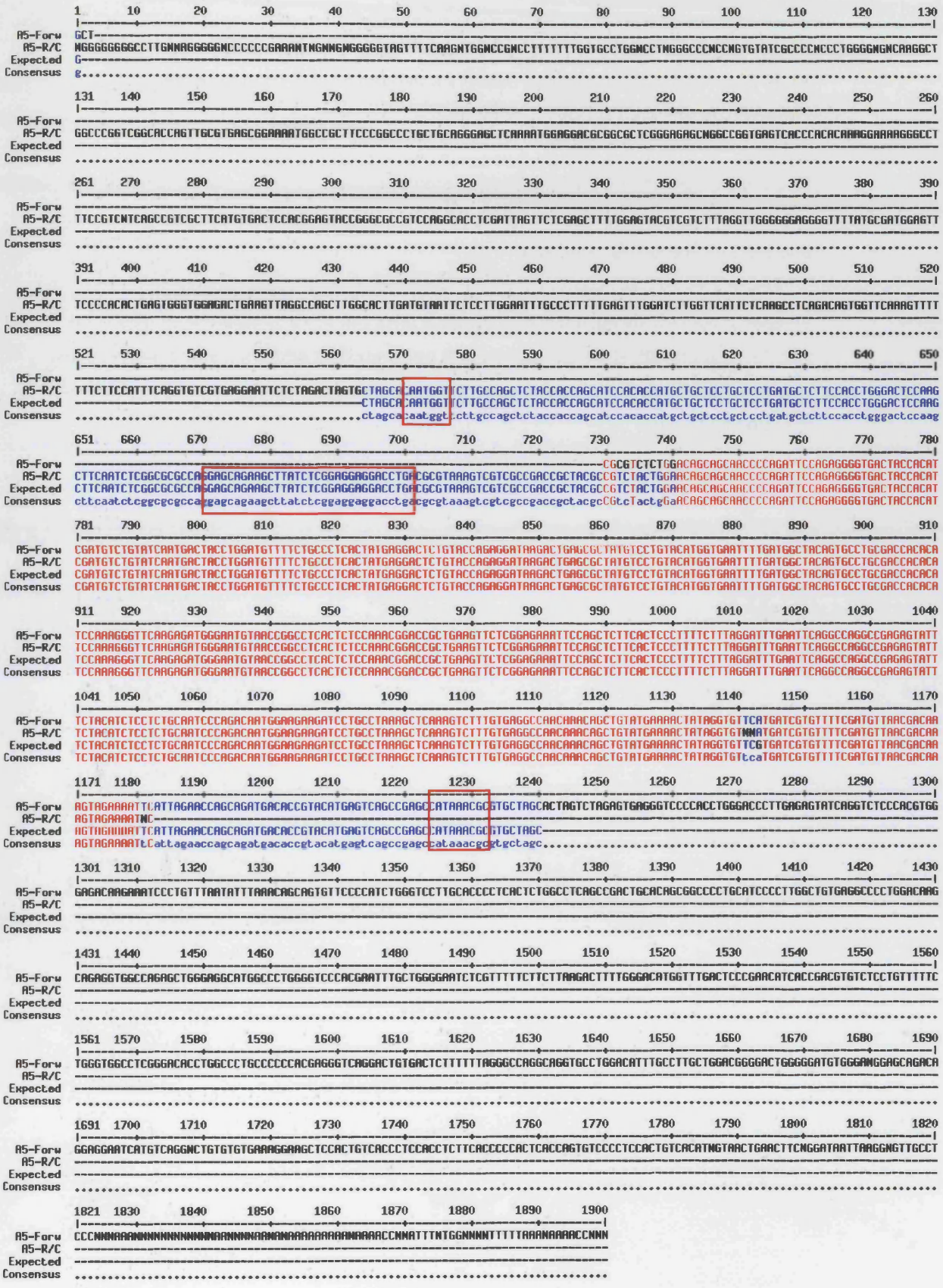
A5-Forw
A5-R/C
Expected
Consensus

Figure 3.M6

EphrinA5 Ectodomain cloned into pCS2+

A5-Forw: Sequence derived from 5' cloning primer.
A5-R/C: Reverse complement of sequence derived from 3' cloning primer.
Expected: Anticipated sequence of clone.

Red boxes highlight the ATG translation start site, the GAGCAGAAGCTTATCCTCGGAGGAGGACCTG sequence encoding the *c-myc* tag and the TAA translation stop site.

Images produced using multiple sequence alignment with hierarchical clustering[432] with red text indicating perfect agreement between both sequences and the expected sequence and blue text highlighting regions where only one sequence agrees with the expected result.

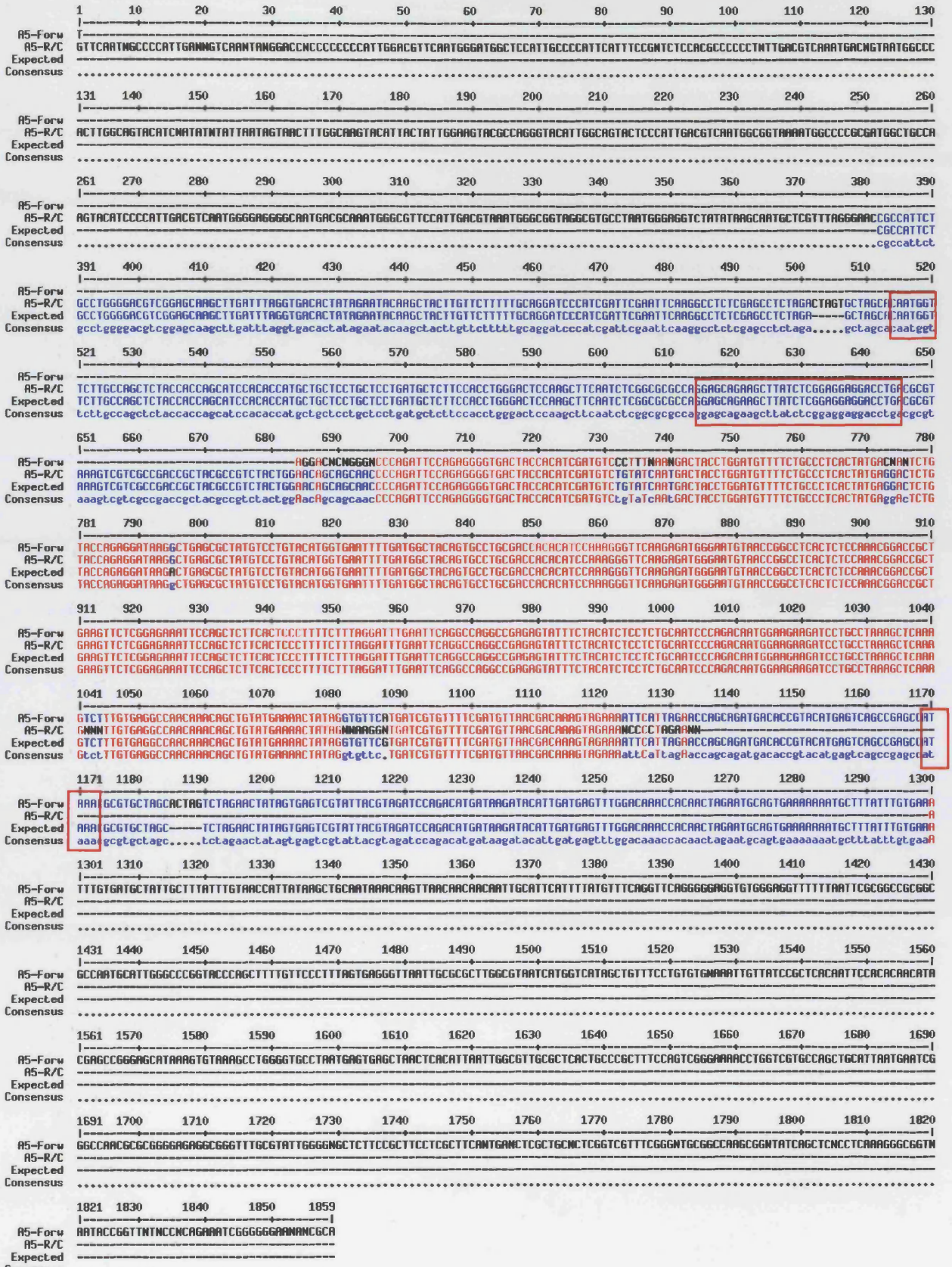
A5-Forw
A5-R/C
Expected
Consensus

Figure 3.M7

EphA7 Ectodomain cloned into pEF-BOS

A7-Forw: Sequence derived from 5' cloning primer.

A7-R/C: Reverse complement of sequence derived from 3' cloning primer.

Expected: Anticipated sequence of clone.

Red boxes highlight the ATG translation start site, the GAGCAGAAGCTTATCCTCGGAGGAGGACCTG sequence encoding the *c-myc* tag and the TAA translation stop site.

Images produced using multiple sequence alignment with hierarchical clustering[432] with red text indicating perfect agreement between both sequences and the expected sequence and blue text highlighting regions where only one sequence agrees with the expected result.

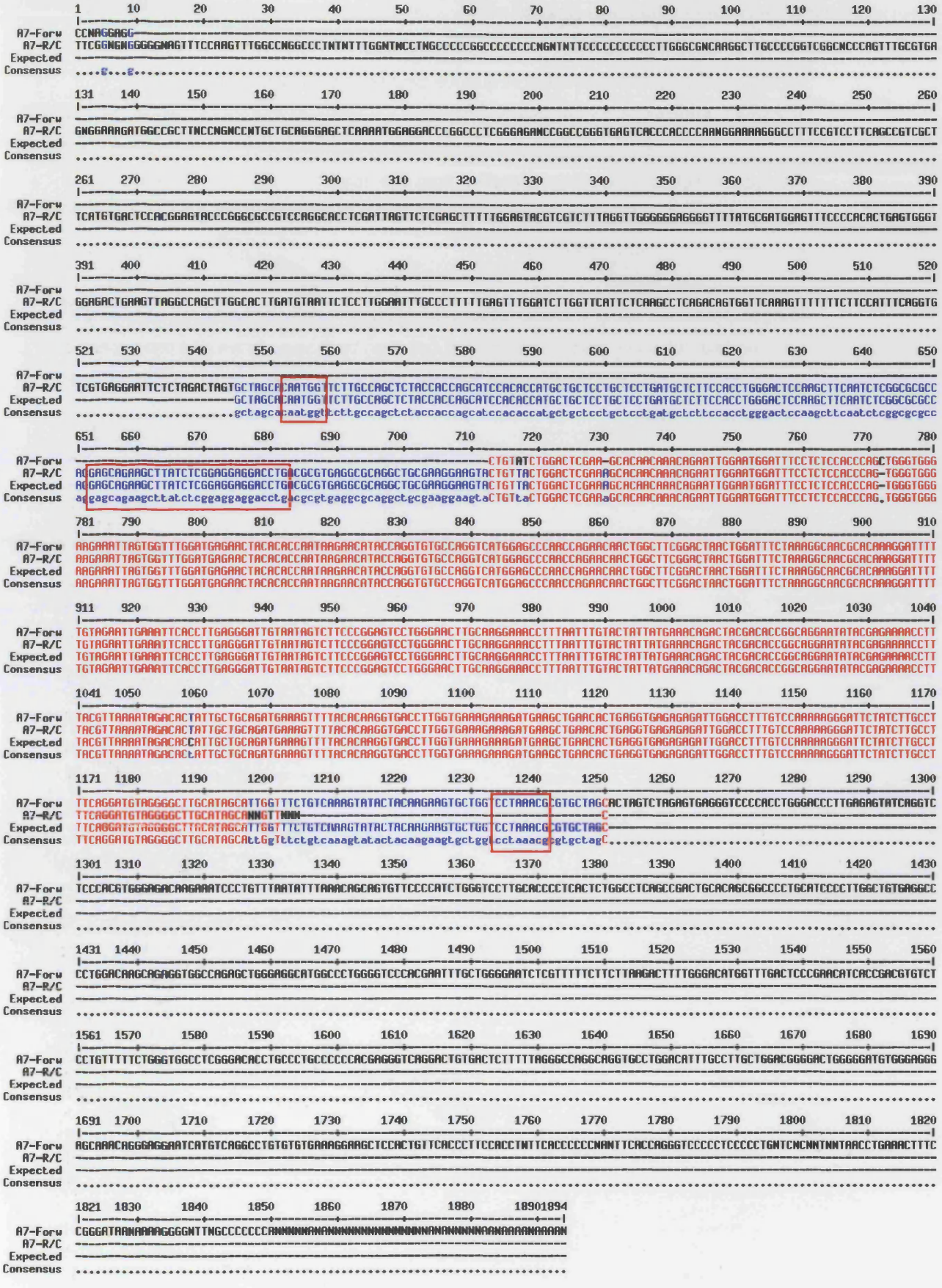
A7-Forw
A7-R/C
Expected
Consensus

Figure 3.M8

EphA7 Ectodomain cloned into pCS2+

A7-Forw: Sequence derived from 5' cloning primer.

A7-R/C: Reverse complement of sequence derived from 3' cloning primer.

Expected: Anticipated sequence of clone.

Red boxes highlight the ATG translation start site, the GAGCAGAAGCTTATCCTCGGAGGAGGACCTG sequence encoding the *c-myc* tag and the TAA translation stop site.

Images produced using multiple sequence alignment with hierarchical clustering[432] with red text indicating perfect agreement between both sequences and the expected sequence and blue text highlighting regions where only one sequence agrees with the expected result.

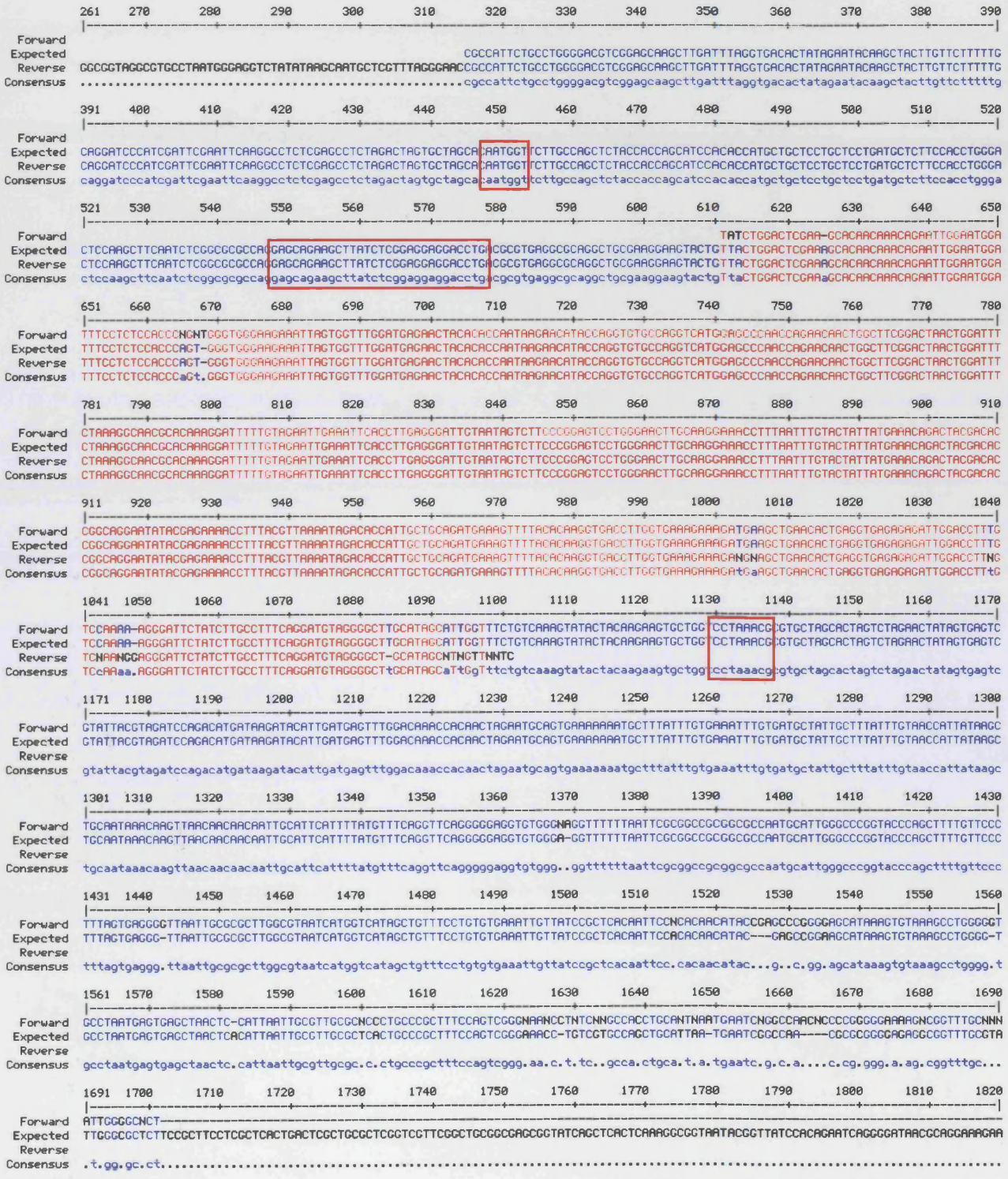

Figure 3.M9

pEF-BOS and pCS2+ vector diagrams

A. Simplified vector diagram of the pEF-BOS vector showing the EF1α (elongation factor 1α) promoter, the IL-3 secretion signal, the MluI cloning site and the XbaI sites used for subsequent sub-cloning.

B. Simplified vector diagram of pCS2+ showing the CMV promoter and XbaI site used for cloning.

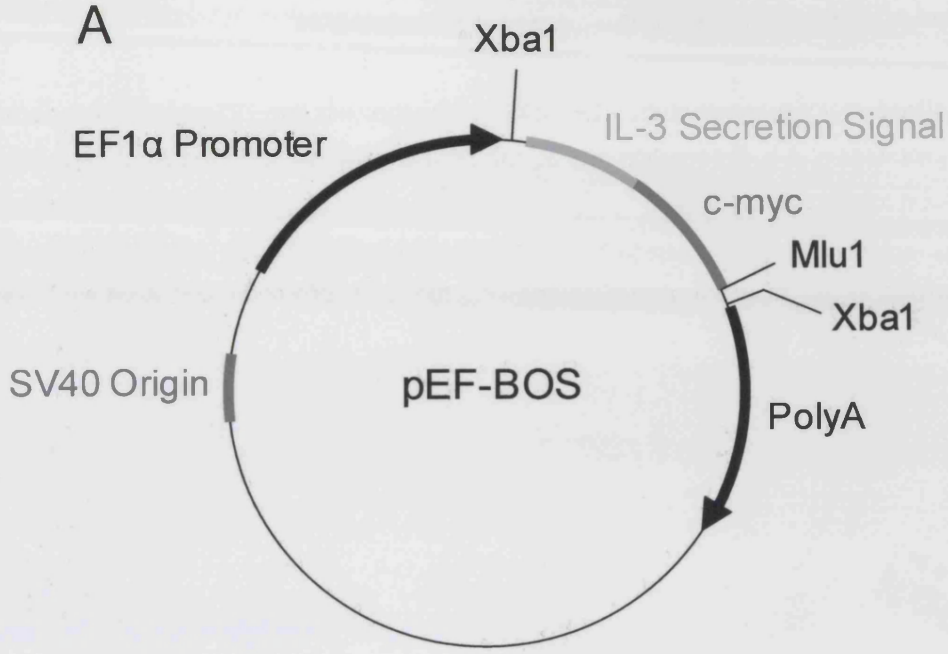
A
Xba1
IL-3 Secretion Signal
EF1α Promoter
c-myc
Mlu1
Xba1
SV40 Origin
pEF-BOS
PolyA

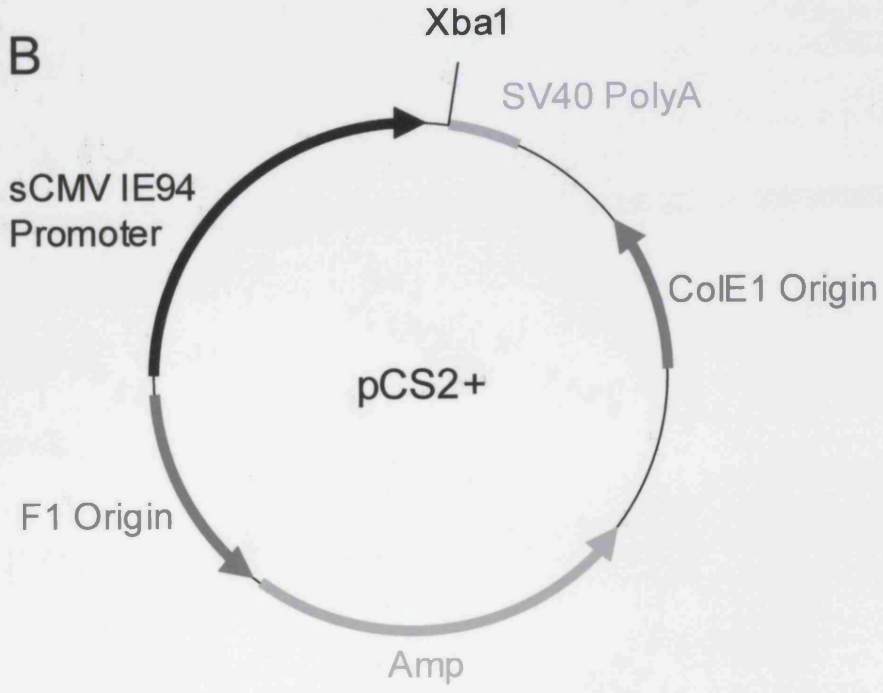
B
Xba1
SV40 PolyA
sCMV IE94
Promoter
ColE1 Origin
pCS2+
F1 Origin
Amp

Figure 3.M10

APtag-1 vector diagram and stripe assay production schematic

A. Figure showing important sites in the APtag-1 vector, including the MoLTR promoter, multiple cloning site and the SEAP domain 3' to the inserted ectodomain.

B. Schematic of stripe assay production using glass coverslips. Blue arrows signify path and direction of flow of injected substrate.

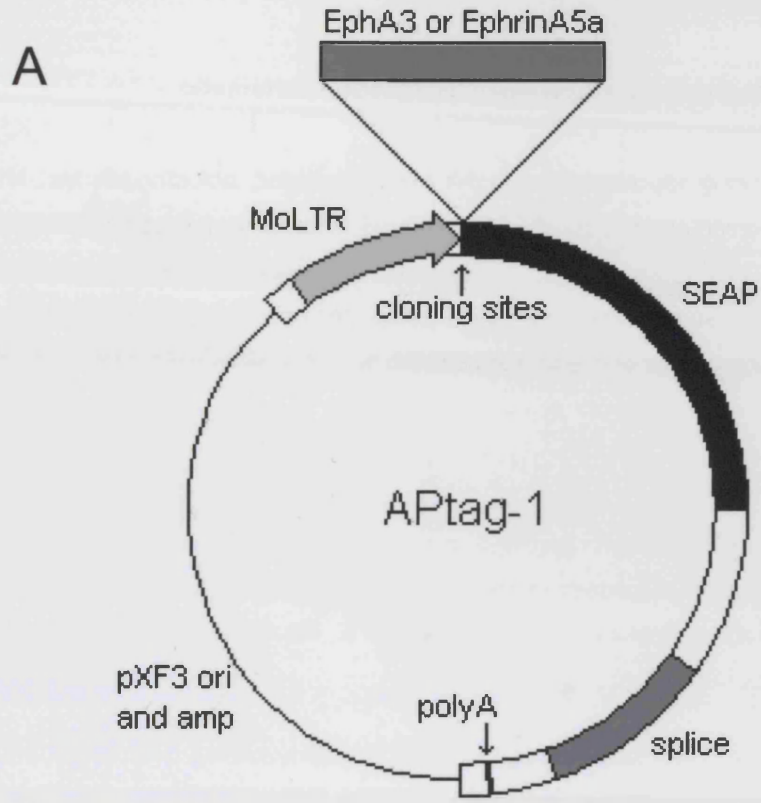
A
EphA3 or EphrinA5a
MoLTR
cloning sites
SEAP
APtag-1
pXF3 ori
and amp
polyA
splice

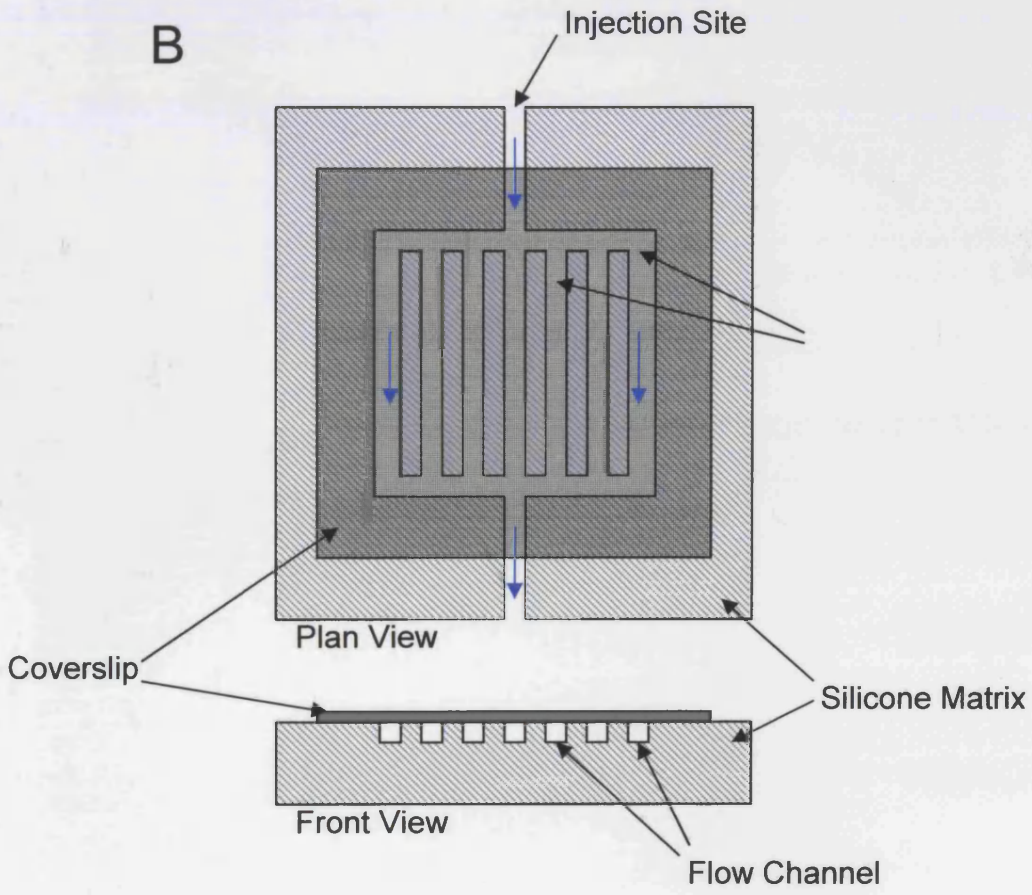
B
Injection Site
Plan View
Coverslip
Silicone Matrix
Front View
Flow Channel

Figure 3.M11

Filter-based stripe production schematic and product

A-B. Schematic of stripe assay production using grilled filters with suction. A shows the formation of the primary stripes as suction through the silicon grid matrix leads to deposition of the suspension at zones of low pressure (blue stripes). Replacing the solution with the secondary stripe suspension and applying suction through a completely porous nylon grid leads to the accumulation of secondary stripe material (red) between the primary lanes where the filter is not occluded. Image redrawn from Walter *et al.*[420].

C. 0.1μm pore Whatman polycarbonate filters with primary stripes of HEK293 membranes and secondary stripes of 1μM BSA-Alexa-594 and 300kDa poly-D-lysine. Visualised after 48hrs in culture medium, 37°C, 5% CO2. Scale bar 75μm.

A

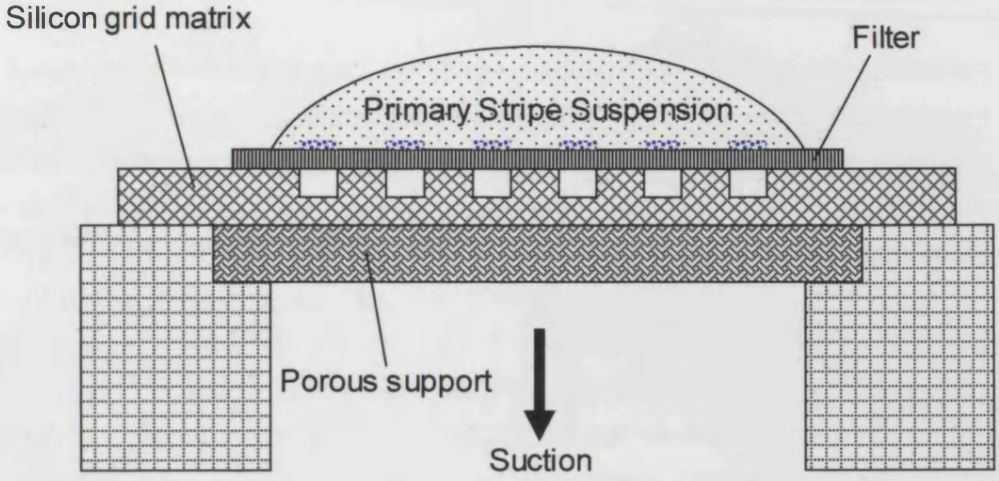
Silicon grid matrix
Filter
Primary Stripe Suspension
Porous support
Suction

B

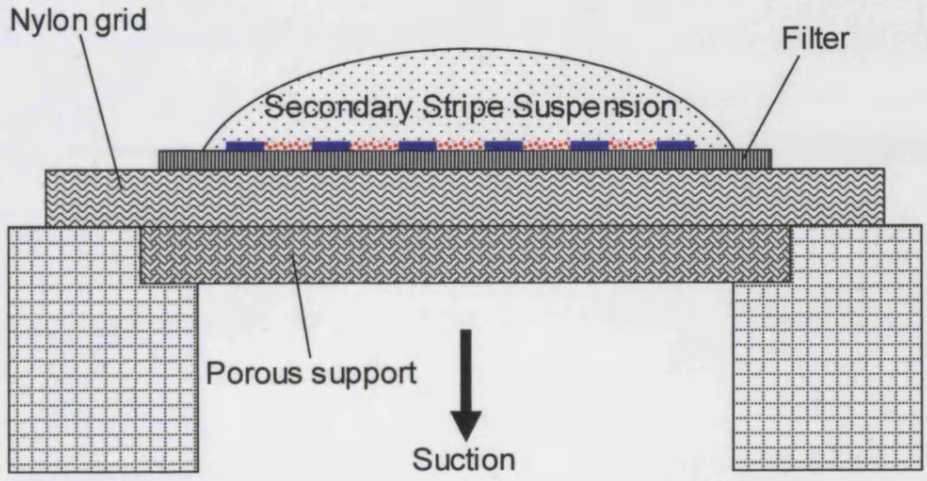
Nylon grid
Filter
Secondary Stripe Suspension
Porous support
Suction

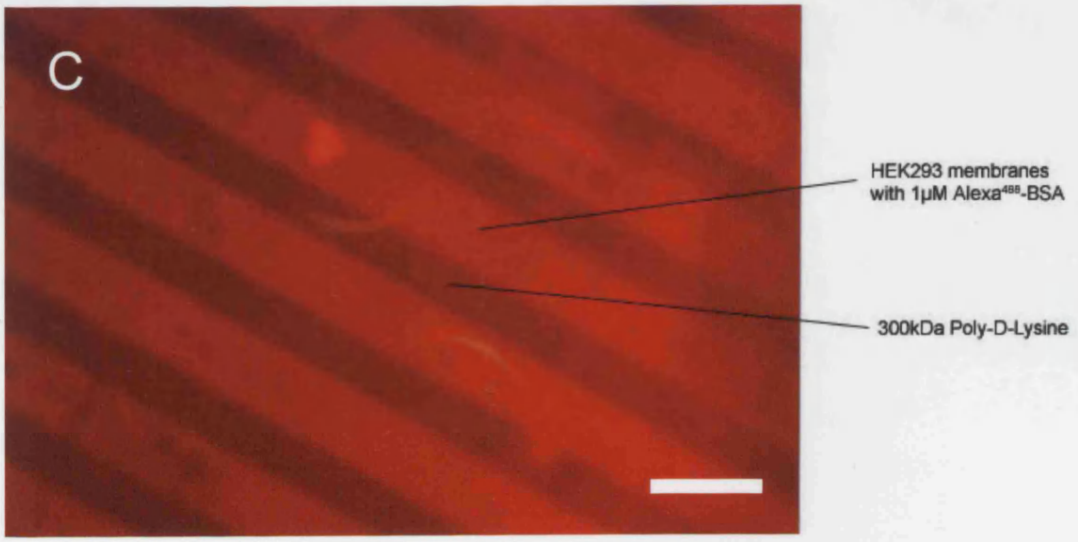
C
HEK293 membranes
with 1μM Alexa488-BSA
300kDa Poly-D-Lysine

Figure 3.M12

Cell line implantation approaches

A. Implantation Method II. A dorsal column lesion was performed at C5 that completely transected the corticospinal tract. Collagen gel foam (orange) seeded with CHO cells was sutured over the top of this lesion site and the dura left open to permit ectodomain (green) access to the lesion. The CST was labelled by BDA injection to the hindlimb region of the motor cortex.

B. Implantation Method III. A dorsal column lesion was performed at C5 that completely transected the corticospinal tract. Collagen gel foam (orange) seeded with CHO cells was sutured 1mm rostral to the site of injury and the dura left open to permit ectodomain (green) access to the lesion. The CST was labelled by BDA injection to the hindlimb region of the motor cortex.

Figure 3.1

Ephrin family member binding promiscuity and ectodomain interactions

A. Diagram highlighting the promiscuity of ephrin interactions. Interactions occur between most ligands and receptors within each receptor/ligand subfamily (not all family members shown). At present the only receptor known to interact with a ligand of the opposing subtype is the EphA4 receptor that binds ephrinB2 and ephrinB3.

B. Diagram illustrating that the four ephrin family members selected for use as blocking ectodomains show promiscuous binding to most ephrins and Eph receptors known to play a role in the spinal cord injury environment.

A

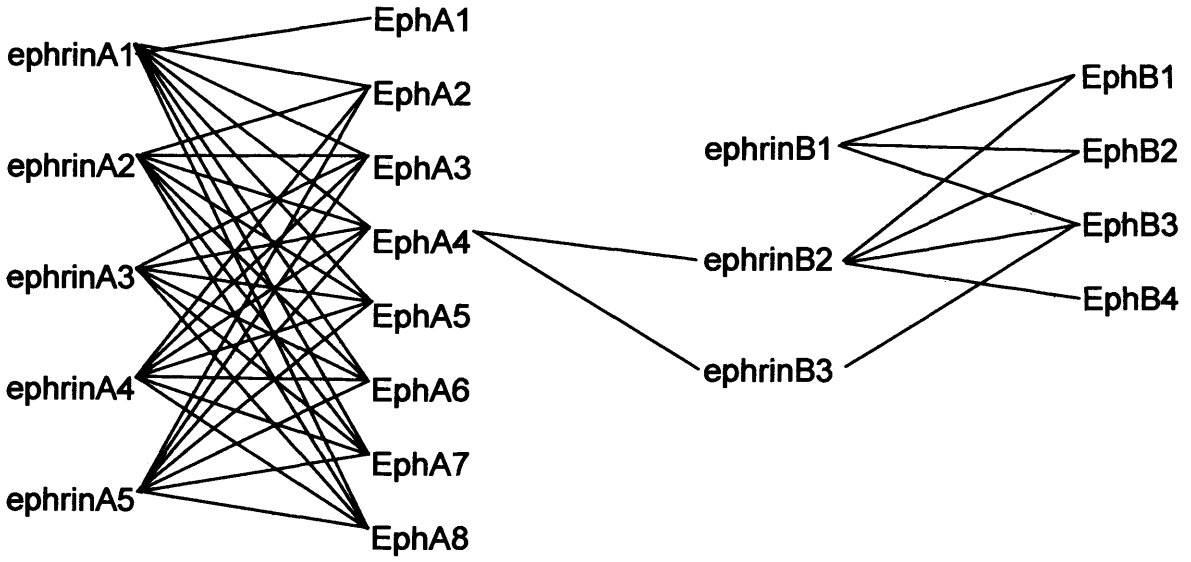

B

Ectodomain	Binds to the following in the spinal cord injury environment			
ephrinB1	EphB2	EphB3		
EphB3	ephrinB2	ephrinB3		
ephrinA5	EphA3	EphA4	EphA6	EphA7
EphA7	ephrinA2	ephrinA3	ephrinA4	ephrinA5

Figure 3.2

Predicted structures of Eph and ephrin ectodomains

A. i, X-Ray crystal structure of the ephrinB2 receptor binding domain; ii, predicted structure of the secreted ephrinB1 ectodomain; iii, predicted structure of the secreted ephrinA5 ectodomain. Showing residues predicted to be important in the dimerisation interface in red and the tetramerisation in green.

B. i, X-Ray crystal structure of the EphB2 receptor binding domain; ii, predicted structure of the secreted EphB3 ectodomain; iii, predicted structure of the secreted EphA7 ectodomain. Showing residues predicted to be important in the dimerisation interface in red and the tetramerisation in green.

C. Predicted arrangement of the secreted ephrinB1 ectodomain complexed with the EphB3 receptor. The primary (red) and secondary (yellow) interaction domains are clearly aligned.

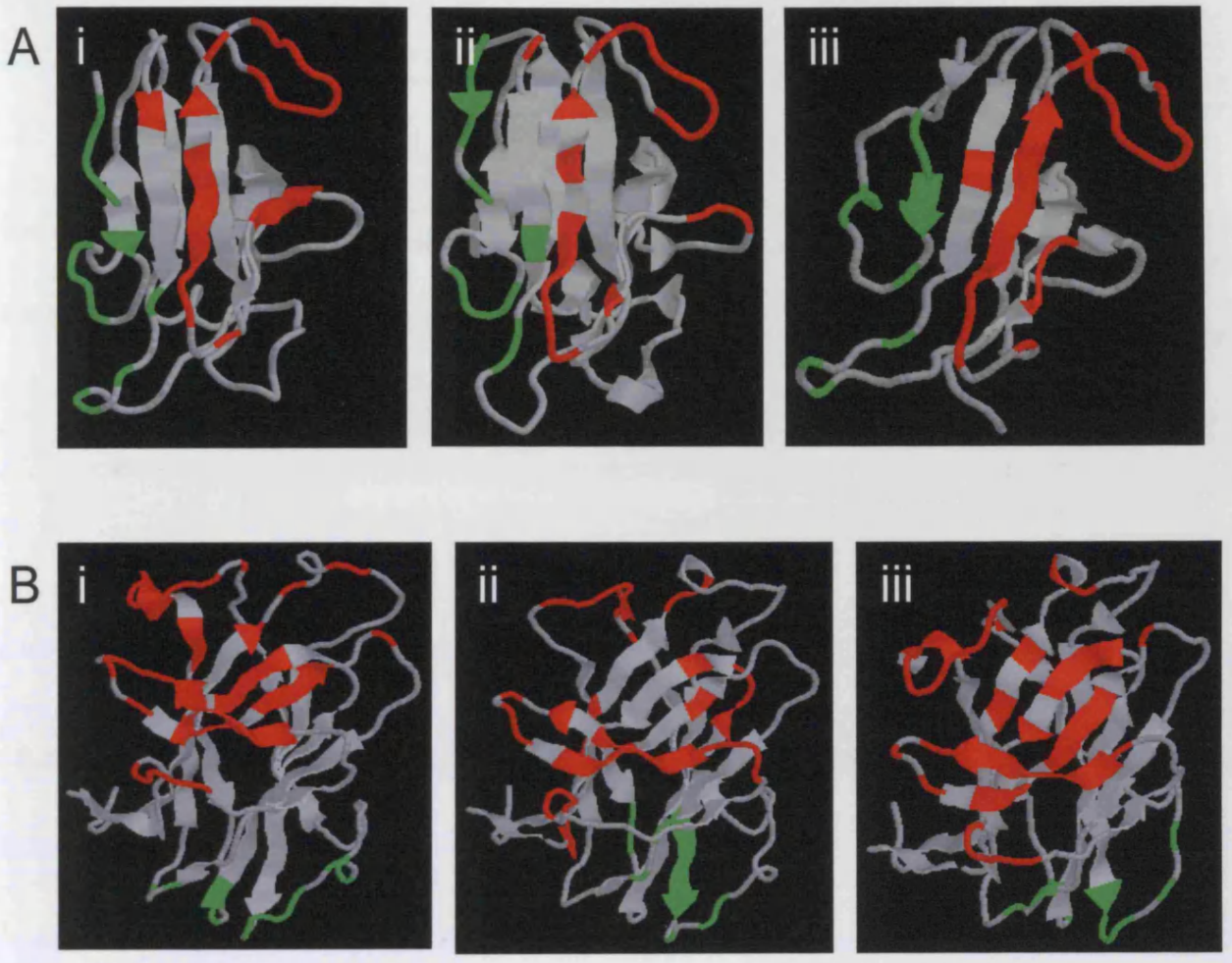
A
i
ii
iii
B
i
ii
iii
C

Figure 3.3

Ectodomain blotting

A. Coomassie stained SDS-PAGE of anti-*c-myc* immunoprecipitated EphA7 and ephrinA5 ectodomains. Secreted ectodomain bands (*) migrate at the expected molecular weight and show a well defined band implying minimal degradation and complete translation.

B. Western blot of an SDS-PAGE of anti-*c-myc* immunoprecipitated EphA7 and ephrinA5 ectodomains. Secreted ectodomains migrate as a well-defined band of the expected molecular weight. Some smearing at molecular weights below the ectodomain suggests a small amount of degradation, however.

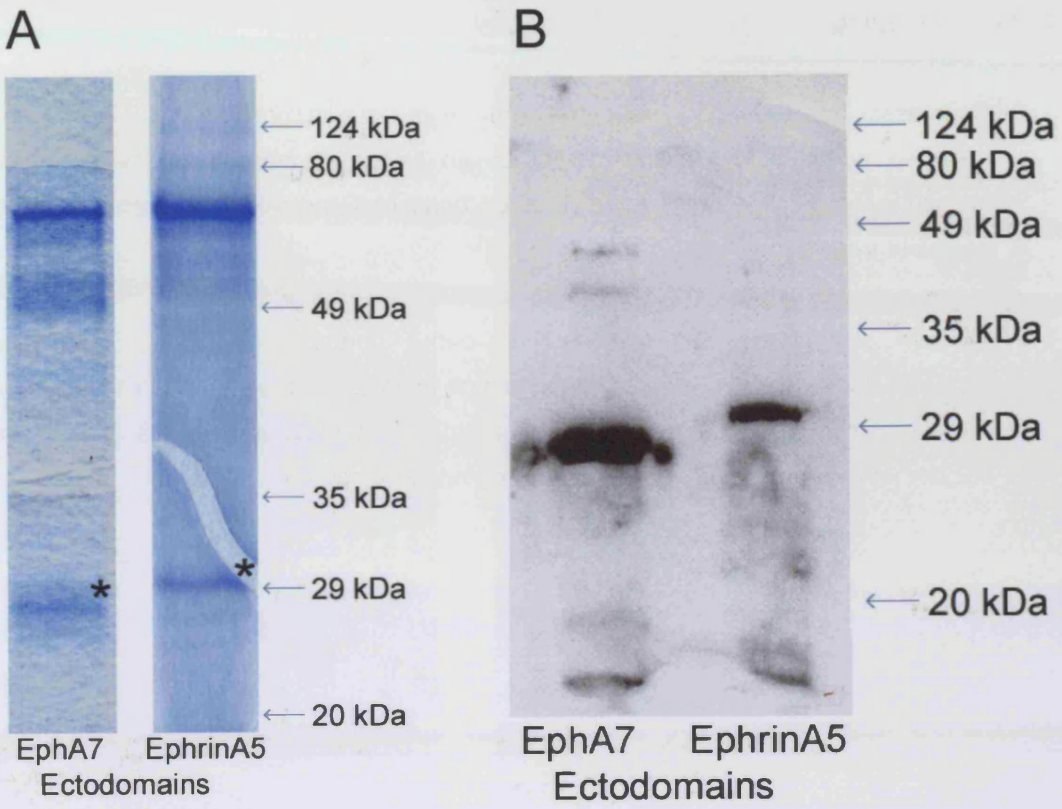
A
124 kDa
80 kDa
49 kDa
35 kDa
29 kDa
20 kDa
*
*
EphA7
EphrinA5
Ectodomains
B
124 kDa
80 kDa
49 kDa
35 kDa
29 kDa
20 kDa
EphA7
EphrinA5
Ectodomains

Figure 3.4

Stripe assays showing growth on ephrinA5-Fc lanes

A-B. Retinal Ganglion cell axons stained with phalloidin-Alexa-488 (i, green) put out long, highly fasciculated axons (direction of growth upwards) on glass coverslip stripe assays. Primary substrate lanes (P) containing ephrinA5-Fc stained with a primary antibody to human Fc (ii, red) show good resolution even after 72hrs in culture. However, the expected avoidance response is not apparent (iii, merge) with RGC axons growing on ephrinA5-Fc lanes and avoiding the 'growth permissive' secondary lanes (S). Scale bars 200μm.

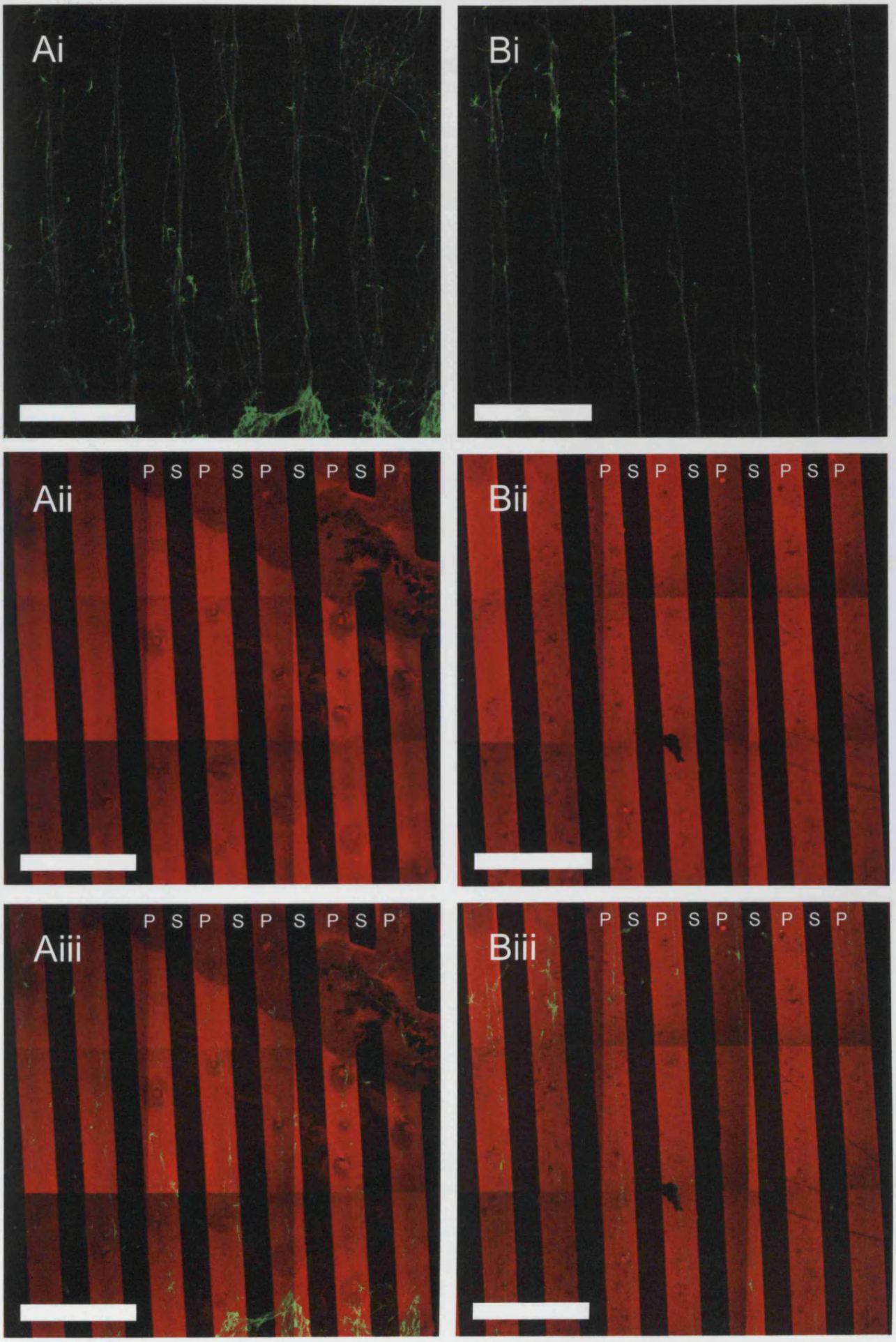
Ai
Bi
Aii
P S P S P S P S P
Bii
P S P S P S P S P
Aiii
P S P S P S P S P
Biii
P S P S P S P S P

Figure 3.5

Outgrowth on control coverslip stripe assays and filter stripe assays

A. Retinal Ganglion cell axons stained with phalloidin-Alexa 488 (i, green) develop long, highly fasciculated axons (direction of growth upwards) on glass coverslip stripe assays produced using human IgG in the primary stripe (P). Substrate lanes containing ephrinA5-Fc stained with a primary antibody to human Fc (ii, red) show RGC processes growing preferentially on these IgG lanes and avoiding control secondary lanes (S). IgG has no known axon guidance properties suggesting some error in stripe generation. Scale bars 200μm.

B. This error is apparent when coverslips coated in poly-L-lysine are exposed to sterile PBS in the silicone mould and then incubated with albumin-Alexa 594. The presence of stripes at this stage of coverslip preparation indicates that the silicone mould removes the poly-L-lysine from the coverslip where it makes contact, resulting in secondary lanes that are bare glass and hence cannot support growth. Scale bar 200μm.

C. Outgrowth of retinal ganglion cells on filter-based stripe assays. Phalloidin-Alexa 488 staining successfully visualised processes (green) but these were frequently short (i) and showed no growth direction response to stripe substrates (ii). Scale bars 50μm.

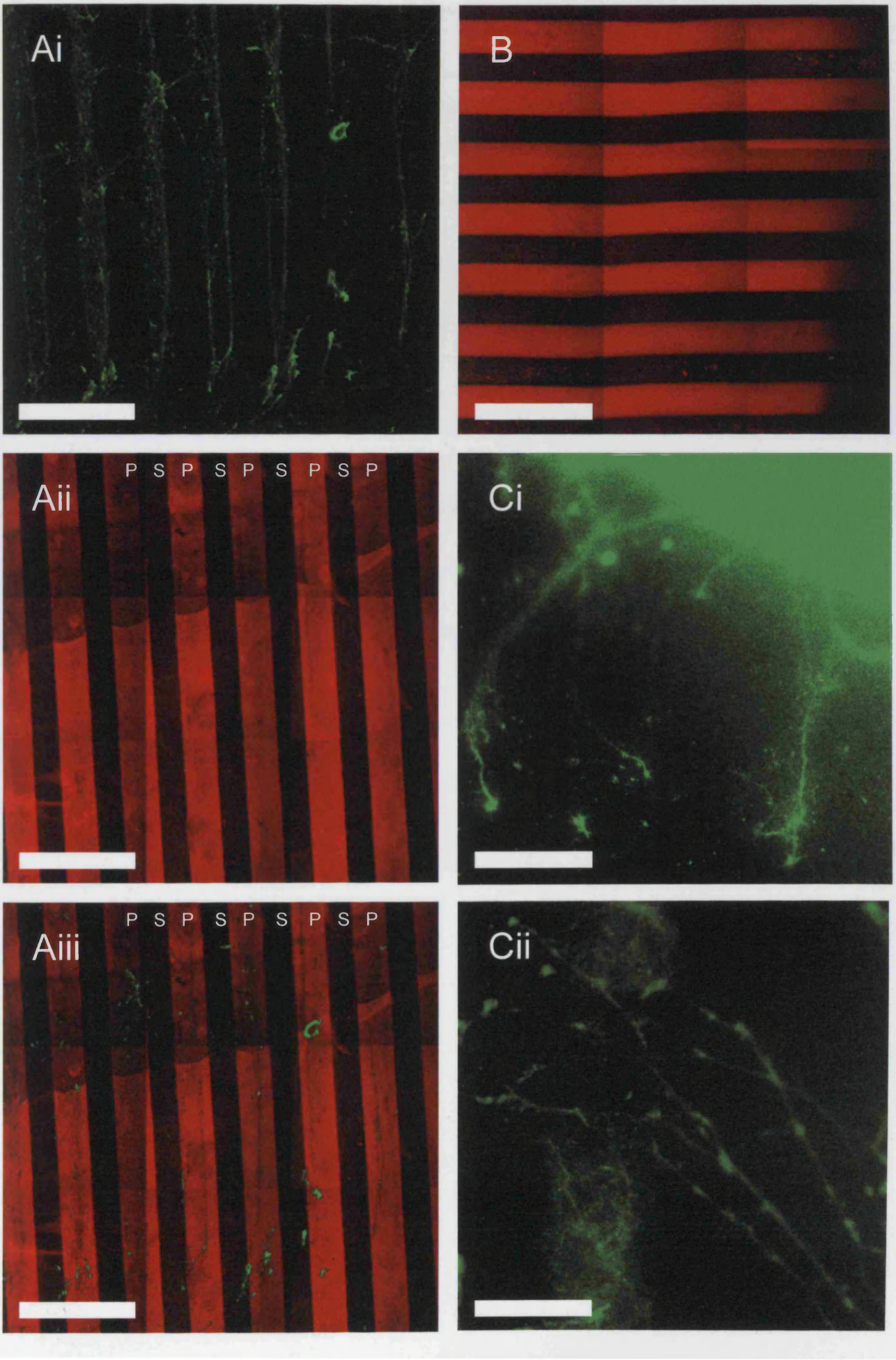
Ai
B
Aii
P S P S P S P S P
Ci
Aiii
P S P S P S P S P
Cii

Figure 3.6

RGC and HEK293 co-culture outgrowth assay

A. Staining of outgrowth in co-culture assay. Immunohistochemistry for neurofilament (200kDa) revealed extensively sprouting retinal ganglion cell axons while only picking up minimal background staining from the co-cultured HEK293 cells. Sprouting was extensive in both control HEK (i) and ephrinA5-expressing HEK (ii) co-cultures. Scale bars 100μm.

B. Graph of outgrowth in co-culture assay. As shown, neurite length in co-cultures of retinal ganglion cells with ephrinA5-expressing HEK cells was greater than that found in control HEK cultures. Mean ± SEM plotted.

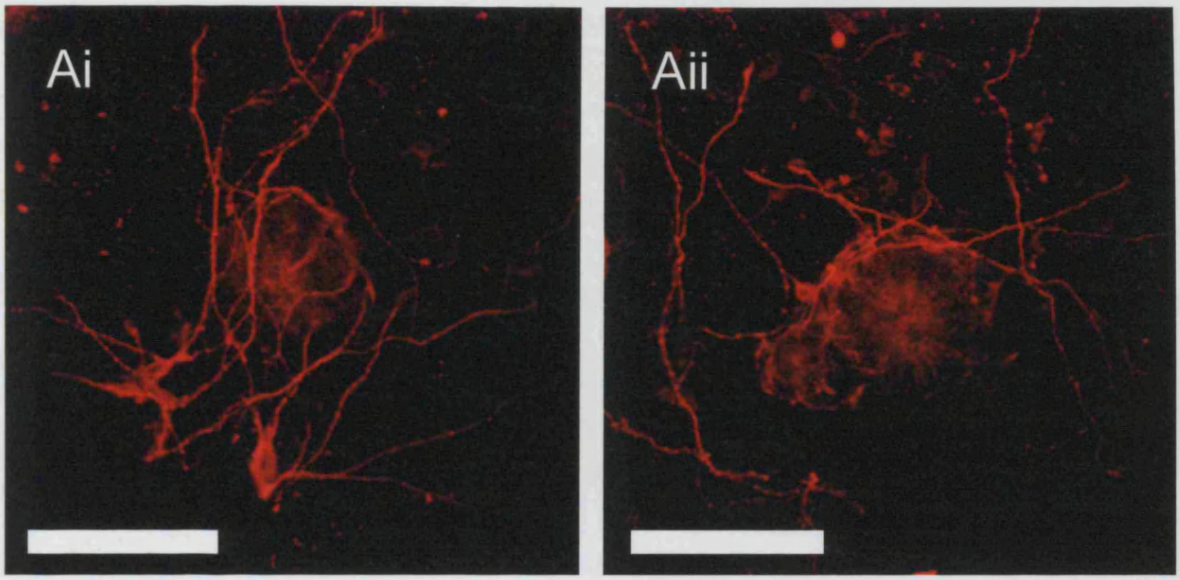
Ai
Aii

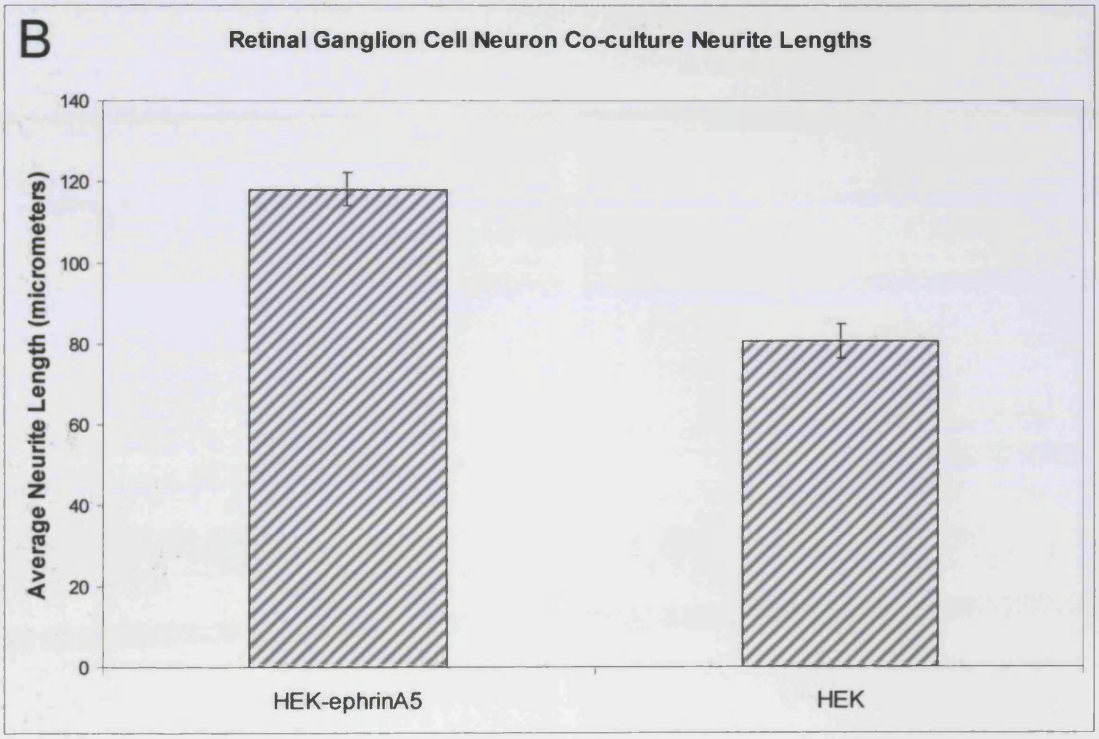
B
Retinal Ganglion Cell Neuron Co-culture Neurite Lengths
Average Neurite Length (micrometers)
140
120
100
80
60
40
20
0
HEK-ephrinA5
HEK

Figure 3.7

RGC collapse assay growth cones

A. Retinal ganglion cell growth cones stained with phalloidin-Alexa 488 show clear morphological differences between the collapsed (B) and uncollapsed (A) states. Uncollapsed growth cones have a wide diameter, show extensive filopodia (arrows) and lamellipodia (triangles) and show raised actin expression compared to the axonal processes but no intense foci. Collapsed growth cones, by comparison, are small, highly actin dense and usually show one filopodial process (arrows) oriented in the direction of the associated axon. Scale bars 20μm.

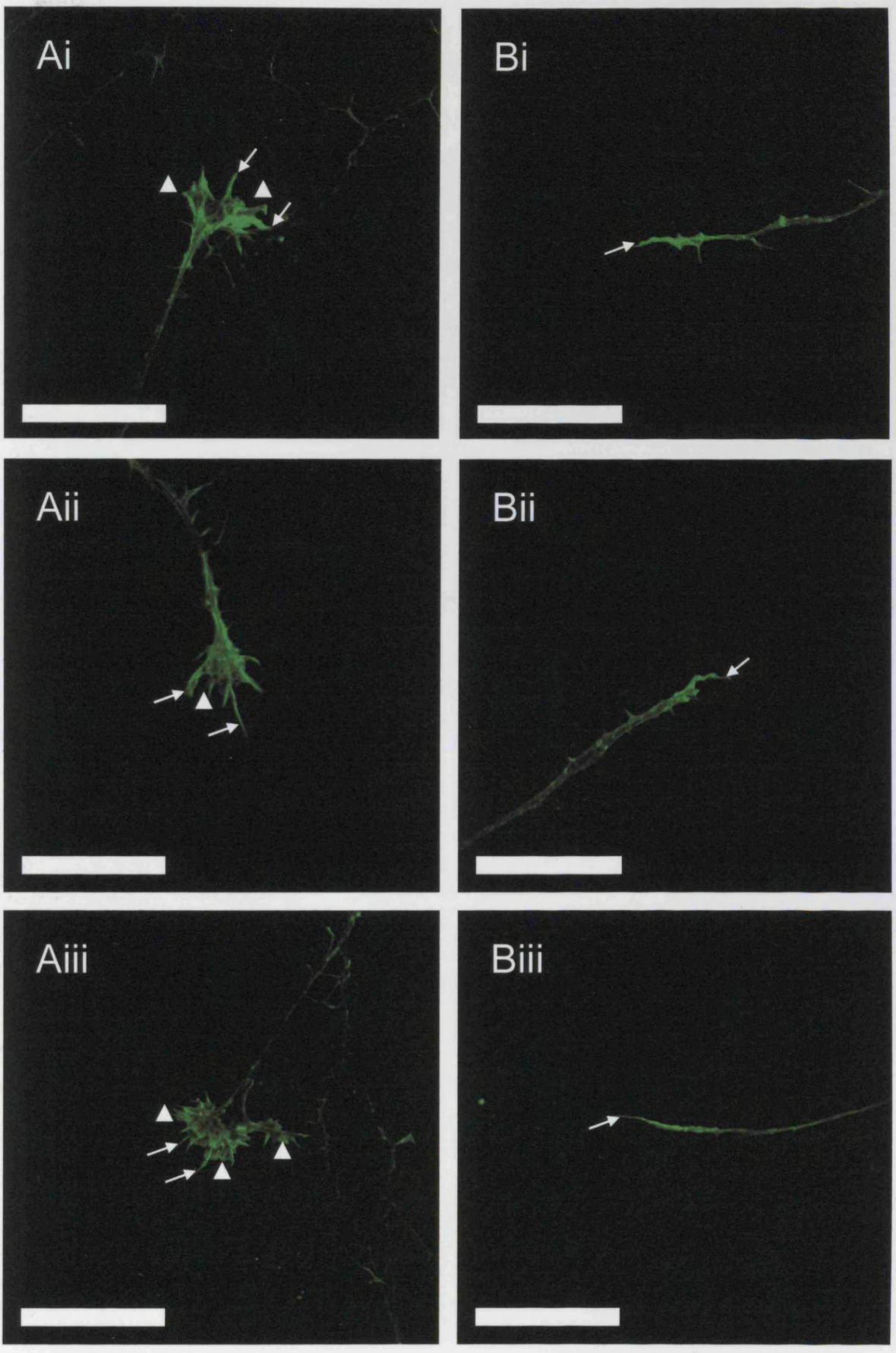
Ai
Bi
Aii
Bii
Aiii
Biii

Figure 3.8

Quantification of RGC collapse assay

A-B. Percentage collapse of retinal ganglion cells growth cones increases following exposure to homodimeric ephrinA5-Fc and this is blocked by application of monomeric ephrinA5 (A) or EphA7 (B) ectodomains. Pre-administration of ephrinA5 ectodomains or pre-incubation of EphA7 ectodomains with the ephrinA5-Fc reduces the growth cone collapse rate to levels very similar to control, sterile PBS exposure. Neither ectodomain induces growth cone collapse when administered alone. Bars show mean ±SEM for each set of cultures.

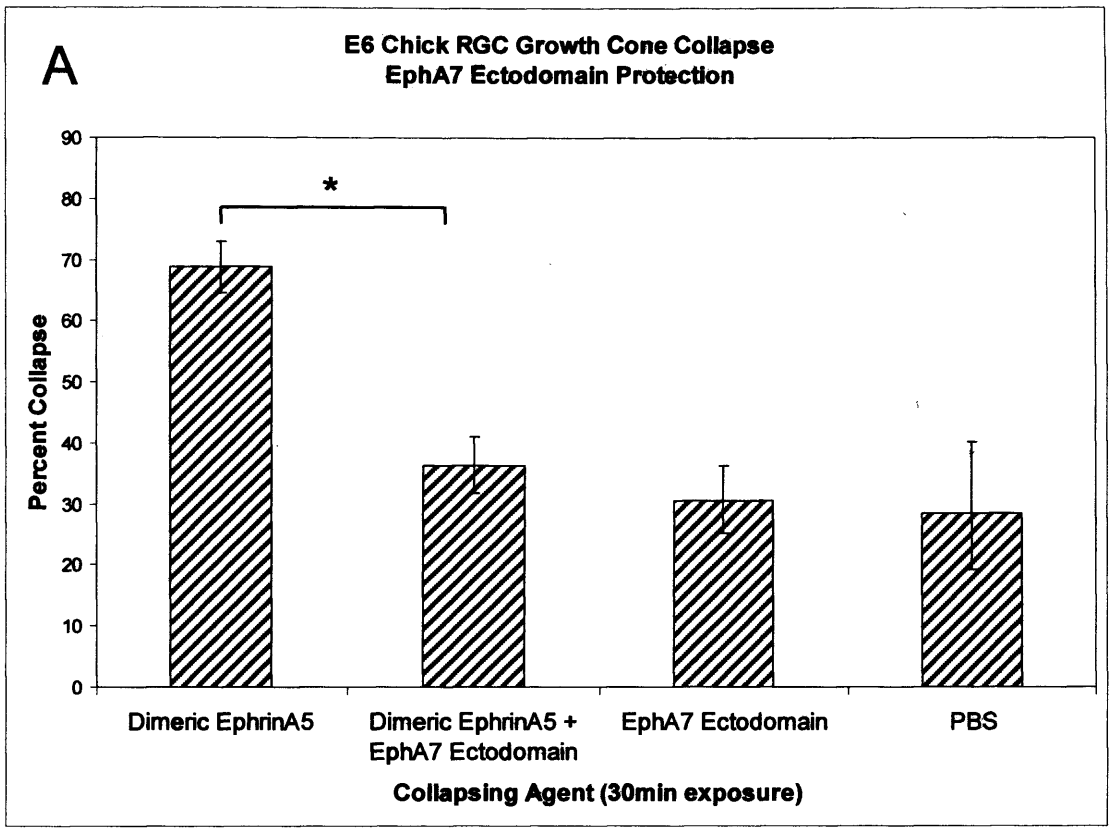
A
E6 Chick RGC Growth Cone Collapse
EphA7 Ectodomain Protection
Percent Collapse
90
80
70
60
50
40
30
20
10
0
*
Dimeric EphrinA5
Dimeric EphrinA5 + EphA7 Ectodomain
EphA7 Ectodomain
PBS
Collapsing Agent (30min exposure)

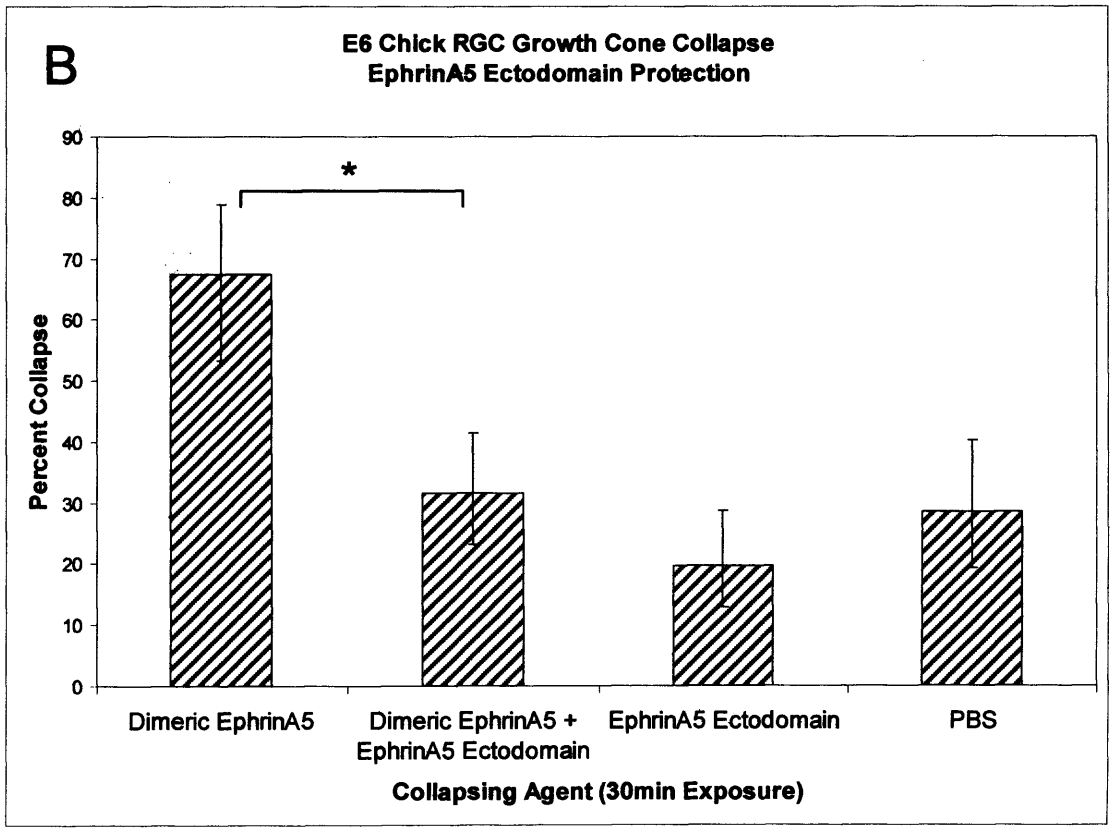
B
E6 Chick RGC Growth Cone Collapse
EphrinA5 Ectodomain Protection
Percent Collapse
90
80
70
60
50
40
30
20
10
0
*
Dimeric EphrinA5
Dimeric EphrinA5 + EphrinA5 Ectodomain
EphrinA5 Ectodomain
PBS
Collapsing Agent (30min Exposure)

Figure 3.9

Implantation of EGFP-CHO cell line into the lateral ventricle

A. CHO cells transduced with an EGFP-expressing lentivirus (CHO-EGFP) grow well in culture at normal growth rates, show normal cellular morphology and good EGFP expression without extensive protein aggregates. Scale bar 100μm.

B. Coronal 40μm section of the lateral ventricle of an adult rat three days following stereotaxic injection of suspended EGFP-CHO cells. Despite immunosuppression with FK506 for three days prior to injection, a strong immune response mediated by macrophages and microglia is identified in OX-42 stained slides (i). This accumulation of immune cells clearly envelops the tissue implant (ii). Scale bars 300μm.

C. Higher magnification images taken from the implant site show EGFP-CHO cells (green, i) surrounded by OX-42 positive macrophages and microglia (red, ii). Scale bars 50μm.

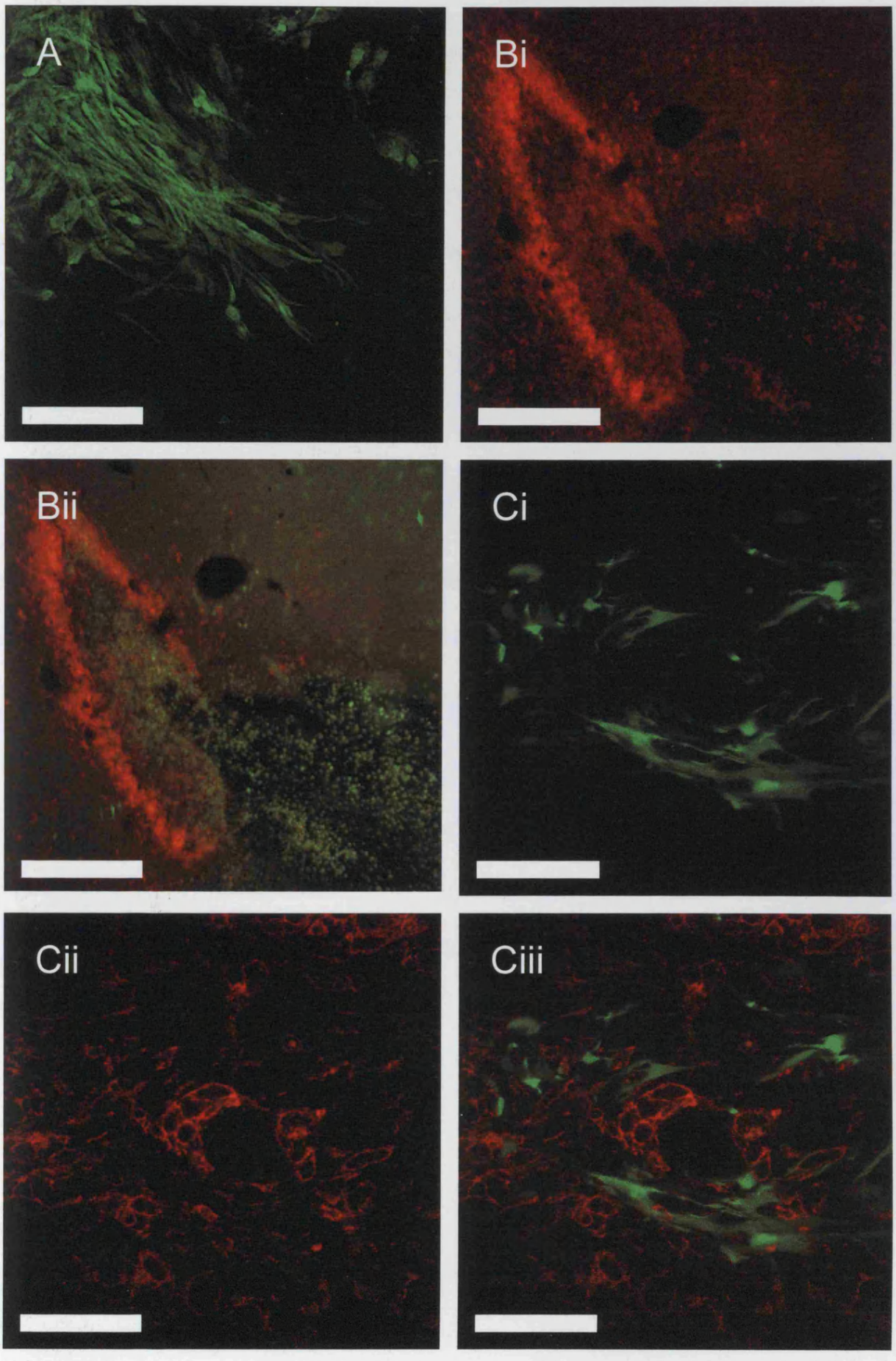
A
Bi
Bii
Ci
Cii
Ciii

Figure 3.10

Implantation methods II and III: cells invading the lesion site and spinal cord

A. Parasagittal 40µm section through the centre of a dorsal column lesion three days following injury and implantation of cells by method II. EGFP-CHO cells (green) cultured on collagen gelfoam (blue) were sutured over the site of the lesion. Immunohistochemistry for GFAP (red) outlines the surviving astrocytes (#) and the margin of the spinal cord (dotted line). As is evident, EGFP-CHO cells have migrated from the collagen gelfoam and invaded the lesion cavity (*). Scale bar 200µm.

B. Horizontal 40µm section through the dorsal column of a spinal cord that underwent cell implantation method III. The animal received a dorsal column transection 1mm caudal to the site of cell implantation (left in image). CHO-ephrinA5 (95% of cells) EGFP-CHO (5% of cells) cells were co-cultured on collagen gelfoam then sutured to the undamaged dura. Three days following surgery animals were transcardially perfused and stained for GFAP. GFAP-positive astrocytes (#) are present in the periphery of the tissue, but the implanted tissue (*, outlined with dotted line) has invaded and displaced the majority of the dorsal columns. Scale bar 500µm.

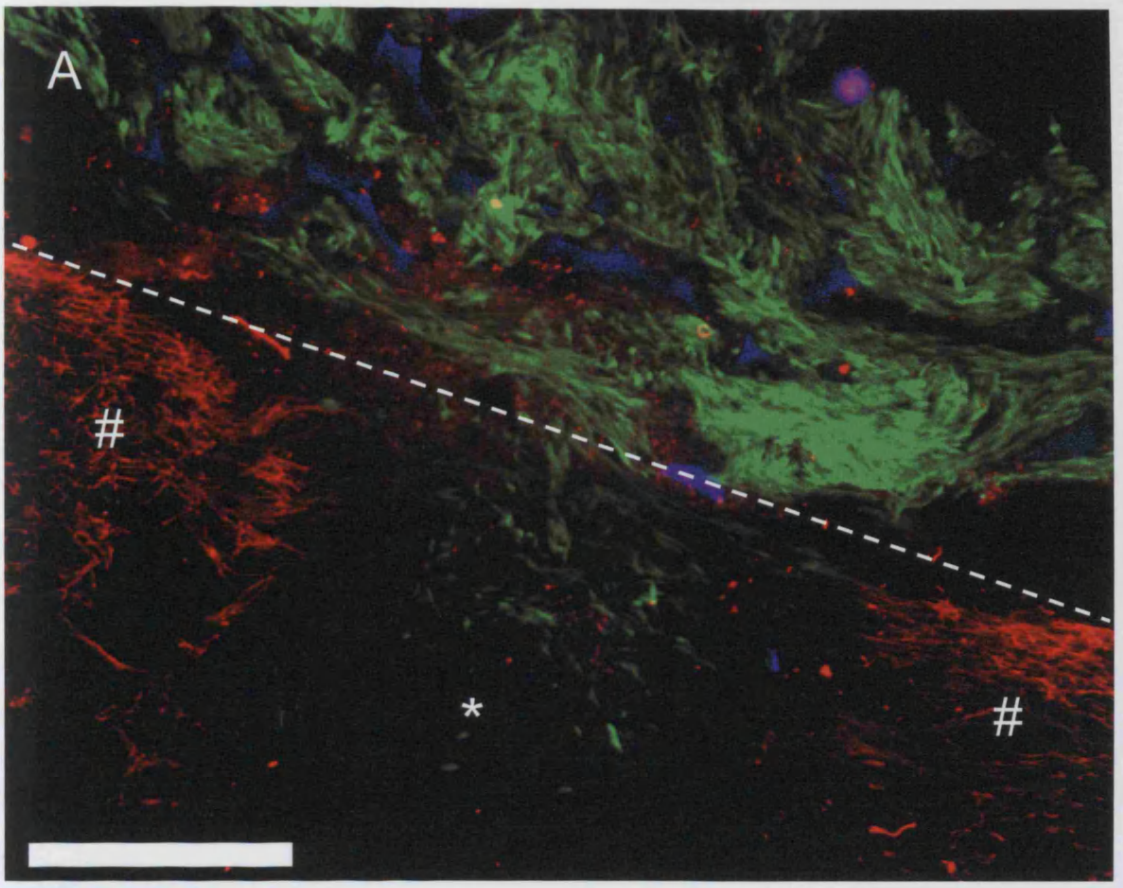
A
#
*
#

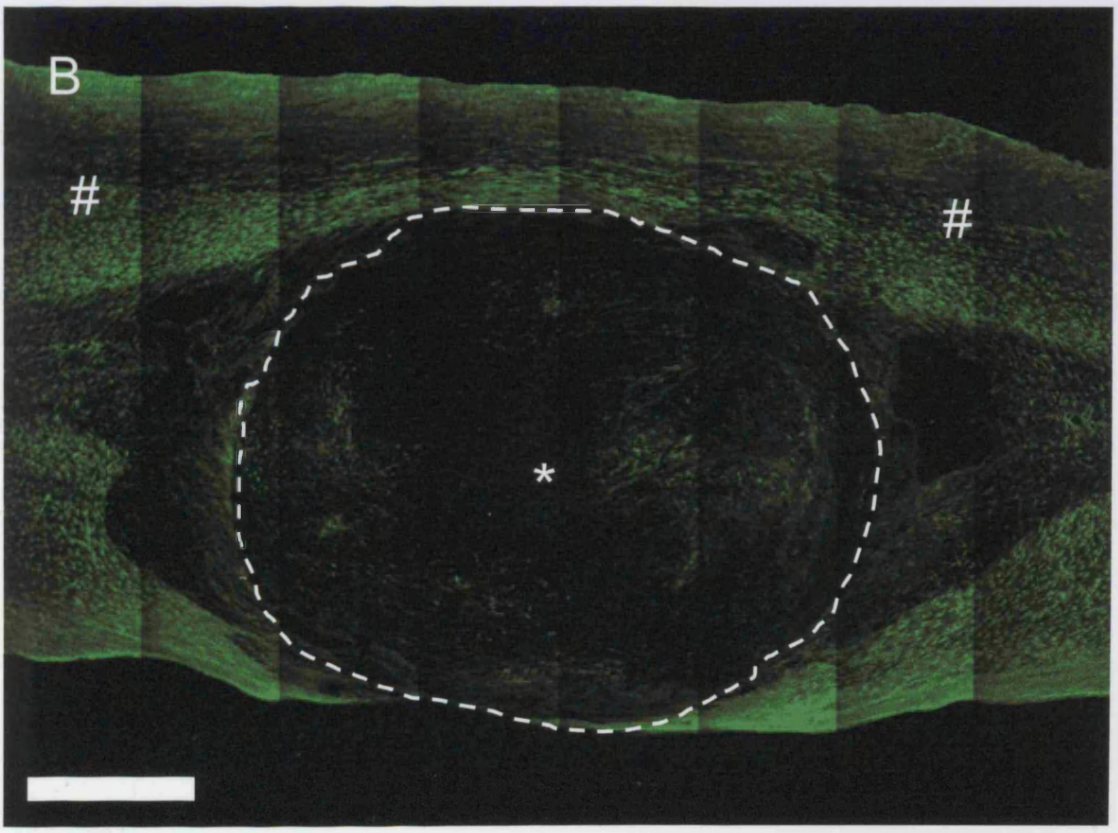
B
#
#
*

Figure 3.11

Improved regeneration of the CST following CHO-ephrinA5 implantation

A-B. Horizontal 40μm section through the dorsal corticospinal tract ten days following transection, injection of BDA to the motor cortex and implantation of control CHO (A) or CHO-ephrinA5 cells (B) that secreted soluble ephrinA5 ectodomains. An improvement in the retraction of the corticospinal tract from the lesion margin (dotted line) was apparent in the ephrinA5 treated animals. Scale bar 200μm.

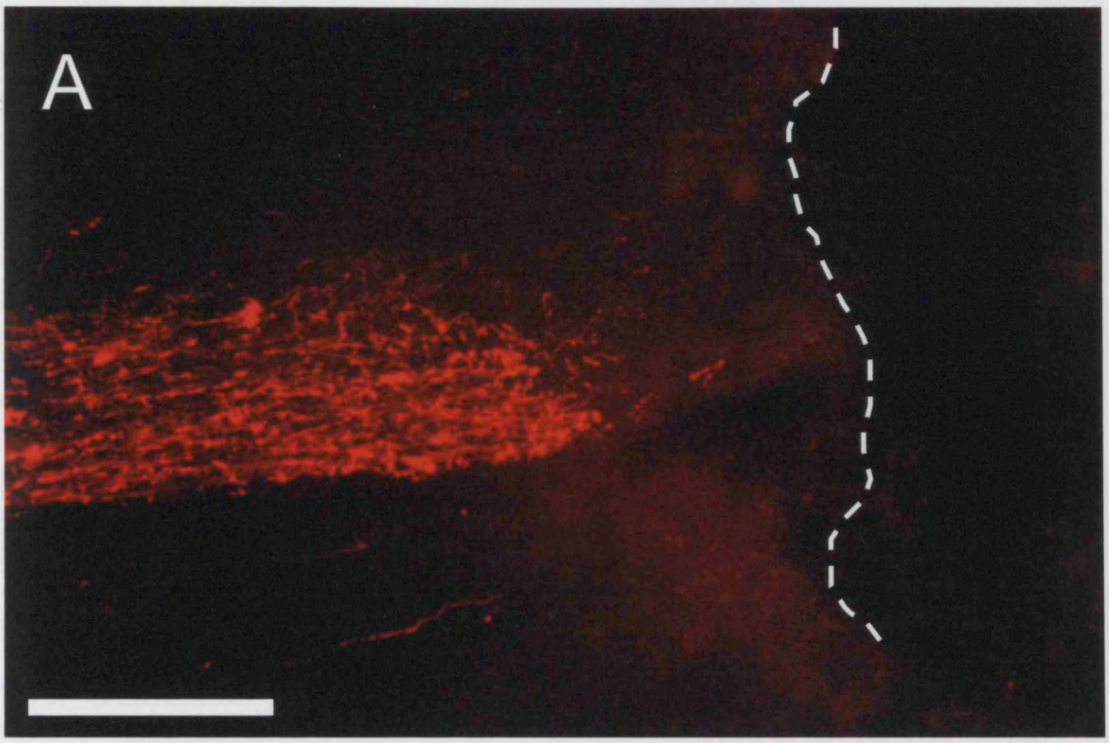
A

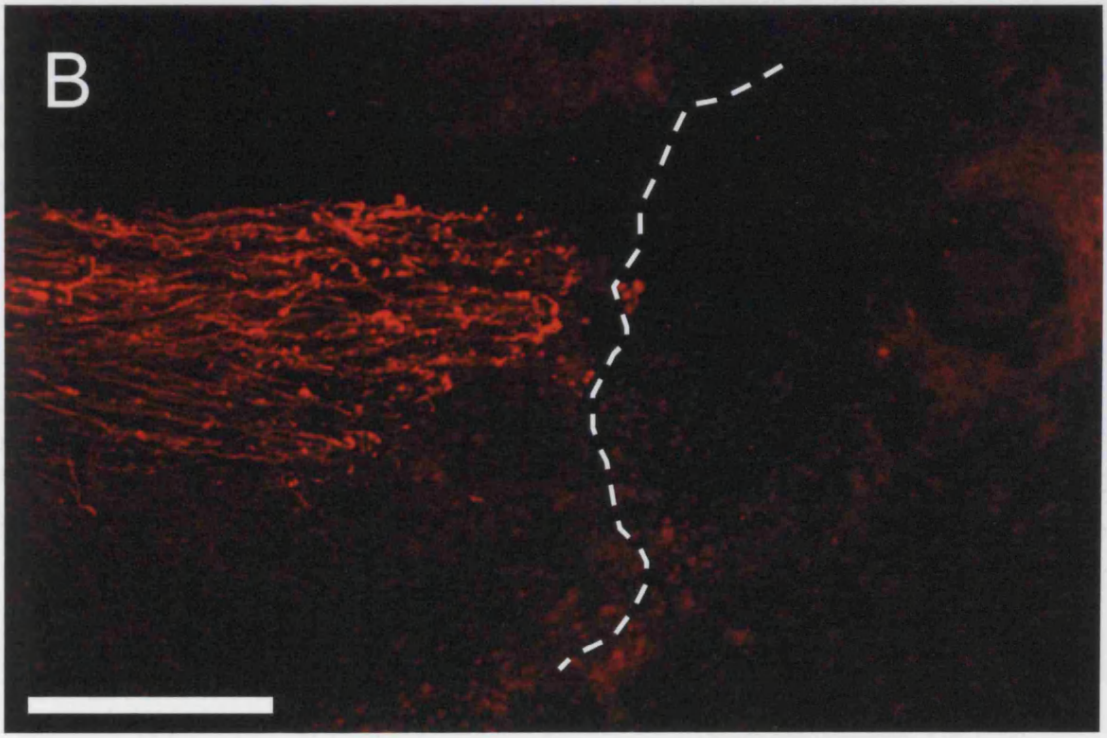
B

Figure 3.12

CST sprouting and astrocyte GFAP expression following CHO-ephrinA5 implantation

A-B. The termination bulbs of lesioned corticospinal tract axons in animals exposed to the ephrinA5 ectodomain show an increased sprouting response ten days after injury. Numerous termination bulbs put forward regenerative sprouts (A, arrows) that grow in the direction of the lesion margin. These sprouts often grow significant distances (Bi) and regenerate as far as the astrocyte margin, as defined by GFAP staining (Bii). Scale bars 100μm (A) and 20μm (B).

C. Reactive astrocyte GFAP expression was unaffected by the exposure to the ephrinA5 ectodomain, with similar astrocyte reactivity and lesion site morphology in control (i) and ephrinA5-treated (ii) animals. Scale bars 200μm.

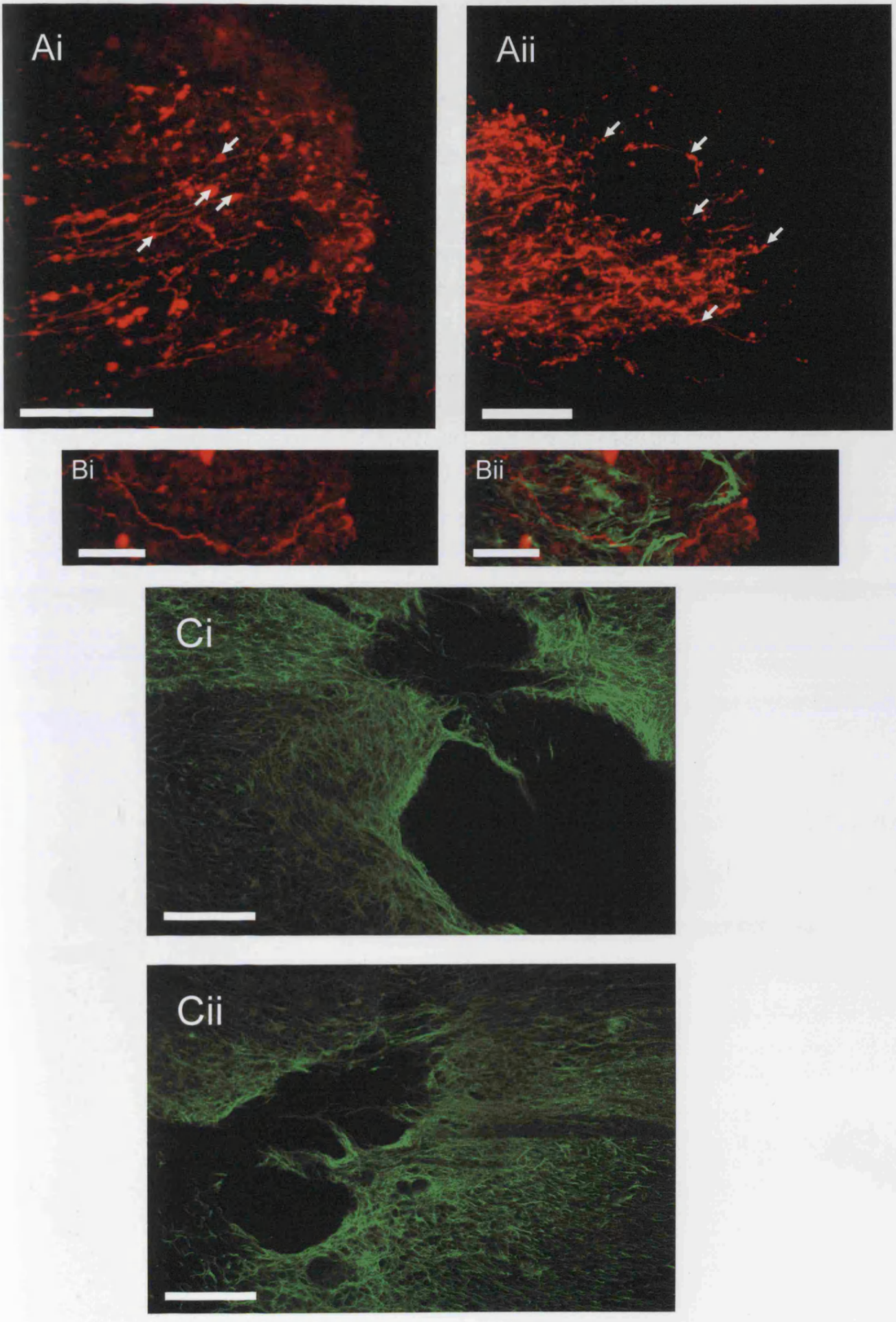
Ai
Aii
Bi
Bii
Ci
Cii

Figure 3.13

Theoretical accumulation of ectodomain within the CSF local to the injury site

The calculation is based on the approximate secretion rate of ectodomain *in vitro*, the number of cells implanted and a 40µl volume of dilution for local CSF. The likely therapeutic threshold of 50nM is based on the work of Murai *et al.*[389] and this concentration should be surpassed within 22hrs of implantation, a feasible time window for beneficial effect.

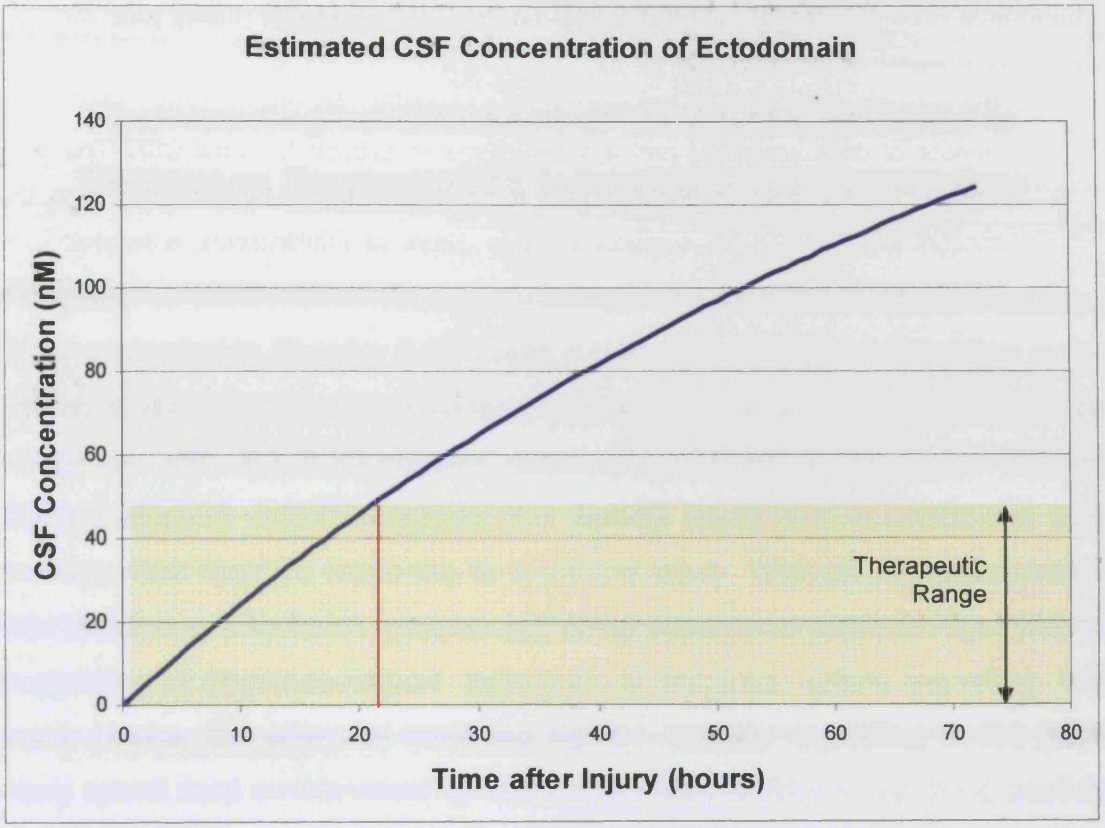
Estimated CSF Concentration of Ectodomain
CSF Concentration (nM)
140
120
100
80
60
40
20
0
0
10
20
30
40
50
60
70
80
Time after Injury (hours)
Therapeutic Range

Chapter IV

Pharmacological Blockade of the EphA4 Receptor to Encourage Regeneration following Spinal Cord Injury

Abstract

Work presented in Chapter II indicates a likely role for EphA4 signalling in the injured corticospinal tract preventing regeneration and sprouting through an interaction with ephrinB2-positive reactive astrocytes at the lesion margin. Other published work[12] suggests that EphA4 expressed in astrocytes may mediate their reactive response to a central injury. Chapter III demonstrated how interfering with EphA receptor signalling appears to improve regeneration suggesting a pharmacological approach to blocking ephrin signalling has merit. Hence, the effect of inhibiting EphA4 receptor signalling in the post-injury spinal cord environment by infusing an EphA4-specific blocking peptide directly into the subdural space was studied. The study was performed on both Sprague-Dawley and Lewis rats and assessed regeneration at 14 and 28 days following injury. This method of intervention was found to improve the sprouting and regenerative capacity of the injured CST and RST following dorsal and lateral lesions. Regenerating axons were seen to navigate significant distances towards the lesion cavity, often reaching the lesion margin. Astrocyte morphology was altered with increased invasion of the lesion cavity by astrocytic processes and axonal sprouts frequently grew along these astrocytic bridges into the lesion cavity. This is a marked improvement over the abortive regenerative response of these descending tracts seen in untreated rats. Functional recovery was also apparent following peptide administration with significant improvements attained in the paw reaching assay.

METHODS

EphA4 Blocking Peptide

Murai *et al.*[389] panned an M13 phage library of 12-mer peptides on immobilised EphA4 ectodomain to identify candidate binding peptides. One peptide sequence identified, termed KYL (full sequence KYLPYWPVLSSL), was selected for use in this study due to its high affinity (K_D 0.5 ±0.06nM) and selectivity for EphA4 over other EphA receptors.

The peptide was synthesised (Alta Bioscience, University of Birmingham, UK) to greater than 95% purity and made up as a 3mM solution in artificial cerebrospinal fluid (ACSF). ACSF was prepared from a 1:1 ratio of sterile filtered Solution A (296mM NaCl, 6.5mM KCl, 2.8mM $CaCl_2.2H_2O$, 1.6mM $MgCl_2.6H_2O$) and Solution B (1.6mM $Na_2HPO_4.7H_2O$, 0.39mM $NaH_2PO_4.H_2O$).

Embryonic Rat Cortical Neuron Culture and Collapse Assay

10mm diameter coverslips (VWR) were washed in pure ethanol in a 24-well plate and then dried in a Class II laminar flow tissue culture hood. 100µL of Poly-L-Lysine (20µg/ml, Sigma) with natural mouse laminin (5µg/ml, Invitrogen) was applied to the coverslips for thirty minutes at 37°C followed by two washes in sterile distilled water and further drying in the hood. E17 Sprague-Dawley rat embryos were dissected from the mother using sterile instruments and placed in oxygenated 4°C Hank's Buffered Saline Solution (HBSS, Sigma). All subsequent dissection was performed in a clean dissection hood in oxygenated 4°C HBSS. Embryos were removed from the amniotic membranes and the skin and other tissue layers covering the brain removed with forceps. The cortical layer was dissected from the brain and placed in 37°C DCC medium (Neurobasal medium containing 2mM L-Glutamine, 2% B27, 2500units/ml Penicillin and 2500µg/ml Streptomycin, all from Invitrogen). DCC medium was replaced with Trypsin solution (0.05%, Sigma) for 15 minutes at 37°C and then replaced with Neurobasal medium containing 10% FBS (Sigma) to quench any remaining trypsin. Trypsinised cortices were triturated repeatedly through a standard 1ml blue pipettor tip and then a 100µl yellow pipettor tip until a fine cell suspension was attained.

Cell density was then counted using a haemocytometer and the suspension diluted in DDC medium such that $2.8x10^4$ cells were added to each well of the 24-well plate together with 300µL of medium. Cultures were left overnight at 37°C 5% CO_2 when processes were apparent when observed under the light microscope.

Cultures received one of five treatments that were blinded subsequent to preparation. 100µl of DCC medium was added at the start of the experiment containing either ACSF (control), or 80, 200 or 400nM blocking peptide in ACSF (peptide only control or blocking assays). 15 minutes later a further 100µl of DCC medium was added to each well containing either ACSF (control) or 100nM homodimeric ephrinA5-Fc in ACSF (final concentration 20nM, R&D Systems). 30 minutes later 1ml of 37°C 4% w/v paraformaldehyde in PBS was added to the cultures and left to fix for 20 minutes.

Treatment	**0min**	**15min**
Control	ACSF	ACSF
100nM Peptide Control	400nM Peptide	ACSF
EphrinA5-Fc	ACSF	100nM EphrinA5-Fc
EphrinA5-Fc + 20nM Peptide	80nM Peptide	100nM EphrinA5-Fc
EphrinA5-Fc + 50nM Peptide	200nM Peptide	100nM EphrinA5-Fc
EphrinA5-Fc + 100nM Peptide	400nM Peptide	100nM EphrinA5-Fc

Three washes with sterile PBS were followed by permeabilisation with 0.1% Triton in PBS for 5 minutes and three washes in PBS. Staining was performed using phalloidin-Alexa 488 (1:40 in PBS, Molecular Probes) for thirty minutes followed by three washes in PBS and mounting on glass slides under DABCO and sealing by nail varnish. Coverslips were analysed blind under the confocal microscope. Fifty growth cones were counted from each coverslip. To ensure that only axonal growth cones were counted, cells were rejected unless they bore a minimum of two growth cones. Only one growth cone was selected from each identifiable cell body and only those whose process was

at least three times as long as all other processes from that cell body. Growth cones were selected from all areas of the coverslip to ensure no artefact developed due to the proximity of the cells to the initial DCC application point.

Mini-Pump and Cannula Preparation

Alzet osmotic mini-pumps (Charles River, UK) were used throughout this study. The 2002 model was used in the two week experiment and subsequently all other work used the 2004 model. Both pumps have the same capacity (approx. 210µl) but the 2002 model pumps at a rate of 0.5µl/hr for two weeks whereas the 2004 model pumps at a rate of 0.25µl/hr for four weeks. Both models required 'priming' to ensure that they were pumping at full speed when implanted. 2002 models were primed in 0.7% NaCl solution in sterile distilled water at 37°C for 8 hours before surgery, 2004 models required 48hrs of priming under identical conditions.

Pumps were filled with either ACSF or ACSF containing peptide using a 1ml syringe and a supplied filling needle. The volume injected into each pump was carefully monitored to ensure no air bubbles were present as this would disrupt the osmotic mechanism and impair the pumping rate. At all times pumps were handled with gloves to maintain sterility and ensure the pumps did not come into contact with skin oils as these are known to disrupt the osmotic mechanism.

Cannulae were made from modified rat intrathecal cannulae (Charles River). Briefly, these cannulae consist of a very fine, flexible segment designed to be placed into the subarachnoid space connected to a larger gauge, more stiff section designed to prevent kinking under the skin. A 4cm section of the thick tubing was tied in a simple knot and superglued in that position. Subsequently a 2cm section of the fine tubing was superglued to one end and a 2cm stretch of even wider gauge, flexible tubing was attached to the other end, designed to be attached to the minipump (Figure 4.M1). This system provided many advantages:

- The thin tubing was readily inserted intrathecally unlike wider bore cannulae.

- The medium gauge tubing was inflexible and hence did not kink. The knot in the tube provided a securement site to the animals' overlying muscle layers to prevent movement of the intrathecal segment.
- The widest bore tubing was sufficiently flexible to fit over the mini-pump attachment.

For the delayed peptide investigation cannulae were trimmed such that, following final attachment of the primed mini-pump, they would contain approximately 20µl of ACSF. With a constant pumping rate of 0.5µl/hr from a 2002 model mini-pump, a 40 hour delay in delivery of the peptide would ensue. In all other experiments the cannula contained the same solution as the mini-pump such that active agent was delivered from the time of implantation onward.

Surgical Techniques

All surgical procedures were approved by the UCL ethical committee and licensed by the Home Office. Adult female 200-220g Sprague-Dawley rats were anaesthetised with a mixture of halothane, nitrous oxide, and oxygen. For cannulation experiments, animals were operated on two days before the spinal cord injury was performed (day of injury defined as Day 0 throughout). Cannulae were filled with either ACSF or EphA4 blocking peptide in ACSF and the wide-bore end sealed with superglue to minimise uptake of blood once inserted and escape of peptide into the CSF before mini-pump attachment. A small hole was created with a fine-bore needle in the dura above cervical segment one of the spinal cord and widened with a scalpel, without damaging the underlying spinal cord tissue. The cannula was then inserted (with the fine end foremost) into this hole and fully inserted until the knot in the cannula sat submerged in the muscle layers overlying the C1-2 spinal cord levels. The cannula was then sutured into place through this knot and the remaining cannula section placed under the skin.

Animals were checked on Day -1 of the surgery for normal locomotion, exploration, feeding and grooming to ensure that no spinal cord damage had

been induced by the cannulation. Any animals showing behavioural changes or locomotor difficulties were removed from the experiment. On Day 0, animals were injected with tracing agents and spinal cord injuries were performed. Where anterograde labelling of the CST was required, 5µl of 10% biotinylated dextran amine (Molecular Probes, Oregon, USA) was injected into the motor cortex using standard coordinates (Paxinos and Watson, 1986). Labelling of the rubrospinal tract was carried out either by stereotaxic injection into the red nucleus of 3µl of replication-deficient HIV vector encoding EGFP (6.5×10^8 TU/ml) or injection of 5µl of 10% BDA. Spinal cord injuries were performed between C4 and C6 in all cases and were either a unilateral incision of the lateral column or, for anatomical and regeneration studies, an overinjury of one side of the dorsal column (Figures 4.M1B and C). For behavioural assays, a unilateral injury was performed designed to encompass the entire dorsal CST on one side while causing as little damage to the contralateral CST as possible (Figure 4.M1D).

At the end of each experiment animals were sacrificed by overdose with halothane and transcardially perfused with 4% w/v paraformaldehyde before removal of the spinal cord. Perfused tissue was stored at 4°C in 30% sucrose, 10% Thiermesol in phosphate buffer until use.

The labelling efficiency of the BDA injections was estimated at 0.5% based on counting the number of labelled fibers in the medulla (Figure 4.M2A) compared to the accepted estimate of rat CST fibre number (approx. 231,500[433, 434]).

Immunohistochemistry

Fixed tissue was cut parasagittally (for dorsal column injuries) or horizontally (for lateral column injuries) at 40µm thickness on a freezing microtome. Samples were permeabilised in TBST buffer (0.1M Tris Buffered Saline with 0.5% Triton-X100, Sigma) for one hour prior to incubation for one hour at room temperature in goat blocking solution (0.1 M TBS, 1% BSA, 0.1% Triton X-100, 10% normal goat serum, Sigma). Sections were incubated in monoclonal mouse anti-GFAP (1:1000 in goat blocking solution, Sigma)

overnight at 4°C and washed three times in TBST before a two hour incubation in goat blocking medium containing streptavidin-Alexa 568 (1:1000, Molecular Probes) and either goat anti-mouse FITC (1:400, Sigma) or goat anti-mouse 633 (1:400, Sigma) at room temperature. Sections were then washed three times in TBST before being mounted on gelatinised slides, coverslipped in DABCO and sealed with nail varnish.

Digital image capture and analysis

Fluorescence images were acquired on a Zeiss 510 confocal microscope using conventional filter based fluorescence optics. Excitation and emission wavelengths were, respectively: FITC and EGFP = 488nm, 505 - 550nm; Alexa 568 = 543nm, >560nm; Alexa 633 = 633nm, >650nm. Imaging of slides labelled with multiple dyes was always sequential with illumination at only one wavelength at any one time.

Analysis of each image for regeneration was performed identically, using the Zeiss Image Analyser Software. The GFAP channel for each image was isolated and the midline of the lesion site was drawn in on the image, using the edge of the GFAP staining as a guide. The 'red' channel was then isolated such that only the BDA-labelled CST or RST and the drawn-in midline marker were visible. The distance of identifiable termination bulbs from the guideline was then established. If both the RST and CST had been labelled, the 'green' channel containing the RST tracing data was then isolated and similar distances calculated. Subsequently these distances were collated and analysed. An example of this analysis is demonstrated in Figure 4.M2B.

GFAP analysis was performed on the Image Analyser Software. Sections of lateral column injuries were only used in analysis if the background streptavidin-Alexa 568 staining (which is an excellent marker for tissue loss) indicated that the entire contents of the lesion cavity were present. The 'cavity' region of the lesion was isolated and the average GFAP staining intensity calculated based on pixel intensity within this region. A 150μm thick 'penumbra' around each lesion was similarly analysed and a control region of contralateral, uninjured, lateral white matter was also analysed for GFAP

intensity (see Figure 4.M3A). The two values were normalised against this control intensity and combined with values from a range of horizontal sections through the spinal cord.

Behavioural Training and Assay

Two behavioural assays were used to assess improvements in functional recovery following peptide administration. The rearing assay and the paw reaching assay, developed by Professor Raisman's laboratory[225], were used to assess locomotor and fine movement respectively for a 28 day period following a dorsal column lesion. Training of animals for the rearing assay was not required as the animals' natural curiosity was sufficient for exploration of their environment once they became comfortable in their surroundings. Animals were placed in a clear Perspex cylinder 40cm high with a diameter of 24cm (Figure 4.M3B). Animals were pre-conditioned for three ten minute periods in the apparatus two weeks before the surgical process was begun to ensure anxiety did not influence the results. During the week before surgery animals were assessed three times to build up a base-line paw usage record to compare with the post-injury data. During result taking, animals were left in the apparatus until they began to groom, signalling that they were relaxed, before data was collected. Each animal was observed until it performed twenty rears, a successful rear defined as the animal facing the Perspex wall directly and showing a fully raised rear with clear weight bearing on the forepaws. The usage of each paw was noted and the proportion of rears using the injured forepaw calculated.

The paw reaching assay required extensive training of the animals. 140g male Sprague-Dawley rats were used in this study as the complete training usually required a month, resulting in animals bring ready for surgery around 240-280g, similar to that used in the anatomical studies. Male rats are also known to be easier to habituate and train and were therefore used. Animals were housed in pairs throughout the entire training and analysis period as often one rat would learn a particular phase of the training more rapidly and stimulate the other rat to follow its actions and learn the task. The apparatus used for this task was designed to slot into the animals' cage and provide a clear

Perspex wall with a 7cm wide and 1.5cm wide slot with a ledge on the external side on which to place food rewards (Figure 4.M4A). The apparatus incorporated an extended 'roof' of Perspex to completely isolate the animals in the cage to minimise external influences. For the first week animals were habituated to the apparatus for 20 minute periods every other day. During this time small amounts of food reward were freely available and animals rapidly accepted the new foodstuff into their diet. Phase two of the training (usually 7-10 days in duration) involved supplying the food reward through the slot in the Perspex with blunt forceps to teach the animals to accept the experimenter's presence and also to accustom them to retrieving the reward from this area. Phase three (usually 10-14 days in duration) taught the animals to retrieve the reward from the ledge. At first the reward would be stabilised by blunt forceps as the animals' grasp and retrieve failure rate was high and this permitted them to maintain interest in the training. At the beginning of phase three animals often showed no preference for either forepaw but rapidly a dominant (termed 'on') paw developed such that by the end of phase three when rapid and reliable retrieval of rewards was attained, the 'off' paw was rarely used.

Animals were only selected for surgery and inclusion in the study if, during the initial training period, they had shown frequent use of both forepaws. An initial pilot study indicated that animals that were strongly trained in only one forepaw rarely learnt to use their off-paw after the lesion and instead persisted in the use of the injured paw until an adapted method of reaching was learnt which involved a 'scooping' use of the forepaw – probably mediated by the RST. The distinctive nature of this reaching action meant that it was readily identified and all animals were monitored closely in subsequent studies to ensure no RST-based recovery occurred. Another important consideration raised during this pilot study was the requirement for weight-bearing on the opposite paw for a successful reach. In the pilot study animals were assessed for recovery in the days immediately following an injury, before weight-bearing on the injured forepaw had been fully restored. Under these circumstances animals were unable to reach with their uninjured forepaw and often persisted with the uncoordinated, injured paw until the RST-mediated reaching technique was learnt. Hence, in the full study, animals were left and only

assessed for rearing when moderate weight-bearing had returned. This was often a period of five days and initial improvements in the rearing assay were apparent around this time point also.

Each pair of animals was trained and analysed three times a week between 9am and 10am as later times of day often yielded poor results due to the nocturnal nature of the rats. Analysis consisted of providing food rewards repeatedly until the animals showed no further interest. The success rate of each forepaw at navigating through the slot and, separately, successfully grasping and retrieving the reward was recorded. During the week before surgery the animals were assessed three times to develop a base-line record with which to compare post-injury data.

RESULTS

In Vitro Analysis of Peptide Inhibition of EphA4 Signalling

E17 Sprague-Dawley rat neocortical neuron growth cones had a typical spread out morphology with multiple filopodial and lamellipodial protrusions (Figure 4.1A). The collapsed growth cones were readily identifiable with a highly F-actin dense appearance and often a single filopodial process (Figure 4.1B). Control cultures showed a low level of basal collapse (37 ± 5%, 95% confidence interval, Figure 4.1C) when exposed to DCC medium alone, comparable to that seen in the E7 chick RGC axon collapse assay (28%, Figure 4.9) and in the literature[235] (32%). Addition of EphA4 blocking peptide alone at a final concentration of 100nM for 45 minutes resulted in no change in this collapse rate (38 ±5%) indicating that binding of the peptide to the EphA4 receptor results in no receptor activation or other side-effects. Addition of ephrinA5-Fc homodimer at a final concentration of 20nM for 30 minutes resulted in an increase in growth cone collapse to 67 ±6%, significantly higher than that seen for the control assays ($p < 0.0001$ Fisher's Exact Two-Tailed Test). This confirms that E17 Sprague-Dawley rat cortical neurons express an EphA receptor that induces repulsive or collapse responses on activation, most likely the EphA4 receptor.

Three peptide concentrations were investigated to give an indication of the likely concentration required *in vivo* to abrogate most EphA4 signalling. As shown in Figure 4.1C, all three concentrations used (20nM, 50nM, 100nM) prevented EphA4-induced growth cone collapse when presented to neocortical neurons for 15 minutes prior to a 30 minute exposure to homodimeric ephrinA5-Fc ($p < 0.0001$, Fisher's Exact Two-Tailed Test for all three concentrations).

These data can be applied to the *in vivo* infusion protocol. Assuming a volume of CSF dilution of 400µL and a 50% CSF turnover rate per hour[435], 3mM peptide delivered at a rate of 0.25µL/hr will rapidly accumulate in the CSF to a concentration expected to block EphA4 (Figure 4.2A). 1.5mM peptide delivered at 0.5µl/hr in the two week study will show a very similar accumulation. As Figure 4.2A shows, 100nM will be reached very rapidly, although in practise diffusion of the peptide and leakage through the region of dural damage are likely to reduce the effective concentration around the injury site. However, the high concentration theoretically attained provide a large margin of error such that even extensive CSF leakage acutely after injury should not prevent effective EphA4 blockade.

Two Week Investigation of CST Regeneration with Immediate and Delayed Peptide Treatment

As is the case for all therapeutic interventions, there is a time window of opportunity during which the treatment will be fully effective. Published work[436] indicates that successful recovery of the CST occurs when olfactory ensheathing cells are implanted as late as six months following injury. Hence, it is critical to determine whether EphA4 blocking peptide infusion is similarly flexible as this will define its use in the clinical scenario. Furthermore, the ideal model for analysis of functional improvements following injury when peptide is administered would be a well established and stable injury to ensure that spontaneous recovery through spared fibres cannot complicate the analysis. Defining the latest viable treatment time will determine whether animals in behavioural studies can be left before treatment to ensure the formation of an established and stable behavioural phenotype.

An initial investigation assessed whether immediate or 48 hour delayed 1.5mM peptide treatment encouraged CST regeneration following dorsal column injury over a short time-course of two weeks. Control spinal cords showed a clear indication of the well-documented 'die back' of the CST from the lesion site[38, 390] with the formation of large, well-established dystrophic end bulbs (Figure 4.4A). There was also a notable lack of regeneration and sprouting from these termination bulbs, typical of the CST following injury but atypical of most CNS tracts in this environment. Furthermore, in all control animals a large cavity had formed with strong indicators of secondary damage such as a 'honeycomb' effect seen in GFAP staining of astrocytes (Figures 4.3A and 4.3C) not seen in uninjured white matter (Figure 4.3D). Animals receiving the delayed peptide treatment showed an identical phenotype to the control animals (Figure 4.4B).

Those animals receiving immediate peptide treatment showed significant improvements in the post-injury architecture of the lesion site. A clear reduction in cavitation and secondary injury were apparent with increased CST axon sprouting from termination bulbs and the formation of regenerative sprouts often oriented towards the lesion site (Figures 4.3B and 4.4C). Analysing termination bulb distances from the lesion epicentre using the Zeiss Image Analysis software for the confocal microscope revealed that immediate peptide delivery permitted a high level of recovery of the lesioned CST (Figure 4.5A). Control termination bulbs were an average of 556 ± 36μm from the lesion centre. In animals receiving peptide however, the mean termination bulb distance was reduced to 204 ±19μm ($p < 0.002$ with an n of 3 for each treatment, paired t-test, Figure 4.5). However, values seen in animals given delayed peptide treatment were not different from controls (Figure 4.5).

Four Week Investigation of CST Regeneration with Immediate Peptide Treatment

While significant CST retraction had occurred in the control animals two weeks following dorsal column injury and the improvements induced by the blocking peptide are obvious, significant recovery is likely to take longer than

two weeks. Hence, 3mM blocking peptide was delivered over a period of four weeks subsequent to a lesion of the dorsal CST. As can be seen in Figure 4.9B, die-back does not appear to worsen over the additional two week period in the control animals. However, cavitation and secondary damage are significantly more extensive at four weeks (Figure 4.6A). Animals treated with blocking peptide, however, show similar improvements in CST regeneration to that seen two weeks after injury (Figure 4.9A-B). The CST in control animals terminated on average 594 ±30μm from the lesion centre. In contrast, in peptide treated animals this value was reduced to 170 ±25μm, significantly smaller ($p < 0.002$ with an n of 3 or more for each treatment, paired t-test).

Few termination bulbs put forward regenerative sprouts and no significant progress towards the lesion margin was apparent in control animals (Figure 4.7A). However, in treated rats the lesion cavity, extensive in control rats, was often diminished to a narrow incision often filled with invading astrocytes (Figures 4.6B-D and 4.8B-D). Furthermore, numerous regenerating axons were seen to migrate along these astrocytic bridges to navigate the lesion site. Numerous termination bulbs were seen to put forward regenerative sprouts, often right up to the lesion margin (Figure 4.8A) and regenerative sprouting into uninjured ascending dorsal column white matter and ipsilateral grey matter was also visibly enhanced (Figure 4.7B- C).

Effects of Peptide Administration on GFAP expression and astrocyte behaviour and morphology following SCI

Lateral white matter injuries do not induce extensive cavitation or astrocyte retraction in control animals and hence are an ideal model on which to study changes in astrocyte behaviour and morphology following lesion (Figure 4.13C). Animals receiving a C5 lateral white matter injury were analysed 28 days post-injury having received either EphA4 blocking peptide or ACSF infusion. Injuries were performed such that they extended just dorsal to the level of the canal (see Figure 4.M1B).

Typical morphological changes were seen in control astrocytes with an upregulation in GFAP expression in a graded fashion with proximity to the

lesion centre. Hypertrophy and reorganisation of astrocytic processes was also seen (Figure 4.10B-E) consistent with many descriptions in the literature[26, 437]. Astrocytes in spinal cord tissue taken from animals that had received EphA4 blocking peptide for the duration of their injury showed very similar responses – with normal hypertrophy (Figure 4.10F) and reorganisation (Figure 4.10G) occurring. GFAP expression was analysed using the Zeiss Image Analyser software and the GFAP expression intensity seen by immunohistochemistry in a 150μm penumbra around the lesion cavity, when normalised to the intensity seen in contralateral uninjured white matter, was similar between the two tissue populations. Normalised control astrocyte GFAP expression was 1.52 ± 0.42 fold greater than control (mean ± SEM) while expression in animals receiving peptide was 2.18 ± 0.26.

However, while the reactivity of astrocytes was clearly unaffected by the presence of the blocking peptide, invasion of the lesion cavity by astrocytes was significantly different. Image analyser software was used to find the average GFAP intensity inside the lesion cavity and this value was normalised to the intensity seen in contralateral uninjured white matter. As Figure 4.11 shows there is a clear and significant difference in the invasion of the lesion site by astrocytes. As noted above for dorsal column injuries, sections stained for GFAP from animals receiving a lateral white matter injury show significantly less cavitation and retraction of surviving astrocytes away from the lesion centre when blocking peptide was infused (Figure 4.12A-C). Also of note is the apparent reduction in secondary tissue damage at sites distant to the original primary lesions (Figure 4.12D-E).

Four Week Investigation of RST Regeneration with Immediate Peptide Treatment

Published behavioural data suggests that the rubrospinal tract in rats is important in forelimb support while rearing, normal gait and for skilled locomotion[438]. As discussed in Chapter II, the RST in rats does not express EphA4 and hence provides a system in which to further test the mechanism of the EphA4 blocking peptide. Furthermore, any useful clinical intervention will be required to improve regeneration of more than one axonal tract, hence this

approach will further assess it's clinical suitability. Labelling of the RST was performed using a single stereotaxic injection of BDA into the red nucleus on the side contralateral to the injury. While the spread of BDA in the brain does present the risk of labelling axons of passage close to the red nucleus, particularly the CST, minimal labelling of other tracts was observed – as evidenced by the lack of dorsal CST labelling (Figure 4.13A) – while good RST labelling was achieved (Figure 4.13B).

The BDA-labelled RST could be clearly traced along the extent of the undisturbed lateral white matter on the contralateral side to BDA injection. Where it approached the lesion site, RST axons terminated at a range of distances from the lesion site and showed large, swollen dystrophic end bulbs some distance from the lesion centre (Figures 4.13D and 4.14). The die-back typical of the CST following injury was not apparent. However, due to the smaller number of labelled RST fibres quantification is required to build a reliable picture of the response of the tract to injury.

As shown in Figure 4.15, the RST retracts further 28 days after lateral white matter injury than at the two week time point (395 ±41μm compared to 302 ±11μm). The RST is seen to retract less far than the CST at this time point after injury (Figure 4.15) however, confirming the concept introduced in Chapter III that the expression of EphA4 on the CST is at least partially responsible for its atypical die-back response following lesion. In animals receiving 3mM EphA4 blocking peptide for the duration of the post-injury period, the RST recovered significantly (Figure 4.14) when compared to control animals treated with ACSF. Control RST termination bulbs were on average located 395 ±40μm from the lesion centre while peptide treated end bulbs were closer, at 250 ±6μm ($p < 0.05$ with an n of 3 for each treatment, paired t-test). The improved recovery of the RST under pharmacological block of EphA4 points to an underlying improvement in the recovery of the CNS to injury additional to the removal of inhibitory EphA4 signalling on axonal growth cones, an effect which will be restricted to the CST. As detailed above, this is most likely due to an effect on astrocytes, possibly by providing structural and trophic support in the lesion site or improved access to the lesion cavity.

As documented above, while there was no significant change in astrocytic GFAP expression or hypertrophy, extensive astrocytic invasion of the lesion site was apparent in peptide treated animals. Furthermore, these astrocytic processes often branched some distance into the cavity, providing a complete bridge across the astrocyte-free zone. There was no apparent reduction in the size of the astrocyte-free zone following peptide treatment, but that is unsurprising as extensive secondary damage and astrocyte retraction is uncommon following lateral white matter injury. RST axons following treatment showed extensive sprouting from termination bulbs and the sprouts often extended in a lesion-ward direction, often navigating the lesion margin scar to successfully migrate along astrocytic bridges (Figures 4.13E and 4.13F). Just as in peptide-treated CST regeneration, no neuronal processes were seen without associated astrocytes suggesting that astrocytes have a trophic or supporting role.

Comparing the Effects of Peptide Treatment on the CST and RST Four Weeks Following Lateral White Matter Injury

To ensure that the improvements seen in regeneration in Sprague-Dawley rats following peptide administration were not a strain-specific phenomenon, spinal cord injury in Lewis rats was investigated. To further our comparison of the CST and RST behaviour subsequent to injury and peptide treatment, a dual tract labelling procedure was employed. Lewis rats were injected stereotaxically with BDA into the motor cortex and an EGFP-expressing virus into the red nucleus. Animals underwent C1 peptide or ACSF cannulation and a lateral white matter spinal cord injury.

Figure 4.17A demonstrates the typical response of the two tracts to injury with the RST extending close to the lesion margin and the CST more retracted. Under control conditions neither tract put forward significant regenerative sprouts (Figures 4.17C and 4.18A) and both terminated in well-defined dystrophic end bulbs. Peptide administration in the Lewis rats induced a very similar response to that seen in the Sprague-Dawley strain with invasion of the lesion cavity by regenerative sprouts from both tracts (Figures 4.17B and

4.18B) and improvements in regenerative sprouting from termination bulbs (Figures 4.17D and 4.18D).

As clearly demonstrated in Figure 4.16A, the story of improvements in both CST and RST regeneration is confirmed statistically for the second rat strain. When compared to data from Sprague-Dawley rats, the fit is remarkably accurate considering the complexity of the study (Figure 4.16B). Lewis rats show an identical die-back of the CST in control conditions when compared to the RST which can be attributed to the difference in EphA4 expression. Furthermore, both the RST and CST respond well to the peptide administration showing a good regenerative response. Similarly to that found in the Sprague-Dawley study, the two tracts recover to very similar extents suggesting that the inhibitory response of EphA4 receptors present on the CST has been completely annulled in Lewis rats.

		Average Distance ± SEM	
Strain	Tract	Control	Treated
Sprague-Dawley	CST	594.40 ±30.51	170.40 ±25.83
Lewis	CST	514.95 ±18.52	226.24 ±7.75
Sprague-Dawley	RST	395.99 ±40.94	250.40 ±5.69
Lewis	RST	380.07 ±11.55	182.45 ±7.70

Functional Recovery Following Peptide Treatment

While anatomical recovery is a good indicator of beneficial changes in CNS regeneration following injury, it does not necessarily translate into functional benefits to the animal. To assess whether application of EphA4 blocking peptide to the site of a dorsal column lesion improves functional recovery following injury we employed the paw reaching assay developed by Professor Raisman's laboratory[225] and the rearing assay.

Control and treated animals showed no functional deficit in either test following intrathecal cannulation indicating that no damage was caused by the procedure, or at least any damage caused did not have any functional

consequences. Inspection of the spinal cord following dissection indicated that on occasion some slight deformation of the dorsal side of the cord occurred due to the presence of the cannula but this did not appear to induce any behavioural phenotype. All animals showed an immediate loss of use of the injured forepaw in both assays with a short (2-5 day) period of clawing in the injured paw and diminished weight bearing on the injured side. Both animal sets showed a similar time course of recovery of function in the rearing assay, typically recovering 60% or more use of the injured paw within 5-10 days (Figure 4.19A). In the paw reaching assay, control animals never regained use of their injured forepaw showing a consistent 100% use of the uninjured paw. The time course for the use of the uninjured, previously non-preferred, paw varied and was probably influenced by the time required for useful recovery of weight bearing ability on the injured paw. Furthermore, the extent of off-paw use during training and the time spent in the final phase of training when the on-paw was used dominantly would also influence the time required to rediscover the ability to reach with the off-paw. Animals receiving EphA4 blocking peptide, however, showed a gradual recovery of function in the injured paw subsequent to preliminary use of the uninjured paw (Figure 4.19B). The time course for this recovery varied with a mean of 10.7 ±1.7 days. Recovery was always limited in these animals with a mean percentage use of the injured forepaw of 30 ±1.9% after Day 10. Figure 4.20A shows a control animal trained to reach with both forepaws 28d following right hand side dorsal column injury, persisting in the use of it's left forepaw. Conversely, an identically trained and operated animal that received a peptide infusion had recovered use of it's right forepaw after 28 days (Figure 4.20B). Recovery occurred in all four animals analysed and no recovery was seen in the control group (Figure 4.20). As shown in Figure 4.19B, the difference in injured forepaw use is clear and statistically significant at $p < 0.05$ (comparing successful vs. unsuccessful recovery with an n of 4 for each animal set, Fischer's exact t-test).

At the end of the 28 day period of functional assessment a subset of animals received a BDA injection into the motor cortex contralateral to the spinal cord injury to ensure that no sparing had occurred, especially in those peptide

animals showing good recovery. All animals investigated showed no sign of sparing and usually a small degree of injury of the contralateral dorsal CST. Another subset of animals received BDA injections into the ipsilateral motor cortex to assess whether sprouting or plasticity from the uninjured contralateral dorsal CST could explain the improvements in functional recovery seen. As shown in Figure 4.21, neither control nor peptide treated animals show any sprouting of uninjured CST axons past the lesion site into contralateral dorsal white matter.

DISCUSSION

In Vitro Analysis of Peptide Inhibition of EphA4 Signalling

The ability of the EphA4 blocking peptide to abrogate ephrinA5-Fc mediated growth cone collapse at a 1:1 molar ratio of antagonist and ligand is highly encouraging. The high binding affinity of the peptide (K_D = 0.5nM[389]), for the receptor permits this efficacious and rapid (15 minutes for full blockade of growth cone collapse activity) action. The high selectivity[389] of the peptide for the EphA4 receptor over other EphA receptors that bear a strong conformational and sequence homology is remarkable and this indicates that it is EphA4 that is mediating the collapse action of ephrinA5-Fc. In the lesion site the selectivity of the peptide is such that it will not be expected to interfere with the interaction of astrocytic ephrinB2 and EphB2 on meningeal fibroblasts. This interaction is essential for the re-formation of the blood brain barrier and exclusion of invading meningeal fibroblasts from the lesion site[21]. The full abrogation of collapse activity by the peptide is also encouraging as this indicates the neurons lack other EphA receptors that might bind cognate ligands *in vivo* following CNS injury. Published expression studies indicate that adult cortical neurons do not express EphB receptors[323], hence application of the EphA4 blocking peptide should be sufficient to prevent all ephrin-mediated signalling affecting the injured CST. The rapid theoretical accumulation of peptide within the CSF, even with generous estimates of CSF turnover and peptide metabolism and leakage, indicates that full block of endogenous EphA4 should be achieved with a short time period following injury.

Two Week Investigation of CST Regeneration with Immediate and Delayed Peptide Treatment

Figure 4.4 clearly demonstrates the significant improvement in the regenerative response of the CST in animals receiving immediate peptide treatment. A detailed study of the response of this tract indicated that the improvements came from a number of sources:

- Increased termination bulb sprouting
- A clear reduction in the die back of the main CST retraction bulb.
- Improvements in the wound healing response of astrocytes

Termination bulbs in control animals rarely put out sprouts (a visual estimate would range from 5-15%) and those that occurred were usually not of any great distance. However, in animals treated with peptide numerous termination bulbs (estimated at 30-70%) put out sprouts many of which grew long distances (often over 200μm) and frequently reached the astrocyte margin. The reduction in the die-back of the main bulk of the CST fibres normally seen after injury is likely to be due to the abrogation of inhibitory/collapsing interactions between strongly expressed astrocytic ephrinB2 at the lesion margin, myelin ephrinB3 and EphA4 receptor accumulated in the termination bulbs of this tract. However, the improved response of hypertrophic astrocytes to the lesion when exposed to peptide may also reduce die-back by providing trophic or structural support. The observed improvements in the wound response of hypertrophic astrocytes is similar to that reported by Goldshmit *et al.*[12] who saw closing of the wound to the extent that the lesion site was often hard to define. While the response of the lesion site is not so dramatic in this shorter duration study (two weeks compared to six) it is still very positive. This closing of the wound and preservation of astrocytic processes into the lesion site may provide trophic support for regenerating axonal processes. Crucially, however, it will provide a stable structural support on which axons can migrate and help close the wound preventing excessive withdrawal of the axonal stump from the lesion centre. Hence, it is likely that improvements in the wound healing process and associated reduction in cavitation and secondary injury, as well as the

improvement in the regenerative response of the CST both contribute to the quantified improvements in regeneration seen in Figure 4.5.

While it is disappointing that the window of therapeutic opportunity appears to be so short, which will preclude a behavioural approach using an established long-term lesion as the treatment model, this does tell us about the likely mechanism of action of the peptide. Interactions between CST-based EphA4 and ephrinB2 and ephrinB3 local to the injury will have occurred during the 40 hour delay of peptide administration and the sequence of events leading to the withdrawal of the CST will have been set in motion. Delayed inhibition of the EphA4 receptor cannot prevent this rapid retraction and die-back of the CST once it has begun, while rapid intervention can (Figure 4.4). This implies that the interaction between CST-based EphA4 and its ligands may be the start of a signalling cascade resulting in CST retraction such that inhibition of EphA4 at a later stage is unable to reverse the mechanism.

Four Week Investigation of CST Regeneration with Immediate Peptide Treatment

As Figure 4.9 indicates, the recovery of the CST seen at two weeks following injury when EphA4 blocking peptide is administered is retained but not significantly improved upon after four weeks. On first inspection this could be attributed to the presence of other inhibitory agents in the vicinity of the spinal cord lesion site, of which there are many. However, while the statistical approach is a good indicator of the behaviour of the main bulk of the CST – the main bullet-shaped mass of retraction bulbs – it does not reflect the behaviour of individual axons effectively.

The clearly improved and reduced lesion cavity containing many more astrocytic processes should provide a fertile ground for axonal regeneration as shown in Figure 4.6. This is borne out by the extensive regenerative sprouting that often extends through the typical lesion margin and into the cavity (Figures 4.7 and 4.8). This sprouting phenomenon, seen in the two week data, has clearly expanded and the additional two week time period has permitted more astrocytes to invade the lesion site as a bridging structure for

the regenerating axons and for these axons to migrate along them. Hence, while the main bulk of the CST termination bulbs show improved sprouting over control rats, this sprouting phenomenon does not appear to have increased during the two-four week period of peptide treatment. However, these processes are increasingly long and show a frequently directional approach to regeneration towards and into the lesion cavity. While many regenerating axons do not appear to be able to migrate through the physical barrier produced by the interaction of reactive astrocytes and invading meningeal fibroblasts, a small proportion of those seen in the four week animals do so. These labelled sprouts, perhaps only representing 0.5% of the actual sprouts present, represent a significant regenerative response that could provide functional improvements following injury. This regenerative sprouting would not be picked up by the statistical approach but is clearly a significant increase in regenerative potential over that seen following two weeks of peptide treatment. Whether the administration of the blocking peptide might diminish the tightness of the astrocytic barrier to regeneration or reduce the barrier's inhibitory nature is difficult to asses. However, Goldshmit *et al.*[12] saw reductions in the expression of CSPG in glial scars in EphA4 knock-out mice and hence a reduction in the inhibitory nature of the scar is a feasible explanation.

Also of note is the interaction between regenerating axons within the lesion margin, as defined by GFAP staining of astrocytes, and astrocytic processes invading the cavity. As axons were never seen in this location without association with an astrocyte it is likely that the astrocytic processes are providing both a 'pioneer' role into the lesion cavity and also structural support for the axons, rather than *vice versa*. Interestingly these processes appear to have abandoned their typical orientation parallel to the lesion margin, as usually seen four weeks after injury[26]; and returned to a morphology more reminiscent of earlier time points in the injury process when the glial scar was more flexible and permeable during the interaction with invading meningeal cells. Hence, these atypical pioneer astrocytes may provide not only the structural support required by regenerating axons to infiltrate the cavity, but also the access points (i.e. a weak link in the new glial limitans) to the cavity.

The debate regarding the role of astrocytes as either positive (trophic, supportive) or negative (CSPG expression, physical barrier to regeneration) is very active with no firm conclusion yet resolved. However, the data presented here suggests that, following pharmacological blockade of the EphA4 receptor, the surface of some, or all, astrocytes becomes an acceptable medium for regeneration and the physical barrier to regeneration induced by the glial scar appears to be relaxed.

Effects of Peptide Administration on GFAP expression and astrocyte behaviour and morphology following SCI

Astrocytes exposed to EphA4 blocking peptide subsequent to a lateral white matter injury showed the normal hypertrophic and reactive response to CNS injury seen in control, ACSF treated animals. However, animals receiving blocking peptide had notably smaller lesions with less secondary tissue damage and much greater numbers of astrocytic processes invading the cavity. Whether this improvement in cavity size is due to the ability of astrocytes to survive the primary/secondary injury phase, a reduction in the astrocytic withdrawal response to CNS injury or improvements in the invasion of the lesion cavity is hard to determine. The reduction in secondary tissue damage seen might suggest either an improved survival of astrocytes in this phase of the injury or a reduction in the severity of secondary damage.

These improvements in astrocytic behaviour cannot be readily explained based on established signalling interactions in the lesion site. A number of possibilities exist however, that might explain the changes in the astrocytic response following EphA4 blockade:

- Prevention of *cis*-interaction between astrocytic EphA4 and ephrinB2
- Stopping the transactivation of EphA4 on astrocytes subsequent to exposure to cytokines
- Interfering with exposed oligodendrocyte myelin ephrinB3 binding to astrocytic EphA4

Cis-interactions have been shown to modulate the effects of both ligands and receptors[278]. EphrinB2 upregulation in astrocytes appears to coincide with meningeal fibroblast invasion following injury[26] and would be expected to interact with co-expressed EphA4. If this interaction mediates part of the astrocytic response to injury then blocking EphA4 may therefore uncouple part, or all, of the activation of astrocytes induced by the invasion of meningeal fibroblasts. The fact that delayed treatment does not induce any improvements in CST regeneration/sprouting or astrocytic invasion of the lesion cavity suggests that the mechanism of action must be rapid and must be on an interaction that occurs rapidly after the initial insult. The time course of the meningeal cell invasion is much longer than this, often taking up to a week for full invasion[26], suggesting that this possibility is unlikely.

Published data[12] indicates that knocking out the EphA4 receptor makes cultured astrocytes unresponsive to cytokine application *in vitro*, hence preventing gliosis. The data contained therein indicates the most likely signalling mechanism at work is a transactivation of EphA4 downstream of a cytokine receptor(s). Hence, pharmacological blockade of the EphA4 receptor would not be expected to interfere with this signalling process. If a conformational change is required as part of the transactivation then the blocking peptide may inhibit part or all of this process. The lack of any change in the hypertrophy and gliosis of astrocytes as shown by swollen cell bodies and upregulated GFAP expression suggests any change induced by the peptide must be subtle, however.

A third possibility is that the sudden exposure of EphA4-positive astrocytes to myelin ephrinB3 following injury might mediate part of the astrogliosis reaction. Hence, in this context blocking the EphA4 receptor would be expected to modulate astrocyte responses to CNS injury. The exposure of the CST to ephrinB3 in the lesion site is likely to be rapid as it is present in uninjured oligodendrocyte myelin. Hence this theory fits well with the probable time course of the CST response to injury and the action of the peptide blocker. However, immunohistochemical visualisation of the ephrinB3 protein is technically difficult which impedes investigation of this interaction.

Hence, while no firm conclusion can be drawn from this study, it is readily apparent that there is a significant change in the astrocytic response to injury. Importantly, a more compact lesion with greater structural support will improve axonal regeneration and functional recovery significantly.

Four Week Investigation of RST Regeneration with Immediate Peptide Treatment

The aim of this approach was to discover if the regenerative improvements seen in the CST due to peptide administration were due solely to inhibition of the EphA4 receptor on the termination bulbs and proximal axonal stumps or whether there was a secondary underlying phenomenon also encouraging regeneration. Labelling of the RST using BDA is significantly more complicated than that of the CST due to the necessity for stereotaxic surgery, and the possibility of labelling axons of close passage. Furthermore, there are relatively fewer numbers of RST axons in comparison to the CST. However, in most animals sufficient RST labelling was seen to permit acquisition of good quantitative data regarding regeneration, while no labelling of the dorsal CST (and hence, by inference also the lateral CST) occurred.

As shown in Figure 4.14, good quantitative improvements in RST regeneration are seen following peptide administration with the associated increases in sprouting from termination bulbs and formation of regenerative sprouts into the lesion. As the RST in rats does not express EphA4[323] this improvement cannot be ascribed to any mechanism intrinsic to the RST. Instead, as discussed above, post-injury changes in astrocytic behaviour induced by block of EphA4 signalling are the most likely candidate. However, the increased invasion of the lesion cavity (Figures 4.11 and 4.12) by astrocytes to provide structural, and possibly trophic, support is unlikely to be sufficient to promote regeneration into the lesion cavity to the extent found in peptide treated animals. The expression of growth inhibitory mediators such as CSPGs on the lesion scar, and the physical barrier produced by tightly interlocked astrocytes, would be expected to prevent significant regeneration into the lesion site, regardless of improvements in the permissive nature of the

cavity. However, the possibility discussed above, that inhibiting EphA4 might reduce certain components of the astrogliosis to make areas of the scar more permissive for growth through reduced CSPG expression (as seen in Goldshmit *et al.*[12]) and interlocking, would account for this increased navigation of the lesion scar.

The improvements seen in this RST study indicate that peptide administration is able to improve regeneration of two crucial descending motor tracts important in locomotion. Furthermore the increases in sprouting apparent will facilitate plasticity-induced recovery through spared white matter and possibly, at longer time points, regeneration through the lesion site to permit reformation of the original neural connections.

Comparing the Effects of Peptide Treatment on the CST and RST Four Weeks Following Lateral White Matter Injury

As shown in Figure 4.16A, the application of EphA4 inhibitory peptide during the 28 days following a lateral white matter injury induces a robust regenerative response from both the RST and CST in this region. The fact that this response directly mirrors that found when both tracts were investigated in a separate strain of rat, is highly encouraging. Furthermore the CST data is very similar to that seen following a dorsal column injury (Figure 4.16B) for both treated and control animals, suggesting similar responses to lesion and similar regeneration mechanisms. The fact that the lateral CST retracts to the same extent as the dorsal CST, despite the nature of the dorsal column injury being significantly less deleterious than the lateral white matter injury, is testimony to the inhibitory nature of the EphA4 expressed on the CST. Furthermore, the dorsal CST recovers to the same extent as the lateral CST suggesting that the peptide is capable of reversing all the negative effects of EphA4 signalling and promote significant recovery.

The astrocytic response to peptide administration is maintained in the Lewis rats as well, with good invasion of the lesion site by astrocytic processes and formation of CST and RST sprouts along these processes. Hence, modulation

of the astrocyte response to injury appears to be a common mechanism in improving recovery following CNS injury in these two rat stains.

Functional Recovery Following Peptide Treatment

The establishment of a reliable assay for recovery of CST function was essential and the final approach appears to give a quantitative and sensitive account of improvements in reaching and rearing associated with dorsal column injury. Ideally, our experimental procedure would allow a period of no treatment to ensure the lesion was stable and that no spontaneous recovery ensued over a period of months. Subsequent to this period, introduction of the treatment or control intervention would permit an assessment of recovery with confidence that no spared fibers could account for this recovery. However, as shown by the initial study into the duration of the window of therapeutic opportunity, a delayed treatment regime is not possible here. The injury type used here is very similar to that used in the work of Raisman and colleagues[225] who find the phenotypic change robust and not prone to spontaneous recovery. The robust change in forepaw usage seen in all control and treated animals for one-two weeks prior to any recovery of function in the injured paw suggests all animals received a complete lesion of the injured CST. Spontaneous recovery from this injury occurs with as little as one percent of spared CST fibers and is sufficient to induce a near-full recovery of reaching ability[225]. However, the time course for this recovery is very rapid and complete and would be identified as such in the analysis. Furthermore, the best recovery seen from any animal only resulted in an approximately 40% recovery of function in the injured paw 28 days after injury suggesting that sparing did not account for the recovery seen. Animals were also labelled with BDA into the motor cortex associated with the injured forepaw after completion of the reaching analysis (day 29-32) , sacrificed ten days later and examined for axonal sparing; none was apparent.

This functional recovery study, while only a small-scale (n of 4 in each group) study to investigate potential physiological improvements following peptide administration, gave excellent results (Figure 4.19). While the clear conclusion

is that the peptide induced significant recovery in the CST, a number of phenomena require closer examination.

The recovery of the use of the injured forepaw in the rearing assay was rapid and appeared to be independent of the treatment protocol applied. This suggests that the uninjured RST was rapidly able to take full control of the weight-bearing and basic locomotion in the injured forepaw. However, lateral white matter injuries of the RST induce a similar rapid recovery response to that seen here and long term, stable loss of use of a forepaw in the rearing assay requires a lateral-central overinjury. Hence, while the RST is obviously a major coordinator of the weight bearing and locomotion required for the rearing assay, it cannot be the only regulatory tract. A likely explanation is that the ascending dorsal column plays a feedback role[438] in controlling the rearing assay locomotion such that, following injury, accommodation or adaptation by the animal is required before confident use of the forepaw is regained.

The animals receiving EphA4-blocking peptide in this study did not show a full recovery of function within the 28 day period, reaching only 30 ±1.9% recovery on average. However, grasp strength recovery in EphA4 knock-out mice following lateral column injury show only a ~40% recovery of function[12] 28 days following injury. Full recovery took three months to develop. Furthermore, mice develop much smaller lesion cavities than mice and the Goldshmit *et al.*[12] study used the less deleterious lateral column injury, compared to the dorsal column injury in this study. Hence extending this study (readily achieved by replacing the mini-pumps every 28 days) to three months would be expected to produce even better recovery of function.

The lack of plasticity or sprouting of the uninjured contralateral CST into the opposing dorsal white matter suggests that the functional recovery seen in peptide treated animals was due to increases in regenerative sprouting of the lesioned CST and the increased invasion of the lesion site by these regenerating processes. While few axons were seen to fully navigate the lesion site, the labelling efficiency for the CST in these experiments could be as low as 0.5%, hence 200-fold as many regenerating axons would be

present in a typical animal. Only minimal regeneration beyond the lesion site would be required for potentially beneficial connections with motor pattern generators or plastic reorganisation of interneurons to provide functional connections to distal motor groups. Furthermore, the extensive sprouting seen on the rostral side of the injury extended significantly into the spared grey matter and interneuronal connections could potentially develop from these plastic changes.

The precise mechanism by which EphA4 blocking peptide improves regeneration following injury is likely to be amenable to investigation due to its specific pharmacology. A number of possible mechanisms of action might be at work:

- A reduction in CSPG, or other growth-inhibitory mediator, expression. An interesting experiment would be to look at CSPG, Nogo, etc. expression in the glial scar following peptide treatment to assess whether there is any change. The apparently growth-permissive or -promoting role of pioneer astrocytes that invade the lesion cavity following peptide administration suggests that they might demonstrate a reduced expression of these highly inhibitory molecules.
- A change in the expression profile of neurotrophins or other secreted factors from astrocytes. A simple experiment to assess any expression changes may explain the growth improvements seen and suggest neurotrophic support regimes tailored for regeneration.
- A change in the reactive nature of responsive astrocytes. The increased invasion of the lesion site seen following peptide infusion suggests that the physical barrier developed by tightly interacting astrocytes may be relaxed. Immunohistochemistry to highlight connexion-based tight junctions would identify any change in this growth-inhibitory mechanism.
- Preventing the initial retraction of the CST by interfering with ephrinB2-EphA4 interactions or promoting regeneration of this tract subsequent to retraction. The fact that delayed peptide treatment does not rescue the CST following injury suggests that the peptide prevents retraction in the first place. However, a time course following injury would permit the

formation of a precise post-injury profile of the CST and RST when exposed to peptide.

Defining the precise mechanism at work would be simplified if the peptide could be traced. During the development of the blocking peptide Murai *et al.*[389] attached the peptide sequence to a display library to pan for binding to the EphA4 receptor. This suggests that the binding affinity is not severely affected by attaching large structures. Hence, the development of a peptide tagged with a fluorescent marker, similar to tagged tetrodotoxin, would permit an accurate analysis of where the peptide bound most strongly and hence indicate the mechanism of action. This construct could also be used to perform high affinity and specificity expression analysis on other tissues.

Work by Weidner *et al.* suggests that spontaneous recovery of forepaw reaching ability following dorsal CST injury in rats may occur through plastic sprouting from the ventral CST[439]. In this study animals were effectively forced to use their injured forepaws and in this situation perhaps the drive for spared CST components to take over dorsal CST functions is very strong. This is perhaps similar to the recovery of function seen in animals in the pilot functional study where due to weight bearing limitations the injured paw was used for reaching. Perhaps in this study the ventral CST also contributed to the recovery of function. However, in the main functional study presented here, no untreated animals recovered paw reaching ability suggesting that ventral CST sprouting was not induced. Furthermore sections through the dorsal spinal cord revealed no CST labelling beyond the lesion site suggesting that ventral CST sprouts did not re-innervate this half of the spinal cord.

CONCLUSION

This study strongly supports the hypothesis that accumulating EphA4 receptor present on the termination bulbs of CST fibres subsequent to either dorsal or lateral column injury is responsible for the atypical die-back of the CST compared to other descending tracts. Furthermore, blocking EphA4 reverses this effect, permitting the CST to regenerate in a similar fashion to the EphA4-negative RST. However, administration of EphA4-blocking peptide also

appears to improve the regeneration of the RST following lesion suggesting that blockade of EphA4 on another cell type in the lesion site is responsible for part of the recovery seen. Astrocytes are known to express EphA4 and this has been linked to cytokine-induced astrocytosis following injury. Astrocytes in lateral column injuries show no changes in their reactive nature when exposed to peptide, but do appear to invade the lesion cavity to a greater extent. The extensive interaction between regenerating axonal sprouts and these invading astrocytic processes suggests that they may provide structural or trophic support. Administration of EphA4-blocking peptide also clearly improves functional recovery of the animals' ability to control voluntary fine locomotion, a hallmark of CST function, demonstrating that the anatomical regeneration is accompanied by physiological benefits.

Hence, pharmacological antagonism of the EphA4 receptor appears to induce significant recovery in animals undergoing spinal cord injury through multiple mechanisms. This effect has been confirmed in two strains of rat, Sprague-Dawley and Lewis, and following both dorsal and lateral column injuries to two descending motor tracts. Further pre-clinical investigation is required to extend this data and to further dissect its mechanism of action.

Figure 4.M1

Cartoons depicting cannulation and spinal cord injury procedures

A. Cartoon of implanted cannula and mini-pump. Cannulae were inserted at the C1 region into the subarachnoid space and sutured through the inflexible tubing loop to the uppermost muscle layers. Mini-pumps were glued to the flexible tubing end of the cannula.

Cannulae were constructed from:

Blue – Wide bore, flexible tubing attached to the mini-pump.

Green – Medium bore, inflexible tubing

Red – Fine bore, flexible tubing

B-D. Cartoons of spinal cord injuries performed. White matter represented by yellow, grey matter by grey and injured regions by overlying diagonal lines. Dorsal side of cartoon is uppermost. Lateral column injuries (A) were designed to completely transect the lateral CST and the RST, usually including a small amount of grey matter to ensure complete transection was performed. Normally the lesion did not extend as ventral as the canal. Dorsal column injuries (B) were performed to completely transect the dorsal CST on one side of the animal. Ipsilateral dorsal horn grey matter and contralateral dorsal column tissue was normally transected to ensure complete lesion. Unilateral CST injuries for the behavioural studies (C) were designed to completely lesion the dorsal CST on one side of the animal but cause as little damage as possible to the contralateral CST.

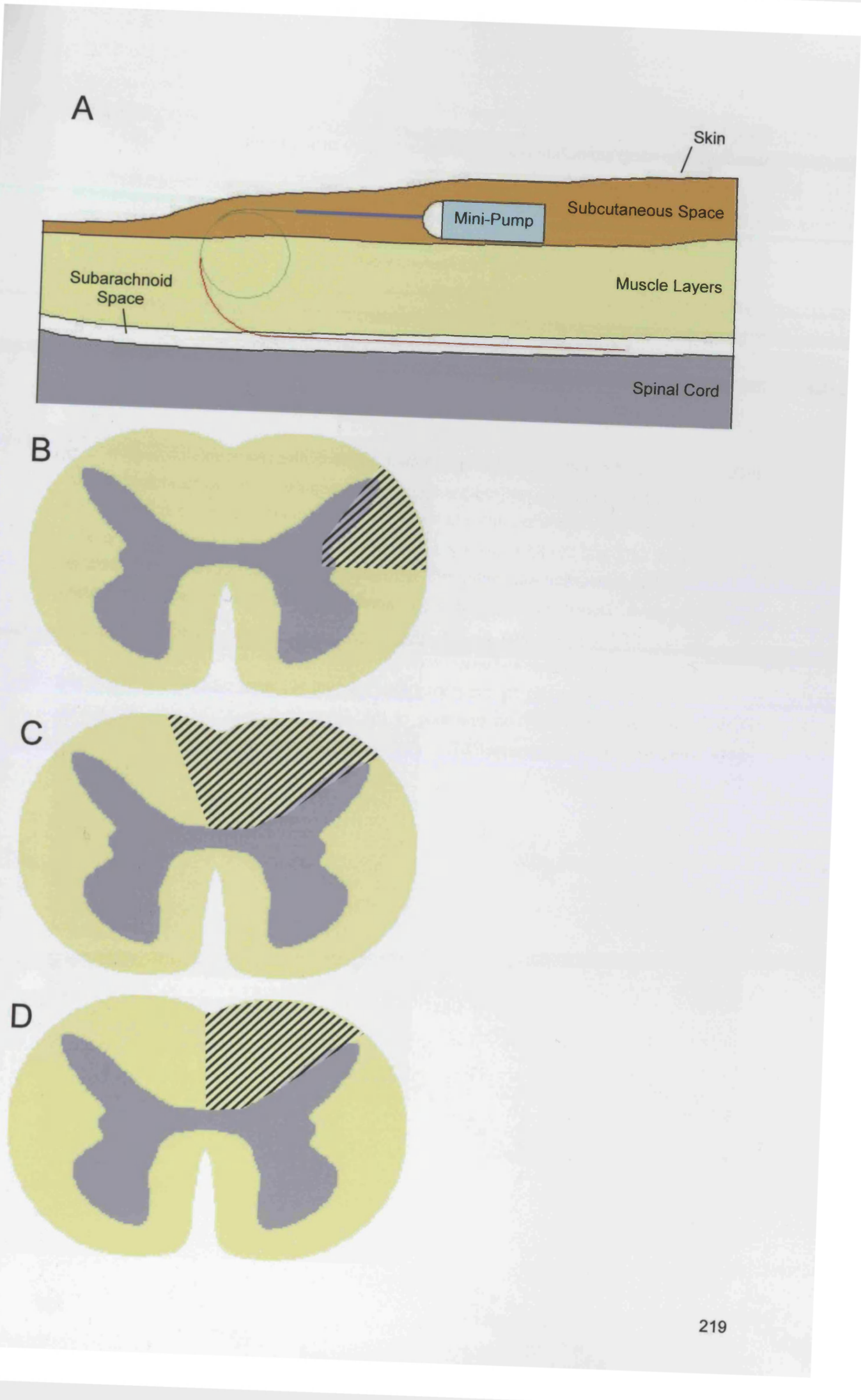
A
Skin
Mini-Pump
Subcutaneous Space
Subarachnoid Space
Muscle Layers
Spinal Cord
B
C
D

Figure 4.M2

Tract labelling and regeneration analysis

A. Coronal 40μm section through the caudal medulla of a rat 28 days following injection of BDA to the motor cortex. The pyramidal tract is clear (dorsal is down in this image) and shows good CST labelling. Scale bar 300μm.

B. An example of the end product of the RST and CST regeneration analysis of a lateral white matter lesion. GFAP immunohistochemistry (blue) identifies astrocytes and hence the midline of the lesion cavity can be drawn (white line). BDA-labelled CST (red) and EGFP-labelled RST (green) termination bulbs are readily visible and the distance between these termination bulbs and the mid-cavity line is measured. Averaging a complete series of sections for both axonal tracts though a spinal cord produces a reliable quantification of the regeneration gap. Horizontal 40μm section, scale bar 200μm.


A

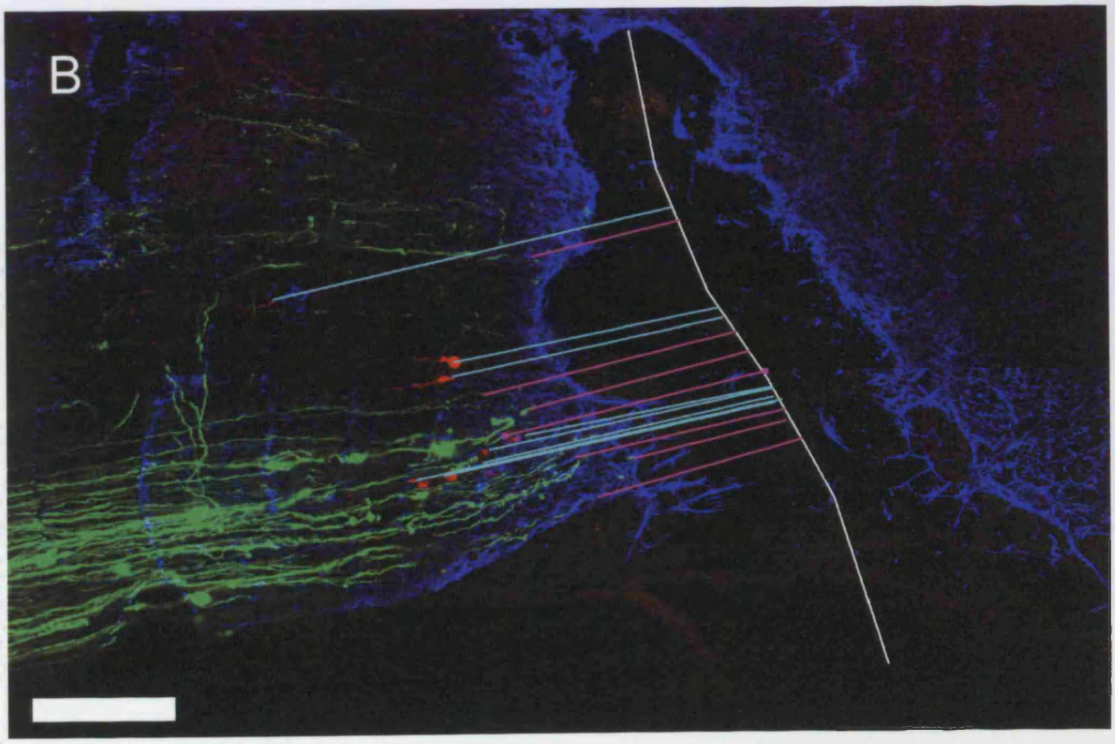
B

Figure 4.M3

GFAP expression analysis and the rearing assay

A. Example of GFAP analysis. Horizontal 40μm section through a lateral white matter injury 28 days after lesion stained for GFAP. Each lesion was divided into two zones for analysis – the lesion cavity as defined by the margin of GFAP expression, and the lesion penumbra, a 150μm wide zone around the cavity. Quantification of the GFAP expression was performed using Zeiss Image Analyser software and normalising values to the contralateral, uninjured white matter GFAP expression.

B. The rearing assay. Animals were placed in a clear plastic tube and given sufficient time to adapt to their surroundings. Exploratory rearing was then recorded and the proportion of use of each forepaw noted. Rears accepted for analysis involved the animal directly facing the glass, with forepaws in front of the body, obvious raising of the body weight to the hind paws and weight bearing on the forepaws in contact with the tube.

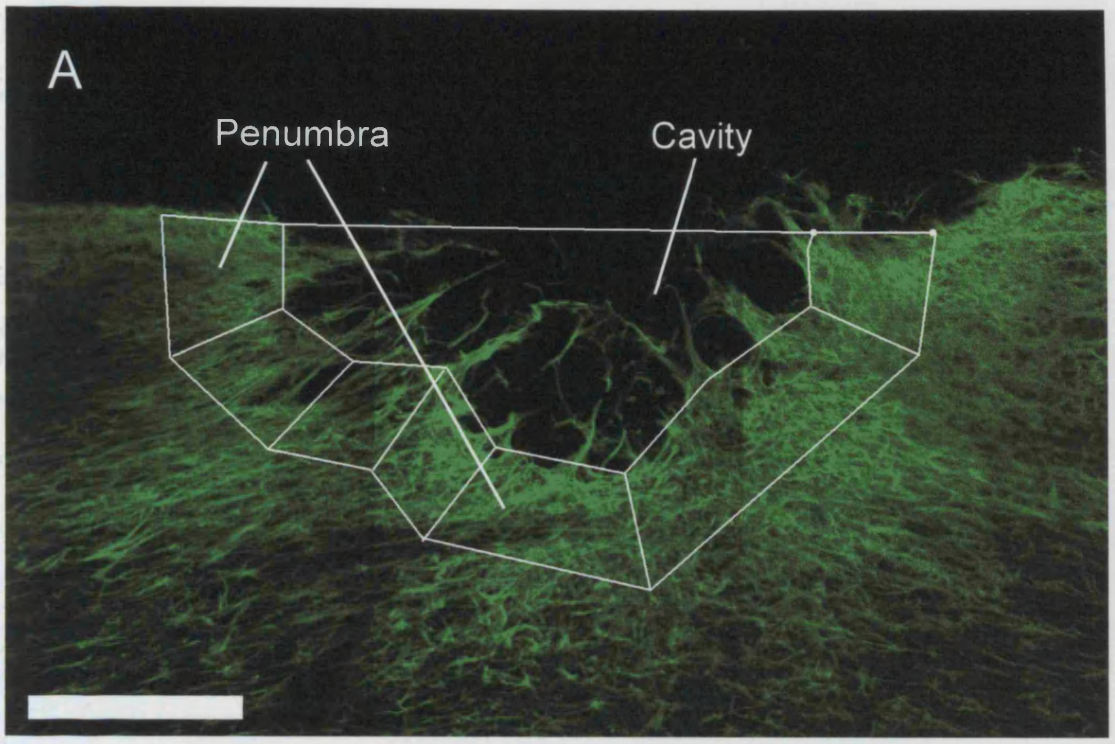
A
Penumbra
Cavity


B

Figure 4.M4

The paw reaching assay

Animals were conditioned to being placed in the apparatus (i) which entirely enclosed two thirds of the cage. Animals were then trained to reach with both forepaws for food rewards placed the other side of a small slot in the front wall of the apparatus (ii). As shown in (ii), animals typically used one forepaw to lean against the plastic front wall of the apparatus and used the other paw to reach for the food reward. Animals were trained, housed and assessed in pairs to increase their learning stimulus.

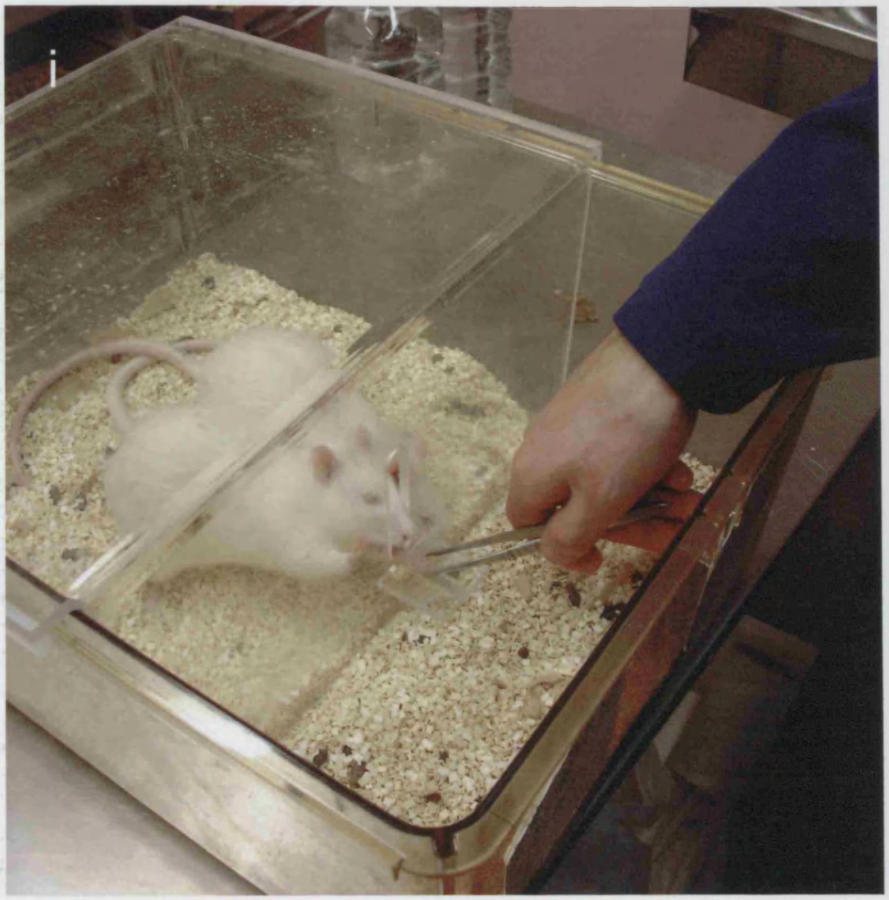
i

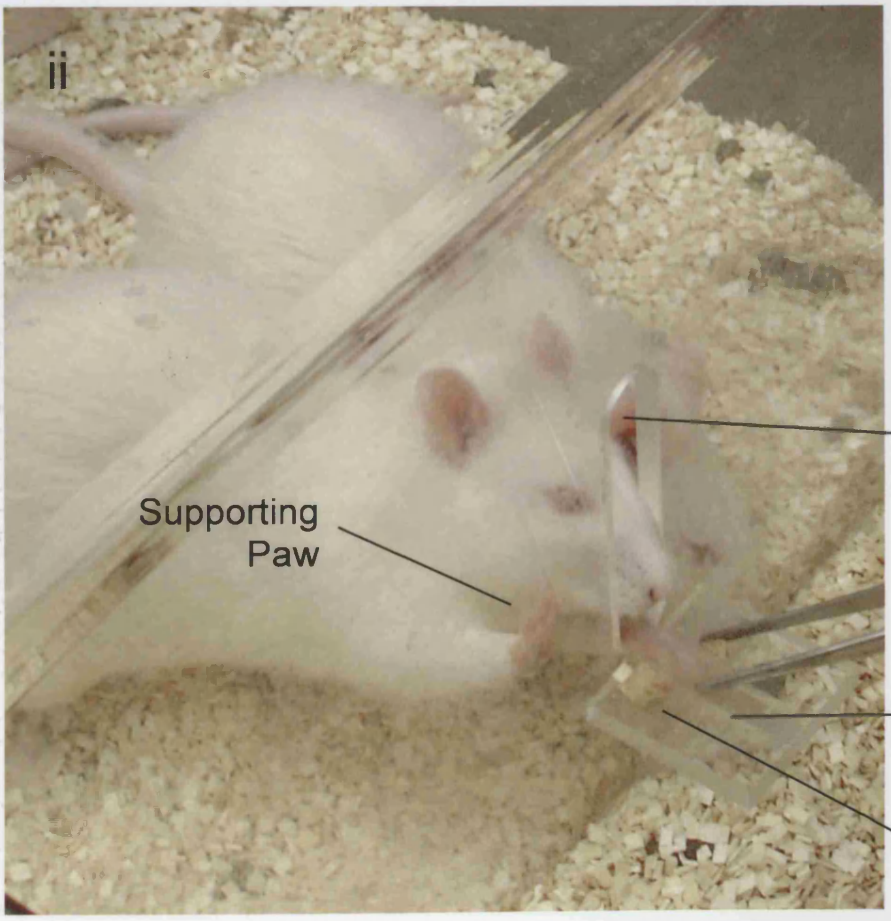
ii
Slot
Supporting Paw
Supporting Ledge
Food Pellet

Figure 4.1

Neocortical cultures and quantification of growth cone collapse rates

A-B. E17 rat neocortical cultures. Control cultures typically have one long, axonal process with a well-extended growth cone showing multiple lamellipodia and filopodia (A) while collapsed growth cones have a small, F-actin dense body with a single filopodial process (B). Scale bars 25µm.

C. Collapse rates of growth cones depending on culture conditions. Base collapse rate in normal culture was 36% and control cultures containing only EphA4 blocking peptide showed a very similar collapse rate. Exposure to homodimeric ephrinA5-Fc induced a collapse rate of 64% that was reduced to 44% by pre-administration of 20nM EphA4 blocking peptide for 10 minutes. Pre-administration of 50 or 100nM peptide prevented all ephrinA5-induced growth cone collapse. All bars mean collapse percentage ± 95% confidence interval, * $p < 0.01$, Fischer's exact t-test.

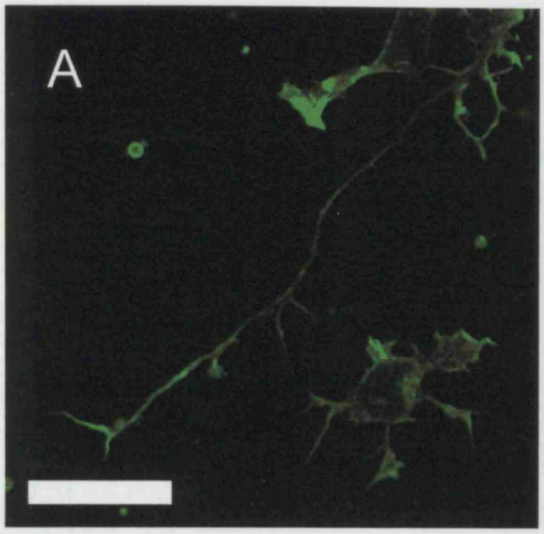
A

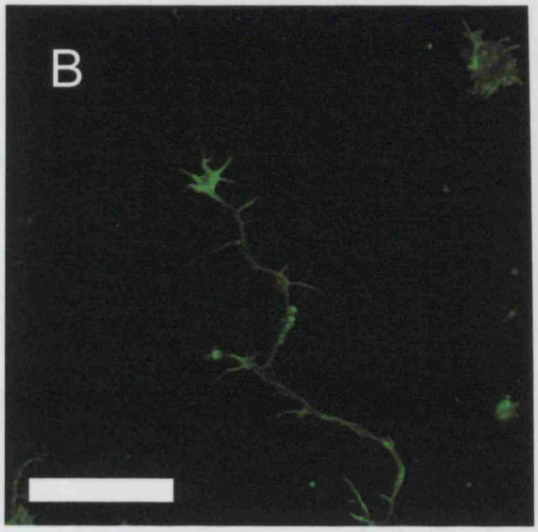
B

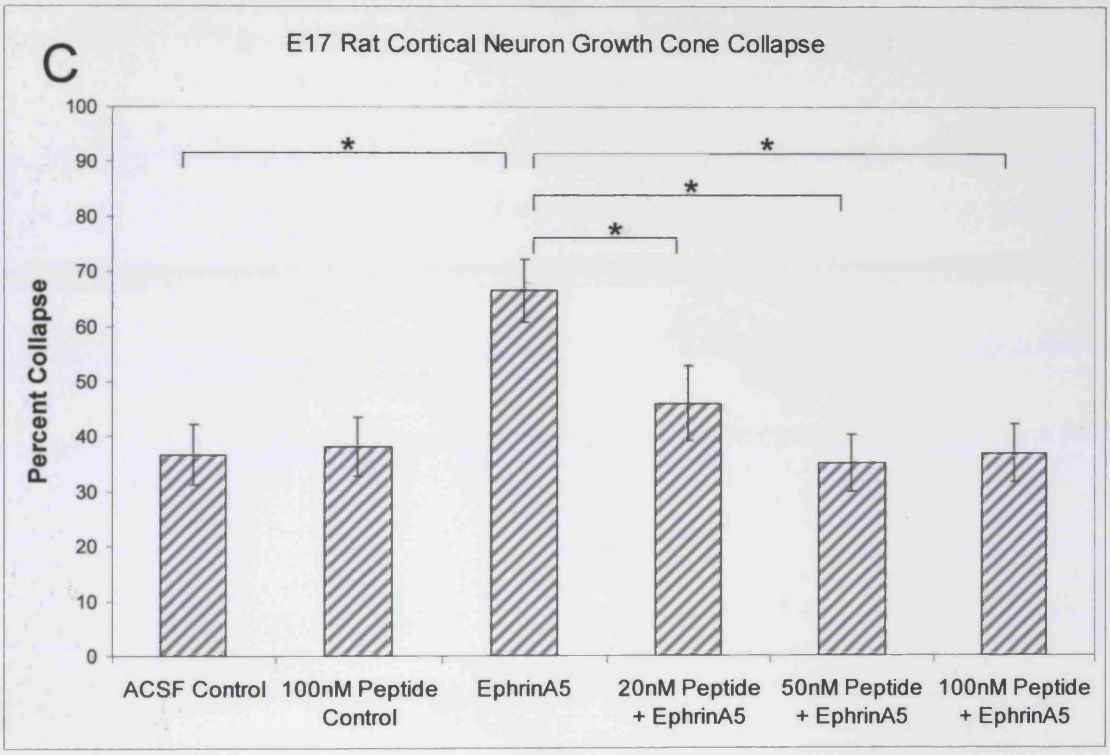
C
E17 Rat Cortical Neuron Growth Cone Collapse
Percent Collapse
100
90
80
70
60
50
40
30
20
10
0
*
*
*
*
ACSF Control
100nM Peptide Control
EphrinA5
20nM Peptide + EphrinA5
50nM Peptide + EphrinA5
100nM Peptide + EphrinA5

Figure 4.2

Theoretical accumulation of EphA4 blocking peptide in the CSF

The calculation is based on the infusion rate of peptide, a turn-over rate for CSF of 50% per hour and a 400µl volume of dilution for local CSF. This theoretical profile suggests that 100nM blocking peptide should develop within the first hour of injury, providing pharmacologically useful levels of peptide to the very acute lesion site.

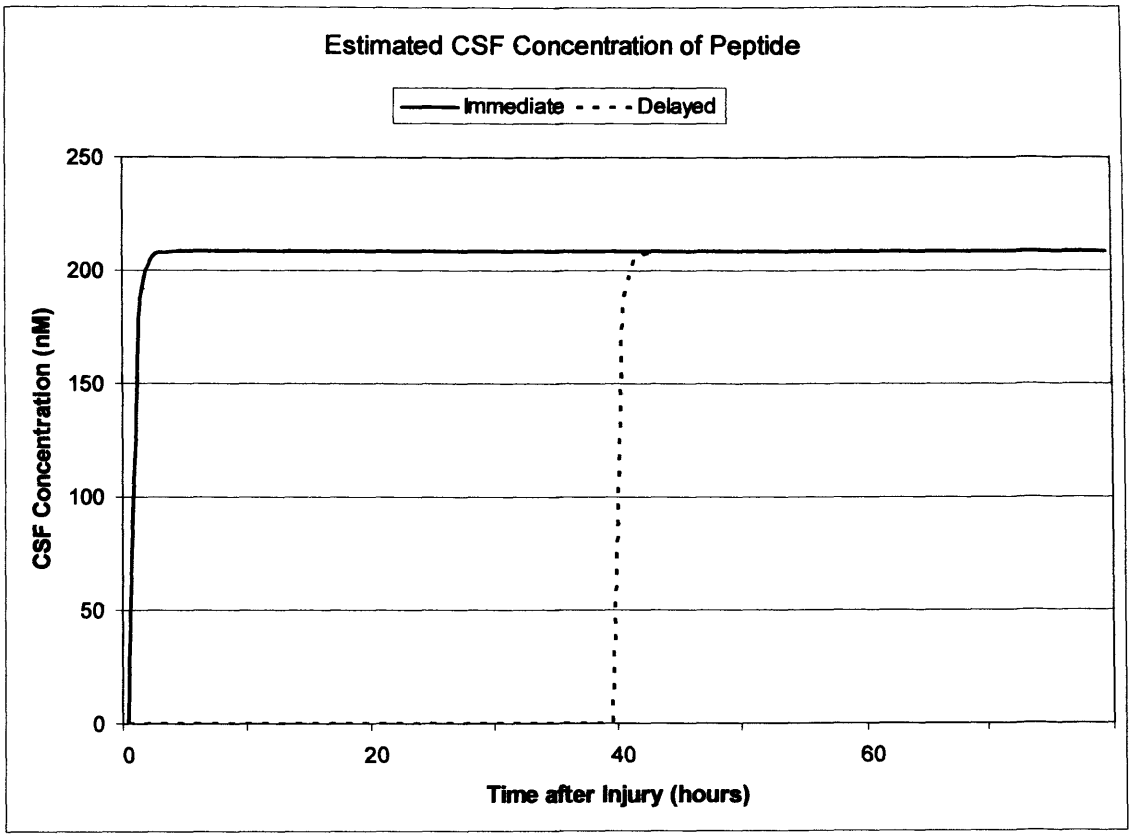
Estimated CSF Concentration of Peptide
Immediate
Delayed
250
200
150
100
50
0
CSF Concentration (nM)
0
20
40
60
Time after Injury (hours)

Figure 4.3

Astrocyte morphology following control or treated spinal cord injury

A-B. Untreated spinal cord two weeks following dorsal column injury showing the extent of cavitation and secondary injury development in both parasagittal (Ai) and horizontal (Aii) sections. Conversely, spinal cords from animals that received EphA4 blocking peptide for the entire duration of the injury showed reduced cavitation and secondary injury both horizontally (Bi) and parasagittally (Bii). Scale bars 1mm.

C-D. Lateral white matter astrocytes following injury commonly developed a 'honeycomb' appearance short distances from the lesion site probably due to necrosis of intervening tissue and hypertrophy in response to the injury (C). In contrast, control astrocytes in the uninjured lateral white matter show a well-organised parallel pattern designed to support axonal processes (D). Scale bars 100μm.

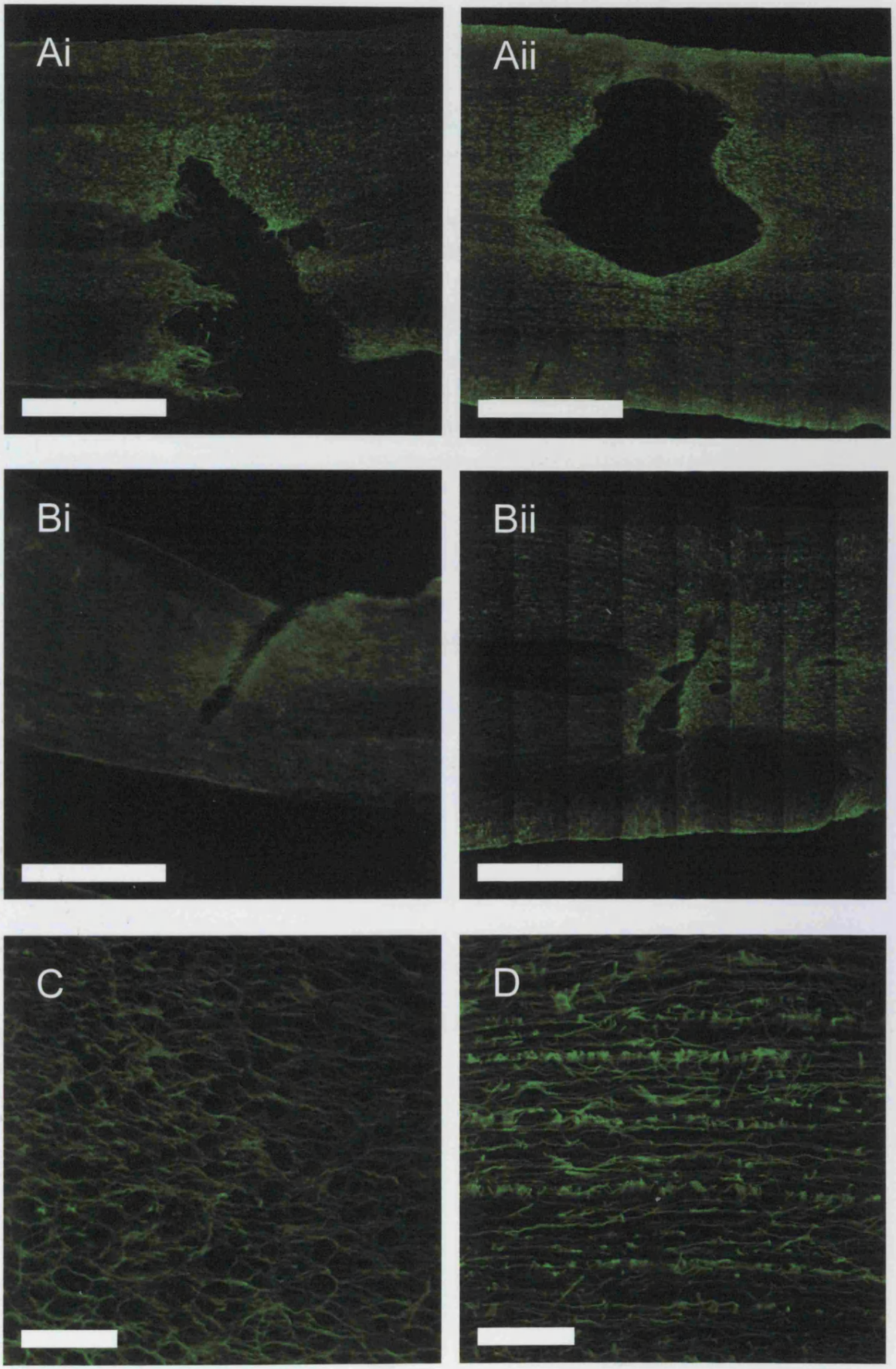
Ai
Aii
Bi
Bii
C
D

Figure 4.4

CST behaviour following control or treated spinal cord injury

A-C. Horizontal 40μm sections taken through the dorsal CST two weeks following lesion stained for GFAP and BDA labelling of the CST. In control animals the lesion site shows cavitation with highly GFAP-positive astrocytes in the developing glial scar (A). The corticospinal tract is clearly retracted form the lesion site and few termination bulbs are seen to have sprouted. Spinal cords from animals that received delayed peptide treatment show an identical phenotype (B). In those animals that received peptide for the entire duration of the post-injury period (C), the CST was significantly less retracted, astrocytic processes were seen to invade the lesion site and provide bridges along which CST processes had advanced. Numerous CST termination bulbs were seen near the lesion margin and some were seen to have invaded the lesion cavity. Scale bars 250μm.

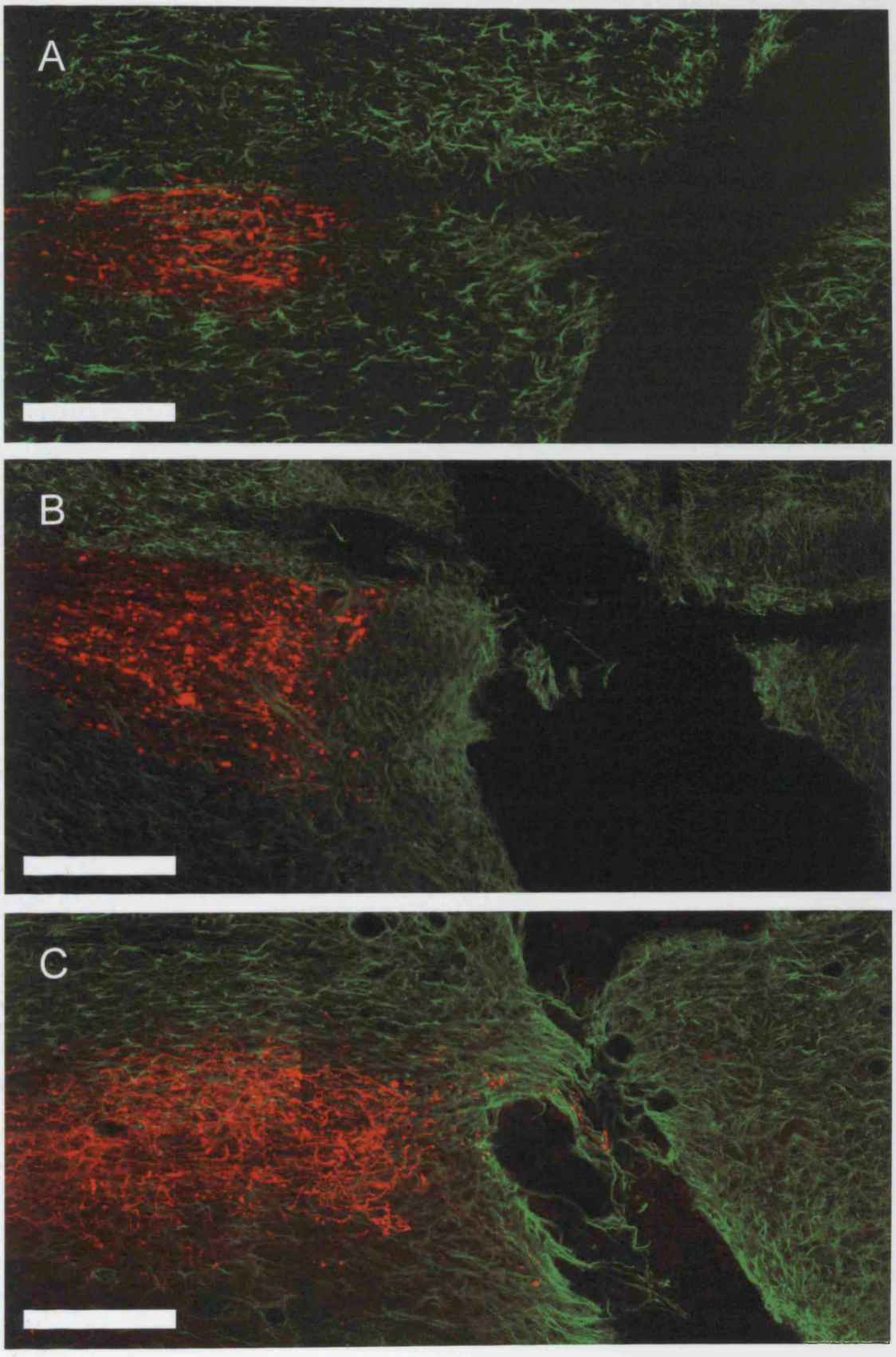
A
B
C

Figure 4.5

CST retraction from the lesion centre following spinal cord injury

Quantification of the distance between CST termination bulbs and the lesion centre. The delayed peptide treatment has no effect on CST retraction while immediate peptide administration induces significant improvements in CST regeneration ($p < 0.01$ Student's t-test, mean of three animals ±SEM).

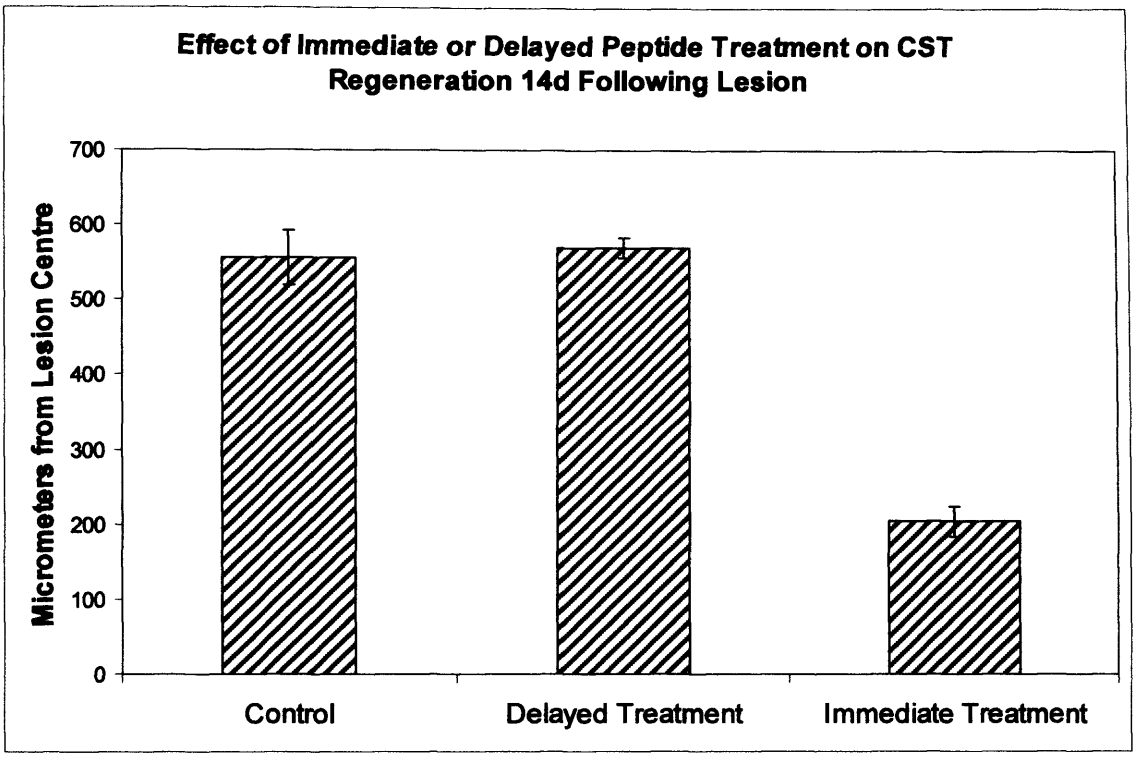
Effect of Immediate or Delayed Peptide Treatment on CST Regeneration 14d Following Lesion
Micrometers from Lesion Centre
700
600
500
400
300
200
100
0
Control
Delayed Treatment
Immediate Treatment

Figure 4.6

Astrocyte morphology 28 days following spinal cord injury

A-B. Parasagittal 40μm sections through spinal cords 28 days following dorsal CST lesion showing staining for GFAP. Control spinal cords (A) show a very similar injury to cords two weeks following injury although secondary necrosis has spread beyond the immediate insult (triangle). Those animals receiving EphA4 blocking peptide for the entire 28 day period show a small lesion site similar to that seen in Figure 4.3B with the progressive formation of astrocytic bridges in the lesion cavity (B). Scale bars 1mm.

C-D. Higher magnification images of the lesion site of animals treated with EphA4 blocking peptide show numerous bridge structures along the length of the cavity that could provide both structural and trophic support for regenerating axons and also act to promote wound closure. Scale bars 400μm (C) and 100μm (D).

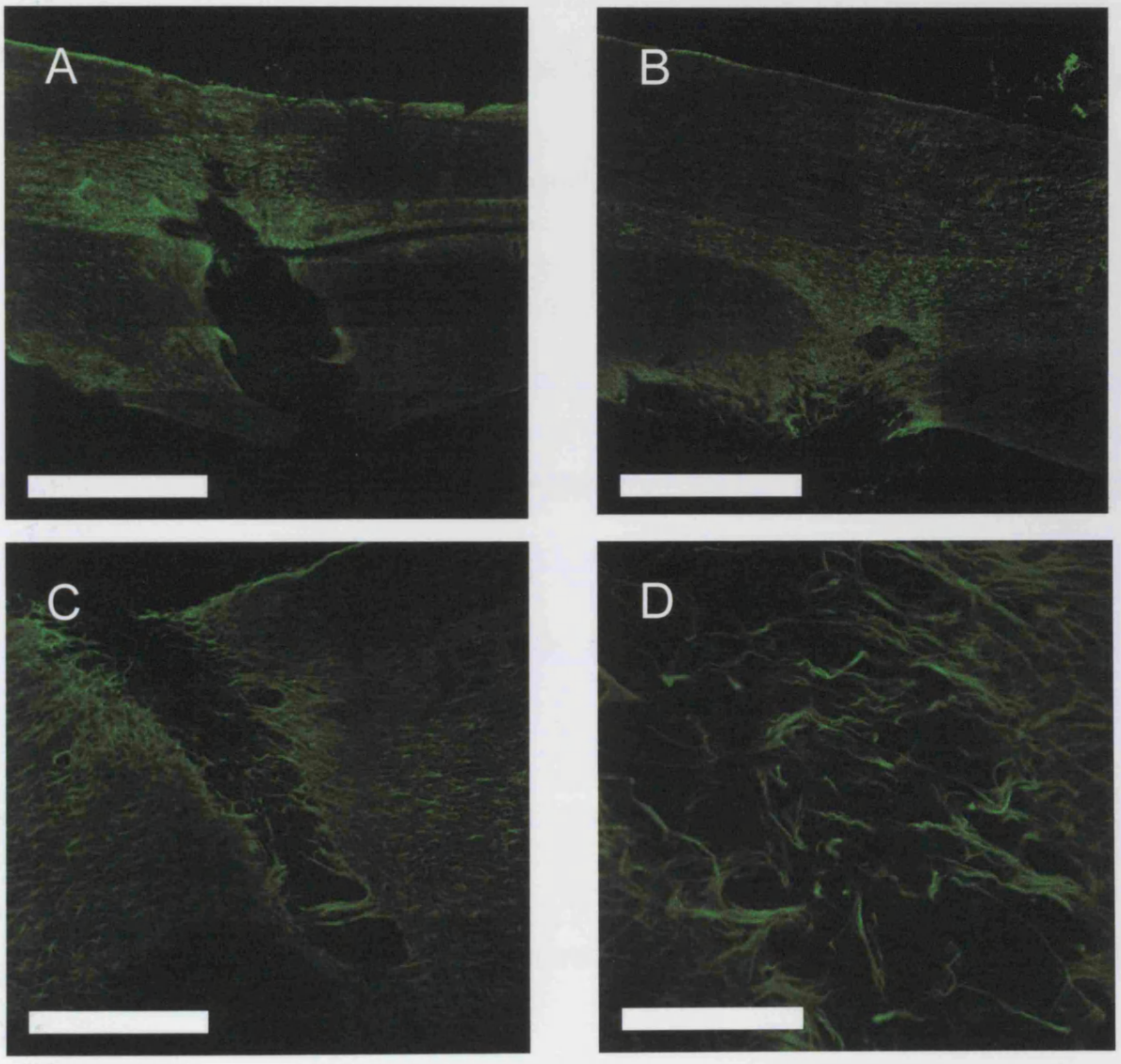
A
B
C
D

Figure 4.7

The CST in control and treated 28 day old spinal cord injuries

A-C. Parasagittal 40μm sections through the BDA-labelled dorsal corticospinal tract 28 days following lesion. ACSF-treated animals show the typical CST retraction bulb with a distinct bullet-shaped morphology (A) and minimal regenerative sprouting. Animals that received an infusion of EphA4 blocking peptide for the entire post-injury period demonstrate less retraction and evidence of regenerative sprouting into spared lateral or dorsal white matter and grey matter (B and C). Scale bars 200μm (A and B), 100μm (C).

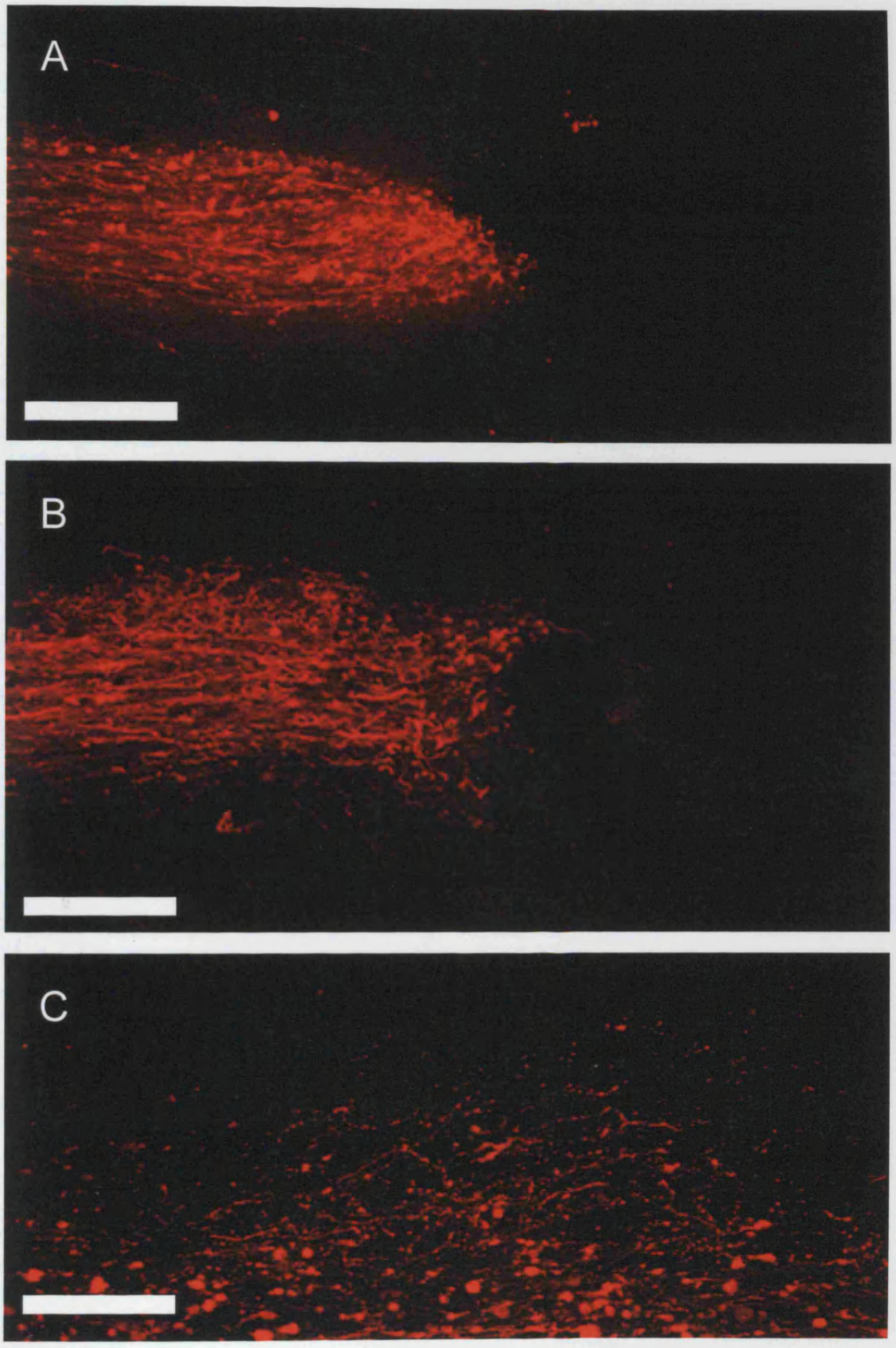
A
B
C

Figure 4.8

CST sprouts regenerating into the lesion margin and cavity following peptide treatment

A-D. Parasagittal 40μm sections through the lesion cavity at the level of the dorsal corticospinal tract. Stained for GFAP (green) and the BDA-labelled CST (red). In animals receiving EphA4 blocking peptide for the 28 day period following a dorsal corticospinal tract injury, regenerative sprouts from the CST were commonly seen to advance through the reactive astrocyte lesion margin (A). Furthermore, astrocytic processes were seen to invade the lesion cavity and provide structural support for axonal processes (no axons were seen without associated astrocytes) regenerating into the lesion site (B-D). Scale bars 25μm.

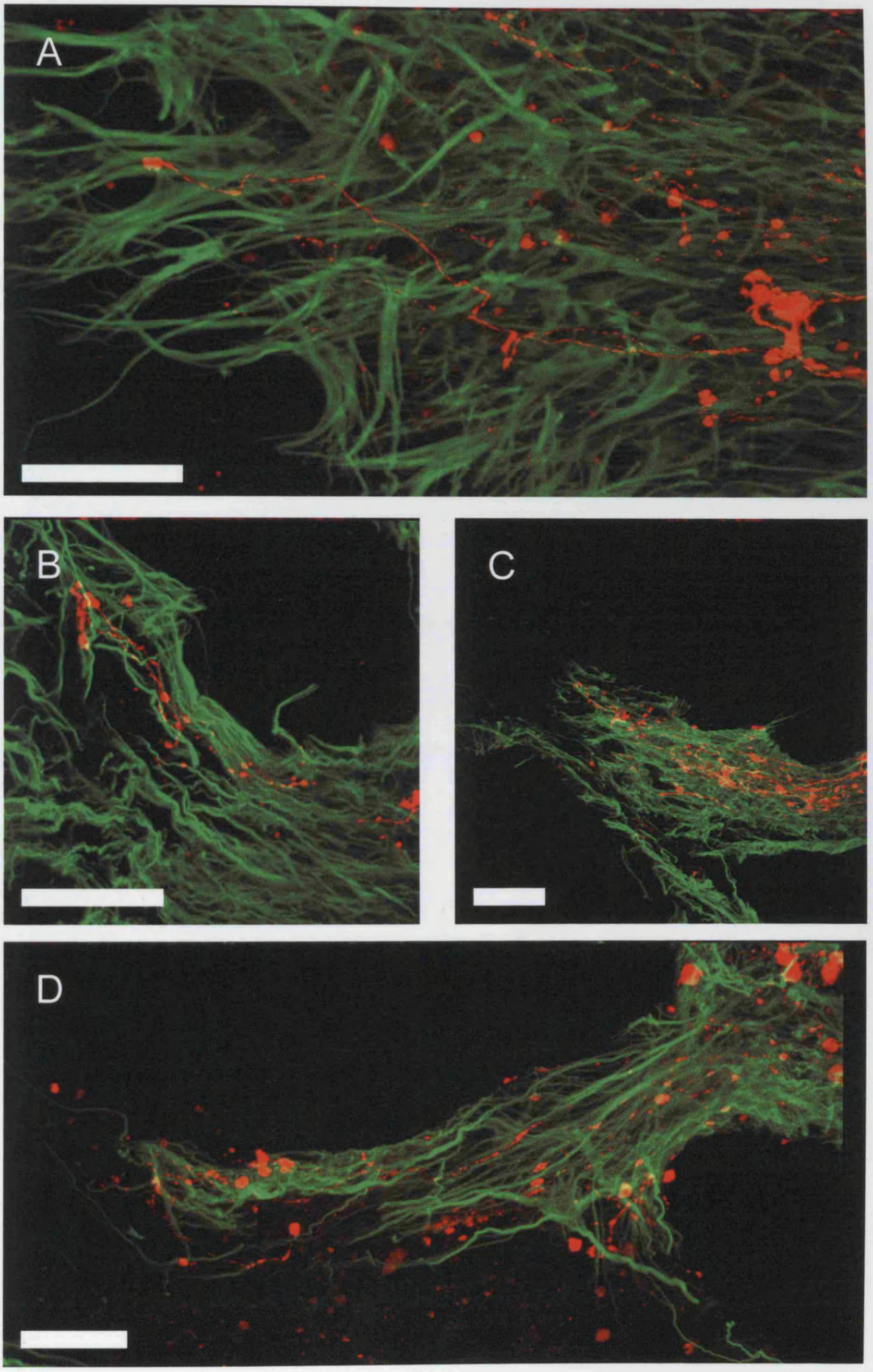
A
B
C
D

Figure 4.9

Peptide administration reduces CST retraction from the lesion margin

A. Quantification of the distance between CST termination bulbs and the lesion centre in animals 28 days following dorsal corticospinal tract transection. Peptide treated animals show significantly less retraction of the CST from the lesion margin ($p < 0.01$ Student's t-test, mean of three animals ±SEM).

B. Comparing CST regeneration two and four weeks following injury with and without peptide treatment. CST retraction does not appear to worsen significantly during weeks two to four following injury. At either time-point EphA4 blocking peptide induces very similar improvements in regeneration. Mean of three animals ±SEM.

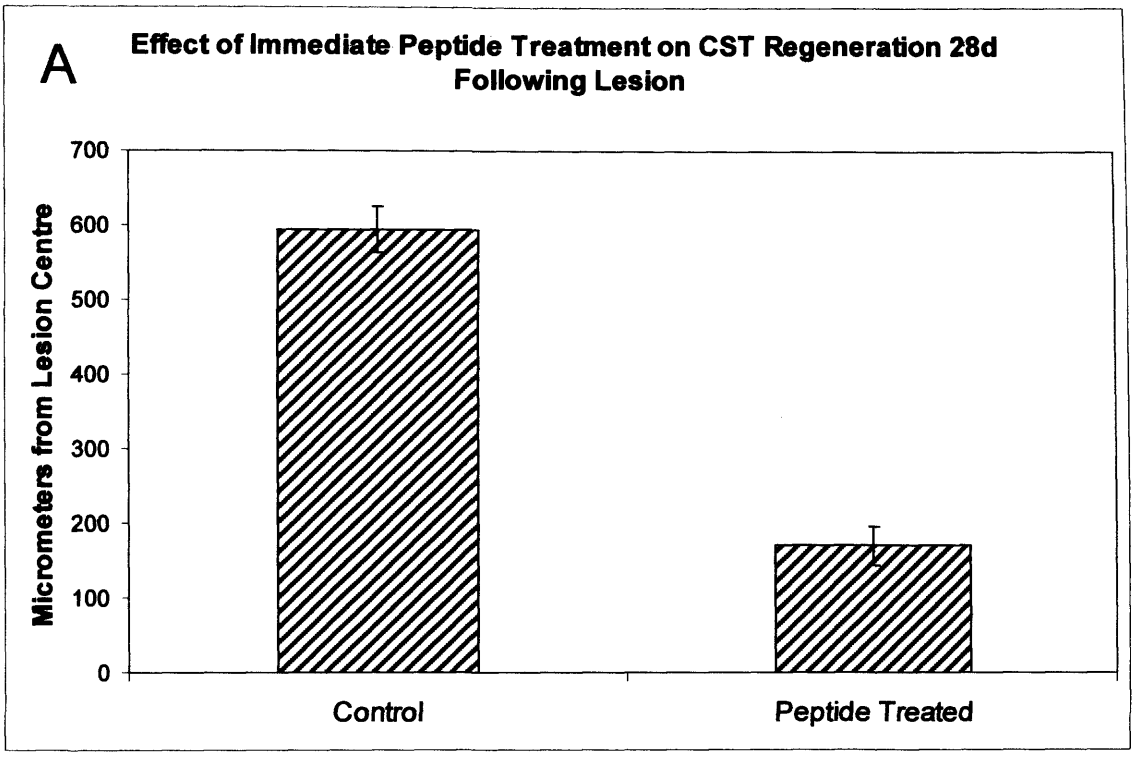
A
Effect of Immediate Peptide Treatment on CST Regeneration 28d Following Lesion
Micrometers from Lesion Centre
700
600
500
400
300
200
100
0
Control
Peptide Treated

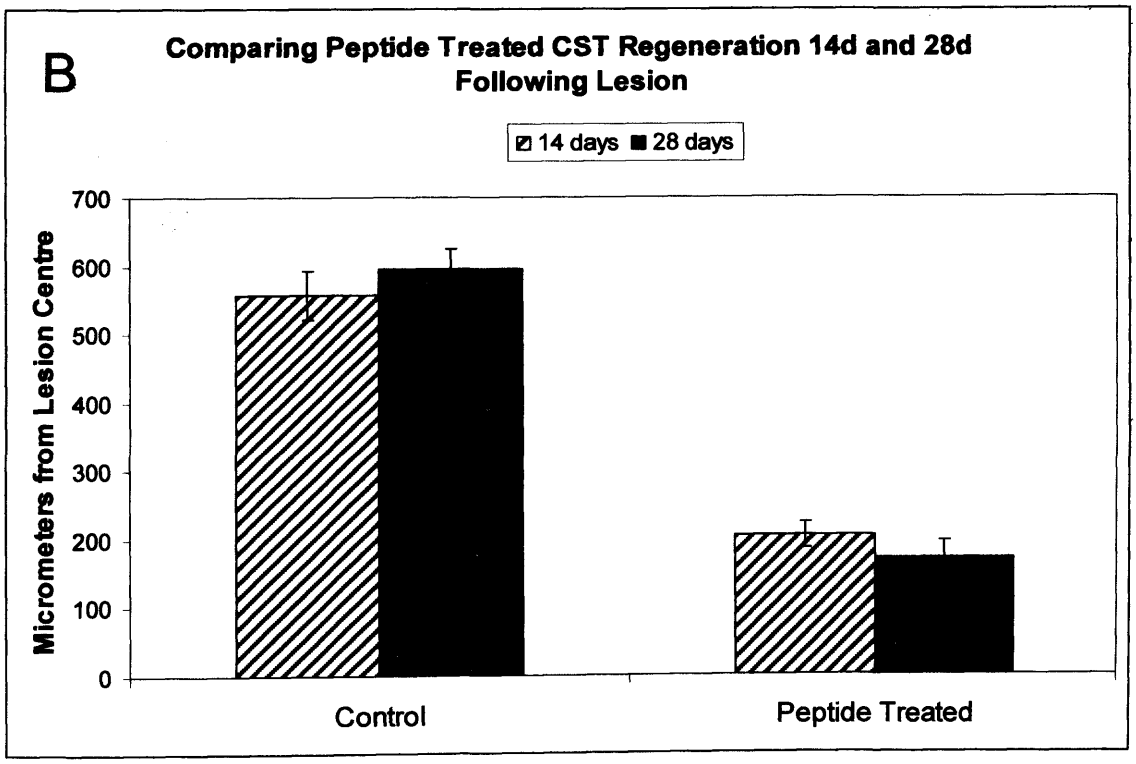
B
Comparing Peptide Treated CST Regeneration 14d and 28d Following Lesion
14 days
28 days
Micrometers from Lesion Centre
700
600
500
400
300
200
100
0
Control
Peptide Treated

Figure 4.10

Astrocyte behaviour following spinal cord injury

A-F. GFAP expression in horizontal sections through a lesion site typically shows a gradient of expression, increasing with proximity to the lesion centre. Following injury grey (A) and white (B) matter astrocytes become highly reactive, upregulate GFAP expression and become hypertrophic (C, triangles). This results in a remarkable change in the appearance of both the grey (C) and white matter (D) with invasion of the lesion margin and penumbra by both migrating astrocytes and processes of less proximal astrocytes. Administration of EphA4 blocking peptide for the 28 day period following lesion has no apparent effect on the gross anatomy of the astrocyte population in either the grey (E) or white (F) matter. Scale bars 100μm.

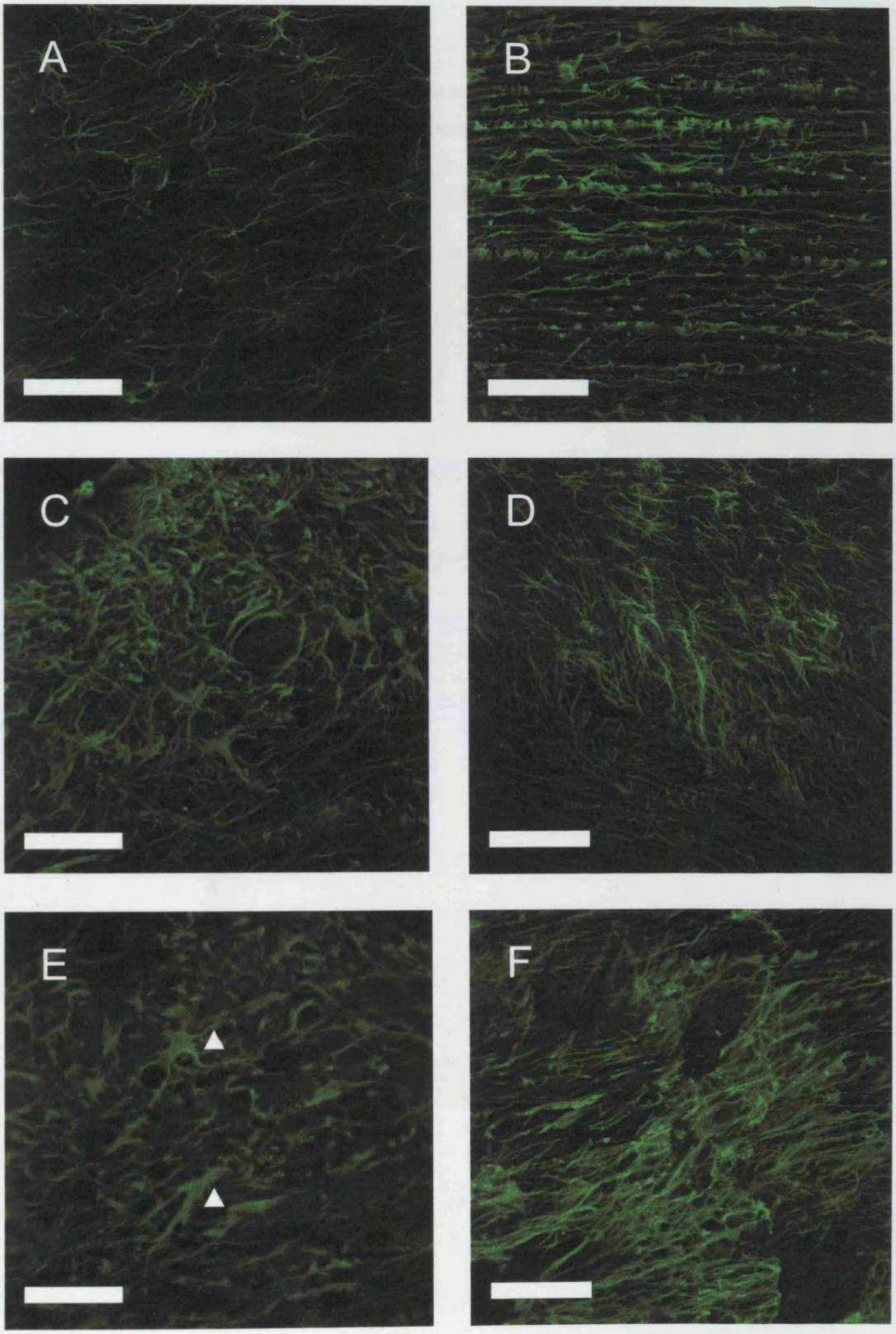
A
B
C
D
E
F

Figure 4.11

Quantification of astrocyte invasion of the lesion cavity

Astrocyte GFAP expression within the lesion cavity was analysed 28 days following lateral white matter injury. Values were normalised against the contralateral uninjured white matter expression of GFAP. Animals receiving EphA4 blocking peptide for the entire duration of the post-injury period show a significantly increased invasion of the lesion site by astrocytic processes (* $p < 0.05$, Student's t-test, mean ± SEM).

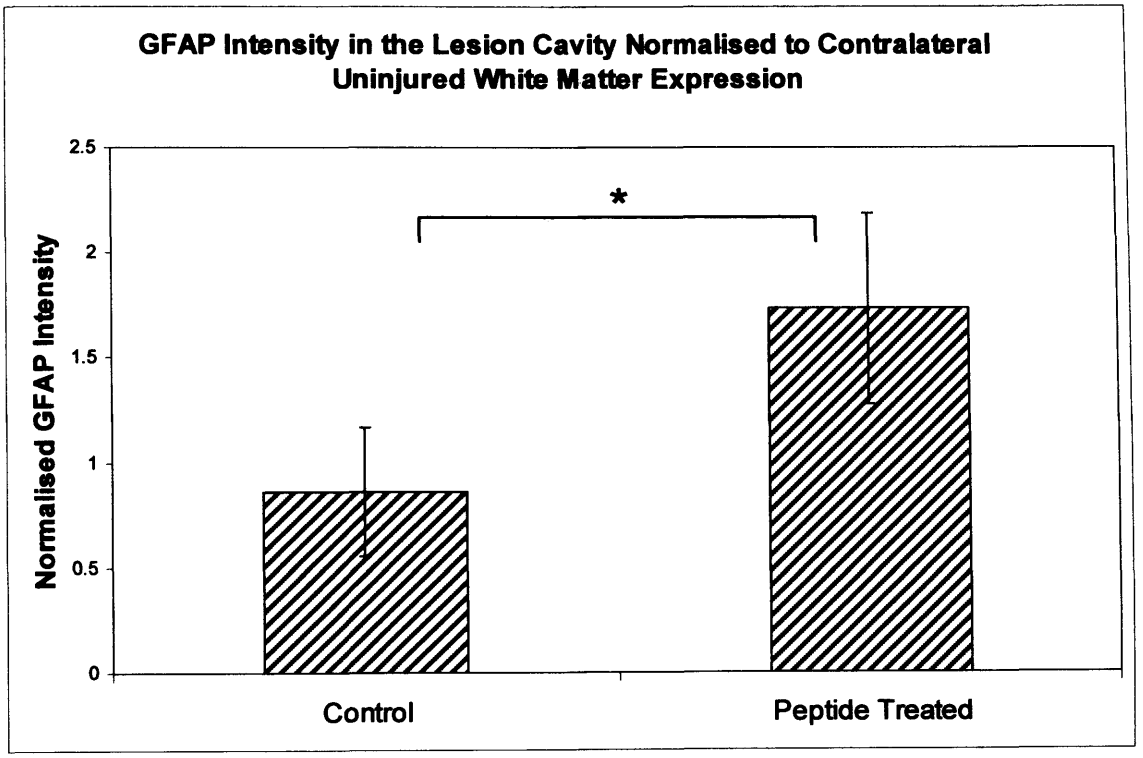
GFAP Intensity in the Lesion Cavity Normalised to Contralateral Uninjured White Matter Expression
Normalised GFAP Intensity
2.5
2
1.5
1
0.5
0
*
Control
Peptide Treated

Figure 4.12

Immunohistochemical data showing astrocyte invasion of the lesion cavity following peptide delivery

A-C. Lateral white matter injuries typically show minimal secondary damage or spread of the injury away from the primary lesion site. However, astrocyte retraction and the absence of significant numbers of astrocytic processes in the lesion site is common (A). Invasion of the lesion cavity by reactive astrocytes is enhanced in animals receiving EphA4 blocking peptide following injury (B and C). Horizontal 40µm sections through a lateral white matter lesion. Scale bars 200µm.

D-E. Secondary damage following spinal cord injury typically leads to areas of necrotic cell death separate from the initial lesion (*, D). In treated animals this secondary damage was less prominent and only a moderate lesion cavity was typically present (E). Parasagittal 40µm sections through a dorsal corticospinal tract lesion, stained for GFAP. Scale bars 1mm.

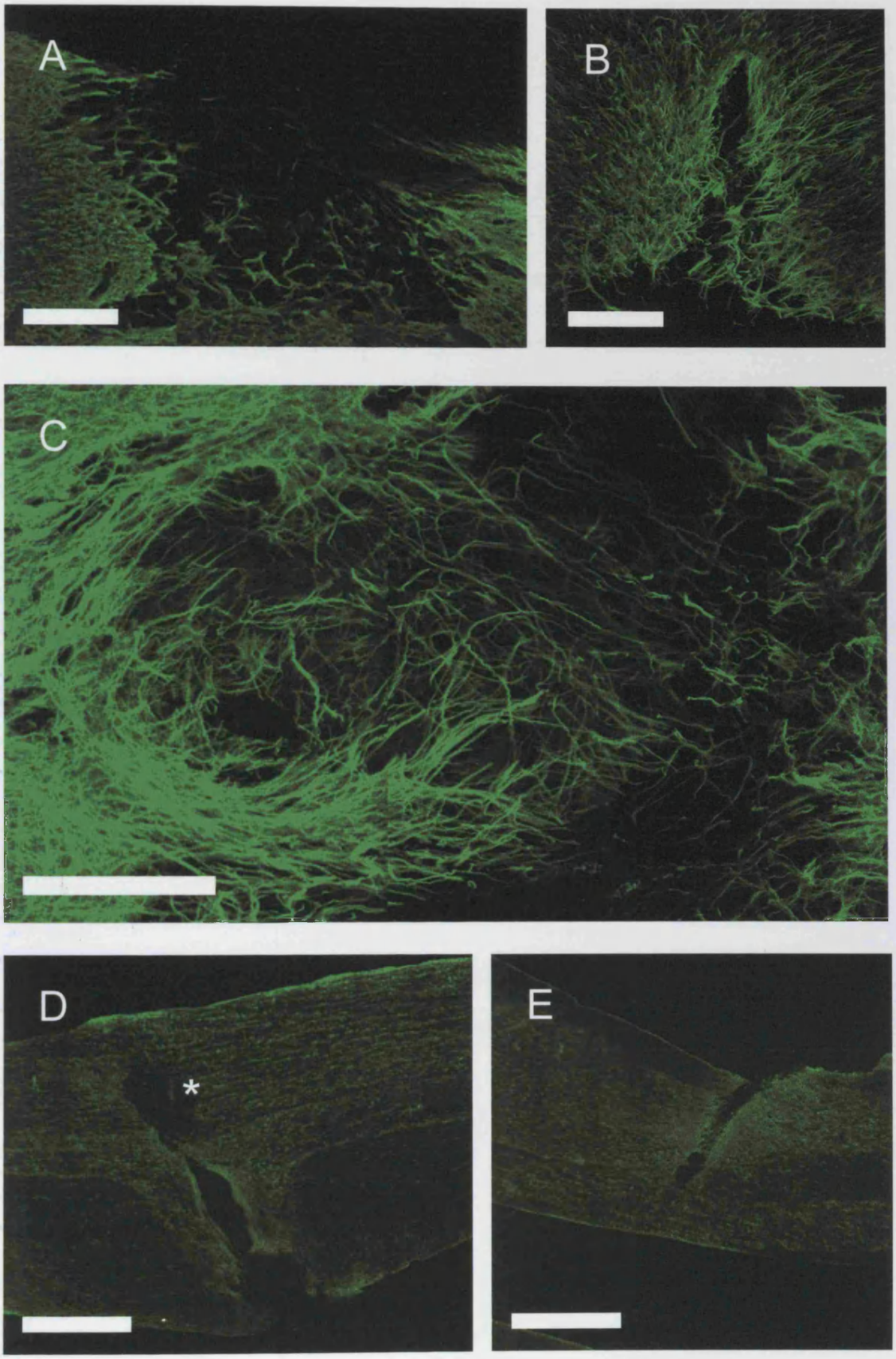
A
B
C
D
*
E

Figure 4.13

Tract labelling permits visualisation of sprouting responses to injury

A. Horizontal 40μm section through the dorsal corticospinal tract ten days following BDA injection into the red nucleus. This procedure did not induce any labelling of the dorsal corticospinal tract. Scale bar 100μm.

B. Horizontal 40μm section through the lateral white matter ten days following BDA injection into the red nucleus. This resulted in good labelling of the rubrospinal tract. Scale bar 300μm.

C. Horizontal 40μm section through the centre of a lateral white matter lesion stained for GFAP. These injuries induce only minimal secondary damage in rats and the extent of cavitation is typically small. Lesions that fully transect the lateral CST and the RST rarely induce damage to the central white matter, as shown. Scale bar 1mm.

D-F. Rubrospinal tract termination bulbs in animals treated with ACSF following lateral white matter lesions show negligible sprouting typical of a post-injury motor tract. Large, swollen dystrophic endbulbs form at various distances from the lesion margin by 28 days after injury (*, D) and these show minimal evidence of regenerative potential. In animals receiving peptide for this period termination bulbs generally occur closer to the lesion margin and there is increased evidence of a regenerative attempt with fine regenerative sprouts approaching the lesion site (arrows, E and F). Scale bars 20μm (D), 25μm (E) and 100μm (F).

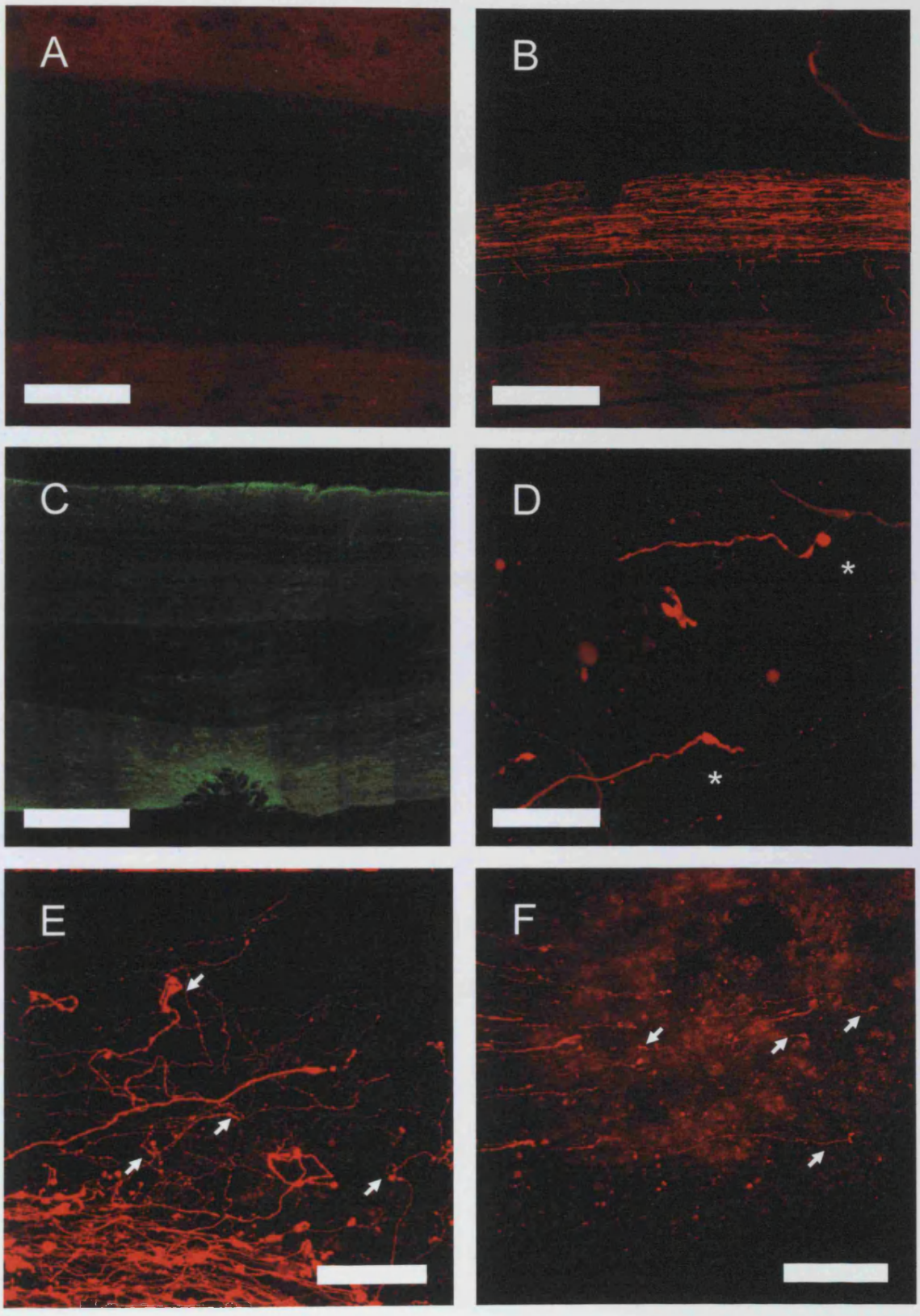
A
B
C
D
*
*
E
F

Figure 4.14

Peptide treatment improves RST regeneration following lesion

Graph illustrating the distance between rubrospinal tract termination bulbs and the lesion centre in animals 28 days following lateral white matter injury that completely transected the RST on one side. Peptide treated animals show a moderate reduction in the retraction of the RST from the lesion margin ($p < 0.01$ Student's t-test, mean of three animals ±SEM).

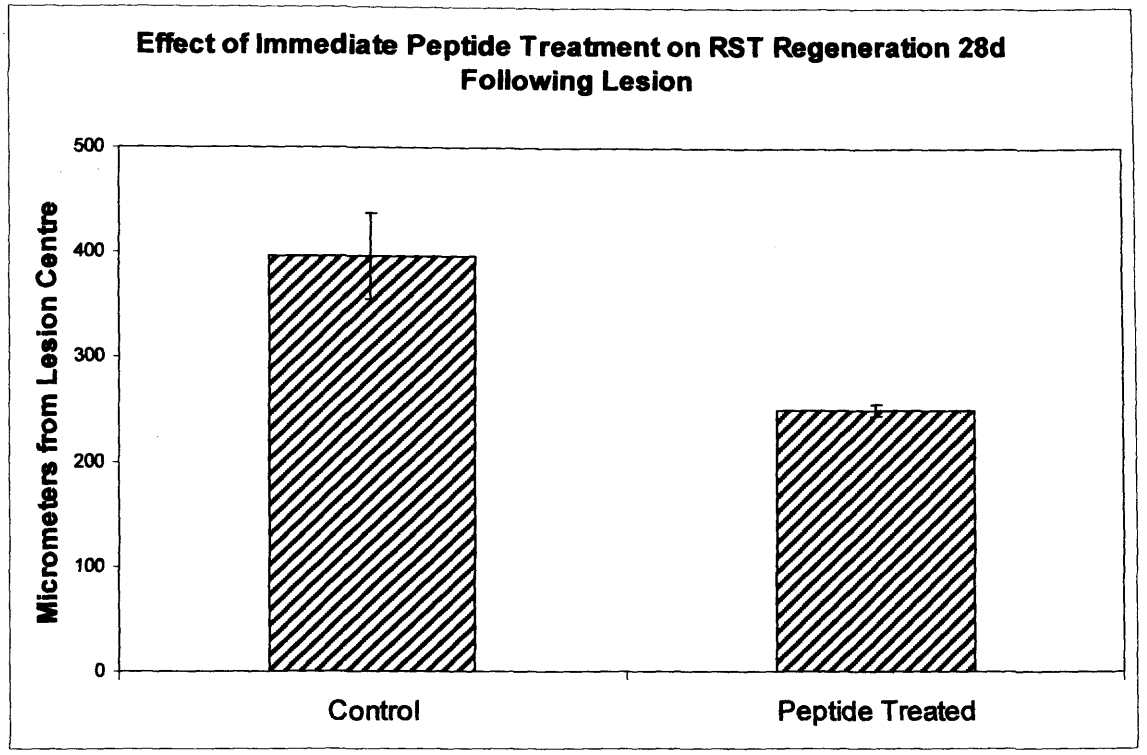
Effect of Immediate Peptide Treatment on RST Regeneration 28d Following Lesion
Micrometers from Lesion Centre
500
400
300
200
100
0
Control
Peptide Treated

Figure 4.15

In the untreated spinal cord the CST retracts further than the RST following injury

The rubrospinal tract retracts less far from the lesion centre than the corticospinal tract both 14 and 28 days following lesion. ($p < 0.01$ Student's t-test, mean of three or more animals ±SEM).

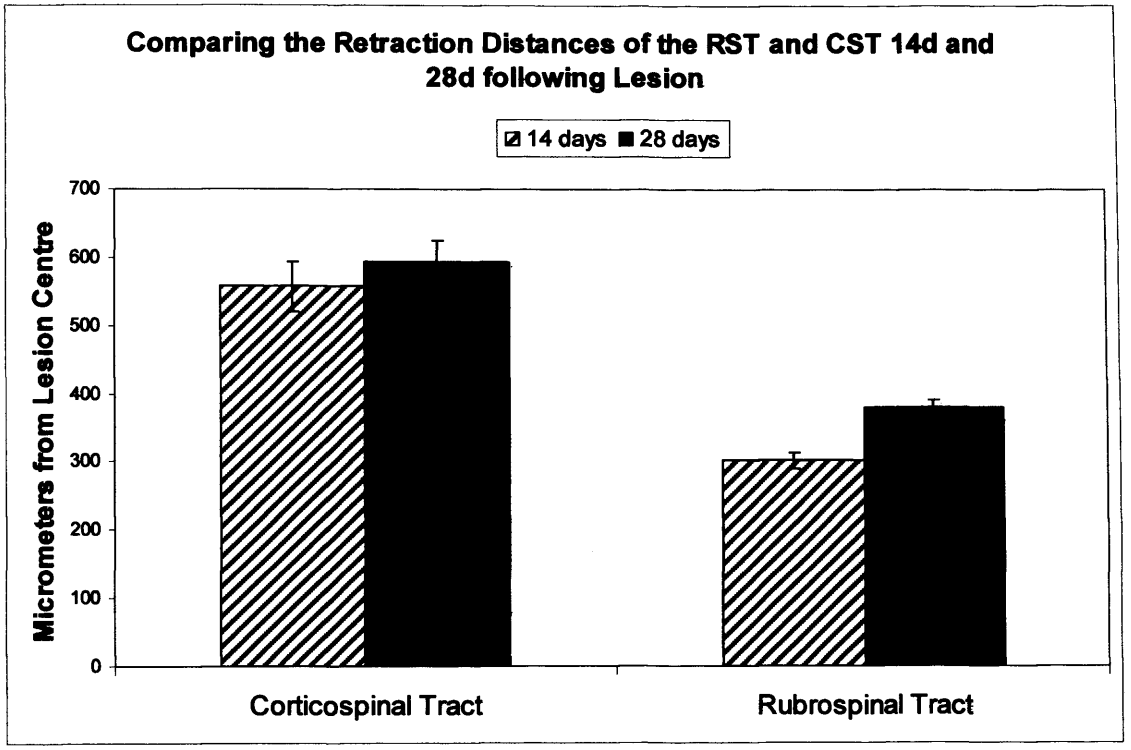
Comparing the Retraction Distances of the RST and CST 14d and 28d following Lesion
14 days
28 days
Micrometers from Lesion Centre
700
600
500
400
300
200
100
0
Corticospinal Tract
Rubrospinal Tract

Figure 4.16

Immediate peptide treatment improves regeneration in two rat strains

A. Graph showing quantification of the termination bulb-lesion centre distances for the rubrospinal and lateral corticospinal tracts in Lewis rats following a lateral white matter injury that completely transects both tracts. Both tracts show a significant reduction in the retraction distance following EphA4 blocking peptide administration ($p < 0.01$, Student's t-test, mean of three or more animals ± SEM).

B. The effect of the peptide on regeneration in both tracts is very comparable between the two species of rat studied. Bars represent the mean of three or more animals ± SEM.

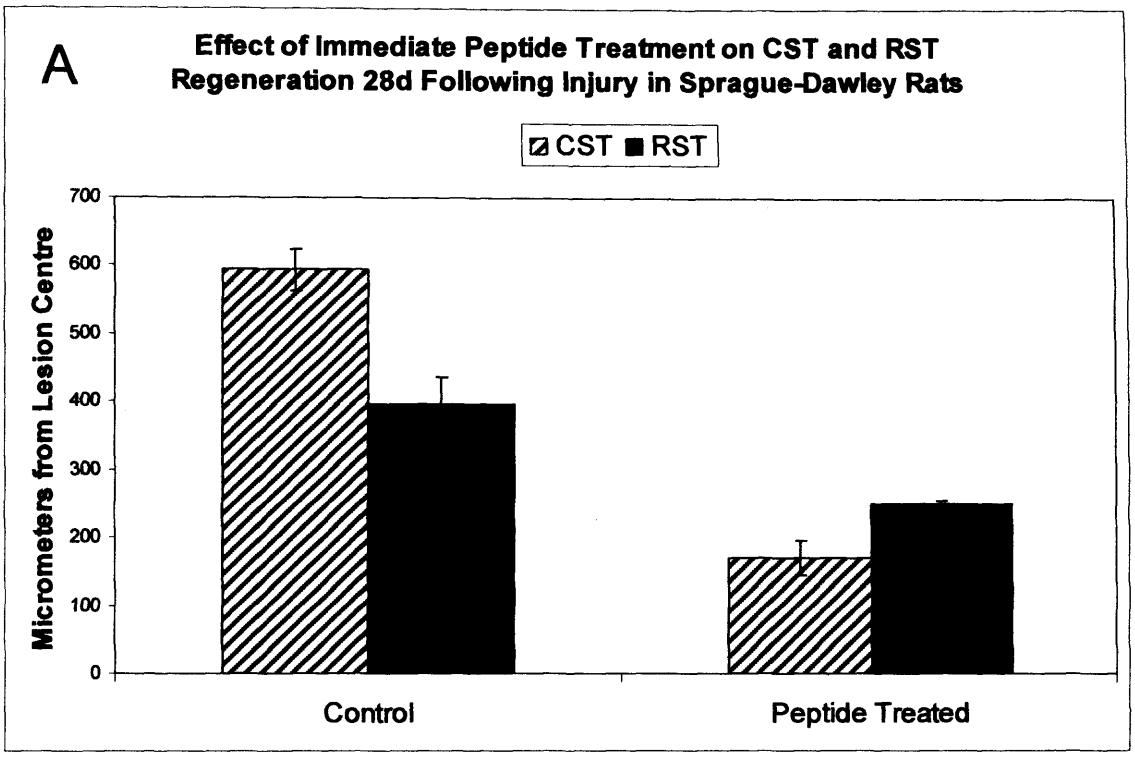
A
Effect of Immediate Peptide Treatment on CST and RST Regeneration 28d Following Injury in Sprague-Dawley Rats
CST
RST
Micrometers from Lesion Centre
700
600
500
400
300
200
100
0
Control
Peptide Treated

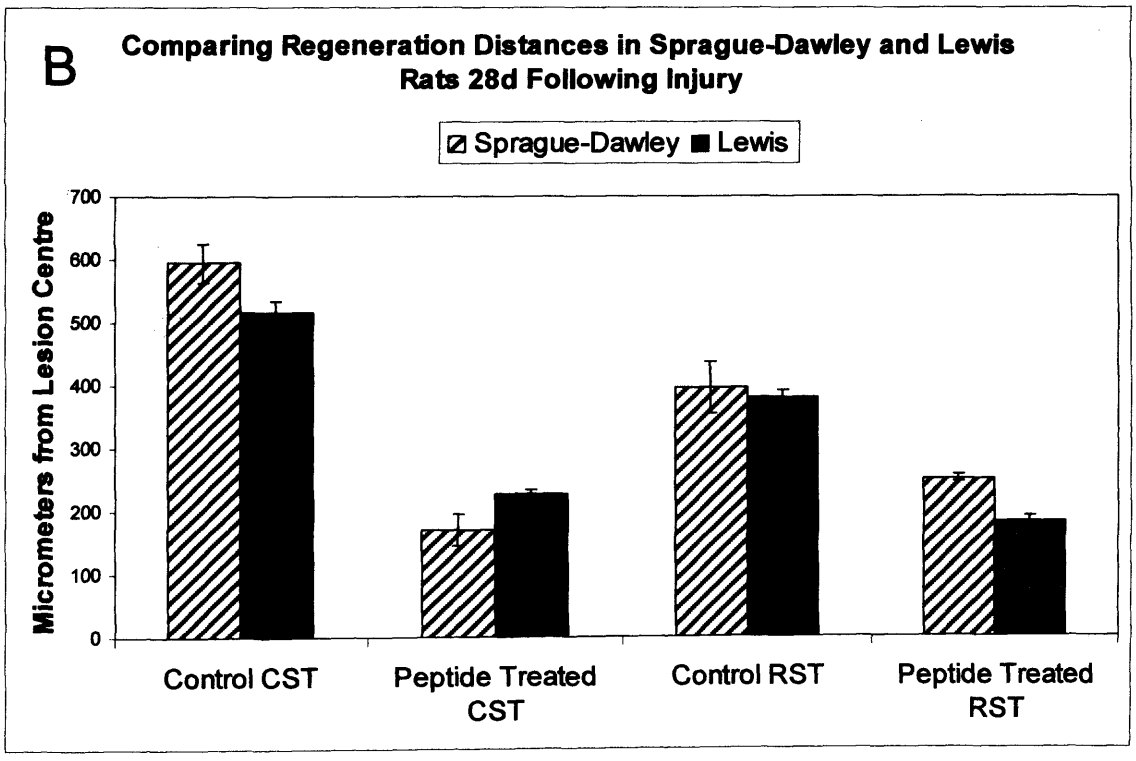
B
Comparing Regeneration Distances in Sprague-Dawley and Lewis Rats 28d Following Injury
Sprague-Dawley
Lewis
Micrometers from Lesion Centre
700
600
500
400
300
200
100
0
Control CST
Peptide Treated CST
Control RST
Peptide Treated RST

Figure 4.17

Peptide administration reduces die-back and improves sprouting

A-D. Horizontal 40μm sections through the lateral white matter 28 days following a lateral white matter lesion completely transecting the lateral corticospinal tract and the rubrospinal tract. The BDA-labelled CST is shown in red, the EGFP-labelled RST is shown in green and GFAP staining for astrocytes is shown in blue. Animals receiving ACSF for the 28 day period following injury show typical retraction of both tracts from the lesion margin (A) while those receiving EphA4 blocking peptide show minimal retraction and processes invading the lesion site (B). Higher magnification images of the termination bulbs illustrates the difference in retraction between the two tracts. ACSF treated CST (*) fibres retract significantly further than comparable RST fibres (C) while in peptide treated animals the CST and RST show a similar regenerative capacity (D). Scale bars 200μm (A and B), 50μm (C and D).

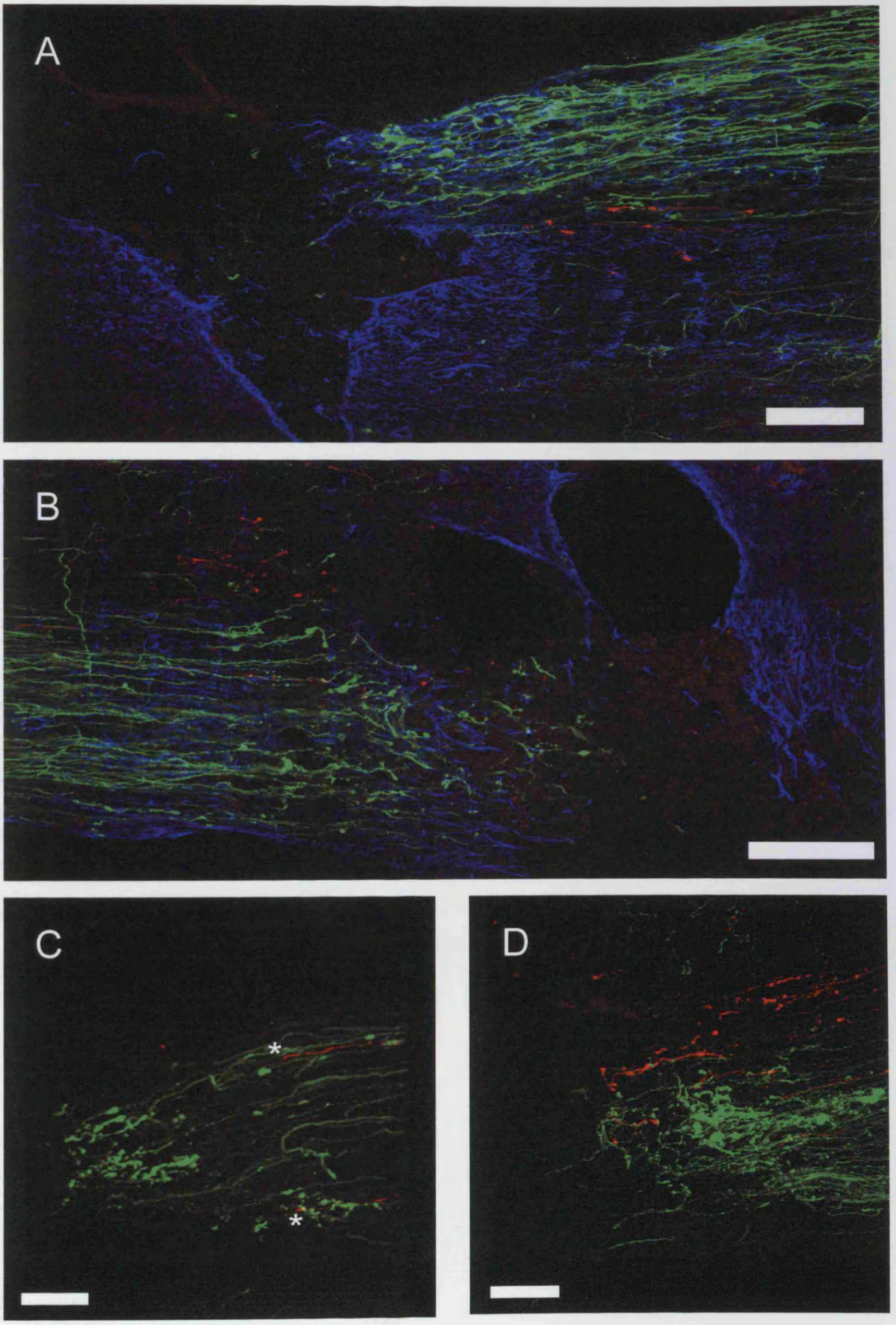
A
B
C
D

Figure 4.18

Regenerative sprouting is enhanced in the presence of peptide

A-D. Horizontal 40μm sections through the lateral white matter 28 days following a lateral white matter lesion completely transecting the lateral corticospinal tract and the rubrospinal tract. The BDA-labelled CST is shown in red, the EGFP-labelled RST is shown in green and GFAP staining for astrocytes is shown in blue. The response of the RST to peptide administration is readily evident using EGFP-labelling. The increased labelling intensity and number of labelled fibres identifies many more regenerating axons. The minimal sprouting and moderately retracted nature of the control RST (A) is completely reversed following peptide administration (B) with extensively sprouting axons that grow to the GFAP-labelled lesion margin. These sprouts also appear to predominately regenerate in a lesionwards direction (C). Sprouting from termination bulbs of both the CST (*) and RST (triangles) is apparent in animals receiving peptide following injury. Scale bars 150μm (A and B), 100μm (C) and 25μm (D).

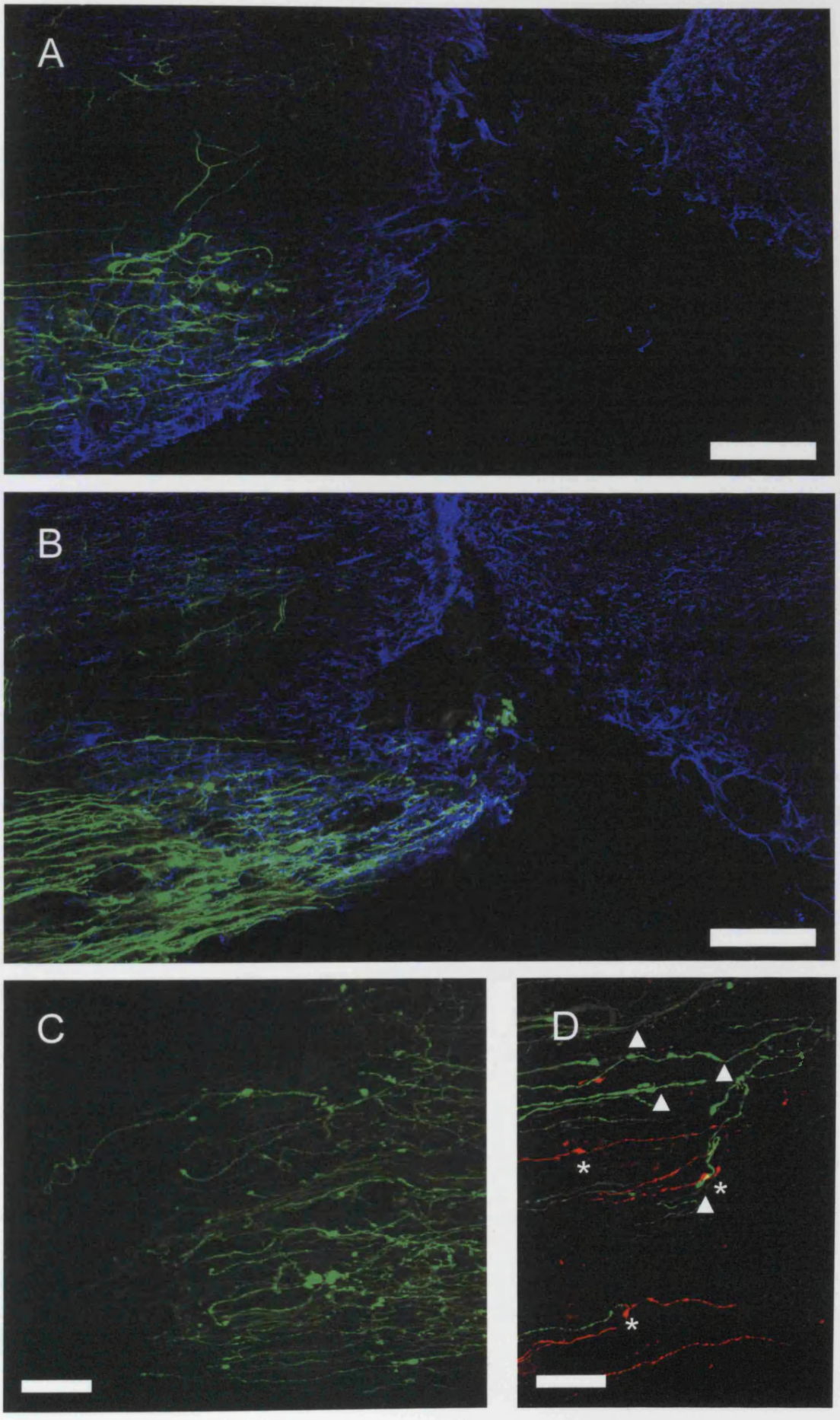
A
B
C
D

Figure 4.19

Peptide infusion induces recovery of paw reaching function following injury

A. Animals recovered rapid use of the injured forepaw in the rearing assay following unilateral dorsal CST injury regardless of the treatment type. Near-complete recovery of function was attained within the 28 day post-injury period of analysis. Graph shows the mean percentage use of the injured forepaw in four animals per treatment regime ± SEM.

B. In the paw reaching assay no recovery of function was achieved by any control animal throughout the period of study. Peptide treated animals showed a progressive recovery of function up to a mean 30% usage by twenty-eight days after injury. Graph shows the mean percentage use of the injured forepaw in four animals per treatment regime ± SEM.

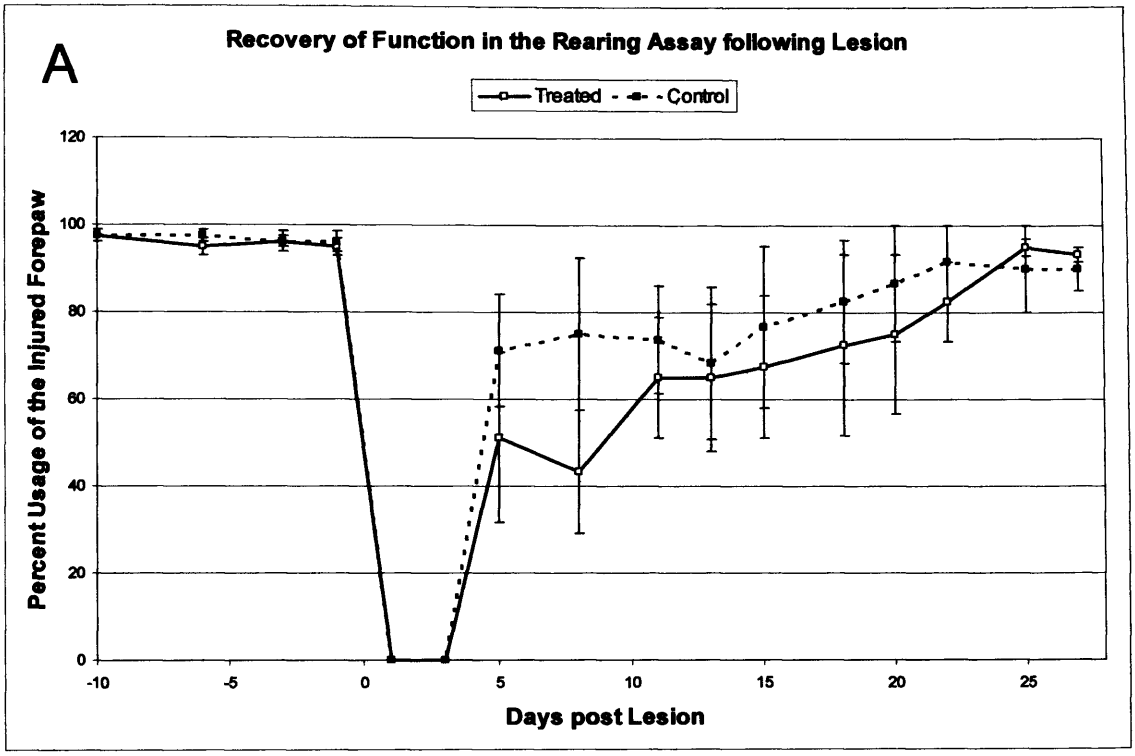
A
Recovery of Function in the Rearing Assay following Lesion
Treated
Control
Percent Usage of the Injured Forepaw
120
100
80
60
40
20
0
-10
-5
0
5
10
15
20
25
Days post Lesion

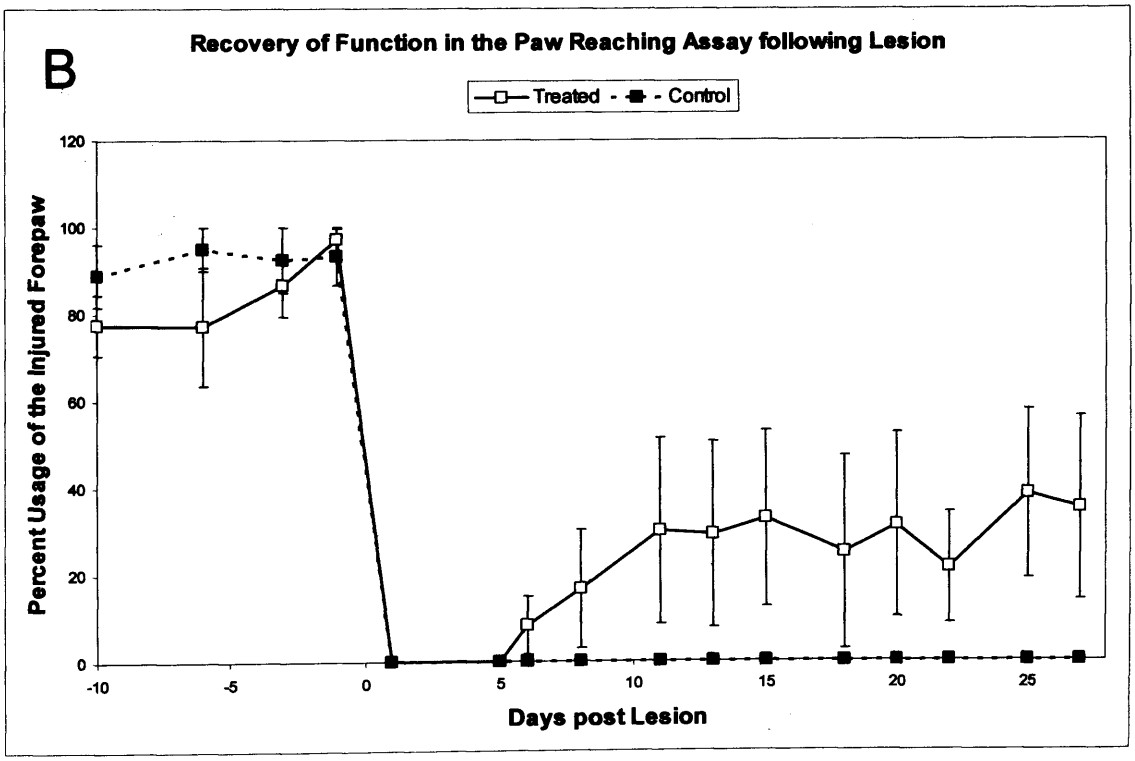
B
Recovery of Function in the Paw Reaching Assay following Lesion
Treated
Control
Percent Usage of the Injured Forepaw
120
100
80
60
40
20
0
-10
-5
0
5
10
15
20
25
Days post Lesion

Figure 4.20

Grasping with the injured forepaw recovers within ten days of injury when EphA4 blocking peptide is infused

A-B. Example images of animals reaching for food pellets in the paw reaching assay. Both animals shown were trained to use both forepaws in the reaching assay and both underwent a right hand side dorsal corticospinal tract lesion. In A the animal received control ACSF only for the duration of the post-injury period. In B the animal received EphA4 blocking peptide. Twenty-eight days following injury the control animal still used its uninjured left forepaw to reach while the peptide treated animal had regained the ability to use its injured forepaw.

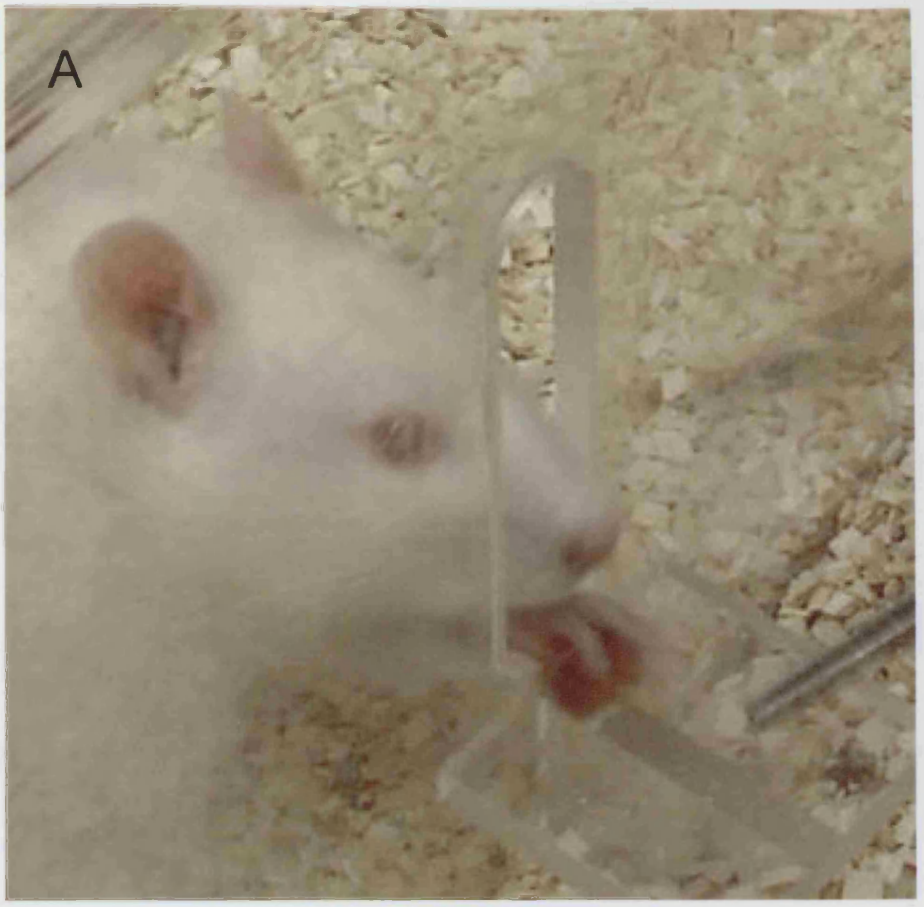
A

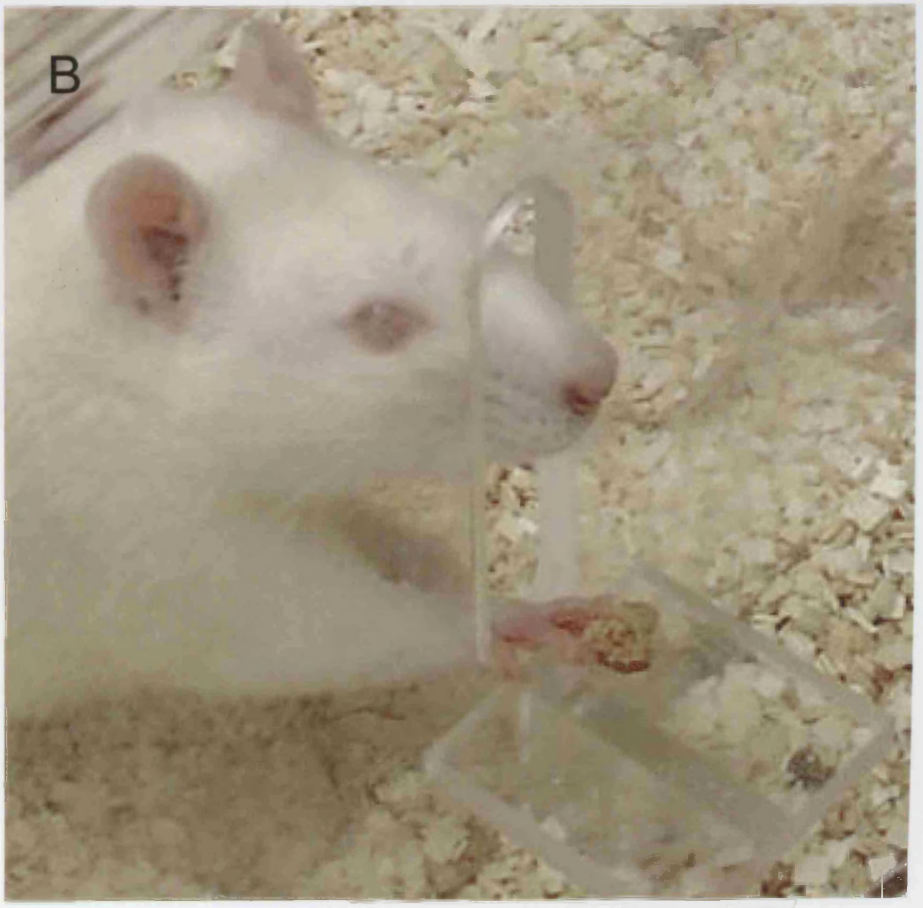
B

Figure 4.21

Plasticity and sprouting from the uninjured contralateral dorsal CST does not appear to mediate recovery of function

A-D. Horizontal 40μm sections through the dorsal CST 38 days after a unilateral dorsal column injury. BDA was used to label the uninjured CST and GFAP staining (green) to define the lesion site. Animals undergoing a unilateral dorsal corticospinal tract lesion show no regenerative sprouting or plasticity from the uninjured, contralateral tract in either control (A and C) or peptide treated (B and D) animals. White squares indicate the regions of higher magnification shown in images C and D. Images C and D highlight the region of the CST just caudal to the injury site and hence a likely site for sprouting. In all images caudal is to the right. Scale bars 400μm (A and B) and 100μm (C and D).

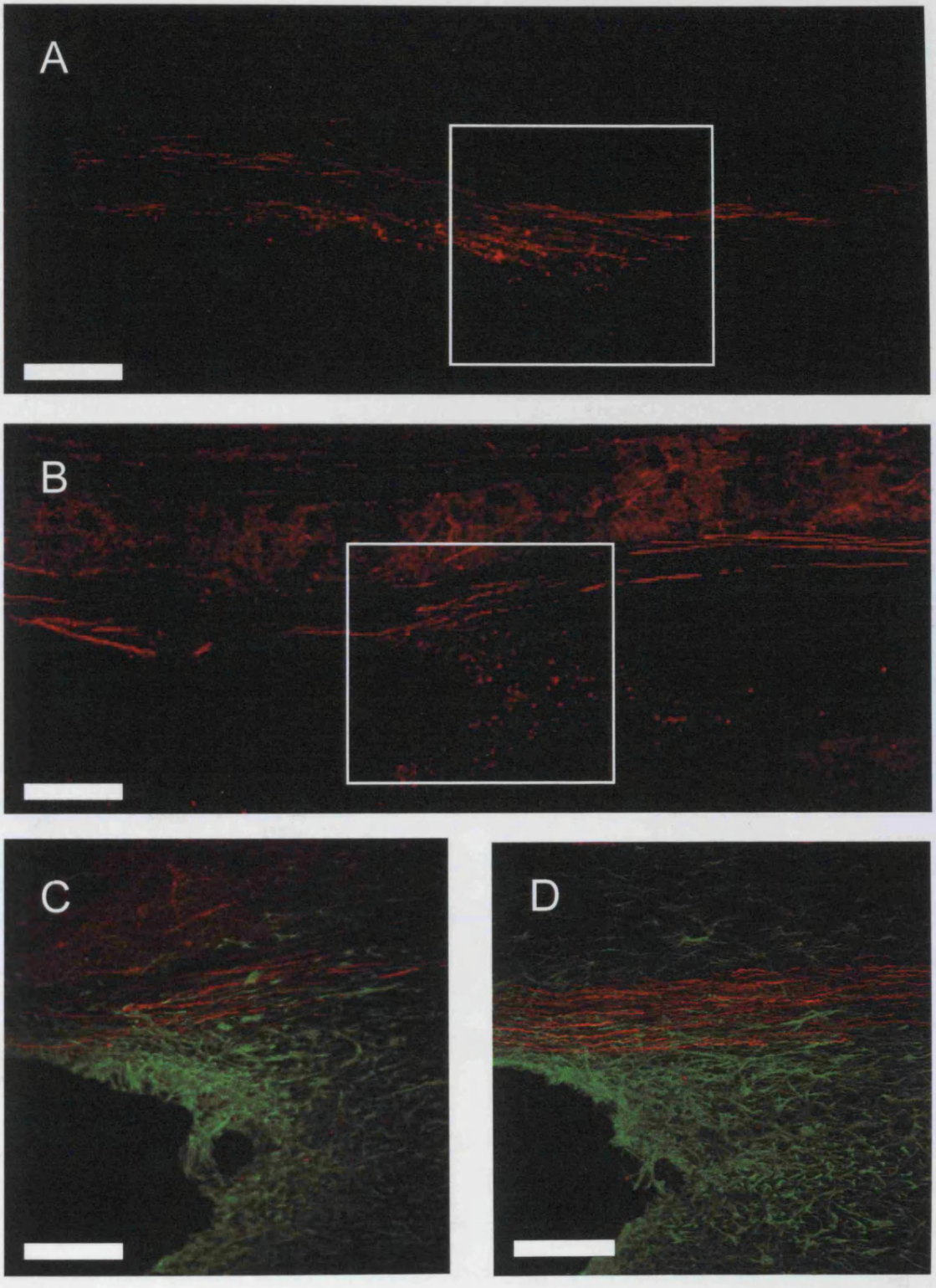
A
B
C
D

Concluding Remarks

The data presented in this thesis identifies a potential interaction between ephrinB2 expressed in reactive astrocytes near the lesion site and the EphA4 receptor in corticospinal tract axons. Furthermore it demonstrates how two approaches to interfere with this interaction promote regeneration of descending motor tracts. The second of these, infusion of a blocking peptide specific for the EphA4 receptor, induces improvements in functional recovery following corticospinal tract lesion and hence may have clinical potential.

The finding that peptide-induced regeneration of neither the corticospinal nor rubrospinal tract increased during the additional two weeks after injury in the extended study is disappointing, if unsurprising. The presence of numerous other growth-inhibitory agents in the lesion site, unaffected by inhibition of EphA4 signalling, would present a significant growth-inhibitory zone through which complete regeneration would be improbable. Hence, blockade of the EphA4 receptor alone is not sufficient for complete regeneration, although it is likely to contribute to any successful combinatorial therapy. The similarities between the work presented here and the work of Goldshmit *et al.*[12] in mice, with improvements in descending fibre regeneration, functional recovery and changes in astrocyte behaviour, suggest that similar ephrin functions are at work in the post-injury spinal cord environment of both rats and mice. This conservation of function indicates that inhibiting EphA4 signalling in human spinal cord injury may also prove pro-regenerative.

As our understanding of ephrin signalling in the post-injury spinal cord environment grows the complex and far-reaching nature of these interactions is becoming apparent. Currently published literature indicates ephrin roles in four of the major CNS injury-related phenomena: astrocyte reactivity[12], meningeal fibroblast invasion and the deposition of the basal lamina[26], growth cone retraction[330] and inflammation[315]. The only published study to date looking at spinal cord injury following abrogation of an ephrin interaction[12] has reported robust and functionally relevant regeneration. Hence, these studies,

combined with the data presented here, suggest that further investigation of ephrin signalling in spinal cord injury is warranted and is very likely to be translated into clinical initiatives.

Bibliography

1. Wolman, L., *The Disturbance of Circulation in Traumatic Paraplegia in Acute and Late Stages: A Pathological Study.* Paraplegia, 1965. **59**: p. 213-26.
2. Dusart, I. and M.E. Schwab, *Secondary cell death and the inflammatory reaction after dorsal hemisection of the rat spinal cord.* Eur J Neurosci, 1994. **6**(5): p. 712-24.
3. Wagner, F.C., Jr. *et al.*, *Pathological changes from acute to chronic in experimental spinal cord trauma.* J Neurosurg, 1978. **48**(1): p. 92-8.
4. Tator, C.H. and D.W. Rowed, *Current concepts in the immediate management of acute spinal cord injuries.* Can Med Assoc J, 1979. **121**(11): p. 1453-64.
5. Kobrine, A.I. *et al.*, *Local spinal cord blood flow in experimental traumatic myelopathy.* J Neurosurg, 1975. **42**(2): p. 144-9.
6. Anderson, D.K. *et al.*, *Spinal cord energy metabolism following compression trauma to the feline spinal cord.* J Neurosurg, 1980. **53**(3): p. 375-80.
7. Sandler, A.N. and C.H. Tator, *Review of the effect of spinal cord trauma on the vessels and blood flow in the spinal cord.* J Neurosurg, 1976. **45**(6): p. 638-46.
8. Faden, A.I. *et al.*, *N-methyl-D-aspartate antagonist MK801 improves outcome following traumatic spinal cord injury in rats: behavioural, anatomic, and neurochemical studies.* J Neurotrauma, 1988. **5**(1): p. 33-45.
9. Panter, S.S. *et al.*, *Alteration in extracellular amino acids after traumatic spinal cord injury.* Ann Neurol, 1990. **27**(1): p. 96-9.
10. Liu, D. *et al.*, *Excitatory amino acids rise to toxic levels upon impact injury to the rat spinal cord.* Brain Res, 1991. **547**(2): p. 344-8.
11. Guha, A. and C.H. Tator, *Acute cardiovascular effects of experimental spinal cord injury.* J Trauma, 1988. **28**(4): p. 481-90.
12. Goldshmit, Y. *et al.*, *Axonal Regeneration and Lack of Astrocytic Gliosis in EphA4-Deficient Mice.* J. Neurosci., 2004. **24**(45): p. 10064-10073.
13. Demediuk, P. *et al.*, *Changes in lipid metabolism in traumatized spinal cord.* Prog Brain Res, 1985. **63**: p. 211-26.
14. Balentine, J.D. and M. Spector, *Calcification of axons in experimental spinal cord trauma.* Ann Neurol, 1977. **2**(6): p. 520-3.
15. Eidelberg, E. *et al.*, *Immediate consequences of spinal cord injury: possible role of potassium in axonal conduction block.* Surg Neurol, 1975. **3**(6): p. 317-21.
16. Schwab, M.E. and D. Bartholdi, *Degeneration and regeneration of axons in the lesioned spinal cord.* Physiological Reviews, 1996. **76**(2): p. 319-70.
17. Popovich, P.G. *et al.*, *Concept of autoimmunity following spinal cord injury: possible roles for T lymphocytes in the traumatized central nervous system.* J Neurosci Res, 1996. **45**(4): p. 349-63.
18. Lawson, L.J. *et al.*, *Quantification of the mononuclear phagocyte response to Wallerian degeneration of the optic nerve.* J Neurocytol, 1994. **23**(12): p. 729-44.

19. Mocchetti, I. and J.R. Wrathall, *Neurotrophic factors in central nervous system trauma.* J Neurotrauma, 1995. **12**(5): p. 853-70.
20. Miyake, T. *et al.*, *Quantitative studies on proliferative changes of reactive astrocytes in mouse cerebral cortex.* Brain Res, 1988. **451**(1-2): p. 133-8.
21. Faulkner, J.R. *et al.*, *Reactive astrocytes protect tissue and preserve function after spinal cord injury.* J Neurosci, 2004. **24**(9): p. 2143-55.
22. Fawcett, J.W. and R.A. Asher, *The glial scar and central nervous system repair.* Brain Research Bulletin, 1999. **49**(6): p. 377-91.
23. Krikorian, J.G. *et al.*, *Origin of the connective tissue scar in the transected rat spinal cord.* Exp Neurol, 1981. **72**(3): p. 698-707.
24. Maxwell, W.L. *et al.*, *The response of the cerebral hemisphere of the rat to injury. I. The mature rat.* Philos Trans R Soc Lond B Biol Sci, 1990. **328**(1250): p. 479-500.
25. Koshinaga, M. *et al.*, *Altered acidic and basic fibroblast growth factor expression following spinal cord injury.* Exp Neurol, 1993. **120**(1): p. 32-48.
26. Bundesen, L.Q. *et al.*, *Ephrin-B2 and EphB2 regulation of astrocyte-meningeal fibroblast interactions in response to spinal cord lesions in adult rats.* J Neurosci, 2003. **23**(21): p. 7789-800.
27. Li, M. *et al.*, *Functional role and therapeutic implications of neuronal caspase-1 and -3 in a mouse model of traumatic spinal cord injury.* Neuroscience, 2000. **99**(2): p. 333-42.
28. Shuman, S.L. *et al.*, *Apoptosis of microglia and oligodendrocytes after spinal cord contusion in rats.* J Neurosci Res, 1997. **50**(5): p. 798-808.
29. Abe, Y. *et al.*, *Apoptotic cells associated with Wallerian degeneration after experimental spinal cord injury: a possible mechanism of oligodendroglial death.* J Neurotrauma, 1999. **16**(10): p. 945-52.
30. Balentine, J.D., *Pathology of experimental spinal cord trauma. I. The necrotic lesion as a function of vascular injury.* Lab Invest, 1978. **39**(3): p. 236-53.
31. Giehl, K.M., *Trophic dependencies of rodent corticospinal neurons.* Rev Neurosci, 2001. **12**(1): p. 79-94.
32. Jacobs, A.J. *et al.*, *Recovery of neurofilament expression selectively in regenerating reticulospinal neurons.* J Neurosci, 1997. **17**(13): p. 5206-20.
33. McBride, R.L. *et al.*, *Retrograde transport of fluoro-gold in corticospinal and rubrospinal neurons 10 and 20 weeks after T-9 spinal cord transection.* Exp Neurol, 1990. **108**(1): p. 83-5.
34. Schnell, L. and M.E. Schwab, *Sprouting and regeneration of lesioned corticospinal tract fibres in the adult rat spinal cord.* Eur J Neurosci, 1993. **5**(9): p. 1156-71.
35. Gilson, B.C. and L.J. Stensaas, *Early axonal changes following lesions of the dorsal columns in rats.* Cell Tissue Res, 1974. **149**(1): p. 1-20.

36. Li, Y. and G. Raisman, *Sprouts from cut corticospinal axons persist in the presence of astrocytic scarring in long-term lesions of the adult rat spinal cord.* Exp Neurol, 1995. **134**(1): p. 102-11.

37. Ramon y Cajal, S., *Degeneration and regeneration of the nervous system (translated by R. M. May)*. 1928, London: Oxford Univ. Press.

38. Pallini, R. *et al.*, *Retrograde degeneration of corticospinal axons following transection of the spinal cord in rats. A quantitative study with anterogradely transported horseradish peroxidase.* J-Neurosurg, 1988. **68**(1): p. 124-8.

39. Kao, C.C. *et al.*, *Electron microscopic observations of the mechanisms of terminal club formation in transected spinal cord axons.* J Neuropathol Exp Neurol, 1977. **36**(1): p. 140-56.

40. Houle, J.D., *Demonstration of the potential for chronically injured neurons to regenerate axons into intraspinal peripheral nerve grafts.* Exp Neurol, 1991. **113**(1): p. 1-9.

41. Guest, J.D. *et al.*, *The ability of human Schwann cell grafts to promote regeneration in the transected nude rat spinal cord.* Exp Neurol, 1997. **148**(2): p. 502-22.

42. Muma, N.A. *et al.*, *Alterations in levels of mRNAs coding for neurofilament protein subunits during regeneration.* Exp Neurol, 1990. **107**(3): p. 230-5.

43. Bisby, M.A. and W. Tetzlaff, *Changes in cytoskeletal protein synthesis following axon injury and during axon regeneration.* Mol Neurobiol, 1992. **6**(2-3): p. 107-23.

44. Yin, H.S. and M.E. Selzer, *Axonal regeneration in lamprey spinal cord.* J Neurosci, 1983. **3**(6): p. 1135-44.

45. Hall, G.F. *et al.*, *Cytoskeletal changes correlated with the loss of neuronal polarity in axotomized lamprey central neurons.* J Neurocytol, 1997. **26**(11): p. 733-53.

46. Fawcett, J.W. *et al.*, *Regenerating sciatic nerve axons contain the adult rather than the embryonic pattern of microtubule associated proteins.* Neuroscience, 1994. **61**(4): p. 789-804.

47. Reh, T. and K. Kalil, *Functional role of regrowing pyramidal tract fibers.* J Comp Neurol, 1982. **211**(3): p. 276-83.

48. Bates, C.A. and D.J. Stelzner, *Extension and regeneration of corticospinal axons after early spinal injury and the maintenance of corticospinal topography.* Exp Neurol, 1993. **123**(1): p. 106-17.

49. Li, D. *et al.*, *Failure of axon regeneration in postnatal rat entorhinohippocampal slice coculture is due to maturation of the axon, not that of the pathway or target.* Eur J Neurosci, 1995. **7**(6): p. 1164-71.

50. Condic, M.L. *et al.*, *Embryonic neurons adapt to the inhibitory proteoglycan aggrecan by increasing integrin expression.* J Neurosci, 1999. **19**(22): p. 10036-43.

51. Cai, D. *et al.*, *Neuronal cyclic AMP controls the developmental loss in ability of axons to regenerate.* The Journal of Neuroscience, 2001. **21**(13): p. 4731-9.

52. Chauvet, N. *et al.*, *Tanycytes present in the adult rat mediobasal hypothalamus support the regeneration of monoaminergic axons.* Exp Neurol, 1998. **151**(1): p. 1-13.
53. Morrison, E.E. and R.M. Costanzo, *Regeneration of olfactory sensory neurons and reconnection in the aging hamster central nervous system.* Neurosci Lett, 1995. **198**(3): p. 213-7.
54. Fouad, K. *et al.*, *Cervical sprouting of corticospinal fibers after thoracic spinal cord injury accompanies shifts in evoked motor responses.* Curr Biol, 2001. **11**(22): p. 1766-70.
55. Hatten, M.E. *et al.*, *Astroglia in CNS injury.* Glia, 1991. **4**(2): p. 233-43.
56. David, S. and A.J. Aguayo, *Axonal elongation into peripheral nervous system "bridges" after central nervous system injury in adult rats.* Science, 1981. **214**(4523): p. 931-3.
57. Richardson, P.M. *et al.*, *Axons from CNS neurons regenerate into PNS grafts.* Nature, 1980. **284**(5753): p. 264-5.
58. Richardson, P.M. and V.M. Issa, *Peripheral injury enhances central regeneration of primary sensory neurones.* Nature, 1984. **309**(5971): p. 791-3.
59. Broude, E. *et al.*, *c-Jun expression in adult rat dorsal root ganglion neurons: differential response after central or peripheral axotomy.* Exp Neurol, 1997. **148**(1): p. 367-77.
60. Neumann, S. and C.J. Woolf, *Regeneration of dorsal column fibers into and beyond the lesion site following adult spinal cord injury.* Neuron, 1999. **23**(1): p. 83-91.
61. Leon, S. *et al.*, *Lens injury stimulates axon regeneration in the mature rat optic nerve.* J Neurosci, 2000. **20**(12): p. 4615-26.
62. Werner, A. *et al.*, *Impaired axonal regeneration in alpha7 integrin-deficient mice.* J Neurosci, 2000. **20**(5): p. 1822-30.
63. Holmes, F.E. *et al.*, *Targeted disruption of the galanin gene reduces the number of sensory neurons and their regenerative capacity.* Proc Natl Acad Sci U S A, 2000. **97**(21): p. 11563-8.
64. de Felipe, C. *et al.*, *The role of immediate early genes in the regeneration of the central nervous system.* Adv Neurol, 1993. **59**: p. 263-71.
65. Fan, M. *et al.*, *Analysis of gene expression following sciatic nerve crush and spinal cord hemisection in the mouse by microarray expression profiling.* Cell Mol Neurobiol, 2001. **21**(5): p. 497-508.
66. Skene, J.H., *Axonal growth-associated proteins.* Annu Rev Neurosci, 1989. **12**: p. 127-56.
67. Widmer, F. and P. Caroni, *Identification, localization, and primary structure of CAP-23, a particle-bound cytosolic protein of early development.* J. Cell Biol., 1990. **111**(6): p. 3035-3047.
68. Wehrle, R. *et al.*, *Role of GAP-43 in mediating the responsiveness of cerebellar and precerebellar neurons to axotomy.* Eur-J-Neurosci, 2001. **13**(5): p. 857-70.

69. Mason, M.R.J. *et al.*, *Transcriptional Upregulation of SCG10 and CAP-23 Is Correlated with Regeneration of the Axons of Peripheral and Central Neurons in Vivo.* Molecular and Cellular Neuroscience, 2002. **20**(4): p. 595-615.

70. Tetzlaff, W. *et al.*, *Response of rubrospinal and corticospinal neurons to injury and neurotrophins.* Prog Brain Res, 1994. **103**: p. 271-86.

71. Doster, S.K. *et al.*, *Expression of the growth-associated protein GAP-43 in adult rat retinal ganglion cells following axon injury.* Neuron, 1991. **6**(4): p. 635-47.

72. Andersen, L.B. and D.J. Schreyer, *Constitutive expression of GAP-43 correlates with rapid, but not slow regrowth of injured dorsal root axons in the adult rat.* Exp Neurol, 1999. **155**(2): p. 157-64.

73. Laux, T. *et al.*, *GAP43, MARCKS, and CAP23 modulate PI(4,5)P(2) at plasmalemmal rafts, and regulate cell cortex actin dynamics through a common mechanism.* J Cell Biol, 2000. **149**(7): p. 1455-72.

74. Mason, M.R. *et al.*, *Corticospinal neurons up-regulate a range of growth-associated genes following intracortical, but not spinal, axotomy.* European Journal of Neuroscience, 2003. **18**(4): p. 789-802.

75. Fernandes, K.J. *et al.*, *Influence of the axotomy to cell body distance in rat rubrospinal and spinal motoneurons: differential regulation of GAP-43, tubulins, and neurofilament-M.* J Comp Neurol, 1999. **414**(4): p. 495-510.

76. Chaisuksunt, V. *et al.*, *Axonal regeneration from CNS neurons in the cerebellum and brainstem of adult rats: correlation with the patterns of expression and distribution of messenger RNAs for L1, CHL1, c-jun and growth-associated protein-43.* Neuroscience, 2000. **100**(1): p. 87-108.

77. Mason, M.R. *et al.*, *Overexpression of GAP-43 in thalamic projection neurons of transgenic mice does not enable them to regenerate axons through peripheral nerve grafts.* Exp Neurol, 2000. **165**(1): p. 143-52.

78. Buffo, A. *et al.*, *Targeted overexpression of the neurite growth-associated protein B-50/GAP-43 in cerebellar Purkinje cells induces sprouting after axotomy but not axon regeneration into growth-permissive transplants.* J Neurosci, 1997. **17**(22): p. 8778-91.

79. Bomze, H.M. *et al.*, *Spinal axon regeneration evoked by replacing two growth cone proteins in adult neurons.* Nature Neuroscience, 2001. **4**(1): p. 38-43.

80. Becker, T. *et al.*, *Readiness of zebrafish brain neurons to regenerate a spinal axon correlates with differential expression of specific cell recognition molecules.* J Neurosci, 1998. **18**(15): p. 5789-803.

81. Thoenen, H. *et al.*, *Trophic support of motoneurons: physiological, pathophysiological, and therapeutic implications.* Exp Neurol, 1993. **124**(1): p. 47-55.

82. Mansour-Robaey, S. *et al.*, *Effects of ocular injury and administration of brain-derived neurotrophic factor on survival and regrowth of axotomized retinal ganglion cells.* Proc Natl Acad Sci U S A, 1994. **91**(5): p. 1632-6.

83. Frisen, J. *et al.*, *Increased levels of trkB mRNA and trkB protein-like immunoreactivity in the injured rat and cat spinal cord.* Proc Natl Acad Sci U S A, 1992. **89**(23): p. 11282-6.
84. Frisen, J. *et al.*, *trkC expression in the injured rat spinal cord.* Neuroreport, 1993. **5**(3): p. 349-52.
85. Follesa, P. *et al.*, *Increased basic fibroblast growth factor mRNA following contusive spinal cord injury.* Brain Res Mol Brain Res, 1994. **22**(1-4): p. 1-8.
86. Reynolds, M.E. *et al.*, *Localization of nerve growth factor receptor mRNA in contused rat spinal cord by in situ hybridization.* Brain Res, 1991. **559**(1): p. 149-53.
87. Meiri, K.F. *et al.*, *Neurite outgrowth stimulated by neural cell adhesion molecules requires growth-associated protein-43 (GAP-43) function and is associated with GAP-43 phosphorylation in growth cones.* J Neurosci, 1998. **18**(24): p. 10429-37.
88. Giehl, K.M. *et al.*, *The survival-promoting effect of glial cell line-derived neurotrophic factor on axotomized corticospinal neurons in vivo is mediated by an endogenous brain-derived neurotrophic factor mechanism.* J Neurosci, 1998. **18**(18): p. 7351-60.
89. Giehl, K.M. and W. Tetzlaff, *BDNF and NT-3, but not NGF, prevent axotomy-induced death of rat corticospinal neurons in vivo.* Eur J Neurosci, 1996. **8**(6): p. 1167-75.
90. Schnell, L. *et al.*, *Neurotrophin-3 enhances sprouting of corticospinal tract during development and after adult spinal cord lesion.* Nature, 1994. **367**(6459): p. 170-3.
91. Reier, P.J. *et al.*, *Intraspinal transplantation of embryonic spinal cord tissue in neonatal and adult rats.* J Comp Neurol, 1986. **247**(3): p. 275-96.
92. Caroni, P. and M.E. Schwab, *Two membrane protein fractions from rat central myelin with inhibitory properties for neurite growth and fibroblast spreading.* J Cell Biol, 1988. **106**(4): p. 1281-8.
93. Schwab, M.E. and P. Caroni, *Oligodendrocytes and CNS myelin are nonpermissive substrates for neurite growth and fibroblast spreading in vitro.* J Neurosci, 1988. **8**(7): p. 2381-93.
94. Caroni, P. *et al.*, *Central nervous system regeneration: oligodendrocytes and myelin as non-permissive substrates for neurite growth.* Prog Brain Res, 1988. **78**: p. 363-70.
95. Schwab, M.E., *Myelin-associated inhibitors of neurite growth and regeneration in the CNS.* Trends Neurosci, 1990. **13**(11): p. 452-6.
96. Pasterkamp, R.J. *et al.*, *Peripheral nerve injury fails to induce growth of lesioned ascending dorsal column axons into spinal cord scar tissue expressing the axon repellent Semaphorin3A.* Eur J Neurosci, 2001. **13**(3): p. 457-71.
97. GrandPre, T. *et al.*, *Nogo-66 receptor antagonist peptide promotes axonal regeneration.* Nature, 2002. **417**(6888): p. 547-51.
98. Oertle, T. *et al.*, *Nogo-A inhibits neurite outgrowth and cell spreading with three discrete regions.* J Neurosci, 2003. **23**(13): p. 5393-406.
99. McKerracher, L. *et al.*, *Identification of myelin-associated glycoprotein as a major myelin-derived inhibitor of neurite growth.* Neuron, 1994. **13**(4): p. 805-11.

100. Kottis, V. *et al.*, *Oligodendrocyte-myelin glycoprotein (OMgp) is an inhibitor of neurite outgrowth.* J Neurochem, 2002. **82**(6): p. 1566-9.
101. Wang, K.C. *et al.*, *Oligodendrocyte-myelin glycoprotein is a Nogo receptor ligand that inhibits neurite outgrowth.* Nature, 2002. **417**(6892): p. 941-4.
102. Huang, J.K. *et al.*, *Glial membranes at the node of Ranvier prevent neurite outgrowth.* Science, 2005. **310**(5755): p. 1813-7.
103. Yang, L.J. *et al.*, *Gangliosides are neuronal ligands for myelin-associated glycoprotein.* Proc Natl Acad Sci U S A, 1996. **93**(2): p. 814-8.
104. Mukhopadhyay, G. *et al.*, *A novel role for myelin-associated glycoprotein as an inhibitor of axonal regeneration.* Neuron, 1994. **13**(3): p. 757-67.
105. Bartsch, U. *et al.*, *Lack of evidence that myelin-associated glycoprotein is a major inhibitor of axonal regeneration in the CNS.* Neuron, 1995. **15**(6): p. 1375-81.
106. Fournier, A.E. *et al.*, *Identification of a receptor mediating Nogo-66 inhibition of axonal regeneration.* Nature, 2001. **409**(6818): p. 341-6.
107. Venkatesh, K. *et al.*, *The Nogo-66 receptor homolog NgR2 is a sialic acid-dependent receptor selective for myelin-associated glycoprotein.* J Neurosci, 2005. **25**(4): p. 808-22.
108. Dimou, L. *et al.*, *Nogo-A-deficient mice reveal strain-dependent differences in axonal regeneration.* J Neurosci, 2006. **26**(21): p. 5591-603.
109. Simonen, M. *et al.*, *Systemic deletion of the myelin-associated outgrowth inhibitor Nogo-A improves regenerative and plastic responses after spinal cord injury.* Neuron, 2003. **38**: p. 201-211.
110. Zheng, B. *et al.*, *Lack of Enhanced Spinal Regeneration in Nogo-Deficient Mice.* Neuron, 2003. **38**(2): p. 213-224.
111. Kim, J.-E. *et al.*, *Axon Regeneration in Young Adult Mice Lacking Nogo-A/B.* Neuron, 2003. **38**: p. 187-199.
112. Caroni, P. and M.E. Schwab, *Antibody against myelin-associated inhibitor of neurite growth neutralizes nonpermissive substrate properties of CNS white matter.* Neuron, 1988. **1**(1): p. 85-96.
113. Rubin, B.P. *et al.*, *A monoclonal antibody (IN-1) which neutralizes neurite growth inhibitory proteins in the rat CNS recognizes antigens localized in CNS myelin.* J Neurocytol, 1994. **23**(4): p. 209-17.
114. Schnell, L. and M.E. Schwab, *Axonal regeneration in the rat spinal cord produced by an antibody against myelin-associated neurite growth inhibitors.* Nature, 1990. **343**(6255): p. 269-72.
115. Raineteau, O. *et al.*, *Sprouting and regeneration after pyramidotomy and blockade of the myelin-associated neurite growth inhibitors NI 35/250 in adult rats.* Eur J Neurosci, 1999. **11**(4): p. 1486-90.

116. Brosamle, C. *et al.*, *Regeneration of Lesioned Corticospinal Tract Fibers in the Adult Rat Induced by a Recombinant, Humanized IN-1 Antibody Fragment.* J. Neurosci., 2000. **20**(21): p. 8061-8068.

117. Bregman, B.S. *et al.*, *Recovery from spinal cord injury mediated by antibodies to neurite growth inhibitors.* Nature, 1995. **378**(6556): p. 498-501.

118. Liebscher, T. *et al.*, *Nogo-A antibody improves regeneration and locomotion of spinal cord-injured rats.* Ann Neurol, 2005. **58**(5): p. 706-19.

119. von Meyenburg, J. *et al.*, *Regeneration and sprouting of chronically injured corticospinal tract fibers in adult rats promoted by NT-3 and the mAb IN-1, which neutralizes myelin-associated neurite growth inhibitors.* Exp Neurol, 1998. **154**(2): p. 583-94.

120. Tang, X. *et al.*, *Changes in distribution, cell associations, and protein expression levels of NG2, neurocan, phosphacan, brevican, versican V2, and tenascin-C during acute to chronic maturation of spinal cord scar tissue.* J Neurosci Res, 2003. **71**(3): p. 427-44.

121. Zhang, Y. *et al.*, *Tenascin-C expression and axonal sprouting following injury to the spinal dorsal columns in the adult rat.* Journal of Neuroscience Research, 1997. **49**(4): p. 433-50.

122. Bareyre, F.M. *et al.*, *Long-lasting sprouting and gene expression changes induced by the monoclonal antibody IN-1 in the adult spinal cord.* J Neurosci, 2002. **22**(16): p. 7097-110.

123. Kartje, G.L. *et al.*, *Corticostriatal plasticity is restricted by myelin-associated neurite growth inhibitors in the adult rat.* Ann Neurol, 1999. **45**(6): p. 778-86.

124. Z'Graggen, W.J. *et al.*, *Functional recovery and enhanced corticofugal plasticity after unilateral pyramidal tract lesion and blockade of myelin-associated neurite growth inhibitors in adult rats.* J Neurosci, 1998. **18**(12): p. 4744-57.

125. Fouad, K. *et al.*, *Regenerating corticospinal fibers in the Marmoset (Callitrix jacchus) after spinal cord lesion and treatment with the anti-Nogo-A antibody IN-1.* Eur J Neurosci, 2004. **20**(9): p. 2479-82.

126. Huang, D.W. *et al.*, *A therapeutic vaccine approach to stimulate axon regeneration in the adult mammalian spinal cord.* Neuron, 1999. **24**(3): p. 639-47.

127. Sicotte, M. *et al.*, *Immunization with myelin or recombinant Nogo-66/MAG in alum promotes axon regeneration and sprouting after corticospinal tract lesions in the spinal cord.* Mol Cell Neurosci, 2003. **23**(2): p. 251-63.

128. Xu, G. *et al.*, *Recombinant DNA vaccine encoding multiple domains related to inhibition of neurite outgrowth: a potential strategy for axonal regeneration.* J Neurochem, 2004. **91**(4): p. 1018-23.

129. Kim, J.E. *et al.*, *Nogo-66 receptor prevents raphespinal and rubrospinal axon regeneration and limits functional recovery from spinal cord injury.* Neuron, 2004. **44**(3): p. 439-51.

130. Zheng, B. *et al.*, *Genetic deletion of the Nogo receptor does not reduce neurite inhibition in vitro or promote corticospinal tract regeneration in vivo.* Proc Natl Acad Sci U S A, 2005. **102**(4): p. 1205-10.

131. Li, S. and S.M. Strittmatter, *Delayed systemic Nogo-66 receptor antagonist promotes recovery from spinal cord injury.* J Neurosci, 2003. **23**(10): p. 4219-27.

132. Li, S. *et al.*, *Blockade of Nogo-66, myelin-associated glycoprotein, and oligodendrocyte myelin glycoprotein by soluble Nogo-66 receptor promotes axonal sprouting and recovery after spinal injury.* Journal of Neuroscience, 2004. **24**(46): p. 10511-10520.

133. Davies, S.J. *et al.*, *Robust regeneration of adult sensory axons in degenerating white matter of the adult rat spinal cord.* J Neurosci, 1999. **19**(14): p. 5810-22.

134. Davies, S.J. *et al.*, *Regeneration of adult axons in white matter tracts of the central nervous system.* Nature, 1997. **390**(6661): p. 680-3.

135. Hunt, D. *et al.*, *Nogo Receptor mRNA Expression in Intact and Regenerating CNS Neurons.* Molecular and Cellular Neuroscience, 2002. **20**(4): p. 537-552.

136. Josephson, A. *et al.*, *Nogo-receptor gene activity: Cellular localization and developmental regulation of mRNA in mice and humans.* Journal of Comparative Neurology, 2002. **453**(3): p. 292-304.

137. Wright, D.E. and W.D. Snider, *Neurotrophin receptor mRNA expression defines distinct populations of neurons in rat dorsal root ganglia.* J Comp Neurol, 1995. **351**(3): p. 329-38.

138. Moreau-Fauvarque, C. *et al.*, *The transmembrane semaphorin Sema4D/CD100, an inhibitor of axonal growth, is expressed on oligodendrocytes and upregulated after CNS lesion.* J Neurosci, 2003. **23**(27): p. 9229-39.

139. Terman, J.R. *et al.*, *MICALs, a family of conserved flavoprotein oxidoreductases, function in plexin-mediated axonal repulsion.* Cell, 2002. **109**(7): p. 887-900.

140. Liu, B.P. and S.M. Strittmatter, *Semaphorin-mediated axonal guidance via Rho-related G proteins.* Curr Opin Cell Biol, 2001. **13**(5): p. 619-26.

141. Mikule, K. *et al.*, *Eicosanoid activation of protein kinase C epsilon: involvement in growth cone repellent signaling.* J Biol Chem, 2003. **278**(23): p. 21168-77.

142. De Winter, F. *et al.*, *Injury-induced class 3 semaphorin expression in the rat spinal cord.* Exp Neurol, 2002. **175**(1): p. 61-75.

143. Manitt, C. *et al.*, *Widespread expression of netrin-1 by neurons and oligodendrocytes in the adult mammalian spinal cord.* J Neurosci, 2001. **21**(11): p. 3911-22.

144. Wehrle, R. *et al.*, *Expression of netrin-1, slit-1 and slit-3 but not of slit-2 after cerebellar and spinal cord lesions.* Eur J Neurosci, 2005. **22**(9): p. 2134-44.

145. Brose, K. *et al.*, *Slit proteins bind Robo receptors and have an evolutionarily conserved role in repulsive axon guidance.* Cell, 1999. **96**(6): p. 795-806.

146. Plump, A.S. *et al.*, *Slit1 and Slit2 cooperate to prevent premature midline crossing of retinal axons in the mouse visual system.* Neuron, 2002. **33**(2): p. 219-32.

147. Sundaresan, V. *et al.*, *Dynamic expression patterns of Robo (Robo1 and Robo2) in the developing murine central nervous system.* J Comp Neurol, 2004. **468**(4): p. 467-81.

148. Berry, M. *et al.*, *Deposition of scar tissue in the central nervous system.* Acta Neurochir Suppl (Wien), 1983. **32**: p. 31-53.

149. Abnet, K. *et al.*, *Interactions between meningeal cells and astrocytes in vivo and in vitro.* Brain Res Dev Brain Res, 1991. **59**(2): p. 187-96.

150. Alonso, G. and A. Privat, *Reactive astrocytes involved in the formation of lesional scars differ in the mediobasal hypothalamus and in other forebrain regions.* J Neurosci Res, 1993. **34**(5): p. 523-38.

151. Eagle, K.S. *et al.*, *Axonal regeneration and limited functional recovery following hippocampal deafferentation.* J Comp Neurol, 1995. **363**(3): p. 377-88.

152. Kawaja, M.D. and F.H. Gage, *Reactive astrocytes are substrates for the growth of adult CNS axons in the presence of elevated levels of nerve growth factor.* Neuron, 1991. **7**(6): p. 1019-30.

153. Saad, B. *et al.*, *Astrocyte-derived TGF-beta 2 and NGF differentially regulate neural recognition molecule expression by cultured astrocytes.* J Cell Biol, 1991. **115**(2): p. 473-84.

154. Privat, A. *et al.*, *Spinal cord injuries: comments on preventive and curative strategy.* Agressologie, 1993. **34**: p. 64.

155. Wilhelmsson, U. *et al.*, *Absence of glial fibrillary acidic protein and vimentin prevents hypertrophy of astrocytic processes and improves post-traumatic regeneration.* J Neurosci, 2004. **24**(21): p. 5016-21.

156. Kalderon, N. and Z. Fuks, *Structural recovery in lesioned adult mammalian spinal cord by x-irradiation of the lesion site.* Proc Natl Acad Sci U S A, 1996. **93**(20): p. 11179-84.

157. Kalderon, N. and Z. Fuks, *Severed corticospinal axons recover electrophysiologic control of muscle activity after x-ray therapy in lesioned adult spinal cord.* Proc Natl Acad Sci U S A, 1996. **93**(20): p. 11185-90.

158. Ridet, J.L. *et al.*, *Effects of spinal cord X-irradiation on the recovery of paraplegic rats.* Exp Neurol, 2000. **161**(1): p. 1-14.

159. Brewer, K.L. *et al.*, *Neuroprotective effects of interleukin-10 following excitotoxic spinal cord injury.* Exp Neurol, 1999. **159**(2): p. 484-93.

160. Canning, D.R. *et al.*, *A potent inhibitor of neurite outgrowth that predominates in the extracellular matrix of reactive astrocytes.* Int J Dev Neurosci, 1996. **14**(3): p. 153-75.

161. McKeon, R.J. *et al.*, *The Chondroitin Sulfate Proteoglycans Neurocan and Phosphacan Are Expressed by Reactive Astrocytes in the Chronic CNS Glial Scar.* J. Neurosci., 1999. **19**(24): p. 10778-10788.

162. Jones, L.L. *et al.*, *The chondroitin sulfate proteoglycans neurocan, brevican, phosphacan, and versican are differentially regulated following spinal cord injury.* Exp Neurol, 2003. **182**(2): p. 399-411.

163. Junghans, U. *et al.*, *Purification of a meningeal cell-derived chondroitin sulphate proteoglycan with neurotrophic activity for brain neurons and its identification as biglycan.* Eur J Neurosci, 1995. **7**(11): p. 2341-50.

164. Davies, J.E. *et al.*, *Decorin suppresses neurocan, brevican, phosphacan and NG2 expression and promotes axon growth across adult rat spinal cord injuries.* Eur J Neurosci, 2004. **19**(5): p. 1226-42.

165. Logan, A. *et al.*, *Decorin attenuates gliotic scar formation in the rat cerebral hemisphere.* Exp Neurol, 1999. **159**(2): p. 504-10.

166. Hynds, D.L. and D.M. Snow, *Neurite outgrowth inhibition by chondroitin sulfate proteoglycan: stalling/stopping exceeds turning in human neuroblastoma growth cones.* Exp Neurol, 1999. **160**(1): p. 244-55.

167. McKeon, R.J. *et al.*, *Injury-induced proteoglycans inhibit the potential for laminin-mediated axon growth on astrocytic scars.* Exp Neurol, 1995. **136**(1): p. 32-43.

168. Schmalfeldt, M. *et al.*, *Brain derived versican V2 is a potent inhibitor of axonal growth.* J Cell Sci, 2000. **113**: p. 807-16.

169. Ughrin, Y.M. *et al.*, *Multiple regions of the NG2 proteoglycan inhibit neurite growth and induce growth cone collapse.* J Neurosci, 2003. **23**(1): p. 175-86.

170. Jones, L.L. *et al.*, *NG2 is a major chondroitin sulfate proteoglycan produced after spinal cord injury and is expressed by macrophages and oligodendrocyte progenitors.* J Neurosci, 2002. **22**(7): p. 2792-803.

171. Moon, L.D. *et al.*, *Relationship between sprouting axons, proteoglycans and glial cells following unilateral nigrostriatal axotomy in the adult rat.* Neuroscience, 2002. **109**(1): p. 101-17.

172. Dow, K.E. *et al.*, *Molecular correlates of spinal cord repair in the embryonic chick: heparan sulfate and chondroitin sulfate proteoglycans.* Exp Neurol, 1994. **128**(2): p. 233-8.

173. McKeon, R.J. *et al.*, *Reduction of neurite outgrowth in a model of glial scarring following CNS injury is correlated with the expression of inhibitory molecules on reactive astrocytes.* J Neurosci, 1991. **11**(11): p. 3398-411.

174. Rudge, J.S. and J. Silver, *Inhibition of neurite outgrowth on astroglial scars in vitro.* J Neurosci, 1990. **10**(11): p. 3594-603.

175. Bahr, M. *et al.*, *Astrocytes from adult rat optic nerves are nonpermissive for regenerating retinal ganglion cell axons.* Exp Neurol, 1995. **131**(2): p. 211-20.

176. Inman, D.M. and O. Steward, *Ascending sensory, but not other long-tract axons, regenerate into the connective tissue matrix that forms at the site of a spinal cord injury in mice.* J Comp Neurol, 2003. **462**(4): p. 431-49.

177. Zhang, Y. *et al.*, *Correlation between putative inhibitory molecules at the dorsal root entry zone and failure of dorsal root axonal regeneration.* Mol Cell Neurosci, 2001. **17**(3): p. 444-59.

178. Lemons, M.L. *et al.*, *Chondroitin sulfate proteoglycan immunoreactivity increases following spinal cord injury and transplantation.* Exp Neurol, 1999. **160**(1): p. 51-65.

179. Bruckner, G. *et al.*, *Acute and long-lasting changes in extracellular-matrix chondroitin-sulphate proteoglycans induced by injection of chondroitinase ABC in the adult rat brain.* Exp Brain Res, 1998. **121**(3): p. 300-10.

180. Pizzorusso, T. *et al.*, *Reactivation of ocular dominance plasticity in the adult visual cortex.* Science, 2002. **298**(5596): p. 1248-51.

181. Bradbury, E.J. *et al.*, *Chondroitinase ABC promotes functional recovery after spinal cord injury.* Nature, 2002. **416**(6881): p. 636-640.

182. Moon, L.D. *et al.*, *Regeneration of CNS axons back to their target following treatment of adult rat brain with chondroitinase ABC.* Nat Neurosci, 2001. **4**(5): p. 465-6.

183. Yick, L.W. *et al.*, *Axonal regeneration of Clarke's neurons beyond the spinal cord injury scar after treatment with chondroitinase ABC.* Exp Neurol, 2003. **182**(1): p. 160-8.

184. Yick, L.W. *et al.*, *Lithium chloride reinforces the regeneration-promoting effect of chondroitinase ABC on rubrospinal neurons after spinal cord injury.* J Neurotrauma, 2004. **21**(7): p. 932-43.

185. Yick, L.W. *et al.*, *Chondroitinase ABC promotes axonal regeneration of Clarke's neurons after spinal cord injury.* Neuroreport, 2000. **11**(5): p. 1063-7.

186. Caggiano, A.O. *et al.*, *Chondroitinase ABCI improves locomotion and bladder function following contusion injury of the rat spinal cord.* J Neurotrauma, 2005. **22**(2): p. 226-39.

187. Lemons, M.L. *et al.*, *Intact aggrecan and chondroitin sulfate-depleted aggrecan core glycoprotein inhibit axon growth in the adult rat spinal cord.* Exp Neurol, 2003. **184**(2): p. 981-90.

188. Grimpe, B. and J. Silver, *A novel DNA enzyme reduces glycosaminoglycan chains in the glial scar and allows microtransplanted dorsal root ganglia axons to regenerate beyond lesions in the spinal cord.* J Neurosci, 2004. **24**(6): p. 1393-7.

189. Gavazzi, I. *et al.*, *Growth responses of different subpopulations of adult sensory neurons to neurotrophic factors in vitro.* Eur J Neurosci, 1999. **11**(10): p. 3405-14.

190. Leclere, P. *et al.*, *Effects of glial cell line-derived neurotrophic factor on axonal growth and apoptosis in adult mammalian sensory neurons in vitro.* Neuroscience, 1998. **82**(2): p. 545-58.

191. Cai, D. *et al.*, *Prior exposure to neurotrophins blocks inhibition of axonal regeneration by MAG and myelin via a cAMP-dependent mechanism.* Neuron, 1999. **22**(1): p. 89-101.

192. Yamashita, T. *et al.*, *Neurotrophin binding to the p75 receptor modulates Rho activity and axonal outgrowth.* Neuron, 1999. **24**(3): p. 585-93.
193. Yamashita, T. *et al.*, *The p75 receptor transduces the signal from myelin-associated glycoprotein to Rho.* J Cell Biol, 2002. **157**(4): p. 565-70.
194. Fu, S.Y. and T. Gordon, *The cellular and molecular basis of peripheral nerve regeneration.* Mol Neurobiol, 1997. **14**(1-2): p. 67-116.
195. Snider, W.D. *et al.*, *Signaling the pathway to regeneration.* Neuron, 2002. **35**(1): p. 13-6.
196. Schwaiger, F.W. *et al.*, *Peripheral but not central axotomy induces changes in Janus kinases (JAK) and signal transducers and activators of transcription (STAT).* Eur J Neurosci, 2000. **12**(4): p. 1165-76.
197. Cafferty, W.B. *et al.*, *Leukemia inhibitory factor determines the growth status of injured adult sensory neurons.* J Neurosci, 2001. **21**(18): p. 7161-70.
198. Zhong, J. *et al.*, *Sensory impairments and delayed regeneration of sensory axons in interleukin-6-deficient mice.* J Neurosci, 1999. **19**(11): p. 4305-13.
199. Romero, M.I. *et al.*, *Functional regeneration of chronically injured sensory afferents into adult spinal cord after neurotrophin gene therapy.* J Neurosci, 2001. **21**(21): p. 8408-16.
200. Ramer, M.S. *et al.*, *Functional regeneration of sensory axons into the adult spinal cord.* Nature, 2000. **403**(6767): p. 312-6.
201. Iwaya, K. *et al.*, *Neurotrophic agents in fibrin glue mediate adult dorsal root regeneration into spinal cord.* Neurosurgery, 1999. **44**(3): p. 589-95; discussion 595-6.
202. Ramer, M.S. *et al.*, *Neurotrophin-3-mediated regeneration and recovery of proprioception following dorsal rhizotomy.* Molecular and Cellular Neurosciences, 2002. **19**(2): p. 239-49.
203. Oudega, M. and T. Hagg, *Neurotrophins promote regeneration of sensory axons in the adult rat spinal cord.* Brain Res, 1999. **818**(2): p. 431-8.
204. Jelsma, T.N. and A.J. Aguayo, *Trophic factors.* Curr Opin Neurobiol, 1994. **4**(5): p. 717-25.
205. Tuszynski, M.H. *et al.*, *NT-3 gene delivery elicits growth of chronically injured corticospinal axons and modestly improves functional deficits after chronic scar resection.* Exp Neurol, 2003. **181**(1): p. 47-56.
206. Blesch, A. and M.H. Tuszynski, *GDNF gene delivery to injured adult CNS motor neurons promotes axonal growth, expression of the trophic neuropeptide CGRP, and cellular protection.* J Comp Neurol, 2001. **436**(4): p. 399-410.
207. Liu, Y. *et al.*, *Transplants of Fibroblasts Genetically Modified to Express BDNF Promote Regeneration of Adult Rat Rubrospinal Axons and Recovery of Forelimb Function.* J. Neurosci., 1999. **19**(11): p. 4370-4387.

208. Grill, R.J. *et al.*, *Robust Growth of Chronically Injured Spinal Cord Axons Induced by Grafts of Genetically Modified NGF-Secreting Cells.* Experimental Neurology, 1997. **148**(2): p. 444-452.

209. Coumans, J.V. *et al.*, *Axonal regeneration and functional recovery after complete spinal cord transection in rats by delayed treatment with transplants and neurotrophins.* The Journal of Neuroscience, 2001. **21**(23): p. 9334-44.

210. Bregman, B.S. *et al.*, *Neurotrophic factors increase axonal growth after spinal cord injury and transplantation in the adult rat.* Exp Neurol, 1997. **148**(2): p. 475-94.

211. Chao, M.V., *Neurotrophins and their receptors: a convergence point for many signalling pathways.* Nat Rev Neurosci, 2003. **4**(4): p. 299-309.

212. Plunet, W. *et al.*, *Promoting axonal regeneration in the central nervous system by enhancing the cell body response to axotomy.* J Neurosci Res, 2002. **68**(1): p. 1-6.

213. Blesch, A. *et al.*, *Neurotrophic factors, gene therapy, and neural stem cells for spinal cord repair.* Brain Research Bulletin, 2002. **57**(6): p. 833-8.

214. Novikova, L.N. *et al.*, *Survival effects of BDNF and NT-3 on axotomized rubrospinal neurons depend on the temporal pattern of neurotrophin administration.* Eur J Neurosci, 2000. **12**(2): p. 776-80.

215. Priestley, J.V. *et al.*, *Stimulating regeneration in the damaged spinal cord.* Journal of Physiology, Paris, 2002. **96**(1-2): p. 123-33.

216. Gautier, S.E. *et al.*, *Poly(alpha-hydroxyacids) for application in the spinal cord: resorbability and biocompatibility with adult rat Schwann cells and spinal cord.* J Biomed Mater Res, 1998. **42**(4): p. 642-54.

217. Li, Y. and G. Raisman, *Schwann cells induce sprouting in motor and sensory axons in the adult rat spinal cord.* J Neurosci, 1994. **14**(7): p. 4050-63.

218. Xu, X.M. *et al.*, *Regrowth of axons into the distal spinal cord through a Schwann-cell-seeded mini-channel implanted into hemisected adult rat spinal cord.* Eur J Neurosci, 1999. **11**(5): p. 1723-40.

219. McDonald, J.W. *et al.*, *Repair of the injured spinal cord and the potential of embryonic stem cell transplantation.* J Neurotrauma, 2004. **21**(4): p. 383-93.

220. Horner, P.J. *et al.*, *Proliferation and differentiation of progenitor cells throughout the intact adult rat spinal cord.* J Neurosci, 2000. **20**(6): p. 2218-28.

221. Wichterle, H. *et al.*, *Directed differentiation of embryonic stem cells into motor neurons.* Cell, 2002. **110**(3): p. 385-97.

222. McDonald, J.W. *et al.*, *Transplanted embryonic stem cells survive, differentiate and promote recovery in injured rat spinal cord.* Nat Med, 1999. **5**(12): p. 1410-2.

223. Cao, Q.L. *et al.*, *Pluripotent stem cells engrafted into the normal or lesioned adult rat spinal cord are restricted to a glial lineage.* Exp Neurol, 2001. **167**(1): p. 48-58.

224. Ramon-Cueto, A. *et al.*, *Functional recovery of paraplegic rats and motor axon regeneration in their spinal cords by olfactory ensheathing glia.* Neuron, 2000. **25**(2): p. 425-35.

225. Li, Y. *et al.*, *Repair of adult rat corticospinal tract by transplants of olfactory ensheathing cells.* Science, 1997. **277**(5334): p. 2000-2.
226. The Eph Nomenclature Committee, *Nomenclature site for the Eph receptors and their ligands, the ephrins.* 2003, http://eph-nomenclature.med.harvard.edu/.
227. Dodelet, V.C. and E.B. Pasquale, *Eph receptors and ephrin ligands: embryogenesis to tumorigenesis.* Oncogene, 2000. **19**(49): p. 5614-9.
228. Flanagan, J.G. and P. Vanderhaeghen, *The Ephrins and Eph Receptors in Neural Development.* Annu. Rev. Neurosci., 1998. **21**(1): p. 309-345.
229. Zhou, R., *The Eph family receptors and ligands.* Pharmacology & Therapeutics, 1998. **77**(3): p. 151-81.
230. Wilkinson, D.G., *Multiple roles of EPH receptors and ephrins in neural development.* Nat Rev Neurosci, 2001. **2**(3): p. 155-64.
231. Pasquale, E.B., *Eph-ephrin promiscuity is now crystal clear.* Nat Neurosci, 2004. **7**(5): p. 417-418.
232. Himanen, J.P. *et al.*, *Repelling class discrimination: ephrin-A5 binds to and activates EphB2 receptor signaling.* Nat Neurosci, 2004. **7**(5): p. 501-9.
233. Gale, N.W. *et al.*, *Elk-L3, a novel transmembrane ligand for the Eph family of receptor tyrosine kinases, expressed in embryonic floor plate, roof plate and hindbrain segments.* Oncogene, 1996. **13**(6): p. 1343-52.
234. Dottori, M. *et al.*, *EphA4 (Sek1) receptor tyrosine kinase is required for the development of the corticospinal tract.* Proc Natl Acad Sci U S A, 1998. **95**(22): p. 13248-53.
235. Kullander, K. *et al.*, *Ephrin-B3 is the midline barrier that prevents corticospinal tract axons from recrossing, allowing for unilateral motor control.* Genes & Development, 2001. **15**(7): p. 877-88.
236. Yokoyama, N. *et al.*, *Forward signaling mediated by ephrin-B3 prevents contralateral corticospinal axons from recrossing the spinal cord midline.* Neuron, 2001. **29**(1): p. 85-97.
237. Schmucker, D. and S.L. Zipursky, *Signaling downstream of Eph receptors and ephrin ligands.* Cell, 2001. **105**(6): p. 701-4.
238. Schlessinger, J., *Cell Signaling by Receptor Tyrosine Kinases.* Cell, 2000. **103**(2): p. 211-225.
239. Gille, H. *et al.*, *A repressor sequence in the juxtamembrane domain of Flt-1 (VEGFR-1) constitutively inhibits vascular endothelial growth factor-dependent phosphatidylinositol 3'-kinase activation and endothelial cell migration.* EMBO Journal, 2000. **19**(15): p. 4064-4073.
240. Wybenga-Groot, L.E. *et al.*, *Structural Basis for Autoinhibition of the EphB2 Receptor Tyrosine Kinase by the Unphosphorylated Juxtamembrane Region.* Cell, 2001. **106**(6): p. 745-757.

241. Kullander, K. *et al.*, *Kinase-Dependent and Kinase-Independent Functions of EphA4 Receptors in Major Axon Tract Formation In Vivo.* Neuron, 2001. **29**(1): p. 73-84.
242. Davis, S. *et al.*, *Ligands for EPH-related receptor tyrosine kinases that require membrane attachment or clustering for activity.* Science, 1994. **266**(5186): p. 816-9.
243. Holland, S.J. *et al.*, *Bidirectional signalling through the EPH-family receptor Nuk and its transmembrane ligands.* Nature, 1996. **383**(6602): p. 722-725.
244. Bruckner, K. *et al.*, *Tyrosine phosphorylation of transmembrane ligands for Eph receptors.* Science, 1997. **275**(5306): p. 1640-3.
245. Stein, E. *et al.*, *Eph receptors discriminate specific ligand oligomers to determine alternative signaling complexes, attachment, and assembly responses.* Genes and Development, 1998. **12**(5): p. 667-678.
246. Himanen, J.P. and D.B. Nikolov, *Eph signaling: a structural view.* Trends in Neurosciences, 2003. **26**(1): p. 46-51.
247. Himanen, J.P. *et al.*, *Crystal structure of an Eph receptor-ephrin complex.* Nature, 2001. **414**(6866): p. 933-8.
248. Patel, B.N. and D.L. Van-Vactor, *Axon guidance: the cytoplasmic tail.* Current Opinion in Cell Biology, 2002. **14**(2): p. 221-9.
249. Noren, N.K. and E.B. Pasquale, *Eph receptor-ephrin bidirectional signals that target Ras and Rho proteins.* Cellular Signalling, 2004. **16**(6): p. 655-666.
250. Lehmann, M. *et al.*, *Inactivation of Rho Signaling Pathway Promotes CNS Axon Regeneration.* J. Neurosci., 1999. **19**(17): p. 7537-7547.
251. Meyer, G. and E.L. Feldman, *Signaling mechanisms that regulate actin-based motility processes in the nervous system.* Journal of Neurochemistry, 2002. **83**(3): p. 490-503.
252. Giniger, E., *How do Rho family GTPases direct axon growth and guidance? A proposal relating signaling pathways to growth cone mechanics.* Differentiation; Research in Biological Diversity, 2002. **70**(8): p. 385-96.
253. Holmberg, J. *et al.*, *Regulation of repulsion versus adhesion by different splice forms of an Eph receptor.* Nature, 2000. **408**(6809): p. 203-6.
254. Klein, R., *Excitatory Eph receptors and adhesive ephrin ligands.* Current Opinion in Cell Biology, 2001. **13**(2): p. 196-203.
255. Cowan, C.A. and M. Henkemeyer, *Ephrins in reverse, park and drive.* Trends in Cell Biology, 2002. **12**(7): p. 339-46.
256. Holmberg, J. and J. Frisen, *Ephrins are not only unattractive.* Trends in Neurosciences, 2002. **25**(5): p. 239-43.
257. Knoll, B. and U. Drescher, *Ephrin-As as receptors in topographic projections.* Trends-Neurosci, 2002. **25**(3): p. 145-9.
258. Kullander, K. and R. Klein, *Mechanisms and functions of Eph and ephrin signalling.* Nature Reviews Molecular Cell Biology, 2002. **3**(7): p. 475-86.

259. Shamah, S.M. *et al.*, *EphA receptors regulate growth cone dynamics through the novel guanine nucleotide exchange factor ephexin.* Cell, 2001. **105**(2): p. 233-44.
260. Bruckner, K. *et al.*, *EphrinB ligands recruit GRIP family PDZ adaptor proteins into raft membrane microdomains.* Neuron, 1999. **22**(3): p. 511-24.
261. Kalo, M.S. and E.B. Pasquale, *Signal transfer by Eph receptors.* Cell and Tissue Research, 1999. **298**(1): p. 1-9.
262. Lin, D. *et al.*, *The carboxyl terminus of B class ephrins constitutes a PDZ domain binding motif.* J Biol Chem, 1999. **274**(6): p. 3726-33.
263. Lu, Q. *et al.*, *Ephrin-B reverse signaling is mediated by a novel PDZ-RGS protein and selectively inhibits G protein-coupled chemoattraction.* Cell, 2001. **105**(1): p. 69-79.
264. Takasu, M.A. *et al.*, *Modulation of NMDA receptor-dependent calcium influx and gene expression through EphB receptors.* Science, 2002. **295**(5554): p. 491-5.
265. Murai, K.K. and E.B. Pasquale, *Can Eph receptors stimulate the mind?* Neuron, 2002. **33**(2): p. 159-62.
266. Knöll, B. and U. Drescher, *Src family kinases are involved in EphA receptor-mediated retinal axon guidance.* Journal of Neuroscience, 2004. **24**(28): p. 6248-6257.
267. Sahin, M. *et al.*, *Eph-dependent tyrosine phosphorylation of ephexin1 modulates growth cone collapse.* Neuron, 2005. **46**: p. 191-204.
268. Schmidt, A. and A. Hall, *Guanine nucleotide exchange factors for Rho GTPases: turning on the switch.* Genes Dev., 2002. **16**(13): p. 1587-1609.
269. Penzes, P. *et al.*, *Rapid Induction of Dendritic Spine Morphogenesis by trans-Synaptic EphrinB-EphB Receptor Activation of the Rho-GEF Kalirin.* Neuron, 2003. **37**(2): p. 263-274.
270. Irie, F. and Y. Yamaguchi, *EphB receptors regulate dendritic spine development via intersectin, Cdc42 and N-WASP.* Nat Neurosci, 2002. **5**(11): p. 1117-8.
271. Mellitzer, G. *et al.*, *Eph receptors and ephrins restrict cell intermingling and communication.* Nature, 1999. **400**(6739): p. 77-81.
272. Kalo, M.S. *et al.*, *In Vivo Tyrosine Phosphorylation Sites of Activated Ephrin-B1 and EphB2 from Neural Tissue.* J. Biol. Chem., 2001. **276**(42): p. 38940-38948.
273. Palmer, A. *et al.*, *EphrinB phosphorylation and reverse signaling: regulation by Src kinases and PTP-BL phosphatase.* Molecular Cell, 2002. **9**(4): p. 725-37.
274. Davy, A. *et al.*, *Compartmentalized signaling by GPI-anchored ephrin-A5 requires the Fyn tyrosine kinase to regulate cellular adhesion.* Genes Dev, 1999. **13**(23): p. 3125-35.
275. Knoll, B. *et al.*, *A role for the EphA family in the topographic targeting of vomeronasal axons.* Development, 2001. **128**(6): p. 895-906.
276. Henkemeyer, M. *et al.*, *Nuk controls pathfinding of commissural axons in the mammalian central nervous system.* Cell, 1996. **86**(1): p. 35-46.
277. Hornberger, M.R. *et al.*, *Modulation of EphA receptor function by coexpressed ephrinA ligands on retinal ganglion cell axons.* Neuron, 1999. **22**(4): p. 731-42.

278. Yin, Y. *et al.*, *EphA receptor tyrosine kinases interact with co-expressed ephrin-A ligands in cis.* Neuroscience Research, 2004. **48**(3): p. 285-295.
279. Eberhart, J. *et al.*, *Expression of EphA4, ephrin-A2 and ephrin-A5 during axon outgrowth to the hindlimb indicates potential roles in pathfinding.* Developmental Neuroscience, 2000. **22**(3): p. 237-50.
280. Iwamasa, H. *et al.*, *Expression of Eph receptor tyrosine kinases and their ligands in chick embryonic motor neurons and hindlimb muscles.* Dev Growth Differ, 1999. **41**(6): p. 685-98.
281. Battaglia, A. *et al.*, *EphB receptors and ephrin-B ligands regulate spinal sensory connectivity and modulate pain processing.* Nat Neurosci, 2003. **6**(4): p. 339-40.
282. Rodger, J. *et al.*, *EphA/ephrin-A interactions during optic nerve regeneration: restoration of topography and regulation of ephrin-A2 expression.* Mol Cell Neurosci, 2004. **25**(1): p. 56-68.
283. Pratt, R.L. and M.S. Kinch, *Activation of the EphA2 tyrosine kinase stimulates the MAP/ERK kinase signaling cascade.* Oncogene, 2002. **21**(50): p. 7690-7699.
284. Tong, J. *et al.*, *Manipulation of EphB2 Regulatory Motifs and SH2 Binding Sites Switches MAPK Signaling and Biological Activity.* J. Biol. Chem., 2003. **278**(8): p. 6111-6119.
285. Lawrenson, I.D. *et al.*, *Ephrin-A5 induces rounding, blebbing and de-adhesion of EphA3-expressing 293T and melanoma cells by CrkII and Rho-mediated signalling.* J Cell Sci, 2002. **115**(5): p. 1059-1072.
286. Miralles, F. *et al.*, *Actin Dynamics Control SRF Activity by Regulation of Its Coactivator MAL.* Cell, 2003. **113**(3): p. 329-342.
287. Egea, J. *et al.*, *Regulation of EphA4 Kinase Activity Is Required for a Subset of Axon Guidance Decisions Suggesting a Key Role for Receptor Clustering in Eph Function.* Neuron, 2005. **47**(4): p. 515-528.
288. Wimmer-Kleikamp, S.H. *et al.*, *Recruitment of Eph receptors into signaling clusters does not require ephrin contact.* J Cell Biol, 2004. **164**(5): p. 661-6.
289. Coonan, J.R. *et al.*, *Development and reorganization of corticospinal projections in EphA4 deficient mice.* J Comp Neurol, 2001. **436**(2): p. 248-62.
290. Kullander, K. *et al.*, *Role of EphA4 and EphrinB3 in Local Neuronal Circuits That Control Walking.* Science, 2003. **299**(5614): p. 1889-1892.
291. Mackarehtschian, K. *et al.*, *Regional differences in the developing cerebral cortex revealed by ephrin-A5 expression.* Cereb Cortex, 1999. **9**(6): p. 601-10.
292. Vanderhaeghen, P. and F. Polleux, *Developmental mechanisms patterning thalamocortical projections: intrinsic, extrinsic and in between.* Trends in Neurosciences, 2004. **27**(7): p. 384-391.
293. Dufour, A. *et al.*, *Area Specificity and Topography of Thalamocortical Projections Are Controlled by ephrin/Eph Genes.* Neuron, 2003. **39**(3): p. 453-465.

294. Gao, P.-P. *et al.*, *Regulation of topographic projection in the brain: Elf-1 in the hippocamposeptal system.* PNAS, 1996. **93**(20): p. 11161-11166.
295. Zhang, J.H. *et al.*, *Detection of ligands in regions anatomically connected to neurons expressing the Eph receptor Bsk: potential roles in neuron-target interaction.* The Journal of Neuroscience, 1996. **16**(22): p. 7182-92.
296. Helmbacher, F. *et al.*, *Targeting of the EphA4 tyrosine kinase receptor affects dorsal/ventral pathfinding of limb motor axons.* Development, 2000. **127**(15): p. 3313-3324.
297. Eberhart, J. *et al.*, *Ephrin-A5 Exerts Positive or Inhibitory Effects on Distinct Subsets of EphA4-Positive Motor Neurons.* J. Neurosci., 2004. **24**(5): p. 1070-1078.
298. Kania, A. and T.M. Jessell, *Topographic motor projections in the limb imposed by LIM homeodomain protein regulation of ephrin-A:EphA interactions.* Neuron, 2003. **38**(4): p. 581-96.
299. Donoghue, M.J. *et al.*, *The Eph kinase ligand AL-1 is expressed by rostral muscles and inhibits outgrowth from caudal neurons.* Molecular and Cellular Neurosciences, 1996. **8**(2-3): p. 185-98.
300. Feng, G. *et al.*, *Roles for ephrins in positionally selective synaptogenesis between motor neurons and muscle fibers.* Neuron, 2000. **25**(2): p. 295-306.
301. Wang, H. *et al.*, *Development of inhibition by ephrin-A5 on outgrowth of embryonic spinal motor neurites.* Journal of Neurobiology, 2000. **47**(3): p. 233-43.
302. Lai, K.O. *et al.*, *Expression of Eph receptors in skeletal muscle and their localization at the neuromuscular junction.* Mol Cell Neurosci, 2001. **17**(6): p. 1034-47.
303. Frisen, J. *et al.*, *Ephrin-A5 (AL-1/RAGS) is essential for proper retinal axon guidance and topographic mapping in the mammalian visual system.* Neuron, 1998. **20**(2): p. 235-43.
304. Brennan, C. *et al.*, *Two Eph receptor tyrosine kinase ligands control axon growth and may be involved in the creation of the retinotectal map in the zebrafish.* Development (Cambridge, England), 1997. **124**(3): p. 655-64.
305. Mann, F. *et al.*, *Topographic mapping in dorsoventral axis of the Xenopus retinotectal system depends on signaling through ephrin-B ligands.* Neuron, 2002. **35**(3): p. 461-73.
306. Pittman, A. and C.B. Chien, *Understanding dorsoventral topography: backwards and forwards.* Neuron, 2002. **35**(3): p. 409-11.
307. Holt, C.E. *Axon guidance in the visual system.* in *Society for Neuroscience Annual Meeting.* 2001. San Diego.
308. Wang, H.U. and D.J. Anderson, *Eph family transmembrane ligands can mediate repulsive guidance of trunk neural crest migration and motor axon outgrowth.* Neuron, 1997. **18**(3): p. 383-96.
309. Krull, C.E. *et al.*, *Interactions of Eph-related receptors and ligands confer rostrocaudal pattern to trunk neural crest migration.* Curr Biol, 1997. **7**(8): p. 571-80.

310. Chen, Z.Y. *et al.*, *Abnormal hippocampal axon bundling in EphB receptor mutant mice.* J Neurosci, 2004. **24**(10): p. 2366-74.
311. Cowan, C.A. *et al.*, *Ephrin-B2 reverse signaling is required for axon pathfinding and cardiac valve formation but not early vascular development.* Dev Biol, 2004. **271**(2): p. 263-71.
312. Coonan, J.R. *et al.*, *Role of EphA4 in defining the position of a motoneuron pool within the spinal cord.* J Comp Neurol, 2003. **458**(1): p. 98-111.
313. Kiehn, O. and K. Kullander, *Central Pattern Generators Deciphered by Molecular Genetics.* Neuron, 2004. **41**(3): p. 317-321.
314. Butt, S.J. and O. Kiehn, *Functional identification of interneurons responsible for left-right coordination of hindlimbs in mammals.* Neuron, 2003. **38**(6): p. 953-63.
315. Sobel, R.A., *Ephrin A receptors and ligands in lesions and normal-appearing white matter in multiple sclerosis.* Brain Pathology, 2005. **15**(1): p. 35-45.
316. Hafner, C. *et al.*, *Differential gene expression of Eph receptors and ephrins in benign human tissues and cancers.* Clin Chem, 2004. **50**(3): p. 490-9.
317. Xiao, D. *et al.*, *Ephrin/Eph receptor expression in brain of adult nonhuman primates: Implications for neuroadaptation.* Brain Res, 2005.
318. Willson, C.A. *et al.*, *Upregulation of EphA receptor expression in the injured adult rat spinal cord.* Cell Transplantation, 2002. **11**(3): p. 229-39.
319. Greferath, U. *et al.*, *Developmental expression of EphA4-tyrosine kinase receptor in the mouse brain and spinal cord.* Gene Expr Patterns, 2002. **2**(3-4): p. 267-74.
320. Karam, S.D. *et al.*, *EphA4 is not required for Purkinje cell compartmentation.* Developmental Brain Research, 2002. **135**(1-2): p. 29-38.
321. Martone, M.E. *et al.*, *Immunolocalization of the receptor tyrosine kinase EphA4 in the adult rat central nervous system.* Brain Research, 1997. **771**(2): p. 238-250.
322. Rogers, J.H. *et al.*, *Eph receptors and ephrins demarcate cerebellar lobules before and during their formation.* Mech Dev, 1999. **87**(1-2): p. 119-28.
323. Liebl, D.J. *et al.*, *mRNA expression of ephrins and Eph receptor tyrosine kinases in the neonatal and adult mouse central nervous system.* Journal of Neuroscience Research, 2003. **71**(1): p. 7-22.
324. Mori, T. *et al.*, *Differential expressions of the eph family of receptor tyrosine kinase genes (sek, elk, eck) in the developing nervous system of the mouse.* Molecular Brain Research, 1995. **29**(2): p. 325-335.
325. Yue, Y. *et al.*, *Specification of Distinct Dopaminergic Neural Pathways: Roles of the Eph Family Receptor EphB1 and Ligand Ephrin-B2.* J. Neurosci., 1999. **19**(6): p. 2090-2101.
326. Lai, C. and G. Lemke, *An extended family of protein-tyrosine kinase genes differentially expressed in the vertebrate nervous system.* Neuron, 1991. **6**(5): p. 691-704.

327. Mori, T. *et al.*, *Localization of novel receptor tyrosine kinase genes of the eph family, MDK1 and its splicing variant, in the developing mouse nervous system.* Molecular Brain Research, 1995. **34**(1): p. 154-160.

328. Taylor, V. *et al.*, *Expression and developmental regulation of Ehk-1, a neuronal Elk-like receptor tyrosine kinase in brain.* Neuroscience, 1994. **63**(1): p. 163-78.

329. Zhou, R. *et al.*, *Isolation and characterization of Bsk, a growth factor receptor-like tyrosine kinase associated with the limbic system.* Journal of Neuroscience Research, 1994. **37**(1): p. 129-43.

330. Fabes, J. *et al.*, *Accumulation of the inhibitory receptor EphA4 may prevent regeneration of corticospinal tract axons following lesion.* Eur J Neurosci, 2006. **23**(7): p. 1721-30.

331. Benson, M.D. *et al.*, *Ephrin-B3 is a myelin-based inhibitor of neurite outgrowth.* PNAS, 2005. **102**(30): p. 10694-10699.

332. Wang, Y. *et al.*, *Induction of ephrin-B1 and EphB receptors during denervation-induced plasticity in the adult mouse hippocampus.* European Journal of Neuroscience, 2005. **21**(9): p. 2336-2346.

333. Klein, R., *Eph/ephrin signaling in morphogenesis, neural development and plasticity.* Current Opinion in Cell Biology, 2004. **16**(5): p. 580-9.

334. Grunwald, I.C. *et al.*, *Hippocampal plasticity requires postsynaptic ephrinBs.* Nat Neurosci, 2004. **7**(1): p. 33-40.

335. Murai, K.K. *et al.*, *Control of hippocampal dendritic spine morphology through ephrin-A3/EphA4 signaling.* Nature Neuroscience, 2003. **6**(2): p. 153-160.

336. Ethell, I.M. *et al.*, *EphB/Syndecan-2 Signaling in Dendritic Spine Morphogenesis.* Neuron, 2001. **31**(6): p. 1001-1013.

337. Henkemeyer, M. *et al.*, *Multiple EphB receptor tyrosine kinases shape dendritic spines in the hippocampus.* J Cell Biol, 2003. **163**(6): p. 1313-26.

338. Murai, K.K. and E.B. Pasquale, *Eph receptors, ephrins, and synaptic function.* Neuroscientist, 2004. **10**(4): p. 304-314.

339. Contractor, A. *et al.*, *Trans-synaptic Eph receptor-ephrin signaling in hippocampal mossy fiber LTP.* Science, 2002. **296**(5574): p. 1864-9.

340. Gerlai, R. *et al.*, *Regulation of learning by EphA receptors: a protein targeting study.* Journal of Neuroscience, 1999. **19**(21): p. 9538-9549.

341. Wahl, S. *et al.*, *Ephrin-A5 induces collapse of growth cones by activating Rho and Rho kinase.* J Cell Biol, 2000. **149**(2): p. 263-70.

342. Vanek, P. *et al.*, *Increased lesion-induced sprouting of corticospinal fibres in the myelin-free rat spinal cord.* Eur J Neurosci, 1998. **10**(1): p. 45-56.

343. Park, S. *et al.*, *Aberrant axonal projections in mice lacking EphA8 (Eek) tyrosine protein kinase receptors.* EMBO J., 1997. **16**(11): p. 3106-3114.

344. Conover, J.C. *et al.*, *Disruption of Eph/ephrin signaling affects migration and proliferation in the adult subventricular zone.* Nat Neurosci, 2000. **3**(11): p. 1091-7.

345. Gerlai, R., *Eph receptors and neural plasticity.* Nat Rev Neurosci, 2001. **2**(3): p. 205-9.

346. Xu, B. *et al.*, *EphA/ephrin-A interactions regulate epileptogenesis and activity-dependent axonal sprouting in adult rats.* Mol Cell Neurosci, 2003. **24**(4): p. 984-99.

347. Aasheim, H.C. *et al.*, *A splice variant of human ephrin-A4 encodes a soluble molecule that is secreted by activated human B lymphocytes.* Blood, 2000. **95**(1): p. 221-30.

348. Luo, H. *et al.*, *EphB6 crosslinking results in costimulation of T cells.* J Clin Invest, 2002. **110**(8): p. 1141-50.

349. Sharfe, N. *et al.*, *Ephrin stimulation modulates T cell chemotaxis.* Eur J Immunol, 2002. **32**(12): p. 3745-55.

350. Huynh-Do, U. *et al.*, *Surface densities of ephrin-B1 determine EphB1-coupled activation of cell attachment through alpha-V-beta-3 and alpha-V-beta-1 integrins.* EMBO J, 1999. **18**(8): p. 2165-73.

351. Zou, J.X. *et al.*, *An Eph receptor regulates integrin activity through R-Ras.* PNAS, 1999. **96**(24): p. 13813-8.

352. Huai, J. and U. Drescher, *An ephrin-A-dependent signaling pathway controls integrin function and is linked to the tyrosine phosphorylation of a 120-kDa protein.* Journal of Biological Chemistry, 2001. **276**(9): p. 6689-94.

353. Magal, E. *et al.*, *B61, a ligand for the Eck receptor protein-tyrosine kinase, exhibits neurotrophic activity in cultures of rat spinal cord neurons.* Journal of Neuroscience Research, 1996. **43**(6): p. 735-44.

354. Stichel, C.C. and H.W. Muller, *The CNS lesion scar: new vistas on an old regeneration barrier.* Cell Tissue Res, 1998. **294**(1): p. 1-9.

355. Eng, L.F. *et al.*, *Astrocyte activation and fibrous gliosis: glial fibrillary acidic protein immunostaining of astrocytes following intraspinal cord grafting of fetal CNS tissue.* Prog Brain Res, 1987. **71**: p. 439-55.

356. Reier, P.J. and J.D. Houle, *The glial scar: its bearing on axonal elongation and transplantation approaches to CNS repair.* Adv Neurol, 1988. **47**: p. 87-138.

357. Xu, Q. *et al.*, *In vivo cell sorting in complementary segmental domains mediated by Eph receptors and ephrins.* Nature, 1999. **399**(6733): p. 267-71.

358. Dubreuil, C.I. *et al.*, *Rho activation patterns after spinal cord injury and the role of activated Rho in apoptosis in the central nervous system.* Journal of Cell Biology, 2003. **162**(2): p. 233-243.

359. Miao, H. *et al.*, *Activation of EphA receptor tyrosine kinase inhibits the Ras/MAPK pathway.* Nat Cell Biol, 2001. **3**(5): p. 527-30.

360. Balasingam, V. and V.W. Yong, *Attenuation of astroglial reactivity by interleukin-10.* J Neurosci, 1996. **16**(9): p. 2945-55.

361. Bechmann, I. and R. Nitsch, *Astrocytes and microglial cells incorporate degenerating fibers following entorhinal lesion: a light, confocal, and electron microscopical study using a phagocytosis-dependent labeling technique.* Glia, 1997. **20**(2): p. 145-54.

362. Deller, T. *et al.*, *Up-regulation of astrocyte-derived tenascin-C correlates with neurite outgrowth in the rat dentate gyrus after unilateral entorhinal cortex lesion.* Neuroscience, 1997. **81**(3): p. 829-46.

363. Savaskan, N.E. *et al.*, *Myelin does not influence the choice behaviour of entorhinal axons but strongly inhibits their outgrowth length in vitro.* The European Journal of Neuroscience, 1999. **11**(1): p. 316-26.

364. Haas, C.A. *et al.*, *Entorhinal cortex lesion in adult rats induces the expression of the neuronal chondroitin sulfate proteoglycan neurocan in reactive astrocytes.* J Neurosci, 1999. **19**(22): p. 9953-63.

365. Deller, T. and M. Frotscher, *Lesion-induced plasticity of central neurons: sprouting of single fibres in the rat hippocampus after unilateral entorhinal cortex lesion.* Prog Neurobiol, 1997. **53**(6): p. 687-727.

366. Wang, Y. *et al.*, *Semi-quantitative expression analysis of ephrin mRNAs in the deafferented hippocampus.* Molecular Brain Research, 2003. **120**(1): p. 79-83.

367. Caron, E. and A. Hall, *Identification of two distinct mechanisms of phagocytosis controlled by different Rho GTPases.* Science, 1998. **282**(5394): p. 1717-21.

368. Etienne-Manneville, S. and A. Hall, *Rho GTPases in cell biology.* Nature, 2002. **420**(6916): p. 629-35.

369. Bergemann, A.D. *et al.*, *Ephrin-B3, a ligand for the receptor EphB3, expressed at the midline of the developing neural tube.* Oncogene, 1998. **16**(4): p. 471-80.

370. Imondi, R. *et al.*, *Complementary expression of transmembrane ephrins and their receptors in the mouse spinal cord: a possible role in constraining the orientation of longitudinally projecting axons.* Development (Cambridge, England), 2000. **127**(7): p. 1397-410.

371. Dergham, P. *et al.*, *Rho signaling pathway targeted to promote spinal cord repair.* J Neurosci, 2002. **22**(15): p. 6570-7.

372. Ellezam, B. *et al.*, *Inactivation of intracellular Rho to stimulate axon growth and regeneration.* Prog Brain Res, 2002. **137**: p. 371-80.

373. Gao, P.-P. *et al.*, *Ephrin-dependent growth and pruning of hippocampal axons.* PNAS, 1999. **96**(7): p. 4073-4077.

374. Castellani, V. *et al.*, *Dual action of a ligand for Eph receptor tyrosine kinases on specific populations of axons during the development of cortical circuits.* J Neurosci, 1998. **18**(12): p. 4663-72.

375. Gao, P.P. *et al.*, *Ephrins stimulate or inhibit neurite outgrowth and survival as a function of neuronal cell type.* Journal of Neuroscience Research, 2000. **60**(4): p. 427-36.

376. Moreno Flores, M.T. *et al.*, *Ephrin-B1 promotes dendrite outgrowth on cerebellar granule neurons.* Mol Cell Neurosci, 2002. **20**(3): p. 429-46.

377. Hindges, R. *et al.*, *EphB forward signaling controls directional branch extension and arborization required for dorsal-ventral retinotopic mapping.* Neuron, 2002. **35**: p. 475–487.

378. Holash, J.A. *et al.*, *Reciprocal expression of the Eph receptor Cek5 and its ligand(s) in the early retina.* Dev Biol, 1997. **182**(2): p. 256-69.

379. King, C.E. *et al.*, *Transient up-regulation of retinal EphA3 and EphA5, but not ephrin-A2, coincides with re-establishment of a topographic map during optic nerve regeneration in goldfish.* Experimental Neurology, 2003. **183**(2): p. 593-599.

380. Biervert, C. *et al.*, *Semiquantitative expression analysis of ephrine-receptor tyrosine kinase mRNA's in a rat model of traumatic brain injury.* Neuroscience Letters, 2001. **315**(1-2): p. 25-28.

381. Miranda, J.D. *et al.*, *Induction of Eph B3 after spinal cord injury.* Experimental Neurology, 1999. **156**(1): p. 218-22.

382. Knoll, B. *et al.*, *Graded expression patterns of ephrin-As in the superior colliculus after lesion of the adult mouse optic nerve.* Mechanisms of Development, 2001. **106**(1-2): p. 119-127.

383. Rodger, J. *et al.*, *Expression of ephrin-A2 in the superior colliculus and EphA5 in the retina following optic nerve section in adult rat.* Eur J Neurosci, 2001. **14**(12): p. 1929-1936.

384. Wang, A.G. *et al.*, *Change of gene expression profiles in the retina following optic nerve injury.* Brain Res Mol Brain Res, 2002. **101**(1-2): p. 82-92.

385. Moreno-Flores, M.T. and F. Wandosell, *Up-regulation of Eph tyrosine kinase receptors after excitotoxic injury in adult hippocampus.* Neuroscience, 1999. **91**(1): p. 193-201.

386. Wohlfahrt, J.G. *et al.*, *Ephrin-A1 suppresses Th2 cell activation and provides a regulatory link to lung epithelial cells.* J Immunol, 2004. **172**(2): p. 843-50.

387. Smith, L.M. *et al.*, *EphA3 is induced by CD28 and IGF-1 and regulates cell adhesion.* Exp Cell Res, 2004. **292**(2): p. 295-303.

388. Savaskan, N.E. and R. Nitsch, *Molecules involved in reactive sprouting in the hippocampus.* Rev Neurosci, 2001. **12**(3): p. 195-215.

389. Murai, K.K. *et al.*, *Targeting the EphA4 receptor in the nervous system with biologically active peptides.* Mol Cell Neurosci, 2003. **24**(4): p. 1000-11.

390. Guest, J.D. *et al.*, *Influence of IN-1 antibody and acidic FGF-fibrin glue on the response of injured corticospinal tract axons to human Schwann cell grafts.* Journal of Neuroscience Research, 1997. **50**(5): p. 888-905.

391. Silver, J. and J.H. Miller, *Regeneration beyond the glial scar.* Nat Rev Neurosci, 2004. **5**(2): p. 146-56.

392. Fitch, M.T. and J. Silver, *Glial cell extracellular matrix: boundaries for axon growth in development and regeneration.* Cell Tissue Res, 1997. **290**(2): p. 379-84.

393. Tang, B.L., *Inhibitors of neuronal regeneration: mediators and signaling mechanisms.* Neurochem Int, 2003. **42**(3): p. 189-203.

394. Nystrom, B. and J.E. Berglund, *Spinal cord restitution following compression injuries in rats.* Acta Neurol Scand, 1988. **78**(6): p. 467-72.

395. Paxinos, G. and C. Watson, *The Rat Brain in Stereotaxic Coordinates.* 1986: New York Academic Press.

396. Demaison, C. *et al.*, *High-level transduction and gene expression in hematopoietic repopulating cells using a human immunodeficiency [correction of imunodeficiency] virus type 1-based lentiviral vector containing an internal spleen focus forming virus promoter.* Hum Gene Ther, 2002. **13**(7): p. 803-13.

397. Pfaffl, M.W., *A new mathematical model for relative quantification in real-time RT-PCR.* Nucl. Acids Res., 2001. **29**(9): p. e45-.

398. Bartsch, S. *et al.*, *Expression of tenascin in the developing and adult cerebellar cortex.* J. Neurosci., 1992. **12**(3): p. 736-749.

399. Zhang, Y. *et al.*, *Molecular basis of interactions between regenerating adult rat thalamic axons and Schwann cells in peripheral nerve grafts I. Neural cell adhesion molecules.* J Comp Neurol, 1995. **361**(2): p. 193-209.

400. de Castro, R.C., Jr. *et al.*, *Metalloproteinase increases in the injured rat spinal cord.* Neuroreport, 2000. **11**(16): p. 3551-4.

401. Duchossoy, Y. *et al.*, *MMP-related gelatinase activity is strongly induced in scar tissue of injured adult spinal cord and forms pathways for ingrowing neurites.* Mol Cell Neurosci, 2001. **17**(6): p. 945-56.

402. Carpenter, M.K. *et al.*, *Ligands for EPH-related tyrosine kinase receptors are developmentally regulated in the CNS.* Journal of Neuroscience Research, 1995. **42**(2): p. 199-206.

403. Parker, M. *et al.*, *Reverse endocytosis of transmembrane ephrin-B ligands via a clathrin-mediated pathway.* Biochem Biophys Res Commun, 2004. **323**(1): p. 17-23.

404. Zimmer, M. *et al.*, *EphB-ephrinB bi-directional endocytosis terminates adhesion allowing contact mediated repulsion.* 2003. **5**(10): p. 869-878.

405. Mann, F. *et al.*, *B-type Eph receptors and ephrins induce growth cone collapse through distinct intracellular pathways.* J Neurobiol, 2003. **57**(3): p. 323-36.

406. Moran, P. and I.W. Caras, *Fusion of sequence elements from non-anchored proteins to generate a fully functional signal for glycophosphatidylinositol membrane anchor attachment.* The Journal of Cell Biology, 1991. **115**(6): p. 1595-600.

407. Mizushima, S. and S. Nagata, *pEF-BOS, a powerful mammalian expression vector.* Nucleic Acids Research (Online), 1990. **18**(17): p. 5322.

408. Turner, D., *pCS2+ Vector Resource.* 2003, http://sitemaker.umich.edu/dlturner.vectors.

409. Flanagan, J.G. and P. Leder, *The kit ligand: a cell surface molecule altered in steel mutant fibroblasts.* Cell, 1990. **63**(1): p. 185-94.

410. Cheng, H.J. and J.G. Flanagan, *Identification and cloning of ELF-1, a developmentally expressed ligand for the Mek4 and Sek receptor tyrosine kinases.* Cell, 1994. **79**(1): p. 157-68.

411. Berger, J. *et al.*, *Secreted placental alkaline phosphatase: a powerful new quantitative indicator of gene expression in eukaryotic cells.* Gene, 1988. **66**(1): p. 1-10.

412. Miska, W. and R. Geiger, *Synthesis and characterization of luciferin derivatives for use in bioluminescence enhanced enzyme immunoassays. New ultrasensitive detection systems for enzyme immunoassays, I.* Journal of Clinical Chemistry and Clinical Biochemistry, 1987. **25**(1): p. 23-30.

413. Brennan, C. and J. Fabes, *Alkaline phosphatase fusion proteins as affinity probes for protein localization studies.* Science STKE, 2003(168).

414. Ciossek, T. *et al.*, *Eph receptor-ligand interactions are necessary for guidance of retinal ganglion cell axons in vitro.* The European Journal of Neuroscience, 1998. **10**(5): p. 1574-80.

415. Klostermann, S. and F. Bonhoeffer, *Investigations of signaling pathways in axon growth and guidance.* Perspectives On Developmental Neurobiology, 1996. **4**(2-3): p. 237-52.

416. Yamada, T. *et al.*, *Analysis of ephrin-A2 in the chick retinotectal projection using a function-blocking monoclonal antibody.* Journal of Neurobiology, 2001. **47**(4): p. 245-54.

417. Vielmetter, J. *et al.*, *In vitro assay to test differential substrate affinities of growing axons and migratory cells.* Experimental Brain Research, 1990. **81**(2): p. 283-7.

418. Chadborn, N. *et al.*, *Direct measurement of local raised subplasmalemmal calcium concentrations in growth cones advancing on an N-cadherin substrate.* The European Journal of Neuroscience, 2002. **15**(12): p. 1891-8.

419. Vielmetter, J. and C.A. Stuermer, *Goldfish retinal axons respond to position-specific properties of tectal cell membranes in vitro.* Neuron, 1989. **2**(4): p. 1331-9.

420. Walter, J. *et al.*, *Recognition of position-specific properties of tectal cell membranes by retinal axons in vitro.* Development (Cambridge, England), 1987. **101**(4): p. 685-96.

421. Dijkstra, S. *et al.*, *Selective stimulation of dendrite outgrowth from identified corticospinal neurons by homotopic astrocytes.* Neuroscience, 1999. **92**(4): p. 1331-1342.

422. Muir, E. *et al.*, *Increased axon growth through astrocyte cell lines transfected with urokinase.* Glia, 1998. **23**(1): p. 24-34.

423. Gallo, G. *et al.*, *Transient PKA activity is required for initiation but not maintenance of BDNF-mediated protection from nitric oxide-induced growth-cone collapse.* J Neurosci, 2002. **22**(12): p. 5016-23.

424. Myshkin, E. and B. Wang, *Chemometrical Classification of Ephrin Ligands and Eph Kinases Using GRID/CPCA Approach.* Journal of Chemical Information and Computer Sciences, 2003. **43**(3): p. 1004-10.

425. Himanen, J.P. *et al.*, *Crystal structure of the ligand-binding domain of the receptor tyrosine kinase EphB2.* Nature, 1998. **396**(6710): p. 486-91.

426. Chrencik, J.E. *et al.*, *Structure and thermodynamic characterization of the EphB4/Ephrin-B2 antagonist peptide complex reveals the determinants for receptor specificity.* Structure, 2006. **14**(2): p. 321-30.

427. Nikolov, D.B. *et al.*, *Crystal structure of the ephrin-B1 ectodomain: implications for receptor recognition and signaling.* Biochemistry, 2005. **44**(33): p. 10947-53.

428. Nathan, A. *et al.*, *Tissue Engineered Perivascular Endothelial Cell Implants Regulate Vascular Injury.* PNAS, 1995. **92**(18): p. 8130-8134.

429. Lu, P. *et al.*, *BDNF-expressing marrow stromal cells support extensive axonal growth at sites of spinal cord injury.* Experimental Neurology, 2005. **191**(2): p. 344-360.

430. Cao, L. *et al.*, *Olfactory ensheathing cells genetically modified to secrete GDNF to promote spinal cord repair.* Brain, 2003.

431. Jaeger, C.B. *et al.*, *Growth of tumour cell lines in polymer capsules: ultrastructure of encapsulated PC12 cells.* Journal of Neurocytology, 1992. **21**(7): p. 469-480.

432. Corpet, F., *Multiple sequence alignment with hierarchical clustering.* Nucleic Acids Res, 1988. **16**(22): p. 10881-90.

433. Leenen, L.P. *et al.*, *A detailed morphometrical analysis of the pyramidal tract of the rat.* Brain Res, 1985. **359**(1-2): p. 65-80.

434. Harding, G.W. and A.L. Towe, *Fiber analysis of the pyramidal tract of the laboratory rat.* Exp Neurol, 1985. **87**(3): p. 503-18.

435. Bass, N.H. and P. Lundborg, *Postnatal development of bulk flow in the cerebrospinal fluid system of the albino rat: clearance of carboxyl-(14 C)inulin after intrathecal infusion.* Brain Res, 1973. **52**: p. 323-32.

436. Keyvan-Fouladi, N. *et al.*, *Delayed repair of corticospinal tract lesions as an assay for the effectiveness of transplantation of Schwann cells.* Glia, 2005. **51**(4): p. 306-11.

437. Schwab, J.M. *et al.*, *Differential Cellular Accumulation of Connective Tissue Growth Factor Defines a Subset of Reactive Astrocytes, Invading Fibroblasts, and Endothelial Cells Following Central Nervous System Injury in Rats and Humans.* Journal of Neurotrauma, 2001. **18**(4): p. 377-388.

438. Webb, A.A. and G.D. Muir, *Unilateral dorsal column and rubrospinal tract injuries affect overground locomotion in the unrestrained rat.* European Journal of Neuroscience, 2003. **18**(2): p. 412-422.

439. Weidner, N. *et al.*, *Spontaneous corticospinal axonal plasticity and functional recovery after adult central nervous system injury.* Proc Natl Acad Sci U S A, 2001. **98**(6): p. 3513-8.